The Scientific World Journal

Bioenergy and Its Environmental Impacts

Guest Editors: Shungui Zhou, Yang-Chun Yong, Bin Cao, Hu-Chun Tao, and Li Zhuang

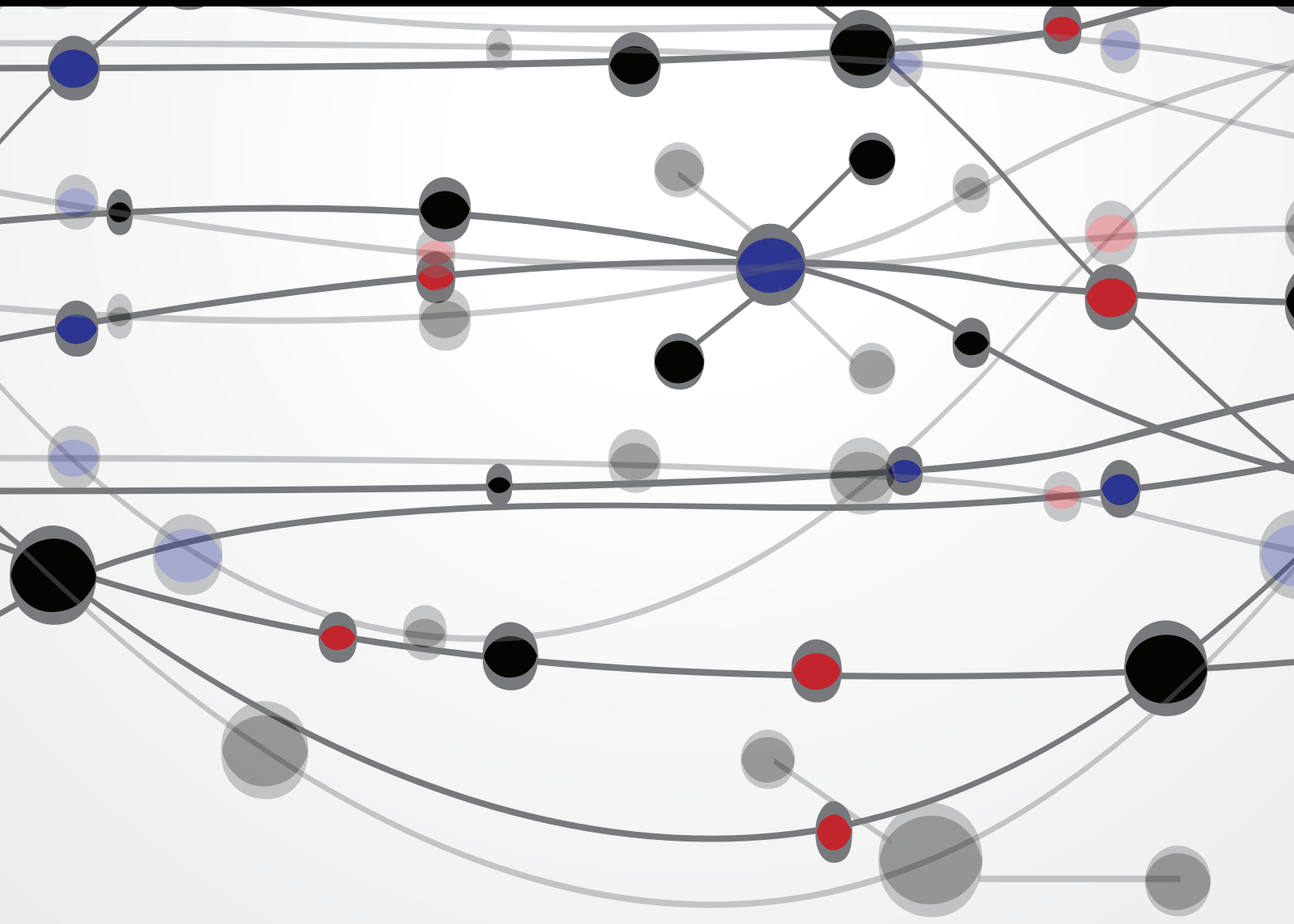

Bioenergy and Its Environmental Impacts

The Scientific World Journal

Bioenergy and Its Environmental Impacts

Guest Editors: Shungui Zhou, Yang-Chun Yong, Bin Cao, Hu-Chun Tao, and Li Zhuang

Contents

Hindawi Publishing Corporation
The Scientific World Journal
Volume 2015, Article ID 508037, 1 page
http://dx.doi.org/10.1155/2015/508037

Editorial

Bioenergy and Its Environmental Impacts

Shungui Zhou,[1] Yang-Chun Yong,[2] Bin Cao,[3] Hu-Chun Tao,[4] and Li Zhuang[1]

[1]*Guangdong Institute of Eco-Environmental and Soil Sciences, Guangzhou 510650, China*
[2]*School of The Environment, Jiangsu University, 301 Xuefu Road, Zhenjiang 212013, China*
[3]*School of Civil & Environmental Engineering and Singapore Centre on Environmental Life Sciences Engineering, Nanyang Technological University, 50 Nanyang Avenue, Singapore 639798*
[4]*School of Environment & Energy, Peking University, Nanshan District, Shenzhen 518055, China*

Correspondence should be addressed to Shungui Zhou; sgzhou@soil.gd.cn

Received 23 December 2014; Accepted 23 December 2014

Bioenergy is renewable energy and offers the promise for reducing dependency on fossil fuels. The main environmental impacts of bioenergy are associated with land use and greenhouse gas emission. This special issue covers multidisciplinary approaches and intensive research orientations for the real challenges in bioenergy and its environmental impacts. For this special issue, we received 35 submissions from all over the world. After an initial screening, 6 submissions were declared "out of scope" and the remaining 29 were sent to reviewers. All manuscripts underwent a very rigorous peer review process. We finally selected 12 full papers and 1 review paper for this special issue. In this issue, bioenergy from algae is highly concerned, including oil production from microalgae, life cycle fossil energy ratio of algal biodiesel, microbial fuel cell (MFC) with photosynthetic algae cathode, and algal biofuel production with wastewater. MFC, a new technology for electricity generation from waste and biomass, is popular in this special issue. The authors reported that the use of nanostructured manganese oxide as cathodic catalyst and the use of carbon nanofiber modified graphite felt as anode can significantly enhance MFC performance. The review paper focused on the state-of-the-art method for assessing the greenhouse gas (GHG) emission reduction by developing energy crops and a new approach combining life cycle analysis (LCA) with biogeochemical process models to assess GHG emission reduction. Although research on bioenergy has increased in recent years, the study of developing and screening the most suitable and economically viable technology needs much further attention.

Acknowledgment

We take this opportunity to thank all the authors for their contribution to the success of this special issue.

Shungui Zhou
Yang-Chun Yong
Bin Cao
Hu-Chun Tao
Li Zhuang

Hindawi Publishing Corporation
The Scientific World Journal
Volume 2015, Article ID 864568, 8 pages
http://dx.doi.org/10.1155/2015/864568

Research Article

Bioelectricity Generation in a Microbial Fuel Cell with a Self-Sustainable Photocathode

Ting Liu,[1,2] Liqun Rao,[3] Yong Yuan,[2] and Li Zhuang[2]

[1]*Orient Science & Technology College, Hunan Agricultural University, Changsha 410128, China*
[2]*Guangdong Institute of Eco-Environmental and Soil Sciences, Guangzhou 510650, China*
[3]*College of Bioscience and Biotechnology, Hunan Agricultural University, Changsha 410128, China*

Correspondence should be addressed to Yong Yuan; yuanyong@soil.gd.cn

Received 22 July 2014; Accepted 7 September 2014

Academic Editor: Shun-Gui Zhou

This study aims to construct an MFC with a photosynthetic algae cathode, which is maintained by self-capturing CO_2 released from the anode and utilizing solar energy as energy input. With this system, a maximum power density of 187 mW/m^2 is generated when the anode off gas is piped into the catholyte under light illumination, which is higher than that of 21 mW/m^2 in the dark, demonstrating the vital contribution of the algal photosynthesis. However, an unexpected maximum power density of 146 mW/m^2 is achieved when the anode off gas is not piped into the catholyte. Measurements of cathodic microenvironments reveal that algal photosynthesis still takes place for oxygen production under this condition, suggesting the occurrence of CO_2 crossover from anode to cathode through the Nafion membrane. The results of this study provide further understanding of the algae-based microbial carbon capture cell (MCC) and are helpful in improving MCC performance.

1. Introduction

Microbial fuel cells (MFCs) are devices that convert organic waste material into electricity energy by using microorganisms as biocatalysts. The environmentally friendly process has been gaining international attention in recent years as an advanced technology for both electricity generation and waste treatment [1–3]. Common MFC is a dual-chamber system, consisting of an anode and a cathode chamber that is separated by a proton exchange membrane (PEM) [4]. In such a system, oxygen must be continuously supplied for the reaction in the cathode, leading to extra energy consumption for aeration [5]. Therefore, requiring continuous aeration is obviously a limitation for real-world applications of MFCs because of its economic and environmental cost.

As a solution to eliminate or maintain minimum energy consumption for cathode aeration, recently studies have proposed the integration of algal photosynthesis with MFCs, which was known as photo MFCs [6–8]. In such a system, oxygen was produced *in situ* in the cathode compartment through the algal photosynthesis. It is known that algae are responsible for ca. 75% of the earth's oxygen production during their uptake of carbon dioxide (CO_2) under solar light illumination [9, 10]. Therefore, the algae-based photo MFCs are capable of simultaneously fixing CO_2, generating electric energy, and treating wastewater, representing a more advanced technique as compared with the conventional MFCs [11–13]. In these cases, CO_2 was required to be continuously supplied to the cathode compartment to maintain high energy generation. Similar to aeration, CO_2 purging consumed extra energy, representing an unsustainable option in terms of economy. In this regard, Wang et al. [14] demonstrated a new microbial carbon capture cell (MCC) in which CO_2 generated from substrate degradation in the anode chamber was directly introduced to the cathode for the O_2 production via algal photosynthesis. This MCC represents an effective technology for simultaneous CO_2 emission reduction and voltage output without aeration. In spite of the advantages, this system is still in its infancy stage. To date, there are still very few attempts regarding how MCCs will work in a more sustainable manner.

The objective of this study was to fully understand MCC systems in terms of electric energy production performance and measure the microenvironments of the photocathode

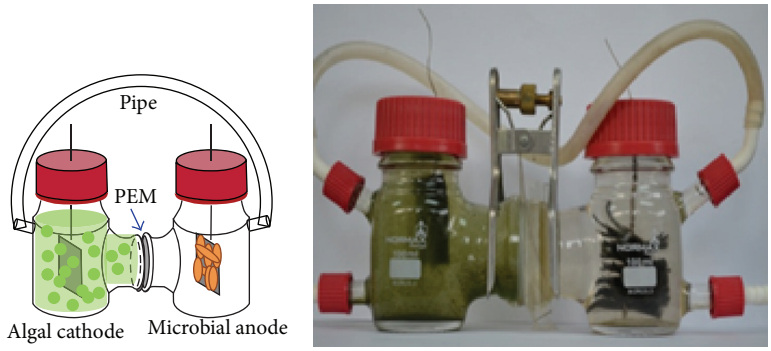

Figure 1: Schematic diagram (a) and experimental setup (b) of an MCC. CO_2 is transported through a silicon tube, fixed on the chambers.

under various circumstances to reveal the underlying mechanisms of cathode reactions. For this purpose we constructed an MCC system and examined its power generation process under light-on and light-off circumstances. Variations in pH and dissolved oxygen in the catholyte were monitored *in situ* with microelectrodes during the circumstances. In addition, conventional electrochemical techniques were used to reveal the catalytic activities of both anode and cathode. Scanning electron microscopy was employed to explore the morphology of biofilms formed on both the anode and the cathode. Generation of bioelectricity by the MCC was related to pH and oxygen variations at the cathode. The results from this study are expected to be helpful in further improving MCC performance.

2. Materials and Methods

2.1. MCCs Setup and Operation. The MCCs consisted of two 100 mL glass bottles as two chambers separated by a piece of PEM as shown in Figure 1. Gas generated from the anode was piped into the catholyte. The anode was made of carbon fiber brushes and the cathode was carbon felt (3 cm × 3 cm) containing 0.1 mg/cm^2 Pt catalyst (10%, Pt loading, HESEN, China). To coat the Pt catalyst to the carbon felt, Pt/C powder was mixed with Nafion solution and then applied to the carbon felt surface with a brush. Both electrodes were connected with titanium wire. A white light LED (light intensity of 2000 lx) was employed to continuously illuminate the cathode. When operated in the dark, the cathode chamber was wrapped with an aluminium foil. All experiments were conducted in duplicate.

The MCC anode chamber was inoculated with 10 mL of activated anaerobic sludge (Liede Sewage Treatment Plant, Guangzhou, China) and 90 mL of culture medium (pH = 7.0). The anode culture medium contained sodium acetate (1,000 mg L^{-1}), $NaH_2PO_4{\cdot}2H_2O$ (2.77 g L^{-1}), $Na_2HPO_4{\cdot}12H_2O$ (11.40 g L^{-1}), NH_4Cl (0.31 g L^{-1}), KCl (0.13 g L^{-1}), a vitamin stock solution (12.5 mL L^{-1}), and a mineral stock solution (12.5 mL L^{-1}) [15]. The acetate-free phosphate buffered solution was used as cathode medium. To start up the MCC, the cathode was firstly purged with oxygen. After the voltage output was stabilized, *Chlorella vulgaris* was introduced into the cathode chamber and the LED lamp was turned on to illuminate the cathode chamber. *C. vulgaris* was purchased from FACHB-Collection (FACHB 1068, China) and cultured in an illuminated autoclaved flask aerated with air. The algae suspension was centrifuged (10,000 ×g) and washed 3 times with DI water before added to the cathode compartment. Then the cathode chamber was purged with N_2 to exclude the influences of the remained oxygen before piping CO_2. The power density curves of the MCC were obtained by changing the circuit resistor from 10,000 to 50 Ω. All tests were conducted in batch mode in a 30°C incubator. The cell voltage was recorded every 2 min by a digital multimeter connected to a computer. The power was normalized by the projected surface area of the cathode.

2.2. Microelectrode Measurements. The cathode pH measurements were conducted continuously using a pH microsensor (50 μm in diameter, response time of ca. 30 s) connected to a multimeter (Unisense, Aarhus, Denmark) for 60 hours. The sensor was calibrated using standard pH buffers before use. Oxygen was measured incessantly using an oxygen microsensor (50 μm in diameter, response time of ca. 5 s) connected to the same equipment for 60 hours. Before taking measurements, the oxygen microsensor was polarized at +800 mV to achieve a stable signal output. The sensor was calibrated in both oxygen-saturated and oxygen-free solutions.

2.3. Analytical Techniques. Cyclic voltammograms (CVs) were conducted in a conventional three-electrode electrochemical system by a potentiostat (CHI660D, Chenhua Instrument, China). A saturated calomel electrode (SCE) was used as reference electrode. The anode and cathode of the MCC were used as working and counter electrode, respectively. The linear sweep voltammetry (LSV) of the cathode was measured with potentials ranging from +0.4 V to −0.7 V (versus SCE) by the potentiostat. Sodium acetate concentration was determined by HPLC (Waters1525, Binary HPLC Pump). Samples were filtered (0.2 μm filter) before HPLC analyses using an Agilent Zorbax SB-C18 (250 × 4.6 mm, 5 μm) column, with 0.01 mol L^{-1} phosphate buffer as the mobile phase (1.0 mL/min). Scanning electron microscopy

(SEM) was used to study the morphologies of the cathode algae and the anode bacteria, respectively. Briefly, biofilms formed on the anode and the cathode were fixed directly with glutaraldehyde (2.5%, final) for 5 h. Furthermore, the biofilms were washed and dehydrated by successive 30 min incubations in 25% ethanol, 50% ethanol, 70% ethanol, and 100% ethanol. After dehydration, the biofilms were dried with a critical-point dryer (HCP-2, Hitachi, Japan). The same treatment was conducted for the cathode. The specimens were observed by SEM (JEOL, JSM-6330F, Japan).

3. Results and Discussion

3.1. Power Generation of the MCC in Response to Light Illumination. After the MCC was started up and produced stable voltage using an MFC mode with an aerated Pt/C cathode, the anode off gas was piped into the catholyte and *C. vulgaris* was introduced into the cathode compartment. As shown in Figure 2(a), after startup of the MCC, the voltage output from the MCC was significantly affected by illumination. The peak voltage reached 0.60 V under illumination at 2000 Ω. Without aeration in this period, the cathode reaction depended on the O_2 generated by algal photosynthesis in the cathode compartment. Once the light was turned off, the voltage started to decline, resulting in a final voltage output of 0.1 V in the dark. It is worth mentioning that the uptake of CO_2 is critical for algal photosynthesis. In this case, CO_2 generated from the anode was piped into the catholyte to support the algal photosynthesis. The variation of the voltage was consistent with the findings by Xiao et al. [8] who purged the algal cathode with CO_2 gas. It was expected that no voltage would be produced if the CO_2 produced in the anode chamber was no longer piped into the cathode. However, considerable although slightly smaller voltage was still generated with the same response on the light.

Furthermore, power densities of the MCCs and individual potentials of electrodes under different operation modes were evaluated and the results were shown in Figures 2(b) and 2(c). When the MCC was continuously illuminated, the maximum power densities were 187 mW/m^2 (1.7 W/m^3 by normalizing to the anode volume) and 146 mW/m^2 (1.3 W/m^3) when CO_2 was piped or not piped into the catholyte, respectively. These values were significantly higher than that of 21 mW/m^2 obtained in the dark. As shown in Figure 2(b), the differences in peak power densities were mainly caused by the performance of cathode. The produced power per anode volume was comparable with the previous results [11, 16], but a little smaller than that reported by Wang et al. [14]. The difference in power density possibly resulted from the different reactor configurations. Here, we used a traditional H-type reactor with easily maintained anaerobic environment for the anode, but such a reactor had a higher internal resistance as compared with that used by Wang et al. [14], resulting from the long distance between the anode and the cathode and the small size of the Nafion membrane [17, 18].

On the other hand, results of previous study showed that light was the most important parameter for MCCs performance. Light dependent performance of the algal photo MFC was also observed by Gouveia et al. [19] However, a self-sustained sediment phototrophic MFC containing both photosynthetic microorganisms and heterotrophic bacteria was reported to generate a higher power density in darkness than that in the light [20]. The inconsistency of results in the effect of light on MFCs is attributed to the different nature of algae [16].

3.2. Electrochemical and Morphological Characteristics of the Electrodes. As mentioned above, the performance of the MCC was mainly limited by the cathode. However, a stable bioanode should be maintained for voltage output during the examined light-on and -off periods. As shown in Figure 3(a), sigmoidal CVs were observed from all anodes for the first 5 days, demonstrating catalytic oxidation of acetate by these bioanodes. At the 9th day, no catalytic current was observed, which suggested the complete consumption of acetate (Figure 3(a), inset). In this case, a nonturnover CV behavior of the bioanode was observed, which showed two major redox couples. The CV was similar to those reported electrochemically active biofilms based on *Geobacter sulfurreducens* [21, 22].

On the other hand, linear sweep voltammetry (LSV) was used to investigate the electrochemical catalytic reaction of the cathode. As shown in Figure 3(b), catalytic current from oxygen reduction was observed when the cathode was piped with the anode off gas and illuminated with light. A decreased catalytic current of the oxygen was observed when the cathode was not piped with the anode off gas, suggesting lower dissolved oxygen in the catholyte under this condition. The catalytic performance of the cathode was well consistent with the voltage and power output as mentioned above, further suggesting the influence of the cathode on the performance of the MCC. After long-term operation, the morphologies of both the anode and the cathode were revealed with SEM. Figures 4(a) and 4(b) showed the present of clustered bacteria on the anode, suggesting formation of electrochemically active biofilm. Similarly, biofilm was also formed on the cathode electrode, demonstrating that algal cells were also possible to adsorb on the surface of the cathode as shown in Figure 4(c). Figure 4(d) showed the algal cells were in round-shape.

3.3. The Cathodic Microenvironments. DO and pH in the cathode chamber are important parameters affecting the electricity generation in the MCC. DO concentration and pH were *in situ* determined using microelectrodes. As shown in Figure 5, the maximal concentration of DO reached 4.5 mg/L when the anode off gas was piped into the cathode and the illuminated cathode compartment. Meanwhile, the maximal concentration of DO reached 1.2 mg/L when the anode off gas was not piped into the illuminated cathode compartment. The unexpected oxygen production was believed to result from algal photosynthesis because oxygen concentration in the catholyte was in response to light illumination. As mentioned above, CO_2 is required for photosynthesis by algae. Therefore, it is deduced that CO_2 generated in the anode chamber had possibly entered the cathode chamber

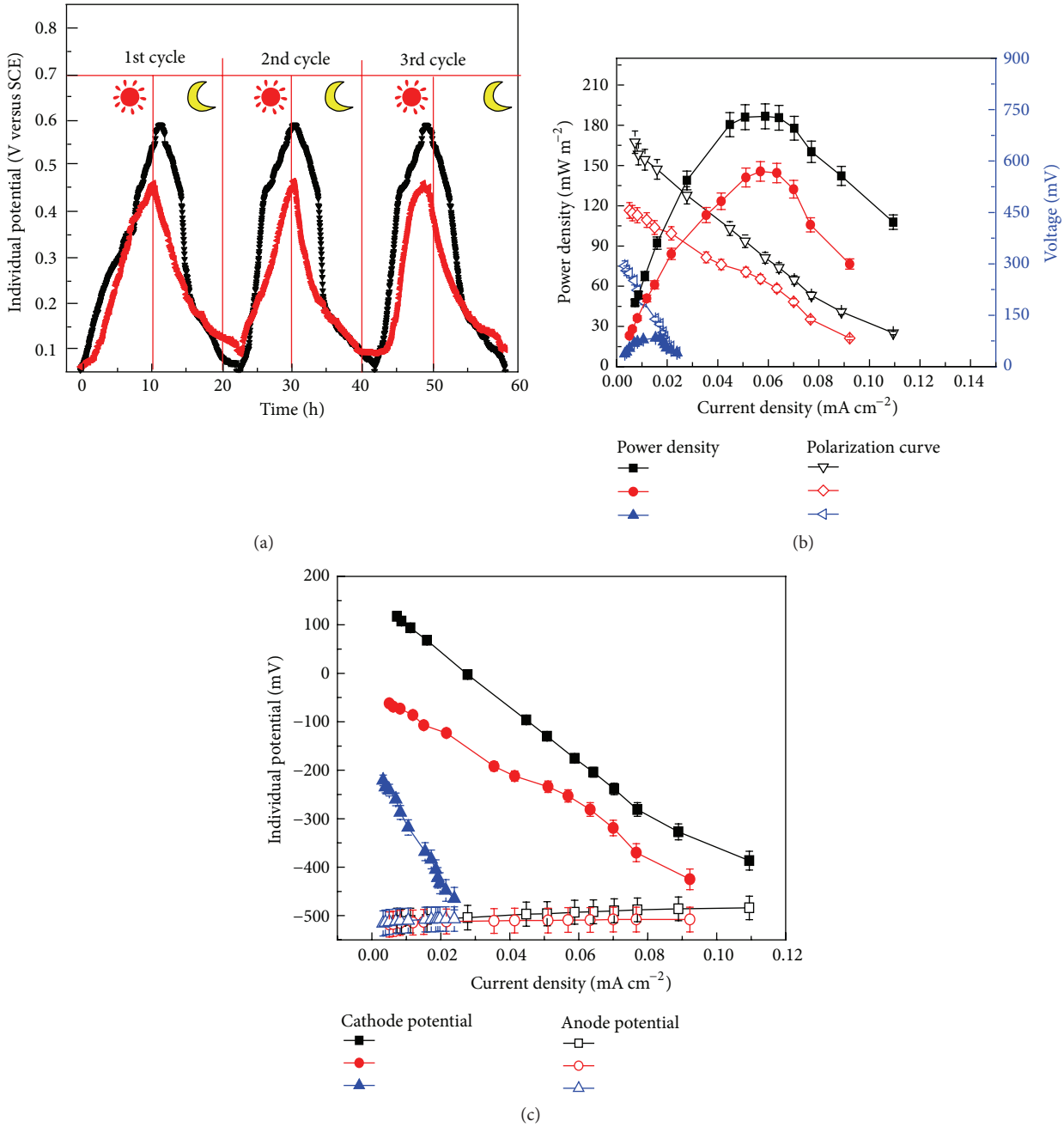

FIGURE 2: (a) Potential changes of the MCCs under different circumstances (black line is when CO_2 travelled through the silicon tube and red line is when CO_2 travel through the silicon tube was blocked with a clip. The symbols of moon and sun represent dark and light conditions, resp.). (b) Power density and polarized curves of the MCCs operated under various conditions. (c) Individual cathode and anode potentials versus current density curves (black line: CO_2 travelled through the tube under light illumination; red line: CO_2 travel through the silicon tube was blocked under light illumination; blue line: CO_2 travelled through the silicon tube in the dark).

through a pathway other than the external pipe. In other words, it is believed that CO_2 crossover through the Nafion membrane from the anode to the cathode compartment took place in the MCC. The phenomenon of CO_2 crossover from the anode to the cathode through the Nafion membrane was previously confirmed in a direct methanol fuel cell [23], which supported our hypothesis.

The pH of the catholyte increased from 7.3 to 8.3 when the CO_2 generated from the anode was piped into the cathode chamber under illumination, which was likely due to oxygen reduction. Note that the pH variation was well associated with the voltage output process during the light-on and -off circumstances. As previously reported, the MFC cathode reaction could elevate the pH of the catholyte to above 12 [24].

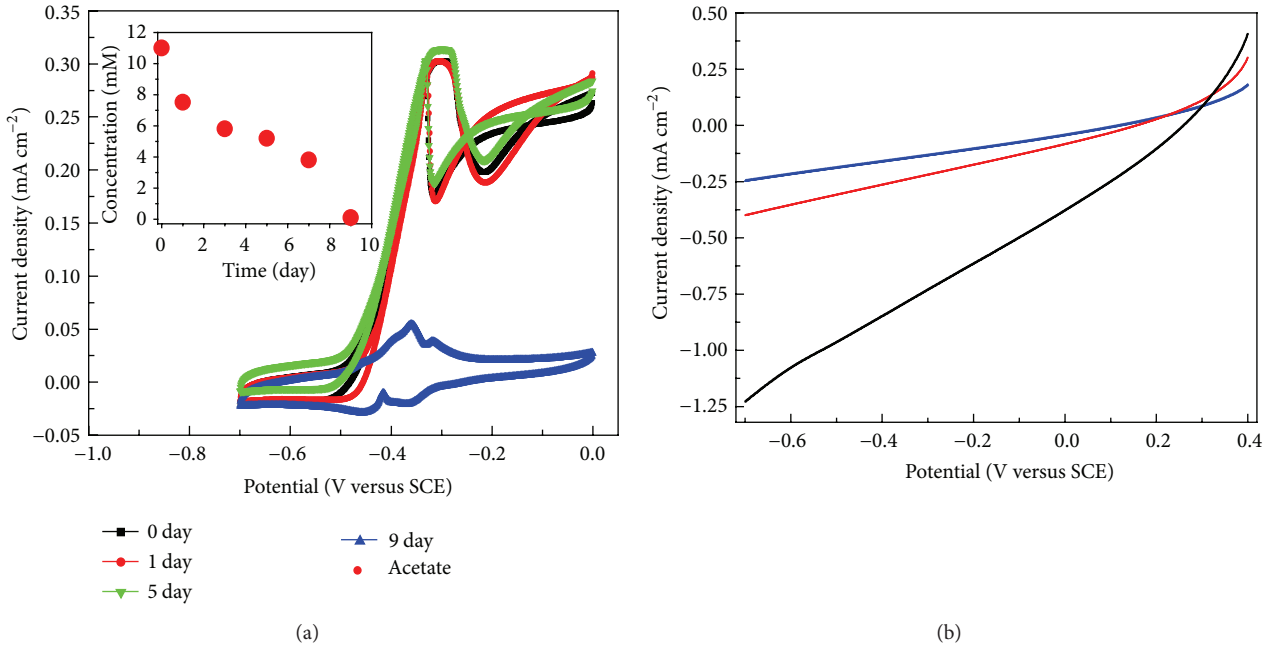

Figure 3: (a) The cyclic voltammograms (CVs) of the anode at different times (inset demonstrates the relationship between time and acetate concentration). (b) The LSV of the cathode under various conditions (black line: CO_2 travel through the tube was allowed under light illumination; red line: CO_2 travel through the silicon tube was blocked under light illumination; blue line: CO_2 was allowed to travel through the tube in the dark).

As expected, the same pH variation trend was observed when the CO_2 was not piped into the cathode, further confirming occurrence of CO_2 crossover from the anode to the cathode through the Nafion membrane in the constructed MCC.

3.4. Mechanisms and Implications. In general, three possible reactions take place in a photocathode chamber, including direct CO_2 reduction, electron transfer through self-produced mediators, and reduction of oxygen generated through photosynthesis. However, Wang et al. [14] previously suggested that reduction of oxygen generated through photosynthesis was the major contributor to the high current generation in an MCC. Oxygen generation relied on the uptake of CO_2 by algae. However, previous study had only considered the CO_2 transportation through the pipe. Here, we showed that the cathodic photosynthesis still took place when the anodic gas was no longer piped into the catholyte. In this case, we deduced that CO_2 crossover from the anode to the cathode through the Nafion membrane contributed to the photosynthetic oxygen generation (Figure 6). In general, the following main reactions occurred in our system.

Anode reaction is as follows:

$$CH_3COO^- + 2H_2O \longrightarrow 2CO_2 + 7H^+ + 8e^- \quad (1)$$

Cathode reaction is as follows:

$$nCO_2 + nH_2O \longrightarrow (CH_2O)_n + nO_2 \quad (2)$$

$$O_2 + 4e^- + 4H^+ \longrightarrow 2H_2O \quad (3)$$

$$O_2 + 2H_2O + 4e^- \longrightarrow 4OH^- \quad (4)$$

Note that oxygen is generally considered to be reduced at the Pt surface in the cathode through reaction (3) [25]. However, alkalization of the catholyte was observed in the MCC, suggesting that oxygen was reduced to produce OH^- as a main product as shown in reaction (4) [26]. It should be noted that the theoretical potential of the ORR in reaction (4) is lower than that in reaction (3), representing a great potential loss because of the alkalization of the catholyte. As previously suggested, decreasing the pH value of the catholyte during the MCC operation can be one solution to achieve higher performance [27].

MFC has been considered as a sustainable technology for energy production and wastewater treatment. However, energy consumption was necessary to maintain MFC operations. Algal photosynthesis provides an option to eliminate or maintain minimum energy consumption in MFC technology by omitting aeration. Therefore, aeration was not required and the greenhouse gas (CO_2) emitted from the anode chamber was self-sequestrated in the MCCs, making real green systems for energy generation. However, it is notable that energy production of the photosynthetic algal MFCs is currently quite low compared with conventional MFCs. Light intensity was proved to be one of the critical parameters in affecting their performance [16]. Other parameters such as reactor configurations, algal species, and electrode materials should be improved in the near future for targeting high-performance algal photo MFC systems.

4. Conclusion

In this study, an MCC was constructed and evaluated in terms of its power output. The results showed that the MCC was

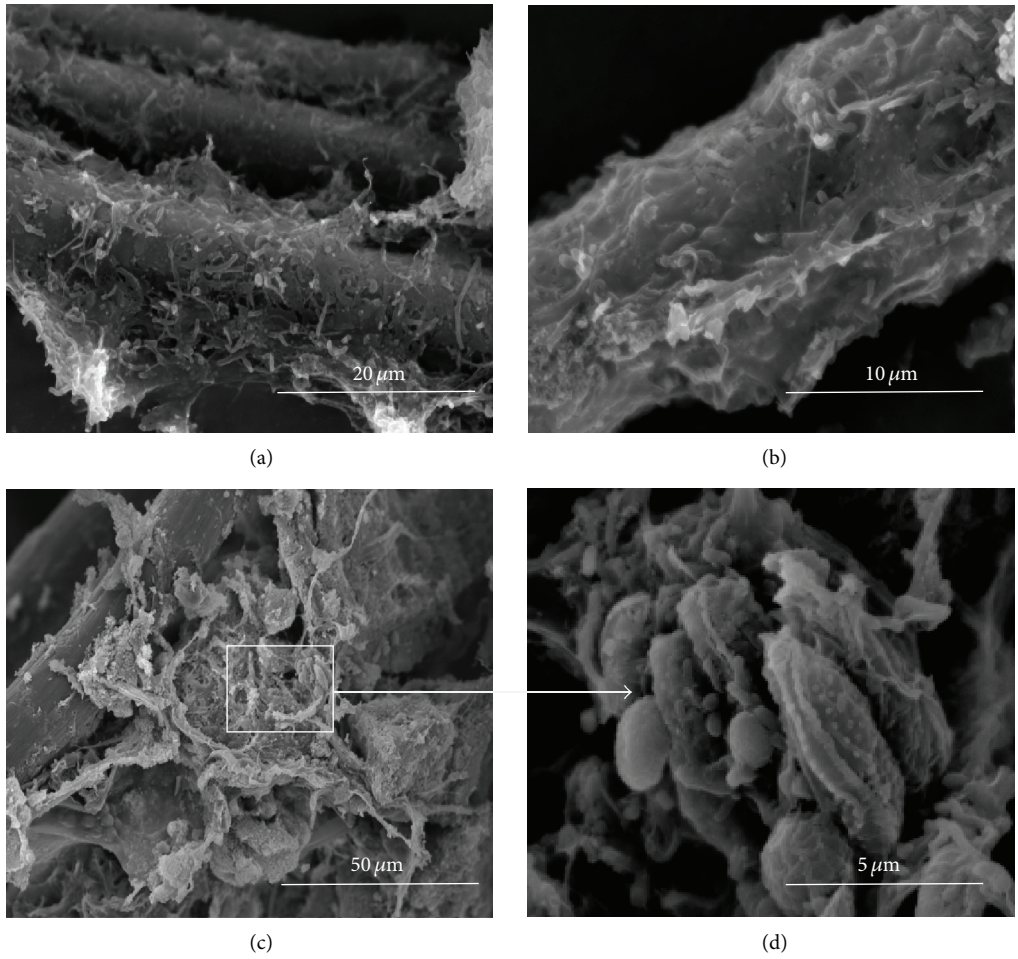

Figure 4: (a) and (b) SEM images of the anode biofilms; (c) and (d) SEM images of the cathode biofilms.

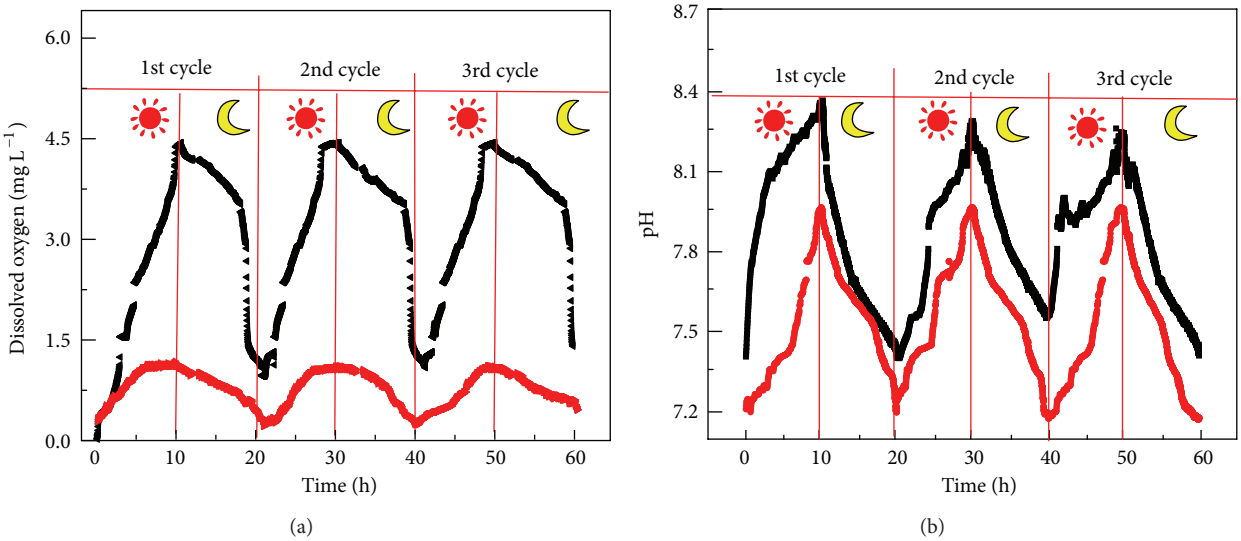

Figure 5: Changes in dissolved oxygen concentration (a) and pH (b) of the cathode electrolyte during illumination and dark circulation. (The symbols of moon and sun represent light and dark conditions, resp.). (Black line: CO_2 was allowed to travel through the tube; red line: CO_2 travel through the silicon tube was blocked.)

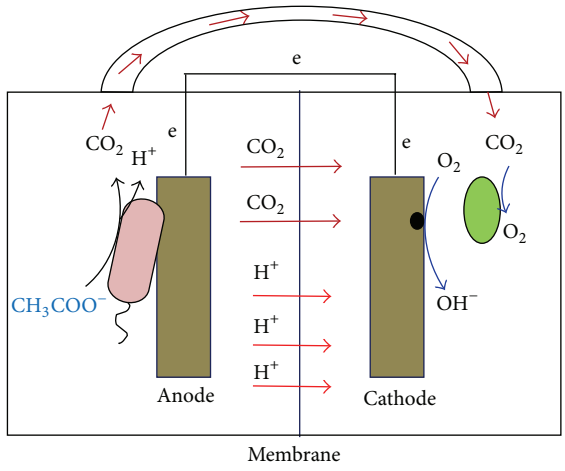

FIGURE 6: Schematic representation of CO_2 transportation and anode and cathode reactions involved.

sensitive to light no matter the anode off gas was piped into the catholyte or not. Oxygen was produced and alkalization occurred in the cathode compartment, suggesting the occurrence of the photosynthetic reaction and oxygen reduction reactions under both conditions. We concluded that the CO_2 crossover through Nafion membrane contributed to the oxygen production when the anode off gas was not piped into the cathode chamber. The results are expected to help further advance the MCC technology.

Conflict of Interests

The authors declare that there is no conflict of interests regarding the publication of this paper.

Acknowledgments

This study was supported jointly by the Guangzhou Science and Technology Development Foundation, China (no. 2011J2200039) and the Cooperation Project in Industry, Education and Research of Guangdong Province, China (no. 2012B091100242).

References

[1] Z. Du, H. Li, and T. Gu, "A state of the art review on microbial fuel cells: a promising technology for wastewater treatment and bioenergy," *Biotechnology Advances*, vol. 25, no. 5, pp. 464–482, 2007.

[2] F. Zhao, R. C. T. Slade, and J. R. Varcoe, "Techniques for the study and development of microbial fuel cells: an electrochemical perspective," *Chemical Society Reviews*, vol. 38, no. 7, pp. 1926–1939, 2009.

[3] B. E. Logan and K. Rabaey, "Conversion of wastes into bioelectricity and chemicals by using microbial electrochemical technologies," *Science*, vol. 337, no. 6095, pp. 686–690, 2012.

[4] B. E. Logan, B. Hamelers, R. Rozendal et al., "Microbial fuel cells: methodology and technology," *Environmental Science and Technology*, vol. 40, no. 17, pp. 5181–5192, 2006.

[5] Z. He, "Microbial fuel cells: Now let us talk about energy," *Environmental Science & Technology*, vol. 47, no. 1, pp. 332–333, 2013.

[6] M. Rosenbaum, Z. He, and L. T. Angenent, "Light energy to bioelectricity: photosynthetic microbial fuel cells," *Current Opinion in Biotechnology*, vol. 21, no. 3, pp. 259–264, 2010.

[7] Y. Zhang, J. S. Noori, and I. Angelidaki, "Simultaneous organic carbon, nutrients removal and energy production in a photomicrobial fuel cell (PFC)," *Energy and Environmental Science*, vol. 4, no. 10, pp. 4340–4346, 2011.

[8] L. Xiao, E. B. Young, J. A. Berges, and Z. He, "Integrated photo-bioelectrochemical system for contaminants removal and bioenergy production," *Environmental Science & Technology*, vol. 46, no. 20, pp. 11459–11466, 2012.

[9] R. Lal, "Sequestration of atmospheric CO_2 in global carbon pools," *Energy and Environmental Science*, vol. 1, no. 1, pp. 86–100, 2008.

[10] G. Venkata Subhash, R. Chandra, and S. Venkata Mohan, "Microalgae mediated bio-electrocatalytic fuel cell facilitates bioelectricity generation through oxygenic photomixotrophic mechanism," *Bioresource Technology*, vol. 136, pp. 644–653, 2013.

[11] D. P. B. T. B. Strik, H. Terlouw, H. V. M. Hamelers, and C. J. N. Buisman, "Renewable sustainable biocatalyzed electricity production in a photosynthetic algal microbial fuel cell (PAMFC)," *Applied Microbiology and Biotechnology*, vol. 81, no. 4, pp. 659–668, 2008.

[12] X. Cao, X. Huang, P. Liang et al., "A completely anoxic microbial fuel cell using a photo-biocathode for cathodic carbon dioxide reduction," *Energy and Environmental Science*, vol. 2, no. 5, pp. 498–501, 2009.

[13] S. Pandit, B. K. Nayak, and D. Das, "Microbial carbon capture cell using cyanobacteria for simultaneous power generation, carbon dioxide sequestration and wastewater treatment," *Bioresource Technology*, vol. 107, pp. 97–102, 2012.

[14] X. Wang, Y. Feng, J. Liu et al., "Sequestration of CO_2 discharged from anode by algal cathode in microbial carbon capture cells (MCCs)," *Biosensors and Bioelectronics*, vol. 25, no. 12, pp. 2639–2643, 2010.

[15] D. R. Lovley and E. J. P. Phillips, "Novel mode of microbial energy metabolism: organic carbon oxidation coupled to dissimilatory reduction of iron or manganese," *Applied & Environmental Microbiology*, vol. 54, no. 6, pp. 1472–1480, 1988.

[16] Y.-C. Wu, Z.-J. Wang, Y. Zheng, Y. Xiao, Z.-H. Yang, and F. Zhao, "Light intensity affects the performance of photo microbial fuel cells with *Desmodesmus* sp. A8 as cathodic microorganism," *Applied Energy*, vol. 116, pp. 86–90, 2014.

[17] S.-E. Oh and B. E. Logan, "Proton exchange membrane and electrode surface areas as factors that affect power generation in microbial fuel cells," *Applied Microbiology and Biotechnology*, vol. 70, no. 2, pp. 162–169, 2006.

[18] K. Raman and J. C.-W. Lan, "Performance and kinetic study of photo microbial fuel cells (PMFCs) with different electrode distances," *Applied Energy*, vol. 100, pp. 100–105, 2012.

[19] L. Gouveia, C. Neves, D. Sebastião, B. P. Nobre, and C. T. Matos, "Effect of light on the production of bioelectricity and added-value microalgae biomass in a photosynthetic alga microbial fuel cell,," *Bioresource Technology*, vol. 154, pp. 171–177, 2014.

[20] Z. He, J. Kan, F. Mansfeld, L. T. Angenent, and K. H. Nealson, "Self-sustained phototrophic microbial fuel cells based on the

synergistic cooperation between photosynthetic microorganisms and heterotrophic bacteria," *Environmental Science and Technology*, vol. 43, no. 5, pp. 1648–1654, 2009.

[21] Y. Liu, F. Harnisch, K. Fricke, R. Sietmann, and U. Schröder, "Improvement of the anodic bioelectrocatalytic activity of mixed culture biofilms by a simple consecutive electrochemical selection procedure," *Biosensors and Bioelectronics*, vol. 24, no. 4, pp. 1006–1011, 2008.

[22] K. P. Katuri, P. Kavanagh, S. Rengaraj, and D. Leech, "Geobacter sulfurreducens biofilms developed under different growth conditions on glassy carbon electrodes: insights using cyclic voltammetry," *Chemical Communications*, vol. 46, no. 26, pp. 4758–4760, 2010.

[23] R. Jiang and D. Chu, "CO_2 crossover through a nafion membrane in a direct methanol fuel cell," *Electrochemical and Solid-State Letters*, vol. 5, no. 7, pp. A156–A159, 2002.

[24] Y. Yuan, S. Zhou, and J. Tang, "In situ investigation of cathode and local biofilm microenvironments reveals important roles of OH^- and oxygen transport in microbial fuel cells," *Environmental Science and Technology*, vol. 47, no. 9, pp. 4911–4917, 2013.

[25] H. Rismani-Yazdi, S. M. Carver, A. D. Christy, and O. H. Tuovinen, "Cathodic limitations in microbial fuel cells: an overview," *Journal of Power Sources*, vol. 180, no. 2, pp. 683–694, 2008.

[26] S. C. Popat, D. Ki, B. E. Rittmann, and C. I. Torres, "Importance of OH^- transport from cathodes in microbial fuel cells," *ChemSusChem*, vol. 5, no. 6, pp. 1071–1079, 2012.

[27] L. Zhuang, S. Zhou, Y. Li, and Y. Yuan, "Enhanced performance of air-cathode two-chamber microbial fuel cells with high-pH anode and low-pH cathode," *Bioresource Technology*, vol. 101, no. 10, pp. 3514–3519, 2010.

Hindawi Publishing Corporation
The Scientific World Journal
Volume 2015, Article ID 597618, 6 pages
http://dx.doi.org/10.1155/2015/597618

Research Article

Microalgae for Bioenergy: Key Technology Nodes

Ywetta Maleterova,[1] Frantisek Kastanek,[1] Milena Rouskova,[1] Martina Matejkova,[1] Petr Kastanek,[2] and Olga Solcova[1]

[1] *Department of Catalysis and Reaction Engineering, Institute of Chemical Process Fundamentals of the ASCR, v.v.i., Rozvojova 135, 16502 Prague 6, Czech Republic*
[2] *Ecofuel Laboratories, s.r.o., Sazavska 721/17, 12000 Prague 2, Czech Republic*

Correspondence should be addressed to Olga Solcova; solcova@icpf.cas.cz

Received 31 July 2014; Accepted 26 November 2014

Academic Editor: A. Abánades

Microalgae have increasingly gained research interest as a source of lipids for biodiesel production. The wet way processing of harvested microalgae was suggested and evaluated with respect to the possible environmental impacts and production costs. This study is focused on the three key steps of the suggested process: flocculation, water recycling, and extraction of lipids. Microalgae strains with high content of lipids were chosen for cultivation and subsequent treatment process. Ammonium hydroxide was tested as the flocculation agent and its efficiency was compared with chitosan. Determined optimal flocculation conditions for ammonium hydroxide enable the water recycling for the recurring microalgae growth, which was verified for the use of 30, 50, and 80% recycled water. For extraction of the wet microalgae hexane, hexane/ethanol and comparative chloroform/methanol systems were applied. The efficiency of hexane/ethanol extraction system was found as comparable with chloroform/methanol system and it seems to be promising owing to its low volatility and toxicity and mainly the low cost.

1. Introduction

Microalgae have been considered as an alternative renewable energy source for biodiesel which could substitute oil from the seed crops. The production of biodiesel from algae has several advantages: high biomass productivity, high content of oil up to 80%, oils with the high lipid content, the need of nonarable lands for their growth, capability of growth in salt water and waste streams, and capability of solar light and CO_2 gas utilizing as nutrients. Therefore, a number of scientists have been reported application of microalgae for biodiesel production [1–4]. Biodiesel produced from microalgae belongs to the third generation of biofuels which overcomes disadvantages of the first (biodiesel produced from palm oil, coconut, sunflower, etc.) and the second (biodiesel produced from *Miscanthus*, *Jatropha*, salmon oil, tobacco seed, etc.) generation of biofuels [5]. Mainly, the microalgal production does not compete for land with food crops [6, 7].

Nevertheless, cost of the microalgal biodiesel production is relatively higher compared to other feedstocks owing to the high energy consuming drying process of harvested microalgae [8]. The most common harvesting methods include sedimentation, centrifugation, filtration, chemical flocculation, and of course drying before the oil extraction [9, 10]. Mechanical press, the use of chemical process, and supercritical extraction rank are among the usually applied extraction techniques. All mentioned processes are energy consuming or could have a negative environmental impact.

From those reasons our work is focused on the new way of the oil production from microalgae. The completely wet treatment, which enables to release the energy consuming drying step, has been studied. The individual key technology nodes have been also evaluated with respect to the possible environmental impacts.

2. Materials and Methods

2.1. Laboratory Cultivation. The applied strain of microalgae, *Chlorella vulgaris* Beijerinck 256, was obtained from the Culture Collection of Autotrophic Organisms (CCALA) of Institute of Botany, ASCR, v.v.i., and contained about 37% of oils. The microalgae were cultivated in the growth

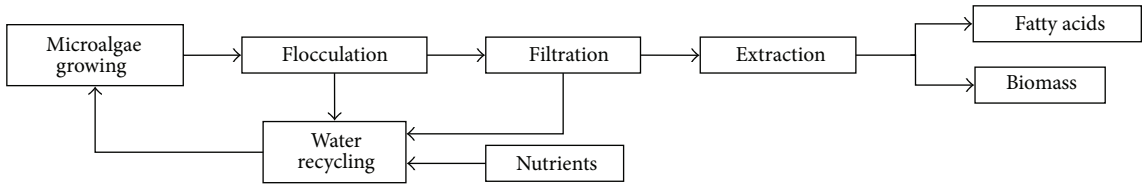

Figure 1: Scheme of the algal treatment with the individual steps.

medium that includes 600 mg/L urea, 1480 mg/L KCl, 988 mg/L $MgSO_4 \cdot 7H_2O$, 340 mg/L KH_2PO_4, 11 mg/L $CaCl_2 \cdot 6H_2O$, 18 mg/L EDTA Fe/Na, 3.09 mg/L H_3BO_4, 1.18 mg/L $MnSO_4 \cdot 4H_2O$, 1.4 mg/L $CoSO_4 \cdot 7H_2O$, 1.43 mg/L $ZnSO_4 \cdot 7H_2O$, 1.4 mg/L $CuSO_4 \cdot 5H_2O$, and 0.88 mg/L $(NH_4)_6Mo_7O_{24} \cdot 4H_2O$ according to the literature [11] with the modification to use urea and KCl instead of KNO_3. The laboratory cultivation units consisted of the glass cylinders (inner diameter 36 mm, height 500 mm), which were placed in a thermostatic bath (29°C) with the continuous illumination by the panel dimmable fluorescent lamps (Philips Master TL-D 36W/840, type warm white) [12] allowing the adjustment of the incident light intensity from 16 to 780 μmol/(m^2s). The cylinders were "aerated" by a mixture of air and CO_2 (2% v/v). Volume of the algal suspension in each cylinder was 300 mL and each cylinder was supplied by gas at a flow rate of 15 L/h. Microalgae were cultivated for 11 days to characterize their growth rates. The microalgal growth in recycling water was tested under continuous illumination with addition of 30, 50, or 80% of recycling water in two (for 80%) or three (for 30 and 50%) consequent experiments.

2.2. Laboratory Flocculation. Chitosan and ammonium hydroxide have been used as flocculation agent. In all experiments the initial concentration of algae varied between 2.70 and 3.25 g/L of dry weight. The algae suspension was placed to graduated cylinders in the amount of 250 mL. To these samples 0.2 to 19 mL of ammonium hydroxide solution (26%) was added to obtain solutions with pH between 8.5 and 10.5. Chitosan diluted in the distilled water was dosed in the amounts 5, 10, 15, and 20 mg/L to obtained pH of value 7. Suspension was intensively agitated for 10 s and in the time intervals 1, 5, 10, 15, and 20 minutes was sampled in the distance of 20 mm below the water level in the graduated cylinder. Samples were analyzed on the photospectrometer SPEKOL 1300 and the optical density (OD) was measured and converted by the calibration curve to the concentration.

2.3. Extraction Experiments. Dry matter in algal suspension was determined before each extraction to assure the exact content of the dry algal biomass in solution (105°C, 7 h to the constant weight). In each experiment, microalgal suspension (containing 10 g dry biomass) was treated by the single-stage extraction with the hexane/ethanol mixture (2/3 v/v) at 1/15 (dw/v) ratio in continuously stirred Erlenmeyer flask for 4 h under inert atmosphere in the absence of light at the ambient temperature. Individual phases (liquid organic extract, water phase, and solid biomass) were separated from the obtained solutions by filtration process on the nutsch. The upper organic phase (extract) was sucked off. The solvent was then removed from the organic phase by rotary evaporation at 40°C after which the total lipid content (extractable part) was determined gravimetrically. An aliquot of the dry extract was taken for the following analysis.

Analysis of fatty acid (FA) profile in the extracts of the tested microalgae was performed at the Department of Food Analysis and Nutrition of the Institute of Chemical Technology Prague. Accredited (ISO 17025) gas chromatographic (GC) method was used. Briefly, following the release of FAs from ester bonds by saponification, their methylation was performed. Target analytes were separated on capillary column and detected by the flame ionization detector (FID). Quantitative determination was carried out by the inner standard technique performed by direct comparison of the addition of the inner standard nonadecane acid (C19:0).

3. Results and Discussion

The whole process of the oil extraction is schematically illustrated in Figure 1, where the schema with individual steps is depicted. Flocculation, water recycling, and extraction belong to the most energy consuming steps and/or could have a negative impact on the environment [10].

3.1. Flocculation. The basic task in the first step of algae suspension treatment past its cultivation is elimination of the major part of water from the algal suspension. Microalgae before harvesting include the really high amount of water. Usually the concentration of algae achieved maximally about 30 g/L of dry weight in dependence of the used growing technology [13]. Therefore, flocculation of algae by coagulants with subsequent separation has been applied to obtain suspension with high concentration of algae.

As a flocculation agent chitosan has been usually used. Nevertheless, to decrease the cost of this operation and enable water recycling the other flocculation agents have been searched and tested [14]. The ammonium hydroxide seems to be the promising coagulant. Application of ammonium hydroxide as the flocculation agent causes the increase of the solution pH value which allows the magnesium hydroxide and/or calcium hydroxide generation.

Hydroxides cover the surface of algae and in combination with neutralization and its adhesion on the cell surface cause formation of heavier flocks which can easily sediment. The ammonium hydroxide seems to be the promising coagulant. Application of ammonium hydroxide as the flocculation agent causes the increase of the solution pH value which allows the magnesium hydroxide and/or calcium hydroxide generation.

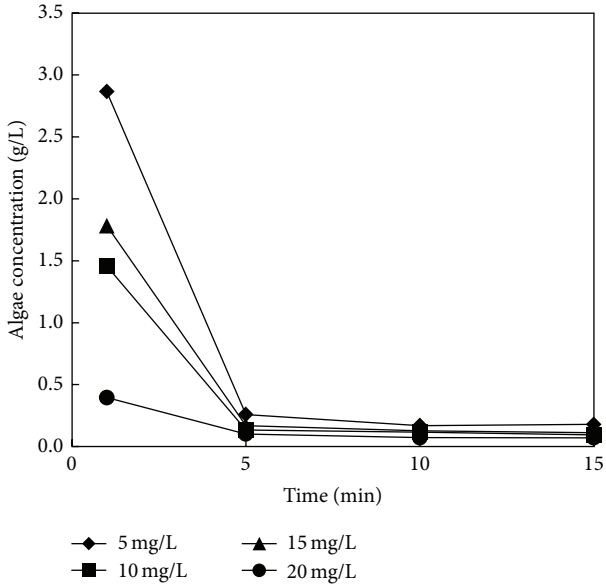

Figure 2: Flocculation by chitosan.

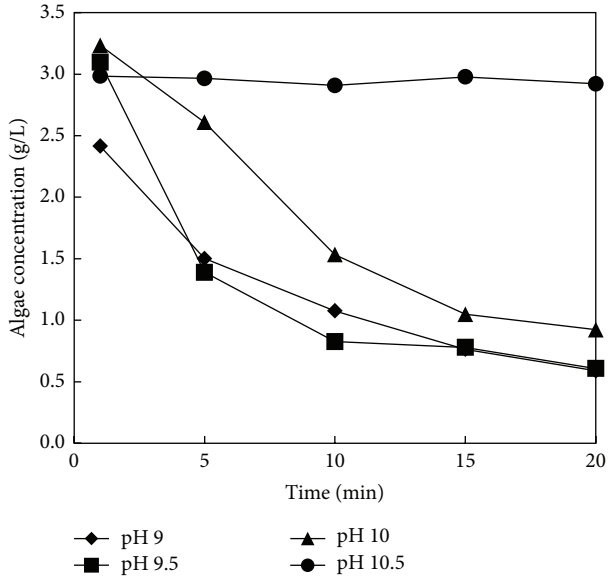

Figure 3: Ammonium hydroxide flocculation.

Rate of flocculation for chitosan and ammonium hydroxide as the flocculation agent is shown in Figures 2 and 3. It can be easily seen that flocculation rate for chitosan depends only slightly on chitosan concentration; see Figure 2. During first 5 minutes the flocculation efficiency of chitosan achieved minimally 95% for the whole range of the tested concentrations (5–20 mg/L). On the contrary, flocculation by ammonium hydroxide significantly depends on pH value of solution and thus on the ammonium hydroxide concentration; see Figure 3. The efficiency about 86% was achieved for pH 9 during 20 minutes. Moreover, the increasing pH value decelerates the flocculation rate and at pH 10.5 the flocculation is completely stopped. For better illustration photos after 20 minutes of flocculation for various agents are shown: Figure 4(a), without flocculation agent; Figure 4(b), ammonium hydroxide at pH 9; and Figure 4(c), chitosan with concentration 5 g/L. Water from both flocculation experiments was decanted and thickened algal solutions were filtrated on the nutsch.

The average efficiency of ammonium hydroxide as the flocculation agent is about 80%; however, it provides the price 3–6 USD per ton of dried biomass while efficiency of chitosan as flocculation agent is higher (95%), but the price per ton of dried biomass is 30–60 USD. Nevertheless, the highest price was estimated for the direct centrifugation of harvesting algae without flocculation step at 60–300 USD per ton of dried biomass.

3.2. Water Recycling. It must be emphasized that ammonium hydroxide not only is the low cost and effective flocculation agent but also brings into the algal water solution only the biogenic elements. This fact is significant for the next step of algal treatment process, the water recycling.

The influence of recycling water was tested on the cultivation growth curve of *Chlorella vulgaris 256* with 50 and 80% of recycled water. In Figure 5 the original cultivation growth

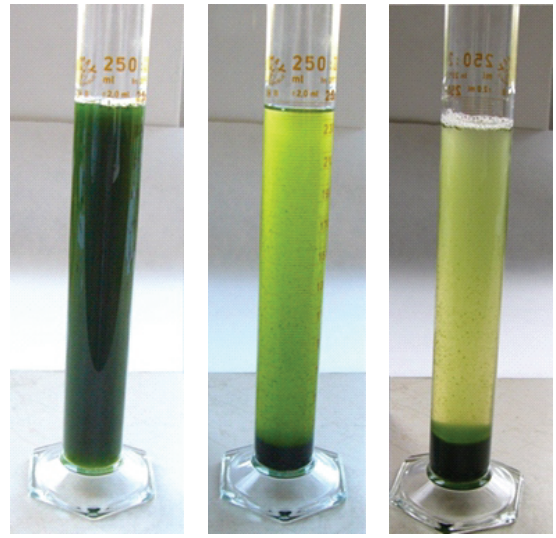

Figure 4: (a) Without any flocculation agent, 0 min; (b) with NH_4OH, pH 9, after 20 min; (c) with chitosan 5 g/L, after 20 min.

curves (line) are compared with the repeated growth curves in water with addition of 50 and 80% of recycled water. It can be seen that utilization of the recycled water has no influence on the growth curves of algae. It is the important fact to the process economy and also to the environmental impact, since during the microalgae treatment the huge amount of water is produced.

3.3. Extraction. One of the crucial key process nodes of the energy production from harvesting algae is the extraction step. Usually, extraction of dry algal biomass of algae has been performed [15–17]; however this work is focused on wet way extraction. It can bring the significantly lower energy

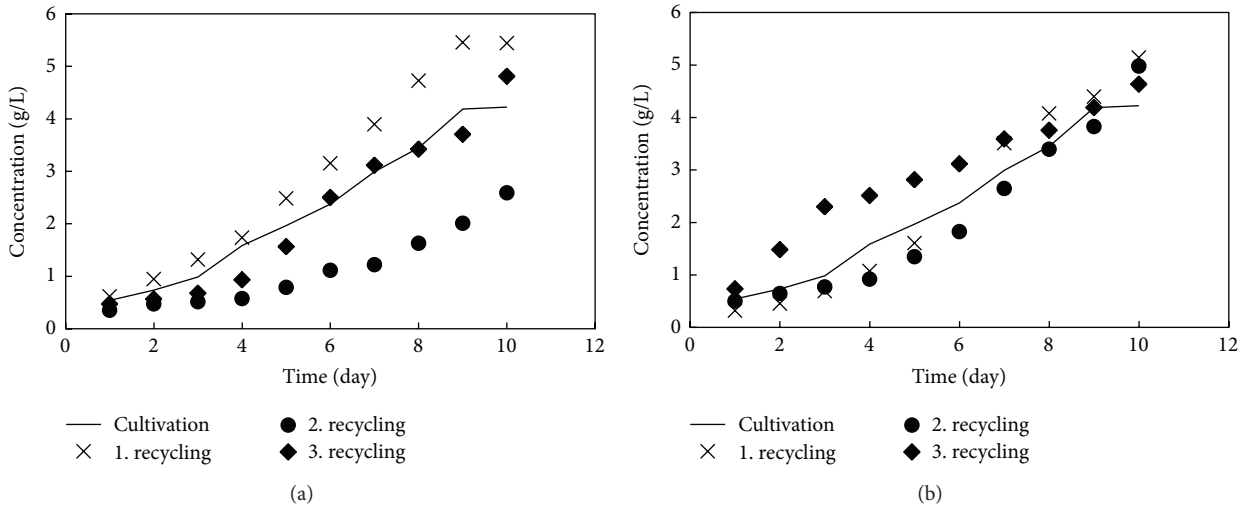

Figure 5: Cultivation growth curve with recycling water: 50 and 80%.

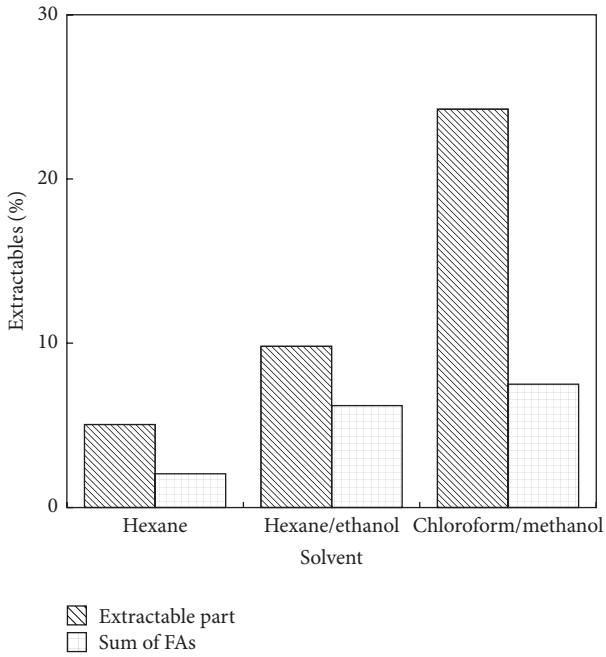

Figure 6: The effect of solvent mixture composition on lipid (extractable part) and sum of FAs content related to dry matter.

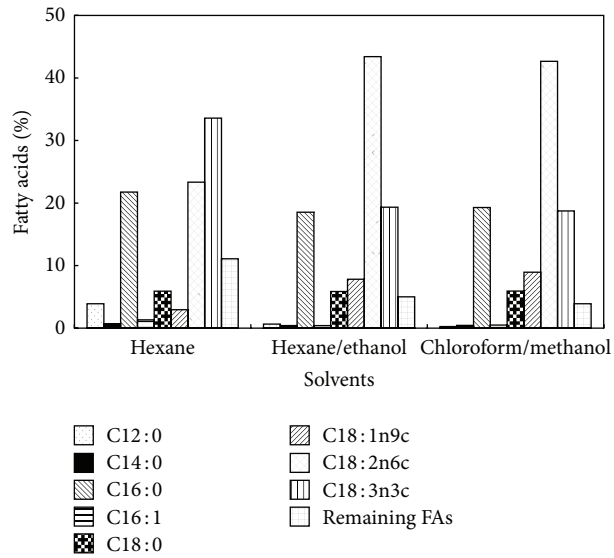

Figure 7: The effect of solvent mixture composition on the profile of fatty acids.

cost and no degradation of valuable fatty acids during the extraction process. Data about the wet extraction process appear only rarely in the literature. Halim et al. [18] obtained the comparable lipid yields by hexane extraction from either dried microalgal powder or wet microalgal paste.

Hexane is often recommended for extraction of the lipid fraction from microalgae. Its advantage is the chemical stability, almost nonsolubility in water, and relatively low boiling point, which is favourable for separation/regeneration.

Generally, hydrocarbons require the use of the other solvents as deemulsifiers to prevent formation of foams and stable emulsions, that is, reduction of interfacial tension. Therefore, ethanol was added to the extraction system due to its relatively low boiling points and favourable regeneration from water phase. For determination of the total lipid content the solvent system of chloroform/methanol mixture has been applied by Bligh and Dyer [19]. This method was primarily developed for determination of lipids in the cod muscle. Therefore, it possesses some limitation for samples of plant/algae origin which contains pigments and the other soluble substances. This solvent system significantly increases the proportion of extractables and its toxicity is not environmental friendly as well. Nevertheless, Bligh and Dyer [19] method has been usually applied as a comparative procedure.

First, the effect of solvent polarity on the extractable part and the total fatty acids in fresh microalgae was tested in this study (Figure 6). Maximal extractable part was obtained by chloroform/methanol system (24.3%) which contains except lipids the other soluble components, for example, pigments.

It can be clearly seen that hexane/ethanol system provides the same amount of the extraction fraction of the total lipids (FAs) as system chloroform/methanol. Figure 7 shows that also profiles of FAs are comparable for both systems. Thus, hexane/ethanol mixture, which is the environmental friendly solvent system, was proved to be a suitable alternative for extraction of lipids/FAs. This system possesses relatively high extraction capacity, low volatility and toxicity for humans as well as environment, and moreover the low cost. The highest proportional content of fatty acids in the lipid fraction was included by hexane/ethanol mixture (63.2%).

Pure hexane showed the lowest extraction capacity for total extractables and extracted 40.6% FAs in the lipid fraction.

These experiments confirmed the conclusion of Halim et al. [18] that efficiency of the microalgal extraction by the wet way is comparable with the dry way and with addition of ethanol it provides the same lipid yields. Moreover, profiles of FA are not affected by presence of water in extracted biomass. It influences only the amount of extraction solvent related to dry microalgae. Hexane/ethanol extraction system enables the subsequent utilization of the residual biomass, for example, as the poultry feed supplement.

4. Conclusions

The three key steps, flocculation, water recycling, and extraction of microalgal treatment for lipid production, have been suggested and evaluated with respect to the possible environmental impacts and production costs. To avoid the energy consuming drying step the completely wet way treatment has been applied. It was verified that ammonium hydroxide can serve as the efficient and the low cost flocculation agent. The optimal flocculation conditions were determined at pH 9. Moreover the application of ammonium hydroxide brings into the algal water solution only the biogenic elements and thus enables the water recycling for the recurring microalgae growth. Water recycling was verified for the use of 50 and 80% recycled water.

It was confirmed that extraction of the wet microalgae can be applied instead of the dry microalgal extraction, which enables to release the energy consuming drying step. The efficiency of hexane/ethanol extraction system was found as comparable with chloroform/methanol system: the comparative method. Moreover, not only the amount of the extraction fraction of the total lipids but also the profiles of fatty acids were the same. Except of the relatively high extraction capacity, hexane/ethanol extraction system possesses the low volatility and toxicity for humans as well as environment and mainly the low cost.

The wet way processing of the harvested microalgae for biodiesel production seems to be the low cost promising biotechnological application with the minimal environmental impact.

Conflict of Interests

The authors declare that there is no conflict of interests regarding the publication of this paper.

Acknowledgment

The financial support of Ministry of Education, program GESHER/MOST, Grant no. LJ12002 is gratefully acknowledged.

References

[1] L. Rodolfi, G. C. Zittelli, N. Bassi et al., "Microalgae for oil: strain selection, induction of lipid synthesis and outdoor mass cultivation in a low-cost photobioreactor," *Biotechnology and Bioengineering*, vol. 102, no. 1, pp. 100–112, 2009.

[2] Y. Chisti, "Biodiesel from microalgae," *Biotechnology Advances*, vol. 25, no. 3, pp. 294–306, 2007.

[3] P. M. Schenk, S. R. T. Hall, E. Stephens et al., "Second generation biofuels: high-efficiency microalgae for biodiesel production," *BioEnergy Research*, vol. 1, no. 1, pp. 20–43, 2008.

[4] Q. Hu, M. Sommerfeld, E. Jarvis et al., "Microalgal triacylglycerols as feedstocks for biofuel production: perspectives and advances," *Plant Journal*, vol. 54, no. 4, pp. 621–639, 2008.

[5] F. Alam, A. Date, R. Rasjidin, S. Mobin, H. Moria, and A. Baqui, "Biofuel from algae—is it a viable alternative?" *Procedia Engineering*, vol. 49, pp. 221–227, 2012.

[6] J. Jakóbiec and M. Wądrzyk, "Microalgae as a potential source for biodiesel production," *Agricultural Engineering*, vol. 6, no. 124, pp. 51–56, 2010.

[7] K. K. Sharma, H. Schuhmann, and P. M. Schenk, "High lipid induction in microalgae for biodiesel production," *Energies*, vol. 5, no. 5, pp. 1532–1553, 2012.

[8] A. Y. A. Saifullah, Md. A. Karim, and A. Ahmad-Yazid, "Microalgae: an alternative source of renewable energy," *American Journal of Engineering Research*, vol. 3, no. 3, pp. 330–338, 2014.

[9] E. Molina Grima, E.-H. Belarbi, F. G. Acién Fernández, A. Robles Medina, and Y. Chisti, "Recovery of microalgal biomass and metabolites: process options and economics," *Biotechnology Advances*, vol. 20, no. 7-8, pp. 491–515, 2003.

[10] S. Rajvanshi and M. Pal Sharma, "Microalgae: a potential source of biodiesel," *Journal of Sustainable Bioenergy Systems*, vol. 2, no. 3, pp. 49–59, 2012.

[11] V. Zachleder and I. Setlík, "Effect of irradiance on the course of RNA synthesis in the cell cycle of *Scenedesmus quadricauda*," *Biologia Plantarum*, vol. 24, no. 5, pp. 341–353, 1982.

[12] J. Degen, A. Uebele, A. Retze, U. Schmid-Staiger, and W. Trösch, "A novel airlift photobioreactor with baffles for improved light utilization through the flashing light effect," *Journal of Biotechnology*, vol. 92, no. 2, pp. 89–94, 2001.

[13] G. Dragone, B. Fernandes, A. A. Vicente, and J. A. Teixeira, "Third generation biofuels from microalgae," in *Current Research, Technology and Education Topics in Applied Microbiology and Microbial Biotechnology*, vol. 2, pp. 1355–1366, Formatex Research Center, 2010.

[14] M. Shilo and M. Shilo, "Conditions which determine the efficiency of ammonium sulphate in the control of *Prymnesium parvum* in fish breeding ponds," *Applied Microbiology*, vol. 1, pp. 330–333, 1953.

[15] B. D. Wahlen, R. M. Willis, and L. C. Seefeldt, "Biodiesel production by simultaneous extraction and conversion of total lipids from microalgae, cyanobacteria, and wild mixed-cultures," *Bioresource Technology*, vol. 102, no. 3, pp. 2724–2730, 2011.

[16] M. Cooney, G. Young, and N. Nagle, "Extraction of bio-oils from microalgae," *Separation and Purification Reviews*, vol. 38, no. 4, pp. 291–325, 2009.

[17] M. G. M. D'oca, C. V. Viêgas, J. S. Lemões et al., "Production of FAMEs from several microalgal lipidic extracts and direct transesterification of the *Chlorella pyrenoidosa*," *Biomass and Bioenergy*, vol. 35, no. 4, pp. 1533–1538, 2011.

[18] R. Halim, B. Gladman, M. K. Danquah, and P. A. Webley, "Oil extraction from microalgae for biodiesel production," *Bioresource Technology*, vol. 102, no. 1, pp. 178–185, 2011.

[19] E. G. Bligh and W. J. Dyer, "A rapid method of total lipid extraction and purification," *Canadian Journal of Biochemistry and Physiology*, vol. 37, no. 8, pp. 911–917, 1959.

Hindawi Publishing Corporation
The Scientific World Journal
Volume 2015, Article ID 920968, 9 pages
http://dx.doi.org/10.1155/2015/920968

Research Article

Life Cycle Analysis on Fossil Energy Ratio of Algal Biodiesel: Effects of Nitrogen Deficiency and Oil Extraction Technology

Hou Jian,[1,2] Yang Jing,[2] and Zhang Peidong[3]

[1]*South China Green Design R&D Center, China Quality Certification Center Guangzhou Branch, Guangzhou, Guangdong 510620, China*
[2]*Qingdao Institute of Bioenergy and Bioprocess Technology, Chinese Academy of Sciences, Qingdao, Shandong 266101, China*
[3]*Qingdao University of Science & Technology, Qingdao, Shandong 266042, China*

Correspondence should be addressed to Hou Jian; houjian@qibebt.ac.cn

Received 29 July 2014; Accepted 4 November 2014

Academic Editor: Shun-Gui Zhou

Life cycle assessment (LCA) has been widely used to analyze various pathways of biofuel preparation from "cradle to grave." Effects of nitrogen supply for algae cultivation and technology of algal oil extraction on life cycle fossil energy ratio of biodiesel are assessed in this study. Life cycle fossil energy ratio of *Chlorella vulgaris* based biodiesel is improved by growing algae under nitrogen-limited conditions, while the life cycle fossil energy ratio of biodiesel production from *Phaeodactylum tricornutum* grown with nitrogen deprivation decreases. Compared to extraction of oil from dried algae, extraction of lipid from wet algae with subcritical cosolvents achieves a 43.83% improvement in fossil energy ratio of algal biodiesel when oilcake drying is not considered. The outcome for sensitivity analysis indicates that the algal oil conversion rate and energy content of algae are found to have the greatest effects on the LCA results of algal biodiesel production, followed by utilization ratio of algal residue, energy demand for algae drying, capacity of water mixing, and productivity of algae.

1. Introduction

With the rapid growth of economy and energy consumption, petroleum resources are gradually depleted and environmental pollution is increasingly serious. It has become emergent to search for alternative energy especially in the field of traffic and to mitigate the environmental problems caused by fossil energy production and using. Biomass energy has the characteristics of renewable raw material and biological carbon sequestration. Development of bioenergy is considered as an effective way to solve energy shortage and improve environment.

Changes of land use and increased emission of greenhouse gases can be caused by production of transportation biofuels from terrestrial energy plants [1]. Using algae as a feedstock for biofuels has led to much excitement and initiative. Although algae based fuels are widely considered as clean energy, fossil energy input during production of biofuels from algae may still aggravate depletion of nonrenewable resources and pollution of environment [2]. It is very necessary to estimate the ratio of energy output to fossil energy consumption (fossil energy ratio) of algal biodiesel based on the concept of life cycle analysis.

Currently, several studies of life cycle analysis on algal biofuels have been carried out. Frank et al. [3], Yang et al. [4], and Clarens et al. [5, 6] have shown that fertilizer input contributes a lot to the overall life cycle fossil energy consumption and global warming of algal biofuel. Sander and Murthy [7] have shown that extraction of oil from dried algae results in high life cycle fossil energy input. With the increasing researches on mass culture of algae and algal oil extraction, several studies have assessed the life cycle fossil energy ratio of algal biofuels produced by new technologies. Life cycle assessment results of Lardon et al. [8] on algal biodiesel produced from *Chlorella vulgaris* with different nitrogen (N) supplies have shown that life cycle fossil energy ratio can be improved when algae grow under low N condition. Some researches show that the productivities, constituents, and calorific values

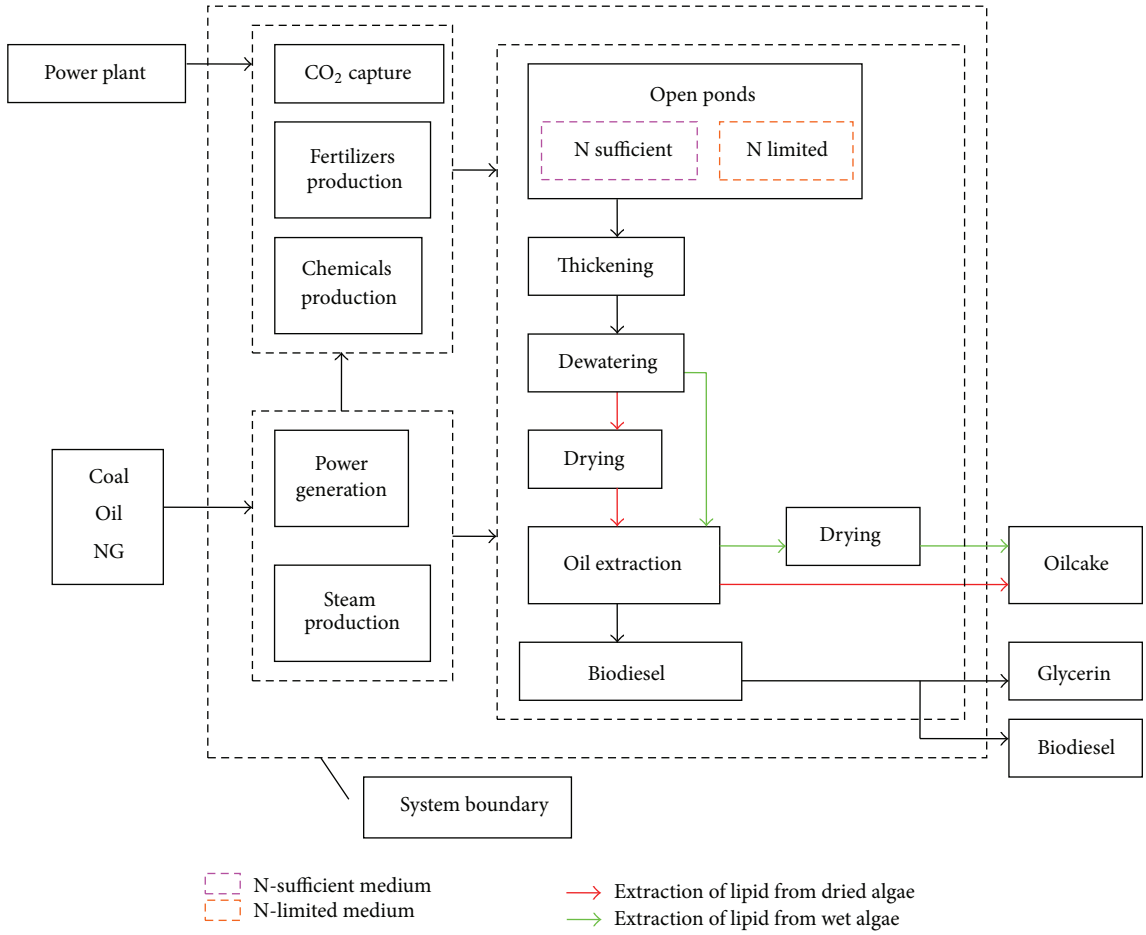

Figure 1: Life cycle system of biodiesel production from algae.

of different algae species may present different changing tendency when the N supply reduces [9–11]. Therefore, in order to identify whether life cycle fossil energy ratio of algal biodiesel can be promoted by low N condition, energy analysis of biodiesel based on different algae species should be carried out. Batan et al. [12] and Brentner et al. [13] compared the life cycle fossil energy use of algal biodiesel by extraction of oil from dried and wet algae. However, the energy consumption for extraction of oil from wet algae is hypothetical data, and reliability of the assessment results remains unknown.

It is thus clear that the existing LCA studies on algal biofuels contain several problems and this results in the fact that life cycle fossil energy ratio of algal biofuel cannot be scientifically identified based on the present research status. To fill up the deficiency above, with algal biodiesel as the objective of our study, we investigate the cell compositions and productivities of *Phaeodactylum tricornutum* and *Chlorella vulgaris* grown with sufficient and limited nitrogen supply. Studies on lipid extraction from wet algae may mainly concern extraction yields of algal oil but often neglect energy required for lipid extraction [14]. In this study, energy demands for extraction of oil from wet algae of pilot production are monitored. Effects of nitrogen supply conditions and algal oil extraction technologies on life cycle fossil energy ratio of algal biodiesel are assessed. To verify the reliability of our study, our results are compared with energy balance of other similar LCA studies on algal biofuel. A sensitivity analysis is performed to identify key parameters affecting life cycle fossil energy ratio of algal biodiesel.

2. Methodologies

2.1. Functional Unit. The functional unit for the LCA in this study is 1 MJ biodiesel produced.

2.2. Life Cycle System Boundary of Algal Biodiesel. Figure 1 shows the simulated life cycle system of algal biodiesel production in this study. Algae are grown in open ponds with sufficient or limited nitrogen supply. 50% of the normal nitrogen supply is used in the N-limited medium. Algae harvesting includes steps of concentration, dewatering, and drying [15]. The content of algal biomass in the fluid from cultivation ponds is lower than 5 wt%. Concentration reduces the water content of the algal biomass from 99 wt% to 95 wt%. Dewatering is needed to further decrease the water content to 60 wt%–80 wt%. Algae have to be dried up to a 90 wt% solid content if the same technology as soybean lipid extraction is applied to extraction of oil from algae.

Chen et al. [16] designed the extraction of oil from wet algae biomass with about 30 wt% solids. Biodiesel is obtained through transesterification reaction of algal lipid and methanol.

2.3. Evaluation Model for Life Cycle Energy Efficiency of Algal Biodiesel

2.3.1. Life Cycle Primary Energy Consumption Calculation. When 1 MJ biodiesel is produced, the life cycle primary fossil energy demand (EC_{LC}) is calculated as the sum of all the primary fossil energy consumptions due to production of all the process energy and materials directly used in all the substages according to the GREET model [17]:

$$EC_{LC} = \sum_i \sum_j EE_{i,j} \times PE_j + \sum_i \sum_n M_{i,n} \times PE_n, \quad (1)$$

where $EE_{i,j}$ is the process energy j consumption during substage i (MJ); PE_j is the life cycle primary fossil energy use for process energy j production (MJ/MJ); $M_{i,n}$ is the material n consumption during substage i (kg); PE_n is the life cycle primary fossil energy use for material n production (kg/MJ).

During algae cultivation, the power demand for mixing (EE_{mixing}) is computed using

$$EE_{mixing} = \frac{M_{algae} \times W_{mixing} \times t_w \times t_r}{C} = \frac{M_{algae} \times W_{mixing} \times t_w}{Y_V}, \quad (2)$$

where M_{algae} is the algae consumption to produce 1 MJ biodiesel (kg); W_{mixing} is the mixing capacity (W/m^3); t_w is the working hours of mixing equipment per day (h/d); t_r is the retention time of algae (d); C is the algal biomass concentration (kg/m^3); Y_V is the volumetric productivity (kg/m^3·d).

The M_{algae} and Y_V are calculated using the following equations, respectively:

$$M_{algae} = \frac{1}{HV_{biodiesel} \times \eta_{ester} \times \eta_{extra} \times \eta_{harve} \times P_{algae,oil} \times P_{nuetr\,oil}}, \quad (3)$$

$$Y_V = Y_A \times \frac{A}{V}, \quad (4)$$

where $HV_{biodiesel}$ is the net caloric value of biodiesel (MJ/kg); η_{harve}, η_{extra}, and η_{ester} are the efficiencies of algae harvesting, algal oil extraction, and esterification, respectively (%); $P_{algae,oil}$ is the total oil content of algae (%); $P_{nuetr\,oil}$ is the percentage of neutral oil in total oil (%); Y_A is the areal productivity (kg/m^2·d); A/V is the ratio of illuminated area to volume (m^{-1}).

Power consumption for pumping ($EE_{pumping}$) is calculated using

$$EE_{pumping} = \frac{M_{algae} \times \rho_{water} \times g \times H}{C \times \eta_{pump}} \times \left(1 + \lambda_{water,evap} + \lambda_{lose}\right), \quad (5)$$

where ρ_{water} is the density of water (kg/m^3); g is the force of gravity (N/kg); H is the liquid head (m); η_{pump} is the pumping efficiency (%); $\lambda_{water,evap}$ and $\lambda_{water,lose}$ are water evaporation rate and water delivering loss rate, respectively (%).

When 1 MJ biodiesel is produced, consumptions of CO_2 (M_{CO_2}) and fertilizer ($M_{fertili}$) are calculated by using the following equations, respectively:

$$M_{CO_2} = \frac{M_{algae} \times P_{algae,C} \times 44/12}{\eta_{fixing}}, \quad (6)$$

$$M_{ferti} = M_{algae} \times P_{algae,N(P)} \times \left(\lambda_{N(P),evap} + \eta_{harve}\right), \quad (7)$$

where $P_{algae,C}$ is the carbon content of algae (%); η_{fixing} is the CO_2 fixing efficiency of algae (%); $P_{algae,N(P)}$ is the nitrogen or phosphorus content of algae (%); $\lambda_{N(P),evap}$ is the nitrogen or phosphorus evaporation rate (%).

2.3.2. Life Cycle Energy Output Calculation. The life cycle energy outputs are calculated based on the energy released from combustion of biodiesel, oilcake, and glycerin [8, 18]:

$$EP_{biodiesel} = 1, \quad (8)$$

$$EP_{oilcake} = M_{algae} \times HV_{algae} - \frac{1}{\eta_{esterification}}, \quad (9)$$

$$EP_{glycerin} = M_{glycerin} \times HV_{glycerin}, \quad (10)$$

where $EP_{biodiesel}$, $EP_{oilcake}$, and $EP_{glycerin}$ are the energy released from biodiesel, oilcake, and glycerin combustion, respectively (MJ); HV_{algae} is the net caloric value of algae (MJ/kg); $M_{glycerin}$ is the glycerin output when 1 MJ biodiesel is produced (kg); $HV_{glycerin}$ is the net caloric value of glycerin (MJ/kg).

HV_{algae} is calculated as

$$HV_{algae} = \sum_i P_{algae,n} \times HV_n, \quad (11)$$

where $P_{algae,n}$ is the percentage of ingredient n in algae (%); HV_n is the net caloric value of ingredient n (MJ/kg).

2.3.3. Life Cycle Fossil Energy Ratio Calculation. The life cycle fossil energy ratio of biodiesel production (η_{fossil}) is the ratio of the life cycle energy output to the life cycle primary fossil energy consumption:

$$\eta_{fossil} = \frac{\sum_m EP_m}{\sum_i EC_i} \times 100\%, \quad (12)$$

where EP_m is the energy output m (MJ); EC_i is the primary energy consumption in substage i (MJ).

Table 1: Productivity and cell composition of algae grown under N-sufficient and N-limited conditions.

Strains	Normal N supply				Limited N supply (50% of normal N supply)			
	Protein/%	Carbonhydrate/%	Lipid/%	Productivity/ $g/m^2 \cdot d$	Protein/%	Carbonhydrate/%	Lipid/%	Productivity/ $g/m^2 \cdot d$
Phaeodactylum tricornutum[b]	32.2	18.5	28.46	25	24.76	16.7	31.8	15.45
Chlorella vulgaris[c]	31	51	18	22	6	54	40	19.85

[b]Source: [9, 21]. [c]Source: [11, 22].

Table 2: CO_2 fixing efficiencies of different algae species.

	Phaeodactylum tricornutum	*Chlorella vulgaris*
CO_2 fixing efficiency/%	64.9[f]	60[g]

[f]Source: [23]. [g]Source: [24].

3. Data Collection

Under conditions with sufficient and limited nitrogen supply, the algal productivities and cell compositions of *Phaeodactylum tricornutum* and *Chlorella vulgaris* grown in open ponds are shown in Table 1. The chemical formulas and net caloric values of carbonhydrate, protein, and lipid are according to Lardon et al. [8]. Phosphorus content of algae is 1 wt% [19]. Algae concentration is 0.5 g/L and pond height is 0.2 m. According to Fagerstone et al. [20], when algae are cultivated in open ponds, the cumulative N_2O emissions over the light and dark periods are 1.53×10^{-5} kg and 6.51×10^{-6} kg per kg N input, respectively. When the concentration of CO_2 injected to algae cultivation ponds is 5%, CO_2 fixing efficiencies of different algae species have been shown in Table 2.

According to the base data in Tables 1 and 2 and formulas of (6) and (9), the calculated nitrogen fertilizer inputs and heat values of algae under conditions of normal and limited N supply are shown in Table 3. As Tables 1 and 3 show, under low N condition, lipid content of *Chlorella vulgaris* increases and algae productivity drops; nitrogen fertilizer and heat value of *Phaeodactylum tricornutum* both decrease.

Operation capacity of paddle wheel and aeration in open ponds is 3.72 W/m^3 [25]. It is assumed that working time of mixing equipment is 12 h per day. Average delivery head of centrifugal pump is 7.5 m with efficiency of 70% [15]. Water evaporation rate during algae cultivation is 10% [6] and water delivering loss is 5% [3].

Energy consumed in algae harvesting is from literature [26]. Dissolved air flotation is used for algae concentration with an electricity requirement of 100 kWh/t dry mass. The electricity demand of centrifuge for algae dewatering is 37 kWh/t dry mass. The energy demand for thermal drying of algae to 10% water content is 615.6 kWh/t dry mass. 10 wt% and 5 wt% of the algal cells are lost in concentration and dewatering, respectively [27].

Energy demands for extraction of oil from dried and wet algae are listed in Table 4. It is assumed that the percentage of neutral lipid in total lipid of algae is 80%. Energy requirements for oil refining are according to literature [28]. Energy consumptions in oil conversion stage are from literature [29]; the conversion efficiency is 96.5% and the net calorific value of biodiesel is 37.2 MJ/kg.

It is assumed that electricity and steam consumed in the assessed system are generated from coal in China. The fertilizers and chemicals are produced using technologies on world average level and the energy demands for fertilizers and chemicals production are from Gabi database [31]. CO_2 applied to algae growth is assumed to be from flue gas discharged from power plant. Flue gas from power or steel plant generally contains substances like sulfur oxide, nitric oxide, and heavy metals which are deleterious to algae growth. CO_2 needs to be separated from the flue gas before it is injected into algae cultivation ponds. Membrane separation of CO_2 is used with steam demands of 73 kWh per ton of recovered CO_2 and a capture efficiency of 85% [32]. CO_2 capture not only provides nutrients for algae growth but also has been required in most coal-fired power stations. Energy demands for carbon capture are allocated between the power plant and the algae farm on an energy basis.

4. Results

4.1. Energy Efficiency Comparison Analysis of Biodiesel Production from Algae Grown with Normal and Limited Nitrogen Supply. With open ponds cultivation of algae, chemical absorption of CO_2, and extraction of oil from dried algae, the calculated life cycle energy production and fossil energy consumed for *Phaeodactylum tricornutum* and *Chlorella vulgaris* based biodiesel with different nitrogen supplies are shown in Figures 2 and 4, and life cycle fossil energy ratios are shown in Figures 3 and 5.

It can be seen from Figure 2 that, under limited nitrogen supply condition, fossil energy consumption for harvesting and oil extraction of *Phaeodactylum tricornutum* and energy production of algae biomass all decrease. This is mainly due to the fact that oil content of *Phaeodactylum tricornutum* increases under low N condition and less algae input for 1 functional unit of biodiesel production is required. However, for the productivity and heat value of *Phaeodactylum tricornutum* both decrease under low N condition, the decline rate of energy production of algal biomass (11.06%) is higher than that of the energy required in algae harvesting and oil extraction (10.64%), and energy consumption for mixing

Table 3: Net calorific values of algae and N fertilizer inputs.

Species of algae	Heat values and nitrogen contents	Normal N	Low N
Phaeodactylum tricornutum	Heat value (MJ/kg)	18.3	18.19
	N content (kg/kg)	0.052	0.040
Chlorella vulgaris	Heat value (MJ/kg)	18.33	23.27
	N content (kg/kg)	0.050	0.010

Table 4: Energy consumptions and efficiency for algal oil extraction.

	Extraction from dried algae[i]	Extraction from wet algae[j]
Power (kWh/t algae)	25	26.46
Steam (MJ/t algae)	1170.8	1239.01
Efficiency (%)	97.5	90

[i]The energy demands for extraction of oil from dried algae are from SEPA (State Environmental Protection Administration of China) of China [30].
[j]The energy demands for extraction of oil wet algae are based on a pilot-scale operation of algal oil extraction plant in China.

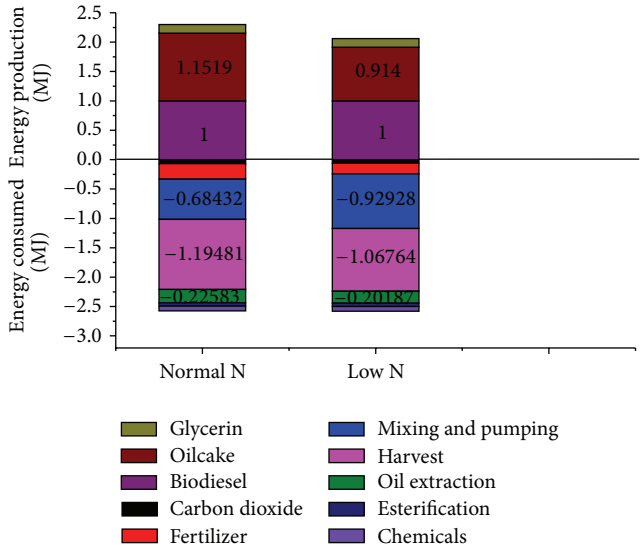

Figure 2: *Phaeodactylum tricornutum*. Energy losses and gains for the production of biodiesel from *Phaeodactylum tricornutum* grown in N-sufficient and N-limited mediums.

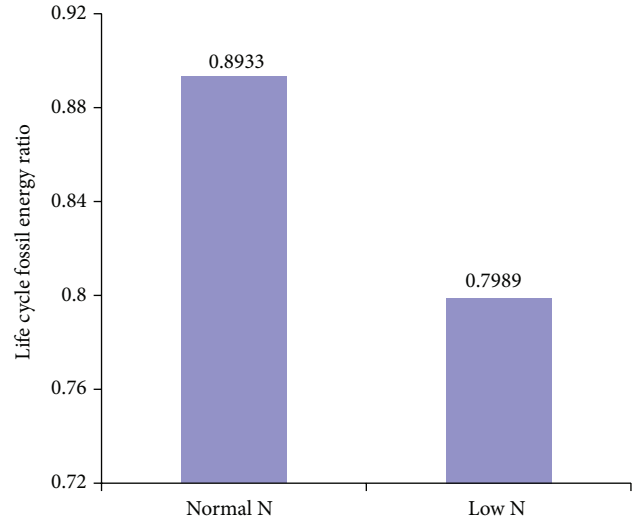

Figure 3: Life cycle fossil energy ratio for the production of biodiesel from *Phaeodactylum tricornutum* grown in normal and limited nitrogen supply conditions.

of cultivation water increases by 35.8%. As a result, life cycle fossil energy ratio for *Phaeodactylum tricornutum* based biodiesel with limited nitrogen supply decreases by 10.56% compared with normal nitrogen supply (Figure 3).

As can be seen from Figure 4, under limited nitrogen supply condition, energy consumption for harvesting and oil extraction of *Chlorella vulgaris* decreases by 54.85% because of higher lipid content compared to normal nitrogen supply. Due to the heat value of *Chlorella vulgaris* increase under low N condition, the total energy production of biodiesel and oilcake only decreased by 14.09%. As a result, life cycle fossil energy ratio for *Chlorella vulgaris* based biodiesel under limited nitrogen supply increases by 30.78% compared with normal nitrogen supply (Figure 5).

4.2. Energy Efficiency Comparison Analysis of Biodiesel Production from Oil Extracted from Dried and Wet Algae. The calculated life cycle energy outputs and fossil energy consumed for algal biodiesel produced from *Chlorella vulgaris* under low N condition in open ponds, with CO_2 from membrane separation, and oil extracted from dried and wet algae are shown in Figure 6, and life cycle fossil energy ratios are shown in Figure 7.

As can be seen from Figure 6, compared to extraction of oil from dried algae, the energy consumed for extraction of oil from wet algae with subcritical cosolvents increases by 14.79% compared to extraction of oil from dried algae, and energy required for mixing increases by 8.1%. This is mainly due to the fact that efficiency for oil extraction from wet algae is lower than from dried algae and more algae input for 1 functional unit of biodiesel production is required. However, algae drying process omitted makes lipid extraction from wet algae perform a 43.83% improvement in the life cycle fossil energy ratio of algal biodiesel compared to extraction of oil from dried algae (Figure 7).

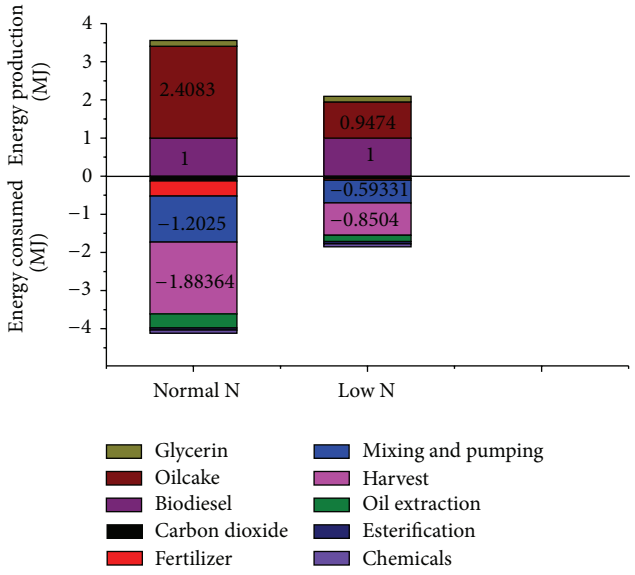

Figure 4: *Chlorella vulgaris*. Energy losses and gains for the production of biodiesel from *Chlorella vulgaris* grown in N-sufficient and N-limited mediums.

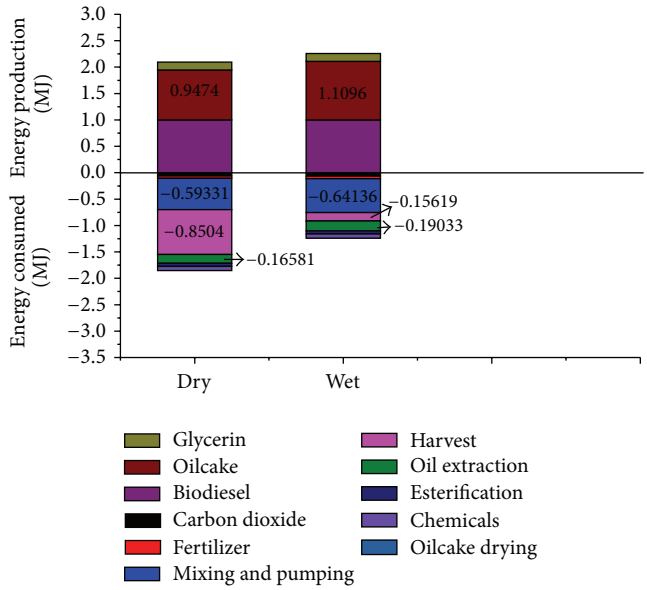

Figure 6: Energy input and output of biodiesel production using oil extracted from dried and wet algae.

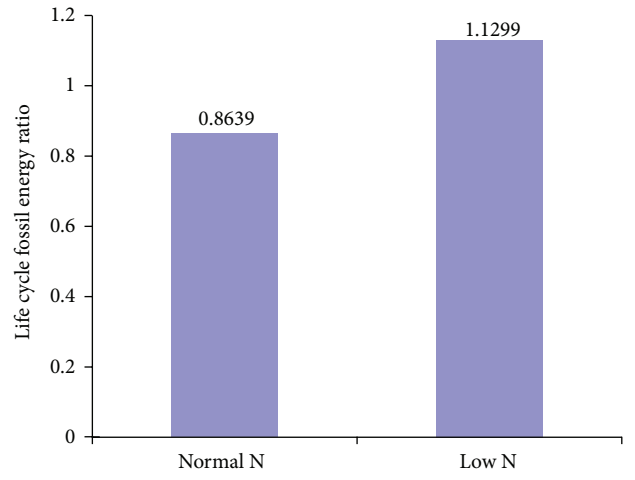

Figure 5: Life cycle fossil energy ratio for the production of biodiesel from *Chlorella vulgaris* grown in normal and limited nitrogen supply conditions.

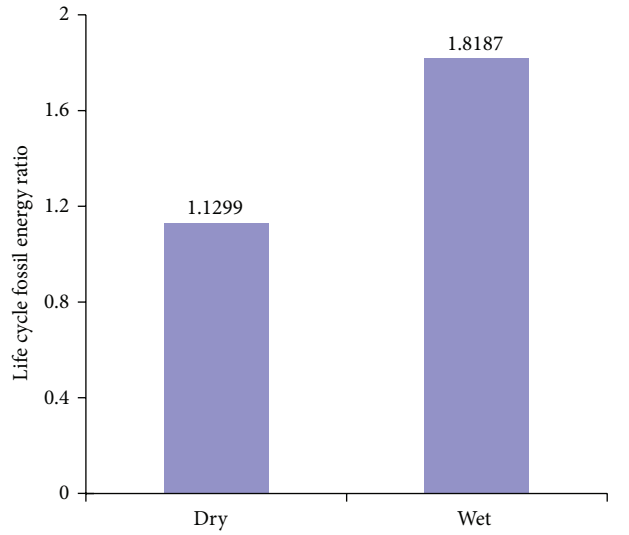

Figure 7: Life cycle fossil energy ratio for the production of biodiesel from algal oil extracted from dried and wet algae.

4.3. Comparison of the Results with Other LCA Studies of Algal Biodiesel. This section has the goal of comparing the results of this study with other similar LCA studies on algal biodiesel and then analyzing the main differences among values for the life cycle fossil energy ratios in different studies. Values of energy demands, energy outputs, and life cycle fossil energy ratios of algae based biodiesel production from two literatures have been collected and are compared in Table 5.

As can be seen from Table 5, when algal biodiesel made from similar pathways is taken as the research object, life cycle fossil energy ratio of biodiesel produced from dried algae is 66.18% higher in this study than in Lardon et al.'s study, and life cycle fossil energy ratio of biodiesel produced from wet algae is 35.82%, 355%, and 28.57% higher in this study than in studies of Lardon et al., Razon and Tan [31], and Batan et al., respectively.

High energy consumption caused by backward algae drying technology is the main reason for the lower life cycle fossil energy ratio of biodiesel produced from dried algae in Lardon et al.'s study. Compared to energy consumption data of algae drying in the study of Zhao and Hu in 2009 on energy consumption of sludge treatment in wastewater treatment plant, energy consumption data of algae drying in study of Lardon et al. is from experimental study of Hassebrauck et al.

Table 5: The primary energy demands, energy outputs, and life cycle fossil energy ratios for algal biodiesel production in different researches.

Oil extraction technology	This study		Lardon et al., 2009 [8]		Yang et al., 2014 [14]	Batan et al., 2010 [12]
	Dry	Wet	Dry	Wet	Wet	Wet
Basic condition						
Oil content/%	40		40		24	50
Productivity/g/m^2·d	19.85		19.25		16	24.9
Primary fossil energy consumption/MJ						
Cultivation	0.65	0.71	0.41	0.59	2.246	0.73
Concentration	0.11	0.11	—	—	0.103	—
Dewatering	0.04	0.04	—	—	—	0.17
Drying	0.7	—	1.39	—	—	—
Oil extraction	0.17	0.19	0.14	0.52	1.895	0.21
Esterification	0.06	0.06	0.03	0.03	—	0.17
Fertilizer production	0.05	0.05	0.08	0.11	1.041	—
Chemicals production	0.08	0.08	0.27	0.43	0.443	—
Biogas generation	—	—	—	—	0.089	—
Sewage treatment	—	—	—	—	0.884	—
Energy production/MJ						
Biodiesel	1	1	1	1	1	1
Oilcake	0.9474	1.1096	0.57	1.23	—	0.79
Glycerin	0.1474	0.1474	—	—	0.565	—
Credit for "fresh" water	—	—	—	—	0.162	—
Biogas	—	—	—	—	1.378	—
Credit for ammonium compounds	—	—	—	—	0.027	—
Life cycle fossil energy ratio	1.13	1.82	0.68	1.34	0.4	1.4

in 1996 on sludge drying by belt dryer and its energy consumption for algae drying is about 2 times higher than results in study of Zhao and Hu [26]. So timeliness of basic data has important effects on the validity of LCA results of algal biodiesel. Compared to energy consumption data of extraction of oil from wet algae in this study based on pilot-scale study of Chen et al., Lardon et al. [8] and Batan et al. [12] calculated the energy consumption for extraction of oil from wet algae based on hypothesis and both of their results are higher than the energy consumed for extraction of oil from wet algae with subcritical cosolvents in study of Sturm and Lamer [15].

In study of Yang et al. [14], complicated algae cultivation process and low yield of algae lead to the high energy input during stages of algae cultivation and oil extraction. It makes algal biodiesel not able to deliver more energy than is required to produce it.

4.4. Sensitivity Analysis. A sensitivity analysis is performed to determine key parameters affecting the life cycle fossil energy ratio of algal biodiesel (see Figure 8). All parameters analyzed vary over equal confidence intervals. The effects of different parameters will be ranked by the change in the life cycle fossil energy ratio of algal biodiesel. Algal biodiesel produced from *Chlorella vulgaris* under low N condition in open ponds, with CO_2 from membrane separation, and oil extracted from dried algae have been taken as the baseline scenario. The change rate of all uncertain parameters is 40%.

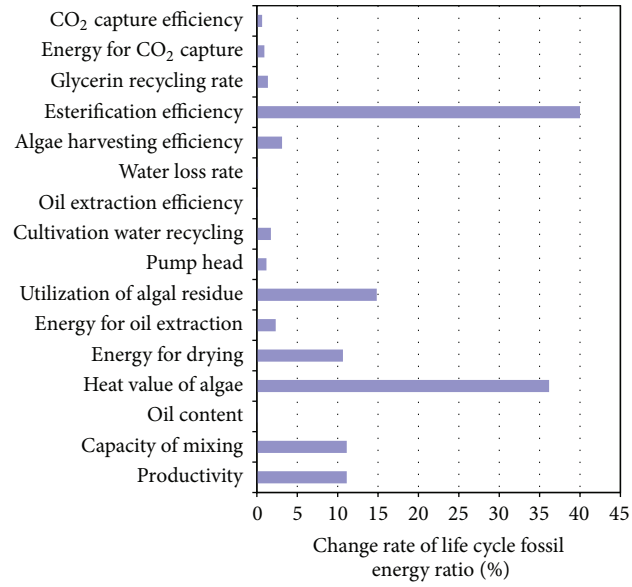

Figure 8: Sensitivity analysis of effects of several parameters on life cycle fossil energy ratio of algae biodiesel.

As can be seen from Figure 8, the changes of esterification efficiency and heat value of algae are found to have the greatest effects on the life cycle fossil energy ratio of algal biodiesel. As esterification efficiency and heat value of algae decrease by 40%, the life cycle fossil energy ratio of algal biodiesel changes by 40% and 36.17%, respectively. The second important parameters are utilization ratio of algal residue, algae cultivation water recycling rate, energy demand for algae drying, capacity of mixing, and productivity of algae and when those parameters separately decrease by 40%, the life cycle fossil energy ratio of algal biodiesel changes between 10 and 15%. When algal oil content, oil extraction energy consumption, pump head, cultivation water recycling rate, oil extraction efficiency, cultivation water loss, algae harvesting efficiency, glycerin recycling rate, CO_2 capture energy consumption, and CO_2 capture efficiency separately decrease by 40%, the life cycle fossil energy ratio of algal biodiesel changes under 5%.

5. Conclusions

(1) Nitrogen deficiency can not only promote the oil content of many species of algae but also decrease the productivity of algae. The change of algae cell composition has certain effects on its energy output. Life cycle fossil energy ratio of biodiesel produced from *Chlorella vulgaris* grown under nitrogen-limited conditions increases by 30.78%. Life cycle fossil energy ratio of biodiesel produced from *Phaeodactylum tricornutum* grown with nitrogen deprivation decreases by 10.56%.

(2) Compared to extraction of oil from dried algae, extraction of oil directly from wet algae with subcritical cosolvents can effectively promote the life cycle fossil energy ratio of algal biodiesel.

(3) Comparison of the results with other LCA studies of algal biodiesel shows that, when algal biodiesel made from similar pathways is taken as the research object, life cycle fossil energy ratio of biodiesel produced from dried algae is 66.18% higher in this study than in Lardon et al.'s. Worse timeliness of data source for energy consumption of algae drying is the main reason. Life cycle fossil energy ratio of biodiesel produced from wet algae is 35.82% and 28.57% higher in this study than in the studies of Lardon et al. and Batan et al., respectively. Compared to Lardon et al. [8] and Batan et al. [12]'s calculation of the energy consumption for extraction of oil from wet algae based on hypothesis, energy consumption data of extraction of oil from wet algae in this study is based on pilot-scale study of Chen et al. So the results are more reliable.

(4) The changes of esterification efficiency and heat value of algae have the greatest effects on the life cycle fossil energy ratio of algal biodiesel, followed by utilization ratio of algal residue, algae cultivation water recycling rate, energy demand for algae drying, capacity of mixing, and productivity of algae. When esterification efficiency and heat value of algae decrease by 40%, the life cycle fossil energy ratio of algal biodiesel changes by 40% and 36.17%, respectively.

Conflict of Interests

The authors declare that there is no conflict of interests regarding the publication of this paper.

References

[1] J. Fargione, J. Hill, D. Tilman, S. Polasky, and P. Hawthorne, "Land clearing and the biofuel carbon debt," *Science*, vol. 319, no. 5867, pp. 1235–1238, 2008.

[2] A. Darzins, P. Pienkos, and L. Edye, *Algae as a Feedstock for Biofuels: An Assessment of the Current Status and Potential for Algal Biofuels Production*, IEA, 2011.

[3] E. D. Frank, J. Han, I. Palou-Rivera, A. Elgowainy, and M. Q. Wang, *Life-Cycle Analysis of Algal Lipid Fuels with the GREET Model*, Argonne National Laboratory, Lemont, Ill, USA, 2011.

[4] J. Yang, M. Xu, X. Zhang et al., "Life-cycle analysis on biodiesel production from microalgae: water footprint and nutrients balance," *Bioresource Technology*, vol. 102, pp. 159–165, 2011.

[5] A. F. Clarens, E. P. Resurreccion, M. A. White, and L. M. Colosi, "Environmental life cycle comparison of algae to other bioenergy feedstocks," *Environmental Science and Technology*, vol. 44, no. 5, pp. 1813–1819, 2010.

[6] A. F. Clarens, H. Nassau, E. P. Resurreccion, M. A. White, and L. M. Colosi, "Environmental impacts of algae-derived biodiesel and bioelectricity for transportation," *Environmental Science and Technology*, vol. 45, no. 17, pp. 7554–7560, 2011.

[7] K. Sander and G. S. Murthy, "Life cycle analysis of algae biodiesel," *International Journal of Life Cycle Assessment*, vol. 15, no. 7, pp. 704–714, 2010.

[8] L. Lardon, A. Helias, B. Sialve, J. P. Steyer, and O. Bernard, "Life-cycle assessment of biodiesel production from microalgae," *Environmental Science and Technology*, vol. 43, no. 17, pp. 6475–6481, 2009.

[9] Q. KaiXian and M. A. Borowitzka, "Light and nitrogen deficiency effects on the growth and composition of *Phaeodactylum tricornutum*," *Applied Biochemistry and Biotechnology*, vol. 38, no. 1-2, pp. 93–103, 1993.

[10] L. Uslu, O. Işik, K. Koç, and T. Göksan, "The effects of nitrogen deficiencies on the lipid and protein contents of Spirulina platensis," *African Journal of Biotechnology*, vol. 10, no. 3, pp. 386–389, 2011.

[11] A. M. Illman, A. H. Scragg, and S. W. Shales, "Increase in Chlorella strains calorific values when grown in low nitrogen medium," *Enzyme and Microbial Technology*, vol. 27, no. 8, pp. 631–635, 2000.

[12] L. Batan, J. Quinn, B. Willson, and T. Bradley, "Net energy and greenhouse gas emission evaluation of biodiesel derived from microalgae," *Environmental Science and Technology*, vol. 44, no. 20, pp. 7975–7980, 2010.

[13] L. B. Brentner, M. J. Eckelman, and J. B. Zimmerman, "Combinatorial life cycle assessment to inform process design of industrial production of algal biodiesel," *Environmental Science and Technology*, vol. 45, no. 16, pp. 7060–7067, 2011.

[14] F. Yang, W. Xiang, X. Sun, H. Wu, T. Li, and L. Long, "A novel lipid extraction method from wet microalga *Picochlorum* sp. at room temperature," *Marine Drugs*, vol. 12, no. 3, pp. 1258–1270, 2014.

[15] B. S. M. Sturm and S. L. Lamer, "An energy evaluation of coupling nutrient removal from wastewater with algal biomass production," *Applied Energy*, vol. 88, no. 10, pp. 3499–3506, 2011.

[16] M. Chen, T. Liu, X. Chen et al., "Subcritical co-solvents extraction of lipid from wet microalgae pastes of *Nannochloropsis* sp," *European Journal of Lipid Science and Technology*, vol. 114, no. 2, pp. 205–212, 2012.

[17] A. Burnham, M. Wang, and Y. Wu, *GREET 2.8 Transportation Vehicle-Cycle Model*, Argonne National Laboratory, Lemont, Ill, USA, 2008.

[18] L. F. Razon and R. R. Tan, "Net energy analysis of the production of biodiesel and biogas from the microalgae: *Haematococcus pluvialis* and *Nannochloropsis*," *Applied Energy*, vol. 88, no. 10, pp. 3507–3514, 2011.

[19] A. C. Redfield, "The biological contral of chemical factors in the environment," *American Scientist*, vol. 46, pp. 205–221, 1958.

[20] K. D. Fagerstone, J. C. Quinn, T. H. Bradley, S. K. de Long, and A. J. Marchese, "Quantitative measurement of direct nitrous oxide emissions from microalgae cultivation," *Environmental Science & Technology*, vol. 45, no. 21, pp. 9449–9456, 2011.

[21] Solar Energy Research Institute (SERI), *Microalgae Culture Collection 1986-1987*, SERI Microlagal Technology Research Group, US, 1986.

[22] L. Boersma, E. W. R. Barlow, J. R. Miner, H. K. Phinney, and J. E. Oldfield, *The Use of Waste Heat in a System for Animal Waste Conversion with By-product Recovery and Recycling*, Oregon State University, 1975.

[23] F. G. Acién Fernández, C. Brindley Alías, M. C. García-Malea López et al., "Assessment of the production of 13C labeled compounds from phototrophic microalgae at laboratory scale," *Biomolecular Engineering*, vol. 20, no. 4–6, pp. 149–162, 2003.

[24] S. Van Den Hende, H. Vervaeren, S. Desmet, and N. Boon, "Bioflocculation of microalgae and bacteria combined with flue gas to improve sewage treatment," *New Biotechnology*, vol. 29, no. 1, pp. 23–31, 2011.

[25] O. Jorquera, A. Kiperstok, E. A. Sales, M. Embiruçu, and M. L. Ghirardi, "Comparative energy life-cycle analyses of microalgal biomass production in open ponds and photobioreactors," *Bioresource Technology*, vol. 101, no. 4, pp. 1406–1413, 2010.

[26] Q. Zhao and K. Hu, "Energy-use analysis of sludge processing in wastewater treatment plant," *Water and Wastewater Information*, vol. 4, pp. 15–20, 2009 (Chinese).

[27] R. W. Harris, M. J. Cullinane, and P. T. Sun, *Process Design and Cost Estimating Algorithms for the Computer Assisted Procedure for Design and Evaluation of Wastewater Treatment Systems (CAPDET)*, US Environmental Protection Agency, 1982.

[28] X. Song and J. Yu, "Study on cost of oil processing," *China Oils and Fats*, vol. 28, pp. 62–64, 2003 (Chinese).

[29] J. Sheehan, V. Camobreco, J. Duffield, M. Graboski, and H. Shapouri, *Life Cycle Inventory of Biodiesel and Petroleum Diesel for Use in an Urban Bus*, US Department of Energy's Office of Fuels Development, 1998.

[30] State Environmental Protection Administration of China (SEPA), *Cleaner Production Standard—Edible Vegetable Oil Industry (Soya-Bean Oil and Soya-Bean Cake)*, SEPA, 2006.

[31] International P. GaBi 4.3 software. PE International, Leinfelden-Echterdingen, Germany, 2006.

[32] H. H. Khoo and R. B. H. Tan, "Life cycle investigation of CO_2 recovery and sequestration," *Environmental Science & Technology*, vol. 40, no. 12, pp. 4016–4024, 2006.

Hindawi Publishing Corporation
The Scientific World Journal
Volume 2014, Article ID 537080, 7 pages
http://dx.doi.org/10.1155/2014/537080

Research Article

Volatile Organic Silicon Compounds in Biogases: Development of Sampling and Analytical Methods for Total Silicon Quantification by ICP-OES

Claire Chottier, Vincent Chatain, Jennifer Julien, Nathalie Dumont, David Lebouil, and Patrick Germain

Laboratoire de Génie Civil et d'Ingénierie Environnementale LGCIE, Université de Lyon, INSA-Lyon, 20 Avenue Albert Einstein, 69621 Villeurbanne, France

Correspondence should be addressed to Vincent Chatain; vincent.chatain@insa-lyon.fr

Received 27 July 2014; Accepted 5 September 2014; Published 15 October 2014

Academic Editor: Bin Cao

Current waste management policies favor biogases (digester gases (DGs) and landfill gases (LFGs)) valorization as it becomes a way for energy politics. However, volatile organic silicon compounds (VOSiCs) contained into DGs/LFGs severely damage combustion engines and endanger the conversion into electricity by power plants, resulting in a high purification level requirement. Assessing treatment efficiency is still difficult. No consensus has been reached to provide a standardized sampling and quantification of VOSiCs into gases because of their diversity, their physicochemical properties, and the omnipresence of silicon in analytical chains. Usually, samplings are done by adsorption or absorption and quantification made by gas chromatography-mass spectrometry (GC-MS) or inductively coupled plasma-optical emission spectrometry (ICP-OES). In this objective, this paper presents and discusses the optimization of a patented method consisting in VOSiCs sampling by absorption of 100% ethanol and quantification of total Si by ICP-OES.

1. Introduction

Biogases (digester gas (DG) and landfill gas (LFG)), issued from anaerobic digestion of wastewater, sewage sludges, or wastes, could be an answer to the lack of energy, and at the same time, could decrease fossil energy consumption and avoid greenhouse gas emissions. Benefits of this renewable energy lead scientists to optimize biogas valorization. However, our daily life and industrial wastes contain silicone polymers or low molecular weight silicones [1] that end in wastewater treatment plants (WWTPs) [2], in landfills or in waste methanization facilities. Also, during the anaerobic waste degradation, silicones and other silicon-containing materials (detergents, soaps, etc.) generate volatile organic silicon compounds (VOSiCs, including siloxanes). Silicon present in biogas originates mainly from those compounds, which are known to be volatile compared to Si mineral. Among them different types of structures could be discriminated, and the most studied are the methyl siloxanes. However, silanols (compounds containing the Si–OH group), such as trimethylsilanol (TMSol), silanes (Si_nH_{2n+2}), such as tetramethylsilane (TMS), or other organic molecules can also be found in biogases [3]. Their structural formulas are shown in Figure 1.

The main cyclic VOSiCs present in biogases are the octamethylcyclotetrasiloxane (D4), the decamethylcyclopentasiloxane (D5), the hexamethylcyclotrisiloxane (D3), and to a lesser extent the dodecamethylcyclohexasiloxane (D6). The main linear VOSiCs are the trimethylsilanol (TMSol), the hexamethyldisiloxane (L2), the octamethyltrisiloxane (L3), and the barely present decamethyltetrasiloxane (L4) [4, 5]. Depending upon the type, origin, and quality of organic waste landfilling, sewage sludge digestion, or sorted biowaste digestion processes, relative proportions of VOSiCs can fluctuate [6].

During combustion, VOSiCs are oxidized into silica and silicates, which deposit in combustion chambers [3, 4, 7, 8]. The accumulation of those abrasive deposits to a thickness of

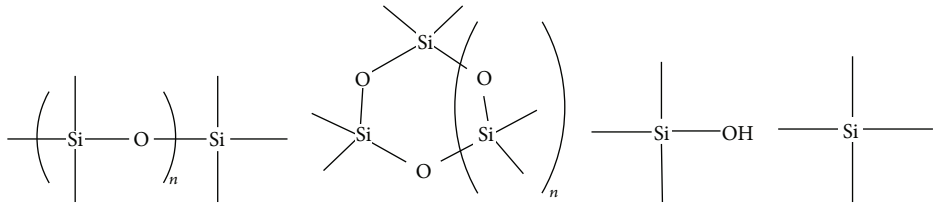

Figure 1: Structural formulas of VOSiCs: (a) linear ($1 < n < 3$), (b) cyclic ($1 < n < 5$), (c) trimethylsilanol (TMSol), and (d) tetramethylsilane (TMS).

several millimeters affects equipment's performances (motor, spark plugs, pistons, cylinder heads, valves, etc.) and contaminates lubricating oils, resulting in an increasing global cost of maintenance and cleaning [9]. Various abatement techniques, such as solvent wash and adsorption on solids, have been developed or adapted to remove those harmful trace constituents from biogas [9–13]. To design and subsequently assess the efficiency of those techniques, a reliable analysis of VOSiCs for DGs/LFGs is required. Previously, there has been no standardized protocol for VOSiCs quantification. First studies have revealed that results can significantly vary depending on the sampling and screening techniques [5, 14, 15]. One of the foremost methods is based on gas chromatography coupled with mass spectrometry (GC-MS), which allows the speciation of VOSiCs [3, 8, 10]. Among hundreds of existing VOSiCs, only 6 to 10 compounds are usually quantified by GC-MS for various reasons; some are better known, more common and/or standards are available. Due to the unavailability of certain analytical standards, most laboratories provide results as toluene (or other) equivalents. Peak areas on chromatograms are reported to a toluene calibration curve in order to derive a numerical value of concentration. Several disadvantages dependent on the analytical chain, linked to the storage, the transport or even the availability of analytical standards, disturb this speciation technique which is nowadays the most employed.

Another technique uses inductively coupled plasma-optical emission spectrometry (ICP-OES) to allow a global quantification of the total silicon content in biogases [7, 16]. Thanks to the use of an absorption method based on an easily transportable device [16], VOSiCs can be quickly and directly trapped (in less than 25 min) into absorbing solutions. All VOSiCs are soluble in various organic solvents, such as oil [9], toluene, acetone, heptane, hexane [17, 18], and methanol [19, 20]. However, some major analytical problems have been highlighted when elementary Si from VOSiCs is analyzed by ICP-OES. For example, the Si content of TMSol aqueous solutions is overestimated by a 17 factor in comparison to the classical Si mineral NIST standard [21]. Hagmann et al. [17] also have shown that Si contents of L2, D3, and D4 solutions in organic solvent are overestimated, respectively, by 8.7, 3.6, and 1.4 in comparison to octaphenylcyclotetrasiloxane standard. Sánchez et al. [22] have shown that it goes the same way for the Si contents of VOSiCs in xylene matrices in comparison to dimethyloctylchlorosilane standard. For example, D4 Si signal is exacerbated by a factor 1.5 and L2 Si signal by a factor 17. So, this phenomenon could occur with any matrices and with the others VOSiC present in biogases. Hagmann et al. [17] and Sánchez et al. [22] mentioned that the origin of the overestimation takes place during the nebulization step in the ICP-OES apparatus. Volatile compounds could desorb outside of the mist and enhance silicon level in the outside atmosphere. In this case, it is a source of analytical bias, which systematically overestimates Si amounts.

Some scientists use both methods to exploit their complementarity. Schweigkofler and Niessner [4] proposed a GC-MS/AES as a detection coupling; VOSiC identification is allowed by the mass spectrometer whereas quantification is performed by atomic emission spectrometry. Chao [23] used GC, to separate VOSiCs, coupled to an atomic emission detector using a microwave-induced He plasma to perform quantification.

This research paper presents and discusses results obtained on several biogases, in using ethanol to absorb VOSiCs and then ICP-OES to quantify total elementary Si. Laboratory development thanks to synthetic matrices and fieldwork validations thanks to biogases sampled on sites will be established to evaluate the efficiency of the analytical methodology developed to overcome the issue of Si overestimation during ICP-OES analyses of VOSiC in organic matrices.

2. Materials and Methods

2.1. Reagents and Solutions. Hexamethyldisiloxane (98.5%), octamethyltrisiloxane (97%), decamethyltetrasiloxane (97%), dodecamethylpentasiloxane (97%), hexamethylcyclotrisiloxane (98%), octamethylcyclotetrasiloxane (98%), and decamethylcyclopentasiloxane (97%) were purchased at Sigma-Aldrich; dodecamethylcyclohexasiloxane (97%) was purchased at ABCR, trimethylsilanol (99.3%) was purchased at Chemos, and absolute ethanol (99.9%) was purchased at Prolabo. All stock solutions and dilutions were made into absolute ethanol. All VOSiCs standards were tested in comparison to a L5 calibration curve, either alone at 0.5, 1, 4, and 5 mgSi/L to assess their individual analytical response in ethanol matrices, or via 300 mgSi/L mixtures showing different VOSiCs distributions diluted to reach 2, 4, and 5 mgSi/L. Individual VOSiC analytical responses are named afterwards as "response factors." Response factor is defined as the measured Si concentration (in comparison to

Table 1: Typical LFGs and DGs compositions in % of Si for each VOSiC by GC-MS and the total Si in mgSi/Nm^3 biogas.

% Si	LFG A	LFG B1	LFG B2	LFG B3	LFG C	DG A	DG B
TMSol	26	11	24	6	36	1	1
L2	10	11	19	19	10	—	—
L3	1	7	1	1	1	—	2
L4	—	—	—	—	—	1	—
D3	2	19	3	3	3	—	2
D4	38	32	46	44	29	20	30
D5	23	19	7	6	21	78	65
Total Si content (mgSi/Nm^3)	9	4	23	29	8	1	1

L5 calibration curve) over the calculated Si concentration by dilution of the standard.

2.2. Real Samples Origins. LFGs produced at 3 French nonhazardous waste landfills (landfill A, B, and C) and DGs produced at 2 French WWTPs (WWTP A and B) were sampled between the conditioning system and a potential pretreatment.

2.3. Sampling and Analysis

2.3.1. Bags Sampling. Tedlar bags of 3 liters with polypropylene fittings were used to sample and store LFGs and DGs. Samples were sent to a private accredited laboratory, able to perform a speciation of VOSiCs by GC-MS analysis. The analysis procedure consists of the direct injection of gaseous samples from bags into the GC-MS device. Laboratory provides VOSiCs concentrations in mg of each analyzed compound per Nm^3 of dry biogas. The analytical relative uncertainty provided by the laboratory is of 15% for each compound.

2.3.2. Liquid Absorption Sampling. The patented method used and developed by Germain et al. [16] is based on a known biogas volume, bubbling at a controlled flow rate thanks to a mass flowmeter (Brooks) calibrated for biogas, into liquid solutions able to absorb VOSiCs. In order to avoid any contamination, a Si-free sampling device has been built (Figure 2).

The absorption device consists of four successive 250 mL HDPE bottles (Azlon) each filled with 150 mL of absolute ethanol. After sampling, bottles are stored at 4°C until analysis.

Samples analyses from each bottle are performed by a radially observed Ultima 2 Horiba Jobin-Yvon ICP-OES (Longjumeau, France) running through an argon flow (4.5; Linde Gas). The apparatus is functioning with a 40.68 MHz radiofrequency generator and a Czerny-Turner grating monochromator. The classical cyclonic spray chamber has been replaced by an IsoMist (Glass Expansion, Australia), which is a programmable temperature cyclonic spray chamber (variable from −10°C to +60°C). The IsoMist allows pure ethanol injection without plasma extinction by decreasing the temperature in the nebulization chamber to −10°C. Moreover this will have a side benefit which is the decrease of analyte volatilization outside of the mist drops and a reduction of the induced overestimation. Si concentrations are determined at 251.6 nm with a viewing height above load coil of 5 mm and a radial plasma viewing mode. The torch was vertical, demountable with a 3 mm i.d. injector. The radiofrequency power used was of 1400 W, the sample uptake was of 0.5 mL/min, the nebulisation pressure was of 1 bar, and plasma gas flow rate and sheath gas flow rate were, respectively, of 16 and 0.35 L/min.

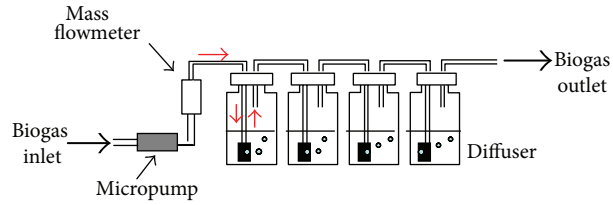

Figure 2: Principle of the liquid absorption bubbling device.

Calibration, ranging from 0 to 5 mgSi/L, is done with L5 standards, a nonvolatile siloxane (vapor pressure < 0.01 kPa at 25°C), logically absent from DGs and LFGs.

Considering the Si levels in the absorbing solutions, the volume of solvent used and the volume of biogas in contact, it is possible to derive the Si content into mgSi/Nm^3 of biogas.

3. Results and Discussion

3.1. LFGs and WWTPs DGs VOSiCs Composition. Table 1 provides a summary of VOSiCs speciation from LFGs and WWTPs DGs sampled in different fieldworks and at different times during the year.

It is noticeable that VOSiCs composition varies in time and space, which will direct our methodology development. Main VOSiCs are different in LFGs (D4, TMSol, D5, and L2) than in WWTPs DGs (D5, D4); as well some VOSiC can be totally absent from one site and in large quantity in other sites. We can cite as examples the cases of TMSol or L2, which are residual in WWTPs DGs and significant in LFGs. About L5 quantification, analyses reveal that its level stays under the detection limit of the device (0.005 mg/Nm^3) whatever the sampling site.

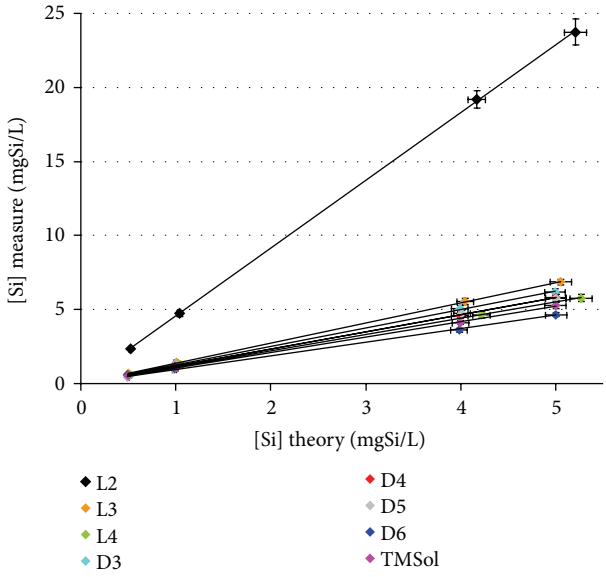

Figure 3: VOSiCs ICP-OES analytical responses (L5 calibration curve) by comparison with the theoretical concentration. Analyses are performed at −10°C and each value is the mean of 3 measurements.

3.2. Development of the ICP-OES Analytical Methodology for VOSiC Total Si Measurements

3.2.1. VOSiCs Individual Analytical Standard Deviation. Figure 3 shows Si measurements for each VOSiCs standard solutions (using L5 calibration curve) on the calibration range routinely used in the analysis procedure, namely, from 0.5 to 5 mgSi/L as a function of the theoretical calculated concentration of each standard solution. In this case, the response factor is equal to the slope for each VOSiC regression line on the studied range. Uncertainties on the x-axis correspond to standard solution preparation and on the y-axis to the standard deviation over 3 measurements of the solution.

Linearity of VOSiCs analytical individual response in ethanol is highlighted (r^2 ranging from 0.9993 to 1). Therefore, it verifies VOSiCs solubility in ethanol in the range from 0.5 to 5 mgSi/L. Furthermore, 7 out of 8 VOSiCs show an individual response factor (equal to the slope for each VOSiC regression on the studied range) close to 1 (considered VOSiC ICP-OES responds as the L5 standard), namely, between 0.9 and 1.4. Only L2 presents a remaining high response factor of 4.6. It is linked to the structure of L2 and its high vapor pressure (*ca.* 5.5 kPa at 25°C), which consequently facilitates its volatilization and increases analytical bias.

According only to vapor pressure, TMSol must show an important residual overestimation in these conditions as its vapor pressure (*ca.* 9.9 kPa at 25°C) is higher than the one of L2. However, the response factor of TMSol is only around 1.1 which is linked to Henry's law through the Henry's law constant which is function of temperature, solute and solvent nature. Indeed, this is explained by the hydrogen bonds between the hydroxyl groups of TMSol and those of ethanol. This phenomenon improves the solute/solvent interactions and annihilates TMSol desorption from the mist drops at low temperature.

Postanalysis adjustments need to be performed on ICP-OES raw data interpretation as no other technical improvement is available to further decrease the temperature in the nebulization chamber and avoid L2 desorption from mist.

Table 2: Determination of the mean response factors observed by ICP-OES at −10°C for the 3 standards solutions at 2, 4, and 5 mgSi/L (L5 calibration).

% of Si/sample coming from L2	Mean response factor	RSD %
0	**1.0**	**2**
10	**1.3**	0
15	**1.4**	7
20	**1.6**	**4**
25	**1.7**	**0**
Median value (excluding 0% Si from L2)	**1.5**	—

3.2.2. Method Adjustment via Synthetic Laboratory Solutions. As explained above, L2, particularly substantial in LFGs, disturbs the accuracy of the ICP-OES analytical method in ethanol matrix. L2 percentage can fluctuate from one site to another, ranging, as shown in Table 1, from 10 to 19% of the total Si LFGs content and be totally absent in WWTPs DGs.

To remain consistent, mixtures of commercial VOSiCs standards (TMSol, L2, L3, D3, D4, and D5) in ethanol, modeled after typical LFGs and DGs GC-MS analyses, have been simulated and analyzed in laboratory by ICP-OES. Five stock solutions of synthetic mixtures have been made with a total Si concentration of 300 mgSi/L. The difference between these 5 mixtures is the Si percentage coming from L2 which was set up at 10, 15, 20, and 25%, proportions of the other VOSiCs are also evolving but ratios remain constant compared to each other. For each synthetic mixture, 3 standards (at 2, 4, and 5 mg of total Si per liter) from stock standard solutions dilution, covering the whole range of L5 calibration, have been realized. The mean ICP-OES response factors between the 3 total Si concentrations for each percentage of L2 are reported in Table 2.

Different percentages of L2, covering classical contents reached in LFGs, have been applied on a typical LFG composition copy, causing a modification of the other VOSiCs silicon amounts represented. The evolution of response factors is linear as a function of the Si percentage coming from L2. A straight line ($y = 0.0284x + 1.0027$) with a correlation coefficient r^2 of 0.9932 is obtained. Moreover, it is noticeable that, for a same Si percentage coming from L2, whatever the mixture composition in terms of total Si amount (2, 4 or 5 mgSi/L), response factors are constant (0% < RSD < 7%).

When L2 is absent from the analyzed mixtures, the ICP-OES result in comparison to L5 calibration curve is accurate (at 0% of L2: response factor of 1.0), which confirms the accuracy of the sampling and analytical methods for WWTPs DGs, without any adjustment. As the Si level coming from L2

Table 3: GC-MS analysis (LFG B3).

	mgSi/Nm^3 biogas
TMSol	2
L2	6
L3	0
L4	<LD
L5	<LD
D3	<LD
D4	13
D5	2
TMS	6
Total	29

Table 4: ICP-OES analysis (LFG B3).

Bottles numbers	Si content
Bottle number 1 (mgSi/L EtOH)	6,0
Bottle number 2 (mgSi/L EtOH)	0,3
Bottle number 3 (mgSi/L EtOH)	<LD
Bottle number 4 (mgSi/L EtOH)	<LD
Si total (mgSi/L EtOH)	6,3
Si total (mg/Nm^3 biogas)	**47**
Si total (mg/Nm^3 biogas) adjusted by a global overestimation factor of:	
1,3	36
1,5	**31**
1,7	28

is higher than 10% for the other solutions, the application of a correction by the mean response factor will only concern LFGs. A global theoretical response factor of 1.5 ± 0.2, covering the whole deviations observed for L2 proportions representative of real LFGs, is established from these results.

3.3. Method Validation for LFG Analysis. Only one validation is presented, the methodology is applicable to all LFG analyses (with a classical L2 percentage less than 25% of the total Si LFGs content).

3.3.1. Experimental GC-MS and ICP-OES Results on LFG B3. Successively, via the absorption device, set up with 4 bottles containing ethanol, and a via 3L Tedlar bag, biogas has been directly sampled from a single tapping point installed upstream from the combustion engine at landfill B to provide a gaseous sample for GC-MS analysis (Table 3) and a liquid sample for ICP-OES analysis (Table 4) which will be compared.

For LFG B3, the GC-MS quantification provides a concentration of 29 ± 5 mgSi/Nm^3. This result will be named *Result 1* afterwards. The ICP-OES quantification with the application of the 1.5 ± 0.2 correction factor (deduced by laboratory experiments) leads to a concentration ranging from 28 to 36 mgSi/Nm^3 for LFG. This result will be named *Result 2* afterwards.

The global relative uncertainty of experimental determination of the total Si amount by ICP-OES in LFG has been calculated and associated with a potential margin of error of 15% and the relative uncertainty calculated for total Si amount provided by GC-MS is also of 15%.

3.3.2. Theoretical ICP-OES Result Calculation in mgSi/Nm^3 LFG. A theoretical calculation of the Si total amount has been carried out. It took into account the percentage of Si coming from L2 furnished by the GC-MS analysis (see Table 1, LFG B3, %Si (L2) = 19%; which is the same analysis to the one presented in Table 4) and the L2 individual response factor in ethanol matrix, that is, 4.6 (see Figure 3). Equation (1) summarizes the different adjustments (due to the operational conditions and L2 theoretical adjustments) to apply to convert the Si level, furnished in mgSi/L of ethanol by the ICP-OES device, in mgSi/Nm^3 of biogas:

$$[\mathrm{Si}]_{\mathrm{mg/Nm^3}} = \frac{a}{1 + (3.6 \times (b/100))} \times \frac{c}{d} \times 1000. \quad (1)$$

The terms of (1) are described as follows: a (mgSi/L): sum of the raw Si concentration in the 4 bottles of the sampling device measured by ICP-OES with L5 calibration. b (%): percentage of Si coming from L2 within the total Si determination by GC/MS analysis. c (L): volume of ethanol in one bottle of the sampling device. d (L): volume of LFG sampled.

The relative uncertainty on the result of the calculated theoretical ICP-OES value has been calculated and is of 15%.

In our example, the application of (1) leads to a theoretical ICP-OES value for LFG B3 of 28±5 mgSi/Nm^3. This result will be named *Result 3* afterwards.

3.3.3. Methods and Results Comparison. Figure 4 is a visual representation of the three results (experimental GC-MS; experimental ICP-OES; and theoretical ICP-OES) with their uncertainties.

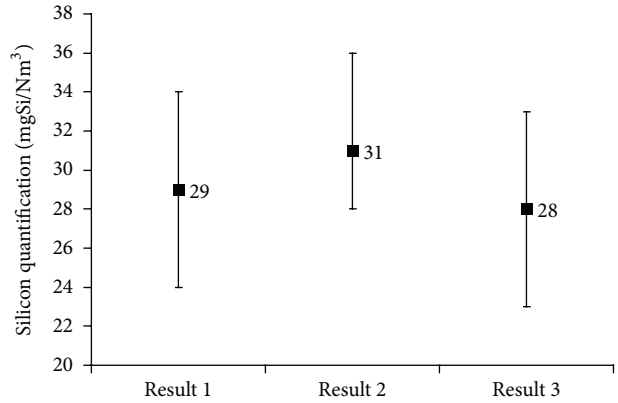

Figure 4: Comparison of experimental quantifications obtained by GC-MS (*Result 1*); ICP-OES (*Result 2*); and the theoretical ICP-OES by calculation (*Result 3*).

Theoretically, the value of 1.5±0.2 of the global correction factor is validated for the present analytical method as the theoretical ICP-OES value of 28 ± 5 mgSi/Nm^3 (*Result 3*), simulated thanks to GC-MS data (%Si from L2 in total Si) and L2 individual response factor for ICP-OES analyses, is recovering in the range of values corresponding to experimental ICP-OES concentrations after correction (28 < mgSi/Nm^3 LFG < 36, *Result 2*).

Experimentally, the conclusive similitude between the GC-MS result (29 ± 5 mgSi/Nm^3 of LFG, *Result 1*) and the corrected experimental ICP-OES results (28 < mgSi/Nm^3 LFG < 36, *Result 2*) confirms the necessity of an adjustment method, using a global correction factor of 1.5 ± 0.2.

By comparison of ICP-OES experimental (*Result 2*) and theoretical results (*Result 3*), it has also been proved that the analytical calculation is able to free ourselves from the analytical deviation linked to L2 presence in LFGs.

All three results added by their uncertainties are recovering each other. These results imply that ICP-OES method (using an adapted correction factor) provides the same results to GC-MS analysis in terms of total Si, which will allow performing more cost-effective analyses of total Si in biogases.

4. Conclusion

A liquid absorption in ethanol, considered more harmless and environmental friendly than methanol or other solvents, such as acetone, toluene, hexane, and heptane, minimizes the risks of biogas and LFG sampling. All VOSiCs are easily solubilized and then analyzed by ICP-OES which allows a global quantification of Si.

The only VOSiC identified as responsible for an analytical bias (L2), which could falsify consequently Si quantification, is absent from WWTPs DGs. Therefore, even if it has been verified, no global deviation needs to be measured for this type of gas, whatever the type of analysis. Finally, only the analysis of VOSiCs from LFGs (with a classical L2 percentage less than 25% of the total Si LFGs content), absorbed in ethanol, requires the use of a 1.5±0.2 corrective factor to apply to the total Si level issued from the ICP-OES analysis.

The easy use of sampling and analysis protocols has revealed that the method uncertainty is acceptable for biogas treatment applications. A first step for Si total quantification in biogases is established and allows an access to a global biogas quality indicator. It can, in addition to a detailed occasional VOSiCs speciation, lead site managers in their equipment choices (type, size, etc.) thanks to a routine assessment. Results are given with a 15% uncertainty, equivalent to private laboratories ones.

Nevertheless, it remains possible to quantify separately polar VOSiCs from the less polar, by using water upstream from the ethanol bottles in charge of trapping the TMSol (thanks to the fact that 95% of Si biogases content is trapped in the first bottle and the 5 remaining percentiles in the second). In this case the methodology will still be applicable, as TMSol will be quantified separately in water over a TMSol calibration, so no bias occurs (*data not shown*) which is similar to its response factor of 1.1 in ethanol in comparison to L5 calibration.

Conflict of Interests

The authors declare that there is no conflict of interests regarding the publication of this paper.

References

[1] D. Graiver, K. W. Farminer, and R. Narayan, "A Review of the Fate and Effects of Silicones in the Environment," *Journal of Polymers and the Environment*, vol. 11, no. 4, pp. 129–136, 2003.

[2] W. Parker, J. Shi, N. Fendinger, H. Monteith, and G. Chandra, "Pilot plant study to assess the fate of two volatile methyl siloxanes compounds during municipal wastewater treatment," *Environmental Toxicology Chemistry*, vol. 18, pp. 172–181, 1999.

[3] R. Dewil, L. Appels, and J. Baeyens, "Energy use of biogas hampered by the presence of siloxanes," *Energy Conversion and Management*, vol. 47, no. 13-14, pp. 1711–1722, 2006.

[4] M. Schweigkofler and R. Niessner, "Determination of siloxanes and VOC in landfill gas and sewage gas by canister sampling and GC-MS/AES analysis," *Environmental Science and Technology*, vol. 33, no. 20, pp. 3680–3685, 1999.

[5] G. Ducom, B. Laubie, A. Ohannessian, C. Chottier, P. Germain, and V. Chatain, "Hydrolysis of polydimethylsiloxane fluids in controlled aqueous solutions," *Water Science and Technology*, vol. 68, no. 4, pp. 813–820, 2013.

[6] J. Stoddart, M. Zhu, J. Staines, E. Rothery, and R. Lewicki, "Experience with halogenated hydrocarbons removal from landfill gas," in *Proceedings of the Sardinia 1999, 7th Sardinia International Waste Management and Landfill Symposium*, Cagliari, Italy, 1999.

[7] A. Ohannessian, V. Desjardin, V. Chatain, and P. Germain, "Volatile organic silicon compounds: the most undesirable contaminants in biogases," *Water Science and Technology*, vol. 58, no. 9, pp. 1775–1781, 2008.

[8] V. Chatain, A. Ohannessian, and P. Germain, "Valorisation du biogaz et traitements épuratoires," in *La Méthanisation*, R. Moletta, Ed., vol. 15, chapter 15, pp. 459–478, Lavoisier Tec & Doc, Paris, France, 2nd edition, 2012.

[9] M. Prabucki, W. Doczyck, and D. Asmus, "Removal of organic silicon compounds from landfill and sewer gas," in *Proceedings of the 8th Sardinia International Waste Management and Landfill Symposium*, Proceedings Sardinia, Cagliary, Italy, 2001.

[10] M. Schweigkofler and R. Niessner, "Removal of siloxanes in biogases," *Journal of Hazardous Materials*, vol. 83, no. 3, pp. 183–196, 2001.

[11] M. Ajhar, M. Travesset, S. Yüce, and T. Melin, "Siloxane removal from landfill and digester gas—a technology overview," *Bioresource Technology*, vol. 101, no. 9, pp. 2913–2923, 2010.

[12] M. Hagmann, E. Hesse, P. Hentschel, and T. Bauer, "Purification of biogas—removal of volatiles silicones," in *Proceedings of the 8th International Waste Water Management and Landfill Symposium*, vol. 2, pp. 641–644, 2001.

[13] S. Rasi, J. Läntelä, A. Veijanen, and J. Rintala, "Landfill gas upgrading with countercurrent water wash," *Waste Management*, vol. 28, no. 9, pp. 1528–1534, 2008.

[14] F. Broto-Puig, "Siloxane analysis in landfill biogas: study on sample capture method and identification—quantification by HRGC-MS," Microphilox Life Project, 2008, http://www.microphilox.com/pdf/FBrotoIQSMICROPHILOX.pdf.

[15] M. Crest, C. Chottier, P. Camacho, A. Ohannessian, V. Chatain, and P. Germain, "Comparison of two analytical methods to quantify volatile organo silicon compounds (VOSiCs) contents in landfill biogas," in *Proceedings of the 12th International Waste Management and Landfill Symposium (Sardinia '09)*, Cagliari, Italy, 2009.

[16] P. Germain, N. Dumont, and V. Chatain, "Quantification of total silicon in biogas," WO Patent 129007, 2006.

[17] M. Hagmann, E. Heimbrand, and P. P. Hentschel, "Determination of siloxanes in biogas from landfills and sewage treatment plants," in *Proceedings of the 7th International Waste Management and Landfill Symposium: Proceedings Sardinia*, Cagliari, Italy, 1999.

[18] Y. Takuwa, T. Matsumoto, K. Oshita, M. Takaoka, S. Morisawa, and N. Takeda, "Characterization of trace constituents in landfill gas and a comparison of sites in Asia," *Journal of Material Cycles and Waste Management*, vol. 11, no. 4, pp. 305–311, 2009.

[19] Air Toxics, *Siloxanes by GC-MS: Introducing the Air Toxics*, vol. 7, Air Methods Ltd, West Midlands, UK, 1st edition, 2002.

[20] A. Narros, M. I. Del Peso, G. Mele, M. Vinot, E. Fernandez, and M. E. Rodriguez, "Determination of siloxanes in landfill gas by adsorption on Tenax tubes and TD-GC-MS," in *Proceeding of the 12th International Waste Management and Landfill Symposium (Sardinia '09)*, Cagliary, Italy, 2009.

[21] J. J. Kennan, L. L. M. Breen, T. H. Lane, and R. B. Taylor, "Methods for detecting silicones in biological matrixes," *Analytical Chemistry*, vol. 71, no. 15, pp. 3054–3060, 1999.

[22] R. Sánchez, J.-L. Todolí, C.-P. Lienemann, and J.-M. Mermet, "Effect of the silicon chemical form on the emission intensity in inductively coupled plasma atomic emission spectrometry for xylene matrices," *Journal of Analytical Atomic Spectrometry*, vol. 24, no. 4, pp. 391–401, 2009.

[23] S. Chao, "Direct measurement and speciation of volatile organosilicons in landfill gas by gas chromatography with atomic emission detection," in *Proceedingsof the 25th SWANA's Annual Landfill Gas Symposium*, Monterey, Calif, USA, 2002.

Hindawi Publishing Corporation
The Scientific World Journal
Volume 2014, Article ID 735431, 14 pages
http://dx.doi.org/10.1155/2014/735431

Research Article

Comparative Evaluation of Biomass Power Generation Systems in China Using Hybrid Life Cycle Inventory Analysis

Huacai Liu, Xiuli Yin, and Chuangzhi Wu

CAS Key Laboratory of Renewable Energy, Guangzhou Institute of Energy Conversion, Chinese Academy of Sciences, Guangzhou 510640, China

Correspondence should be addressed to Xiuli Yin; xlyin@ms.giec.ac.cn

Received 7 March 2014; Accepted 18 August 2014; Published 14 October 2014

Academic Editor: Li Zhuang

There has been a rapid growth in using agricultural residues as an energy source to generate electricity in China. Biomass power generation (BPG) systems may vary significantly in technology, scale, and feedstock and consequently in their performances. A comparative evaluation of five typical BPG systems has been conducted in this study through a hybrid life cycle inventory (LCI) approach. Results show that requirements of fossil energy savings, and greenhouse gas (GHG) emission reductions, as well as emission reductions of SO_2 and NO_x, can be best met by the BPG systems. The cofiring systems were found to behave better than the biomass-only fired system and the biomass gasification systems in terms of energy savings and GHG emission reductions. Comparing with results of conventional process-base LCI, an important aspect to note is the significant contribution of infrastructure, equipment, and maintenance of the plant, which require the input of various types of materials, fuels, services, and the consequent GHG emissions. The results demonstrate characteristics and differences of BPG systems and help identify critical opportunities for biomass power development in China.

1. Introduction

With the rapid development of economy, electricity demand continues to grow in China. Significant attention has been focused on the high dependence of electricity generation on coal, including greenhouse gases (GHG) emissions and environmental pollution. Alternate approaches are being sought. Biomass is the only renewable fuel available for combustion-based electricity generation. Moreover, straw is no longer the primary fuel for cooking and space heating in many rural communities. A large amount of straw is abandoned or incinerated in the fields, resulting in environmental pollution and a waste of resources. For these reasons, biomass power generation (BPG) has gained significant attention in China. By the end of 2010, the overall installed capacity of biomass power had reached 5.5 GW. In addition, China has set the goals in State Plans for Medium and Long-Term Development of Renewable Energy to achieve 30 GW of biomass power capacity by 2020 [1].

There are currently three kinds of biomass power plants in China: biomass-only fired power plant, biomass-coal co-firing power plant, and biomass gasification power plant. These plants may vary significantly in technology, scale, and feedstock and consequently in their performances. In the short term, large-scale electricity generation based on biomass-only fired or cofiring is the most promising alternative to achieve expected biomass electricity market contribution and to fulfill GHG emissions targets, mainly due to better technological reliability and maturity [2]. However, biomass is usually characterized by massive volume and dispersed distribution, which may incur high energy and economic costs during collection. Small- and medium-scale biomass gasification power generation technology may be more feasible than large-scale direct-fired and cofiring technology [3, 4]. A full assessment and comparison of potential of each system for sustainable development should be conducted.

Several studies have been undertaken using life cycle assessment (LCA) to analyze benefits and drawbacks of BPG

Table 1: Coefficient matrices for the hybrid LCI analysis.

		BPG systems		IO sector		Functional unit	Total output
		Process commodity ($c = 1, 2, \ldots, l$)	Process activity ($p = 1, 2, \ldots, m$)	Energy sector ($i = 1, 2, \ldots, n_e$)	Nonenergy sector ($j = 1, 2, \ldots, n$)		
BPG systems	Process commodity ($c = 1, 2, \ldots, l$)		$\mathbf{U}^{CP}$			$\mathbf{F}$	$\mathbf{Q}$
	Process activity ($p = 1, 2, \ldots, m$)	$\mathbf{V}^{PC}$		$\mathbf{V}^{PE}$	$\mathbf{V}^{PN}$		$\mathbf{G}$
IO sector	Energy sector ($i = 1, 2, \ldots, n_e$)		$\mathbf{U}^{EP}$	$\mathbf{U}^{EE}$	$\mathbf{U}^{NE}$		$\mathbf{x}_E$
	Nonenergy sector ($j = 1, 2, \ldots, n$)		$\mathbf{U}^{NP}$	$\mathbf{U}^{NE}$	$\mathbf{U}^{NN}$		$\mathbf{x}_N$

Table 2: Accounting framework for BPG systems.

		BPG systems		IO sector		Functional unit	Total output
		Process commodity ($c = 1, 2, \ldots, l$)	Process activity ($p = 1, 2, \ldots, m$)	Energy sector ($i = 1, 2, \ldots, n_e$)	Nonenergy sector ($j = 1, 2, \ldots, n$)		
BPG systems	Process commodity ($c = 1, 2, \ldots, l$)	$\mathbf{A}_{ff}$	$\mathbf{B}^{CP}$	$\mathbf{A}_{fn}$	$\mathbf{A}_{fn}$	$\mathbf{F}$	$\mathbf{Q}$
	Process activity ($p = 1, 2, \ldots, m$)	$\mathbf{D}^{PC}$					$\mathbf{G}$
IO sector	Energy sector ($i = 1, 2, \ldots, n_e$)	$\mathbf{A}_{ef}$		$\mathbf{A}_{ee}$	$\mathbf{A}_{en}$		$\mathbf{x}_E$
	Nonenergy sector ($j = 1, 2, \ldots, n$)	$\mathbf{A}_{nf}$		$\mathbf{A}_{ne}$	$\mathbf{A}_{nn}$		$\mathbf{x}_N$

systems in China because LCA considers all the processes involved in each alternative in a cradle-to-grave manner [5–8]. However, direct comparisons on the same bases are difficult to find. Therefore, five typical power plants are studied in this study through a detailed life cycle inventory (LCI) approach: 25 MW biomass-only fired plant, 140 MW cofiring plant, 25 MW cofiring plant, 1 MW gasification plant, and 5.5 MW gasification plant. The results demonstrate characteristics and differences of BPG systems and help identify critical opportunities for biomass power development in China.

2. Methodology

LCI analysis is one of the four phases of LCA involving the compilation and quantification of inputs and outputs. The two basic methods for compiling an LCI are the process-based analysis and the input-output (IO) analysis. Most LCIs have been conducted based on a process-based analysis where the physical quantities of energy and material use and environmental releases from the main production processes are assessed in detail, but nevertheless the process-based analysis suffers from a systematic truncation error due to the delineation of product system by a finite boundary and the omission of contributions outside the boundary [9]. In contrast, input-output analysis is a top-down technique that uses sectoral monetary transaction matrixes describing complex interdependencies of industries within a national economy. Input-output analysis can overcome the "truncation error" and solve the traditional system boundary limitation by taking into account capital goods and overheads as inputs to a product system, which are often deliberately left out by most of process-based LCIs [9]. However, it also has limitations associated with high levels of aggregation in industry or commodity classifications, as well as potential uncertainty [9, 10]. Moreover, monetary value, the most commonly used representation of interindustry transactions in input-output tables, may distort physical flow relations between industries due to price inhomogeneity [9].

The hybrid LCI method seeks to use advantages of both methods while mitigating their respective limitations. One of the practical examples has been presented by Inaba and his coworkers [11]. He developed a production equilibrium hybrid model to assess reductions in CO_2 emissions by food waste biogasification by using a matrix representing the input-output relationship of energy and materials among the processes and sectors. The method presented and utilized in this research takes a similar approach to that used by Inaba et al. [11]. To gain more insight into contributions of energy consumptions and emissions of BPG systems, each lifecycle stage was considered as a subsystem of the larger group of Chinese industrial sectors in the LCI model.

2.1. Goals and Scope. In a consequential LCA, the differences in environmental impact stemming from changes made to a reference system are quantified. Fossil fuel system substituted

Table 3: Classifications of IO sectors in hybrid LCI model.

Sector code	Sectors
1-1	Raw coal
1-2	Cleaned coal
1-3	Other washed coal
1-4	Coke
1-5	Coke oven gas
1-6	Other gases
1-7	Other coking products
1-8	Crude oil
1-9	Gasoline
1-10	Kerosene
1-11	Diesel oil
1-12	Fuel oil
1-13	Liquefied petroleum gas
1-14	Refinery gas
1-15	Other petroleum products
1-16	Natural gas
1-17	Electricity
1-18	Heat
2	Farming, forestry, animal husbandry, fishery, and water conservancy (agriculture)
3	Ferrous and nonferrous metals mining and dressing
4	Nonmetal and other minerals mining and dressing
5	Food processing, food production, beverage production, and tobacco processing
6	Textile
7	Garments and other fiber products, leather, furs, down and related products
8	Timber processing, bamboo, cane, palm and straw products, and furniture manufacturing
9	Papermaking and paper products, printing and record medium reproduction, and cultural, educational, and sports articles
10	Raw chemical materials and chemical products, medical and pharmaceutical products, and chemical fiber, rubber, and plastic products
11	Nonmetal mineral products
12	Smelting and pressing of ferrous and nonferrous metals
13	Metal products
14	Ordinary machinery, equipment for special purpose
15	Transport equipment
16	Electric equipment and machinery
17	Manufacture of communication equipment, computers, and other electronic equipment
18	Instruments, meters, and cultural and office machinery
19	Artwork and other manufacturing
20	Recycling and disposal of waste
21	Water production and supply
22	Construction
23	Transport, storage, postal, and telecommunications services
24	Wholesale, retail trade, hotels, and catering service
25	Other service activities

or most likely to be substituted by biomass energy system is usually chosen as the reference system. Compared with the reference system, biomass power plants' performances may vary depending on other factors such as the normal routes of biomass disposal and local energy consumption structure. For the sake of comparison, some simplifications have been made in this study. Credits are not taken for the avoided operations of normal routes of biomass disposal such as field burning. Coal-fired plant before retrofitting for cofiring is chosen to be the reference system of biomass cofiring systems. It was assumed that the specific portion of coal cofired with biomass has the same electric efficiency and emissions as those before cofiring. The differences of electric output and emissions between cofiring and the specific portion of coal cofired with biomass were allocated to biomass. Biomass is assumed to substitute part of the coal without changing the performance of the rest part of coal in power generation. A simple and useful comparison can be carried out this way. For the biomass-only system and biomass gasification system, the reference system is the electricity sector in IO table (see Table 3), which represents the national average of electricity production. Despite this, useful information can be obtained since power generation from coal accounts for more than 80% of annual power generation in China [12].

Two main objectives were pursued in this study: firstly, to determine the reduction of GHG emissions, the primary energy (PE) savings that could actually be attained when biomass power is compared to conventional electricity production, and secondly, to evaluate which BPG system is more beneficial on the same basis. We have established that the LCI is done from the production process of the biomass to the electric output suitable for consumption of power plants.

2.2. System Boundaries. A consistent scope of system boundaries which mainly includes three life cycle stages is adopted to facilitate comparison between technologies, as shown in Figure 1. In all of the stages, the energy, material, and other services during the entire life time of the plant were considered, which includes supports from background economy such as fuel production, extraction/production of essential materials, and manufacturing and commissioning of equipment. The ash will be either disposed or used as industrial raw material and it is not taken into account in this study, neither are the end-use of electricity and the decommissioning of power plant.

2.3. Model Description. The previously described inventory data were summarized into an input-output format, and the energy and material flow between processes in the system was calculated. A make-use input-output framework was used to illustrate the BPG systems, as shown in Table 1.

Energy and materials in the system are defined as a process commodity sector ($c = 1, \ldots, l$), and a process itself is defined as a process activity sector ($p = 1, \ldots, m$). Thereby, matrix $\mathbf{U}^{CP}$ represents input to each process activity (p) of a process commodity (c), and matrix $\mathbf{V}^{PC}$ represents the quantity of output of a process commodity (c) from a process activity (p).

Energy and material inputs from IO sector are described as matrixes $\mathbf{U}^{EP}$ and $\mathbf{U}^{NP}$, respectively, which comprises the

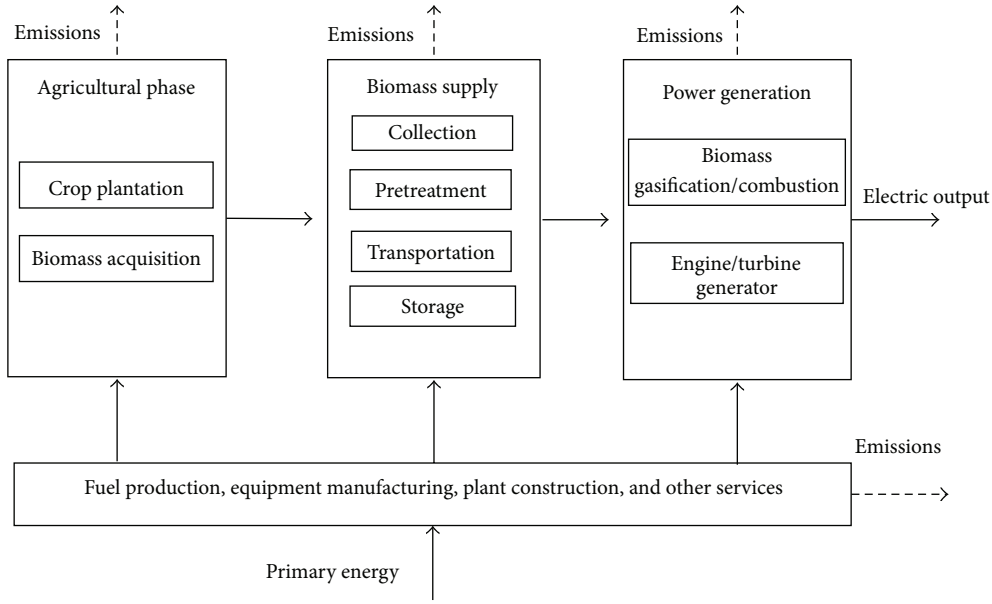

Figure 1: System boundaries of BPG system.

IO sector and the process activity sector in the BPG systems. The matrix $\mathbf{U}^{EP}$ represents input to each process activity (p) from a energy sector ($i = 1, 2, \ldots, n_e$), and matrix $\mathbf{U}^{NP}$ represents input to each process activity (p) from a nonenergy sector ($j = 1, 2, \ldots, n$).

Output of commodities from a process activity sector in the system (p) to IO energy sector (i) and nonenergy sector (j) is shown as matrixes $\mathbf{V}^{PE}$ and $\mathbf{V}^{PN}$. The matrixes $\mathbf{U}^{EE}$, $\mathbf{U}^{NE}$, $\mathbf{U}^{EN}$, and $\mathbf{U}^{NN}$ denote annual commodity transactions based on the energy and monetary unit between IO sectors.

A production equilibrium model for hybrid LCI analysis was established using a matrix representing the input-output relationship of materials and energy among the processes and sectors described above. The accounting framework is shown in Table 2.

The matrices $\mathbf{B}^{CP}$ and $\mathbf{D}^{PC} = \mathbf{V}^{PC}$ were calculated using (1) and (2), respectively. The squarely arranged input coefficient $\mathbf{A}_{ff}$ derived from (3) is composed of the commodity sector in the BPG systems. Vector $\mathbf{G}$ is the total output of the process sectors. Vector $\mathbf{Q}$ is the total amount of commodities. The symbol "$\widehat{\ }$" indicates a diagonal matrix. Consider the following:

$$\mathbf{B}^{CP} = \mathbf{U}^{CP}\widehat{\mathbf{G}}^{-1}, \tag{1}$$

$$\mathbf{D}^{PC} = \mathbf{V}^{PC}\widehat{\mathbf{Q}}^{-1}, \tag{2}$$

$$\mathbf{A}_{ff} = \mathbf{B}^{CP}\mathbf{D}^{PC}. \tag{3}$$

The matrices $\mathbf{A}_{ef}$ and $\mathbf{A}_{nf}$ are inputs from energy sector and nonenergy sector of the BPG systems, respectively, as described below:

$$\begin{aligned}\mathbf{A}_{ef} &= \left(\mathbf{U}^{EP}\widehat{\mathbf{G}}^{-1}\right)\mathbf{D}^{PC} + \left(-\left(\mathbf{V}^{PE}\right)^{T}\widehat{\mathbf{G}}^{-1}\right)\mathbf{D}^{PC},\\ \mathbf{A}_{nf} &= \left(\mathbf{U}^{NP}\widehat{\mathbf{G}}^{-1}\right)\mathbf{D}^{PC} + -\left(\left(\mathbf{V}^{PN}\right)^{T}\widehat{\mathbf{G}}^{-1}\right)\mathbf{D}^{PC},\end{aligned} \tag{4}$$

where T represents the transpose of a matrix.

The matrixes $\mathbf{A}_{ee}$, $\mathbf{A}_{en}$, $\mathbf{A}_{ne}$, and $\mathbf{A}_{nn}$ describe the intersectoral requirements in the background economy:

$$\begin{pmatrix}\mathbf{A}_{ee} & \mathbf{A}_{en}\\ \mathbf{A}_{ne} & \mathbf{A}_{nn}\end{pmatrix} = \begin{pmatrix}\mathbf{U}^{EE} & \mathbf{U}^{EE}\\ \mathbf{U}^{NE} & \mathbf{U}^{NN}\end{pmatrix}\widehat{\mathbf{x}}^{-1},$$
$$\mathbf{x} = \begin{pmatrix}\mathbf{x}_E\\ \mathbf{x}_N\end{pmatrix}. \tag{5}$$

Electricity was assumed to be the only product of BPG systems. Therefore, the total energy requirement matrix $\mathbf{L}$ can be written as follows:

$$\mathbf{L} = \begin{pmatrix}\mathbf{I} - \mathbf{A}_{ff} & -\mathbf{A}_{fe} & -\mathbf{A}_{fn}\\ -\mathbf{A}_{ef} & \mathbf{I} - \mathbf{A}_{ee} & -\mathbf{A}_{en}\\ -\mathbf{A}_{nf} & -\mathbf{A}_{ne} & \mathbf{I} - \mathbf{A}_{nn}\end{pmatrix}^{-1}. \tag{6}$$

Direct and indirect emissions within a system $\mathbf{y}_1$ and outside of the system $\mathbf{y}_2$ were calculated by premultiplying $\mathbf{L}$ with direct emissions data and postmultiplying by demand for the good in question, as represented by the following equation:

$$\begin{pmatrix}\mathbf{y}_1 & \mathbf{y}_2\end{pmatrix} = \begin{pmatrix}\mathbf{d}_1 & \mathbf{d}_2\end{pmatrix}\begin{pmatrix}\mathbf{I} - \mathbf{A}_{ff} & -\mathbf{A}_{fe} & -\mathbf{A}_{fn}\\ -\mathbf{A}_{ef} & \mathbf{I} - \mathbf{A}_{ee} & -\mathbf{A}_{en}\\ -\mathbf{A}_{nf} & -\mathbf{A}_{ne} & \mathbf{I} - \mathbf{A}_{nn}\end{pmatrix}^{-1}\begin{pmatrix}\mathbf{u}\\ 0\end{pmatrix}, \tag{7}$$

where $\mathbf{d}_1$ and $\mathbf{d}_2$ are the emissions per unit activity of sector in the system and of the emissions per unit activity of sector t in the IO table and $\mathbf{u}$ represents the functional unit vector of the system.

Table 4: Allocation of energy consumptions for energy sectors.

Energy-related sectors in IO table and energy statistical yearbook	Energy sectors in hybrid LCI model	Allocation method of energy consumptions
Coal mining and dressing	1-1 Raw coal 1-2 Cleaned coal 1-3 Other washed coal	Ratio of energy consumptions of raw coal (1-1) and washed coal (1-2, 1-3) was assumed to be 25 : 9, based on Grade 3 of clean production standard of coal mining and processing industry [24]
Petroleum and natural gas extraction	1-8 Crude oil 1-16 Natural gas	Crude oil and refinery gas are consumed in Crude oil extraction. Natural gas is consumed in natural gas extraction
Petroleum processing, coking, and processing of nuclear fuel	1-4 Coke 1-5 Coke oven gas 1-6 Other gases 1-7 Other coking products 1-9 Gasoline 1-10 Kerosene 1-11 Diesel oil 1-12 Fuel oil 1-13 Liquefied petroleum gas 1-14 Refinery gas 1-15 Other petroleum products	Coking products are consumed in coking. Crude oil and refinery gas are consumed in processing of petroleum. Ratios of refining efficiency of gasoline, kerosene, diesel, liquefied petroleum gas, and fuel oil are assumed to be 85% : 87% : 89% : 93.5% : 95% [25]. Refining efficiency of refinery and other petroleum are assumed to be the same as fuel oil
Electric power and steam production and supply	1-17 Electricity 1-18 Steam	The equivalent value of electricity to heat is assumed to be 2.78 [14]
Gas production and supply	1-5 Coke oven gas 1-13 Liquefied petroleum gas 1-16 Natural gas	

3. Data Sources and Assumptions

3.1. Classification of IO Sectors and Sectoral Energy Consumptions. China's 2007 monetary input-output table [13], the latest data of China national economy, was used to construct the hybrid LCI model. To make full use of data from energy statistics and to overcome the price inhomogeneity of energy, the energy-related sectors in IO table were divided into 18 specific energy production sectors. The 2008 China Energy Statistical Yearbook [14] was used to calculate sectoral energy intensity vector. Moreover, the IO table was aggregated into a 24-nonenergy-sector format to be consistent with the Chinese energy statistics based on the standards of classification of national economic industries [15]. The 18 energy sectors and 24 nonenergy sectors are shown in Table 3. The sectoral energy consumptions were transformed from physical units to energy units with data from the yearbook [14]. It should be noted that the energy statistics were accomplished based on industry sectors while the IO table was established based on commodity sectors. Thus the data of energy statistics was transformed into commodity-sector based data before integrating into the IO table.

The energy consumptions of the 5 energy-related sectors in the 2008 China Energy Statistical Yearbook [14] are categorized into 18 kinds of energy. Correspondingly, the 5 energy-related sectors in IO table were divided into 18 specific energy sectors to be consistent with the Chinese energy statistics, as shown in Tables 3 and 4. The energy consumptions of the 5 energy-related sectors were allocated to the 18 specific energy sectors, as shown in Table 4. For example, energy consumption of petroleum and natural gas extraction was allocated to 1-8 crude oil and 1-16 natural gas. In other words, it was allocated to petroleum extraction and natural gas extraction. Most of the energy allocation was done on energy basis while some exceptions are listed in Table 4.

Some of the energy is used as feedstock into different industrial processes. The 2008 China Energy Statistical Yearbook gives the total nonenergy use in the industrial sectors. It was assumed that all the nonenergy use is in the chemical sectors [16]. The "other petroleum products" in all sectors and coke use in smelting of metals are assumed to be completely nonenergy use [16].

3.2. Sectoral Air Emissions. GHG emissions particularly CO_2, CH_4, and N_2O expressed as CO_2 equivalent (CO_2-eq) have been assessed in this study. In addition, SO_2 and NO_x emissions were taken into consideration when carrying out comparisons between options. The SO_2 emissions of industries recorded in the China statistics yearbook [17] were used for creating the sectoral intensity matrix. The current Chinese statistic system does not provide any national or sectoral data on GHG and NO_x emissions. Thus, the GHG and NO_x emissions were generally calculated by multiplying the energy data by emission factors.

Chinese specific values for the carbon emission factor of each fuel and the fraction of carbon oxidized for each fuel in each sector from Peters et al. [16] were used to construct the

Table 5: GHG emissions of nonenergy use from industrial processes.

Sector code	Sector category	Industrial processes	GHG emissions
10	Raw chemical materials and chemical products, medical and pharmaceutical products, and chemical fiber, rubber, and plastic products	Manufacturing of ammonia, soda ash, and calcium carbide	105.78 Mt CO_2
11	Nonmetal mineral products	Manufacturing of cement and plain grass	683.93 Mt CO_2
12	Smelting and pressing of ferrous and nonferrous metals	Smelting and pressing of ferrochromium, silicon metal and ferro-unclassified, and coke as a reducing agent	873.59 Mt CO_2
2	Farming, forestry, animal husbandry, fishery, and water conservancy (agriculture)	Enteric fermentation, manure management, rice cultivation, and field burning of agricultural residues	18.44 Mt CH_4
1-1	Raw coal	Coal mining	19409.97 kt CH_4
1-8, 1-16	Crude oil, natural gas	Oil and natural gas systems	258.31 kt CH_4
2	Farming, forestry, animal husbandry, fishery, and water conservancy (agriculture)	Manure management, cropland, and field burning of agricultural residues	614.97 kt N_2O
10	Raw chemical materials and chemical products, medical and pharmaceutical products, and chemical fiber, rubber, and plastic products	Nitric acid, adipic acid	74.55 kt N_2O

Table 6: NO_x emissions of nonenergy use from industrial processes.

Category	Industrial processes	Quantity (Mt)	NO_x emission factors (t/t)	NO_x emissions (Mt)
10 raw chemical materials and chemical products, medical and pharmaceutical products, and chemical fiber, rubber, and plastic products	Nitric acid	2.009	0.012	0.0241
	Adipic acid	0.215	0.0081	0.0017
12 smelting and pressing of ferrous and nonferrous metals	Iron	494.889	0.000076	0.3761
	Ferrochromium-silicon	0.043	0.0117	0.0005
	Silicon metal	0.81	0.0117	0.0095
	Aluminum	9.358	0.00215	0.0201
13 metal products	Steel rolling	60.927	0.00004	0.2437

CO_2 emissions data. Meanwhile, IPCC (Intergovernmental Panel on Climate Change) default emission factors of CH_4 and N_2O of fuel combustion in each sector [18] were used to calculate the sectoral CH_4 and N_2O emissions data. The GHG emissions of nonenergy use from industrial processes were also taken into consideration, including CO_2 emission from smelting and pressing of ferrous metals, CH_4 emission from enteric fermentation, and N_2O emission from cropland [19], as shown in Table 5.

Based on the country specific values of sectoral NO_x emission factors [16] and the industrial outputs [20], NO_x emissions from the main industrial processes can be estimated, as presented in Table 6.

3.3. Agricultural Phase. Biomass power plants' main features vary depending on several factors: amount of available resources and their properties, pretreatments required, and generation technology employed. For the sake of comparison, some representative average characteristics in biomass production and supply had to be selected in this case.

Corn stover is considered as feedstock for biomass power plants in this study. Life cycle data for the production, collection, and transportation of the feedstock include the energy and emissions associated with fertilizers, herbicides, and fuel to operate harvesting equipment. Data for the agricultural phase for corn originate mainly from national statistics [21], which represents the national average in 2007 (Table 7). Inputs were assigned to corn stover based on the purchased price of stover and grain, which is 120 yuan/t and 1500 yuan/t, respectively [21].

Energy allocation was rejected as grain has been considered an alimentary product and not a fuel. It has been considered that agricultural residues resources would not be collected without an energy demand and no economic

Table 7: Inputs and allocation in agricultural phrase.

Inputs	Plantation inputs (yuan/mu)	Assigned input of corn stover (yuan/GJ)
Seed	26.92	0.308
Chemical fertilizers[a]	88.43	1.013
Farmyard manure	8.66	0.099
Pesticide	7.96	0.091
Agricultural film	2.62	0.030
Field machinery, irrigation, and animal power	55.64	0.637
Fuels	0.03	0.393
Technical service	0.03	0.143
Tools and materials	2.1	0.061
Maintenance	1.27	0.101
Others	0.12	0.000

Note: [a]the amount of N-fertilizer applied in physical unit is 10.27 kg N/mu [21]. An emission rate of 1.3% of N-fertilizer for N_2O [25] was adopted. On the other hand, emissions associated with land use change were not taken into account in this study. The average exchange rate of currency in 2007, 1 yuan = 0.132 USD and 1 yuan = 0.096 EUR.

value would be obtained. For this reason, partitioning on an economic basis using the share in revenues (grain and straw) was the method finally chosen.

3.4. Biomass Supply. The agricultural production is mainly carried out based on households in China, which results in a small average planted area and thus scattered straw resources. Thus the feedstock supply has become a bottleneck for large-scale use. There are mainly two patterns for biomass supply in China, which can be referred to as centralized pattern and distributed pattern. The centralized pattern involves a centralized storage site by the plant which can receive straw and ensure the plant's operation. Straw is mainly collected by farmers manually and then delivered to storage site by tractors. The distributed pattern involves a bunch of straw-receiving stations, which also serve as intermediate storage sites where biomass is baled and stacked [22]. The distributed pattern was employed by the 25 MW biomass-only fired plant and the 140 MW cofiring plant, while the centralized pattern was employed by the 25 MW cofiring plant, the 1 MW gasification plant, and the 5.5 MW gasification plant. The model established in our early study [22] was adopted to calculate the inputs of biomass supply system, including fuel, machinery, labor, and other services. Major parameters for biomass supply are listed in Table 8.

3.5. Biomass Power Stations. The combustion characteristics of biomass are well-understood and already wildly used in biomass applications worldwide. However, the development of biomass-only fired technologies starts fairly late in China. Advanced oversea technology and equipment have been employed in most cases. In recent years, some domestically developed boilers have met the basic operating requirements

Table 8: Major parameters for biomass feedstock supply.

Items	Value
Straw/grain ratio	0.75
Corn production (kg/mu)	422.4
Lower heating value (LHV) of corn stover (MJ/kg, dry basis)	15.6
Moisture content of corn stover (wt%)	10
Sulfur content of corn stover[a] (wt%)	0.21
Distribution density of biomass[b] (t/km)	103.3
Average transport distance from straw-receiving station to the plant[c] (km)	30
CO_2 emission factor of diesel[d] (g/GJ)	74100
SO_2 emission factor of diesel[e] (g/GJ)	93.78
NO_x emission factor of diesel[f] (g/GJ)	643.19

Note: [a]an average value of sulfur content of corn stover from Liao et al. [26] was adopted to ensure that the BPG systems were comparable.
[b]The transport distance for centralized pattern was calculated using a farmland coverage rate of 0.7 and a availability factor of 0.4 in the model [22]. It was assumed that the collection area is assumed to be a circle centered at the straw-receiving station and the centralized storage site, where the straw is evenly distributed [22].
[c]The average transport distance is used for the distributed pattern in the cases of 25 MW biomass-only fired and 140 MW cofiring.
[d]CO_2, CH_4, and N_2O emission factors for diesel utilization were adopted from IPCC road transport default values, the latter two of which are 3.9 g/GJ [18].
[e]The Chinese specific value for sulfur content of diesel was taken from Song [27]. And the emission rate of sulfur was assumed to be 100%.
[f]The Chinese specific value of NO_x emission for diesel vehicles is 27.4 kg/t [28].

and have been put into operation but the performance still needs to be confirmed. A 25 MW biomass power plant in Anhui province was taken as an example in this study, which mainly consists of a 130 t/h high-temperature and high-pressure steam boiler with vibrating grate and a condensing steam turbine generator unit.

On the other hand, the R&D activity of BPG technology started since the 1960s, characterized by rice hull gasification and power generation system with sizes from 60 to 200 kW. A number of demonstration plants have been erected over the past few decades and some of them have been in operation for several thousands of hours. A demonstration project of 1 MW circulating fluidized bed biomass power plant which was established by the Guangzhou Institute of Energy Conversion, Chinese Academy of Sciences in Putian, Fujian Province, in 1998, was the first project of a MW-scale biomass power plant in China. Many improvements had been made in the 1 MW system as compared to the former 200 kW system. However, the overall efficiency of 1 MW system is still less than 20% [12], mainly due to the limited efficiency of internal gas engine generator. The 1 MW gasification and power generation system in this study consisted of an air-blown fluidized bed gasifier, a combined gas cleaner, five 200 kW gas engines, and a wastewater treatment system. For the first time a more efficient system that combines gas engine and steam turbine is employed in the 5.5 MW project [12], which is located in Xinghua, Jiangsu Province. But there

Table 9: Major parameters for biomass power plant.

Items	25 MW biomass-only fired	140 MW cofiring	25 MW cofiring	1 MW gasification	5.5 MW gasification
Electric efficiency[a]	25.6%	35.4%	27.6%	18.0%	27.0%
Electric efficiency before cofiring		36.1%	28.0%		
Cofiring ratio by energy		20%	15%		
Auxiliary power consumption rate[b]	8%	10%	8%	10%	10%
Annual operating hours (h)	6500	7000	7000	6000	6000
Annual power supply[c] (GJ)	538200	571536	78246	19440	106920
Life expectancy (year)	15	10	10	15	15
Capital investment (10^4 yuan)[d]	24145	8413	1155	428	3350
Annual cost (10^4 yuan)[e]	3255	1148	230	92	572
CH_4 emission[f] (kg/GJ biomass)	0.0037	0.0037	0.0037	0.0037	0.0037
N_2O emission[f] (kg/GJ biomass)	0.0105	0.0105	0.0105	0.0105	0.0105
SO_2 emission[g] (kg/GJ biomass)	0.2393	0.0299	0.0299	0.0008	0.0008
NO_x emission[h] (kg/GJ biomass)	0.0590	0.3291	0.3300	0.1733	0.1733

[a] Utility boiler efficiency decrease: 1% for each 10% of coal replaced by biomass (on an energy basis) [2].

[b] Energy consumption of biomass crushing is included.

[c] The energy inputs of the boiler in cofiring plant remain the same as before. The biomass-related power output was listed as the annual power supply of cofiring plant.

[d] Investment on feedstock supply system is not included.

[e] The annual cost consists of depreciation cost, maintenance, materials, and personnel. The cost of feedstock supply is not included.

[f] Since all the carbon in the biomass is recycled, it has been assumed that biomass fuel combustion does not produce GHG emissions due to CO_2. The CH_4 and N_2O emission factors of biomass-only fired plant and biomass gasification system were taken from Wang [25]. In addition, the CH_4 and N_2O emission of internal engine is assumed to be the same as that of IGCC from Wang [25]. As in the cofiring case, the emission factors of CH_4 and N_2O were assumed to be the same as that of biomass-only fired system.

[g] For biomass gasification power plant, the SO_2 emission may vary significantly from one to another. The data of the 5.5 MW gasification system adopted here is converted from Jia [29]. And the 1 MW gasification system is assumed to have the same emission. Desulphurization device is not usually commissioned in a biomass-only fired plant, since sulfur content of biomass is usually low. The SO_2 emission of biomass-only fired plant is estimated to be 80% of that of feedstock. On the other hand, the SO_2 emission factor of cofiring plant is estimated to be 10%, for desulphurization is commonly used. The sulfur content of coal in the cofiring case is 1.29 wt% [16].

[h] The NO_x emission factor of biomass-only fired plant was converted from Liu et al. [8]. For biomass gasification power plant, the NO_x emission is converted from Jia [29]. And the 1 MW gasification system is assumed to have the same NO_x emission factor. NO_x emissions reduction can be achieved by cofiring and is calculated using an equation from Tillman [30], which can be expressed as $RNO_x = 0.0008C^2 + 0.0006C + 0.075$, where C is the percentage biomass cofiring on a calorific basis. The NO_x emission factor of coal before cofiring is 335.94 g/GJ coal [16].

are problems that remain to be solved, including lack of proper gas purification process and short continuous working time of the engine system. The 5.5 MW gasification power plant mainly comprises an atmospheric CFB gasifier, a gas-purifying system, 10 sets of 450 kW gas engines, a waste heat boiler, a 1.5 MW steam turbine, wastewater treatment and ash discharging systems, and so forth [12]. The data of biomass gasification plants in this study were mainly obtained from site-specific data and information.

Compared to biomass-only fired plants, cofiring offers two important advantages. Firstly, cofiring can take advantage of the higher efficiency of large-scale coal-fired power plants, even though boiler efficiency may decrease. Secondly, investment costs required to achieve bioelectricity production might be greatly reduced. However, there is still no subsidiary policy to support biomass cofiring in China. Only a few demonstration cases exist, like the Shiliquan Power Plant and several others. In addition, biomass price keeps increasing rapidly, leading to enormous fuel costs, and therefore the scheme has not been adopted in other power plants in China. The Shiliquan Power Plant is the first cofiring plant in China. Essential facilities were commissioned in a 140 MW generator set and crushed biomass is pneumatically conveyed into two cyclone burners in the boiler. The Shiliquan Power Plant and a 25 MW cofiring plant were taken as an example in this study. Data of cofiring plants was mainly collected from a report [23].

The major parameters of biomass power plants are shown in Table 9.

3.6. Data Classification for Biomass Power Generation (BPG) Systems. Inputs of BPG system from background economy consist of fuels, machinery, and other essential facilities. Corresponding IO sectors in the LCI model mainly include diesel, electricity, transport equipment, and ordinary machinery, equipment for special purpose, as indicated in Table 10. It is difficult to precisely classify the inputs into IO sectors, since the inputs involve almost all economic sectors and some data is highly aggregated. Thus data classification in this study follows rules below.

Table 10: Major expenditures and corresponding IO sectors.

Inputs	Sector category
Diesel	1-11 diesel
Electricity	1-17 electricity
Boiler, steam turbine, internal gas engine, handling equipment, air blower, drying equipment, and auxiliary equipment	14 ordinary machinery, equipment for special purpose
Transport vehicles	15 transport equipment
Generator, electricity transmission, and distribution equipment	16 electric equipment and machinery
Construction engineering, wiring, piping, and installation of electric equipment	22 construction
Transportation of equipment and materials[a]	23 transport, storage, postal, and telecommunications services
Technical service, insurance	25 other service activities

[a] The freight and miscellaneous charges of boiler, internal engine, steam turbine, and generator set were evaluated to be 0.6% of the purchase cost. The freight and miscellaneous charges of other equipment and materials were evaluated to be 7%.

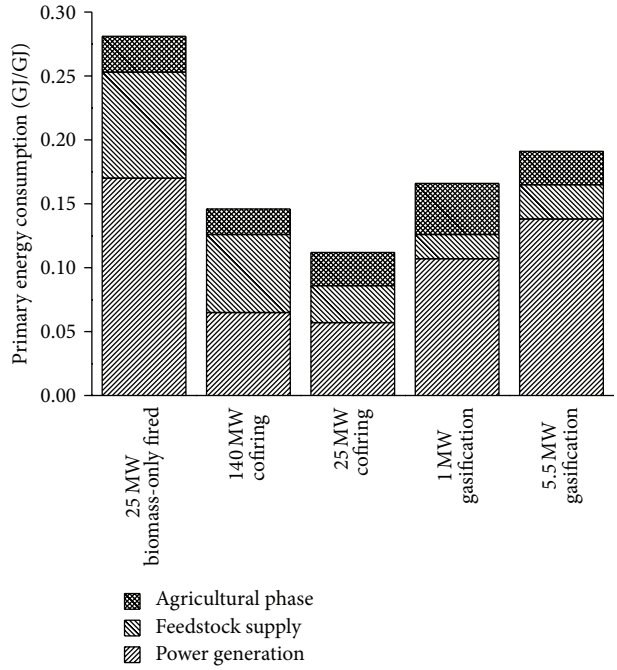

Figure 2: Comparison of PE consumptions of BPG systems.

(1) All inputs with clear category were classified according to the standards of classification of national economic industries [15]. For instance, boiler and steam turbine generator come from the sector "ordinary machinery, equipment for special purpose."

(2) Inputs without clear category were classified into the most related sectors based on evaluations of engineers.

(3) Maintenance inputs were classified into sectors of corresponding equipment and services.

(4) Purchase cost of equipment consists of prime cost and freight and miscellaneous charges. The freight and miscellaneous charges were classified into sector "transport, storage, postal, and telecommunications services."

4. Results and Discussion

4.1. Primary Energy (PE) Consumption. PE consumption represents the sum of direct and indirect consumptions of fossil fuel energy associated with unit output of electricity from biomass. The PE consumption of BPG systems can also be defined as the fossil fuel energy consumed within the system per electric energy delivered to the utility grid. The results expressed in GJ/GJ are shown in Figure 2. All the values related to each life cycle process are included. Taking into account the inputs of agricultural phase, the PE consumption of BPG systems is 0.11–0.28 GJ/GJ. The PE consumption of the electricity sector obtained by the model is 2.85 GJ/GJ in this study. Thus, a large amount of PE can be saved by using biomass in power generation.

The 25 MW cofiring system exhibits a lower PE consumption, followed by the 140 MW cofiring system, the 1 MW gasification system, the 5.5 MW gasification system, and the 25 MW biomass-only fired in an ascending sequence: 0.11 < 0.15 < 0.17 < 0.19 < 0.28 GJ/GJ, respectively. Without the agricultural inputs, BPG systems appear to be of the same sequence of PE consumption, ranging from 0.09 GJ/GJ to 0.25 GJ/GJ. The major reason may be that cofiring systems avoid inputs of plant construction that are found in intensively invested system such as biomass-only fired system. Another reason is that depreciation of original coal power plant property has not been allocated to biomass power. The agricultural inputs play a noticeable role, especially in the 1 MW gasification system. PE consumption in Figure 2 of agricultural phase is 0.02–0.04 GJ/GJ, which becomes 0.01-0.02 GJ/GJ when the inputs of chemical fertilizers are removed. The chemical fertilizers account for over 50% of the PE consumption in agricultural phase.

The PE consumption of feedstock supply accounts for a significant portion in the case of the 25 MW biomass-only fired system and the 140 MW cofiring system (see Figure 2). Despite a higher electric efficiency, the 140 MW cofiring system consumes more PE than the 25 MW cofiring system, mainly owing to significant inputs in feedstock supply. The distributed pattern can ensure a quality and stable feedstock supply for large-scale BPG systems, but requires intensive investments for construction and operation of straw-receiving stations. In addition, fuel consumptions may also increase significantly as a result of pretreatments and additional intermediate handlings. On the other hand, the centralized pattern involves less investments and fuel consumption, which may be the first choice for small-scale systems. But more attention needs to be paid to road maintenance and

Table 11: Energy saving performance of BPG systems.

Items	25 MW biomass-only fired	140 MW cofiring	25 MW cofiring	1 MW gasification	5.5 MW gasification
Energy savings[a] (GJ/GJ)	2.57	3.44	4.42	2.68	2.66
Cost of energy saving (yuan/GJ)	29.5	10.5	8.3	21.8	22.3
Cost of energy saving (GJ biomass/GJ)	1.66	0.99	0.98	2.30	1.55

[a] In the case of cofiring systems, coal transportation in reference system was not taken into consideration.

utilization, for there would either be more capacity to be built or more traffic jams.

In addition to PE consumption, two other measures for assessing energy use can be defined:

$$\text{Energy savings} = \text{PE}_{\text{ref}} - \text{PE}_{\text{bio}},$$
$$\text{Cost of energy savings} = \frac{C_{\text{bio}}}{\text{PE}_{\text{ref}} - \text{PE}_{\text{bio}}}, \quad (8)$$

where PE_{ref} is the PE consumption of reference system, PE_{bio} is the PE consumption of BPG system, C_{bio} is the cost of biomass power generation, and C_{bio} can be expressed either in yuan/GJ or in GJ biomass/GJ. Due to the scarcity of biomass resources, the consumption of biomass may be regarded as another kind of cost.

The energy savings represent the amount of PE saved when unit electric energy from biomass is delivered to the utility grid. The cost of energy savings measures the amount of investment for every unit of PE saved by the BPG system. These two indicators may provide a better means of assessing the BPG systems. Comparing the results presented in Table 11, it can be observed that cofiring biomass resources in a coal power plant give better energy saving behavior than their conversion in biomass-only fired plant and biomass gasification plant. The highest energy savings are found in the 25 MW cofiring system, which means 4.42 GJ of PE can be saved when 1 GJ of electricity produced from biomass is delivered. The highest energy saving cost in yuan/GJ is found in the 25 MW biomass-only fired system, due to its intensive capital investments. On the other hand, the 1 MW gasification system appears to have a much higher energy saving cost in GJ biomass/GJ than the other BPG systems, as a result of low electric efficiency.

4.2. GHG Emissions. The GHG emission intensity of BPG systems is defined as the GHG emission by the system per electric energy from biomass delivered to the utility grid, which includes the direct and indirect GHG emissions. By the commonly referred IPCC global warming potentials ($CO_2 : CH_4 : N_2O = 1 : 21 : 310$), the GHG emissions of each BPG system assessed are shown in Figure 3. The GHG emission intensity of BPG systems is 26–44 kg CO_2 eq/GJ, out of which the inputs of agricultural phase account for about 13%. A GHG emission intensity of 264 kg CO_2 eq/GJ of the electricity sector is obtained in this study. Large amounts of GHG emission can be avoided by using biomass to substitute fossil energy in power generation. It should

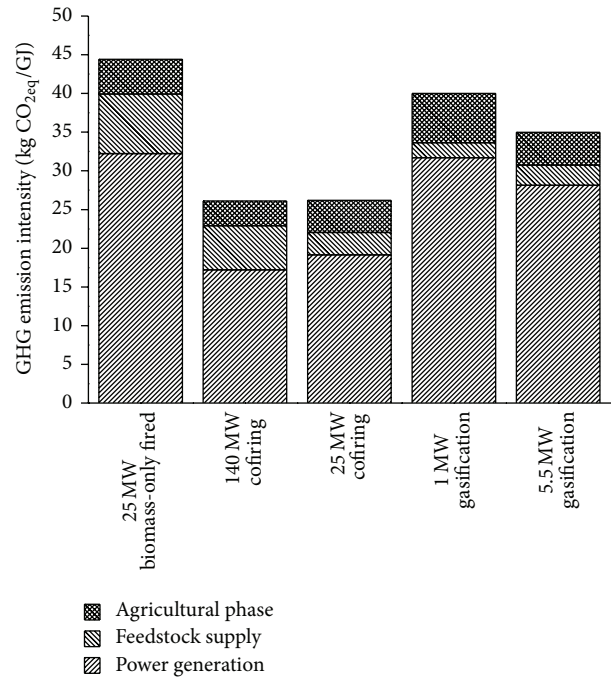

Figure 3: Comparison of GHG emission intensities of BPG systems.

be noted that the 1 MW gasification system has a higher GHG emission intensity but a lower PE consumption than the 5.5 MW gasification system. Due to the lower electric efficiency, more biomass feedstock is consumed by the 1 MW gasification system per unit electric energy delivered, leading to more GHG emission from agricultural phase and biomass combustion.

For all systems, the majority of GHG emission comes from the life stage of power generation. N_2O emission, specifically, from combustion of biomass fuels has significant contributions. In the cofiring cases, the results might differ widely from that obtained by the other researchers. According to Sebastián et al., biomass pretreatments account for more than 50% of biomass-related GHG emissions [2]. The major reason for this discrepancy may be that the energy consumption of feedstock crushing, which is the most energy-intensive operation, has been regarded as self-consumption of plants in this study. Other than that, the results are in good agreement with Liu et al. [8]. GHG emissions in the agricultural phase account for 10–16% of the

Table 12: GHG emission reduction of BPG systems.

Items	25 MW biomass-only fired	140 MW cofiring	25 MW cofiring	1 MW gasification	5.5 MW gasification
GHG emission reductions (kg CO_2 eq/GJ)	220	404	517	224	229
Cost of GHG emission reductions (yuan/kg CO_2 eq)	0.34	0.09	0.07	0.26	0.26
Cost of GHG emission reductions (GJ biomass/kg CO_2 eq)	0.019	0.008	0.008	0.028	0.018

total, mainly due to fertilizer production and the N_2O emission caused by N-fertilizer utilization. Another important aspect that should be noticed is the significant contribution of infrastructure, equipment, and maintenance of the plant, which require the input of various types of materials, fossil fuels, and the consequent GHG emissions. For the 1 MW gasification system, the inputs of infrastructure, materials, and maintenance of the plant account for about 25% of the system's GHG emission. In some way, the importance of system completeness when conducting an LCA is testified. On the other hand, contributions of CO_2 emissions from tractor operation during biomass transportation are relatively small.

Similar to the energy saving indicators, two other measures for assessing GHG emission reduction can be defined:

$$\text{GHG emission reductions} = \text{EM}_{\text{ref}} - \text{EM}_{\text{bio}},$$
$$\text{Cost of GHG emission reductions} = \frac{C_{\text{bio}}}{\text{EM}_{\text{ref}} - \text{EM}_{\text{bio}}}, \quad (9)$$

where EM_{ref} is the GHG emission intensity of reference system and EM_{bio} is the GHG emission intensity of BPG system.

The GHG emission reductions represent the amount of GHG emission avoided per electric energy from biomass delivered to the utility grid. The cost of GHG emission reductions measures the amount of investment for every unit of GHG emission avoided by the BPG system. The cofiring plant performs better than the biomass-only fired plant and the biomass gasification plants in GHG emission reductions, as indicated in Table 12. The comparison results of GHG emission reductions are similar to that of energy savings, since the GHG emission reductions are roughly linear to the energy consumption savings.

4.3. SO_2 and NO_x Emissions. The SO_2 (or NO_x) emission intensity of BPG systems is defined as the SO_2 (or NO_x) emission by the system per electric energy from biomass delivered to the utility grid. The SO_2 emission intensity of BPG systems is 0.13–1.20 kg SO_2/GJ. The SO_2 emission intensity of BPG systems is 0.36–1.34 kg NO_x/GJ. For all systems, the majority of SO_2 and NO_x emission comes from the combustion of biomass fuel, as shown in Figures 4 and 5.

The sulfur content of biomass is much lower than that of coal. On the other hand, desulphurization involves a large amount of investment. For these two reasons, desulphurization device is not usually equipped in the biomass-only fired system in China. Desulphurization device of the coal-fired power plant can effectively remove the SO_2 for the cofiring system, just as the water scrubber does for the biomass gasification systems. As expected, the worst SO_2 emission performance is that of the 25 MW biomass-only system.

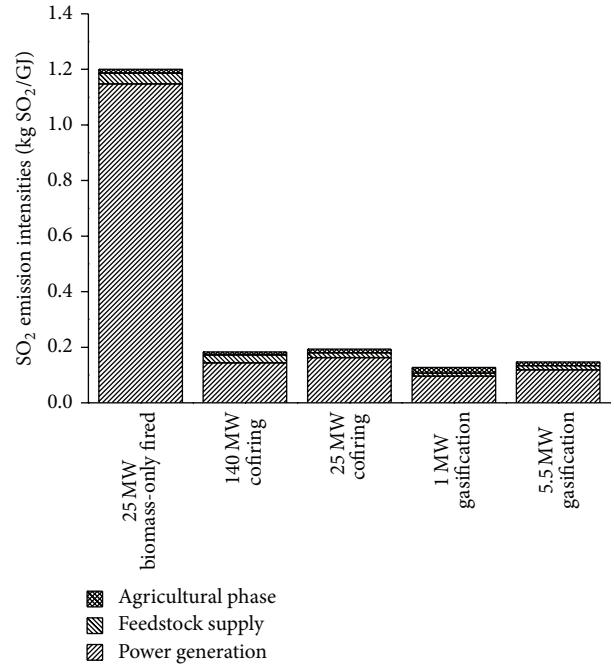

Figure 4: Comparison of SO_2 emission intensities of BPG systems.

Comparing the SO_2 emission intensities of 1.79 kg SO_2/GJ of the electricity sector obtained by the hybrid LCI model, BPG systems can anyhow provide a significant reduction in SO_2 emissions, due to the very low sulfur content of biomass. Despite the relatively low SO_2 emissions intensities, the cofiring systems exhibit a small capacity for reducing SO_2 emissions (Table 13). An explanation can be given by the assumptions made in this study: the SO_2 emission factor of the cofiring system was 10%, while only 48% of coal power plants were estimated to use desulphurization in the calculation associated with electricity sector.

NO_x emission of BPG systems is mainly from biomass fuel combustion. The NO_x formation is influenced by many

Table 13: SO_2 and NO_x emission reductions of BPG systems.

Items	25 MW biomass-only fired	140 MW cofiring	25 MW co-firing	1 MW gasification	5.5 MW gasification
SO_2 emission reductions (kg SO_2/GJ)	0.59	0.46	0.62	1.67	1.64
NO_x emission reductions (kg NO_x/GJ)	0.80	0.21	0.30	0.04	0.39

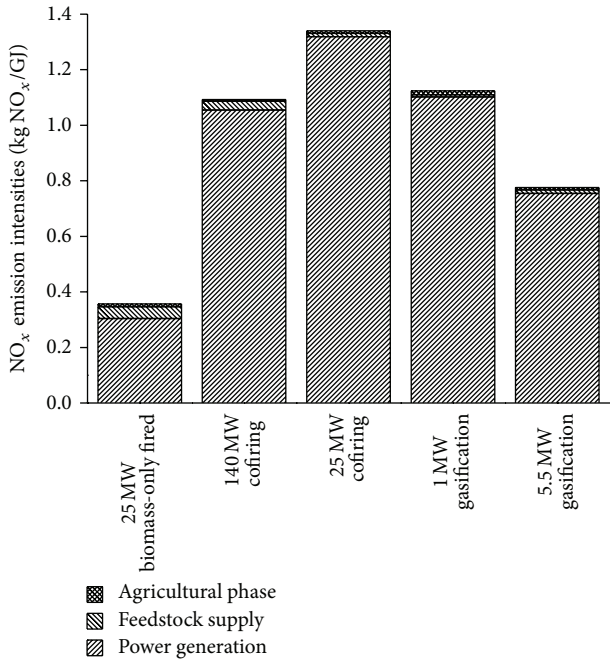

Figure 5: Comparison of NO_x emission intensities of BPG systems.

factors such as combustion temperature, concentration of oxygen, residence time, and the content of fuel-bound nitrogen. The cofiring systems and the biomass gasification systems can slightly decrease the NO_x emission, whereas the 25 MW biomass-only fired system performs significantly better in NO_x emission reductions, despite the fact that no denitrification measures are considered (Table 13).

5. Conclusions

Methodological constraints of process-based life-cycle analysis, particularly a problem associated system boundary selection, may lead to some uncertainties in the LCI results. A hybrid LCI framework can ensure the completeness of system boundary and provide a desirable method for quantifying a system's environmental footprint.

There are currently a number of biomass power plants in China. The government has not offered any guidance on preferred type, leaving the market open. A comparative study is necessarily important. In this paper, a hybrid LCI model is used to comparatively evaluate five BPG systems, which may represent the present state-of-the-art in China. A preliminary feasibility estimation of the biomass power in China is provided in terms of primary energy (fossil energy) savings, GHG emission reductions, and avoided emissions of SO_2 and NO_x.

To get 1 GJ electricity from corn stovers, only 0.11–0.28 GJ of primary energy (PE) is consumed by BPG systems, whereas primary energy as much as 4.42 GJ can be saved by substituting conventional electricity. At the same time, the BPG systems only contribute 26–44 kg CO_2 eq of GHG emissions, while up to 517 kg CO_2 eq of GHG missions can be avoided. The cofiring systems, especially the 1 MW cofiring system, can achieve the highest PE savings and GHG emission reductions per electric energy from biomass delivered to the utility grid. Moreover, the PE savings and GHG emission reductions are accomplished at a lower cost of biomass resource and monetary investment. Thus the cofiring systems give better behavior than the biomass-only fired system and the biomass gasification systems. For all systems, the life stage of power generation is responsible for the largest share of PE consumptions and GHG emissions. N_2O emission from combustion of biomass fuels has made a significant contribution to GHG emission. Another important aspect that should be addressed is the significant contributions of infrastructure, equipment, and maintenance of the plant, which may be easily ignored in a process-based LCI. Inputs of various types of fossil fuels, materials, and services are required in construction and operation of a biomass plant. And the consequent PE consumptions and GHG emissions should be taken into consideration.

The emission intensities of SO_2 and NO_x of BPG systems are evaluated to be 0.13–1.20 kg SO_2/GJ and 0.36–1.34 kg NO_x/GJ, respectively, the majority of which come from the combustion of biomass fuels. Compared with conventional electricity, emission reductions of SO_2 and NO_x can be achieved by all BPG systems.

The innovative base of comparison between BPG systems has allowed assessment and comparison of the five electricity production system alternatives with agricultural residues. From the case presented, it is shown that BPG systems could be a high-potential alternative for electricity generation. In addition to the environmental benefits quantified in this LCI, BGP systems will provide other benefits as they are deployed in China, such as rural economic development through the creation of new markets and jobs. A specific LCI study should take into consideration local conditions such as the normal routes of biomass disposal and energy consumption structure, which may have significant effects on results. Moreover, it has to be noted that, by expanding the scope of analysis in hybrid LCA, the level of precision is lost due to the use of highly coarse and aggregated data in input-output table that involved significant amounts of uncertainties and assumptions. The choice of process

parameters and allocation procedures can have significant effects on results as well. Although much work is currently being undertaken to determine several values used in this analysis in a more precise way, the main conclusion that can be highlighted is that, based on the values and assumptions used, the cofiring system is more beneficial than biomass-only fired power plant and biomass gasification system, when the PE savings and GHG emission reductions are taken into account.

Conflict of Interests

The authors declare that there is no conflict of interests regarding the publication of this paper.

Acknowledgments

This study has been supported by the National Key Technology R&D Program in the 12th Five-Year Plan of China (Grant no. 2012BAA09B03), the National Natural Science Foundation (Grant no. 51176194), and in part by the Strategic Emerging Industries of Guangdong (Grant no. 2012A032300019).

References

[1] National Development and Reform Commission, *State Plans for Medium and Long-Term Development of Renewable Energy*, National Development and Reform Commission, 2007.

[2] F. Sebastián, J. Royo, and M. Gómez, "Cofiring versus biomass-fired power plants: GHG (Greenhouse Gases) emissions savings comparison by means of LCA (Life Cycle Assessment) methodology," *Energy*, vol. 36, no. 4, pp. 2029–2037, 2011.

[3] D. Y. C. Leung, X. L. Yin, and C. Z. Wu, "A review on the development and commercialization of biomass gasification technologies in China," *Renewable and Sustainable Energy Reviews*, vol. 8, no. 6, pp. 565–580, 2004.

[4] C. Z. Wu, X. L. Yin, L. L. Ma, Z. Q. Zhou, and H. P. Chen, "Design and operation of A 5.5 MWe biomass integrated gasification combined cycle demonstration plant," *Energy and Fuels*, vol. 22, no. 6, pp. 4259–4264, 2008.

[5] Y. J. Jia, Z. Yu, and C. Z. Wu, "Life cycle assessment of 4MWe biomass integrated gasification gas engines-steam turbine combined-cycle power plant," *Acta Energiae Solaris Sinica*, vol. 25, no. 1, pp. 56–62, 2004.

[6] W. Wang, D. Q. Zhao, H. L. Yang, J. Y. Cai, and P. Chen, "Life cycle analysis on biomass gasification and power generation system and inquiry to assessment method," *Acta Energiae Solaris Sinica*, vol. 26, no. 6, pp. 752–759, 2005.

[7] L. Lin, D. Q. Zhao, G. P. Wei, and S. Y. Liu, "Life cycle assessment of biomass direct combustion power generation system," *Water Conservancy & Electric Power Machinery*, vol. 28, no. 12, pp. 18–23, 2006 (Chinese).

[8] H. T. Liu, K. R. Polenske, Y. M. Xi, and J. Guo, "Comprehensive evaluation of effects of straw-based electricity generation: a Chinese case," *Energy Policy*, vol. 38, no. 10, pp. 6153–6160, 2010.

[9] S. Suh, M. Lenzen, G. J. Treloar et al., "System boundary selection in life-cycle inventories using hybrid approaches," *Environmental Science and Technology*, vol. 38, no. 3, pp. 657–664, 2004.

[10] M. Lenzen, "Errors in conventional and input-output-based life-cycle inventories," *Journal of Industrial Ecology*, vol. 4, no. 4, pp. 127–148, 2001.

[11] R. Inaba, K. Nansai, M. Fujii, and S. Hashimoto, "Hybrid life-cycle assessment (LCA) of CO_2 emission with management alternatives for household food wastes in Japan," *Waste Management and Research*, vol. 28, no. 6, pp. 496–507, 2010.

[12] C. Z. Zhu, "Discussion of coal power related to China's energy security," *Sino-Global Energy*, vol. 17, no. 1, pp. 29–32, 2012 (Chinese).

[13] National Bureau of Statistics (NBS), *Input-Output Tables of China*, China Statistic Press, Beijing, China, 2009 (Chinese).

[14] CESY, *China Energy Statistical Yearbook*, China Statistical Publishing House, Beijing, China, 2008, (Chinese).

[15] GB/T 4754-2002, *Classification of National Economic Industries*, Standards Press of China, 2002.

[16] G. Peters, C. Weber, and J. Liu, "Construction of Chinese energy and emissions inventory," Norwegian University of Science and Technology Industrial Ecology Programme Reports and Working Papers, 2006.

[17] CSY, *China Statistical Yearbook*, National Bureau of Statistics of China, 2008, http://www.stats.gov.cn/tjsj/ndsj/2008/indexch.htm.

[18] IPCC, *The 2006 IPCC Guidelines for National Greenhouse Gas Inventories (2006 Guidelines)*, 2006.

[19] G. Q. Chen and B. Zhang, "Greenhouse gas emissions in China 2007: inventory and input-output analysis," *Energy Policy*, vol. 38, no. 10, pp. 6180–6193, 2010.

[20] CIESY, *China Industry Economics Statistical Yearbook 2008*, China Statistical Publishing House, Beijing, China, 2008, (Chinese).

[21] NPCS, "National Product Cost Survey," Price Department of National Development and Reform Commission, 2008, http://www.npcs.gov.cn/web/Column.asp?ColumnId=13.

[22] H. C. Liu, X. L. Yin, and C. Z. Wu, "Cost analysis of crop residue supplies," *Transactions of the Chinese Society of Agricultural Machinery*, vol. 42, no. 1, pp. 106–112, 2011.

[23] ESD and CRED, *Reasearch on Market Innovation Mechanisms and Policies and Regulations of Development of Biomass Co-Firing in China*, 2007.

[24] "Cleaner production standard for coal mining ans processing industry," HJ446-2008, Ministry of Environmental Protection, 2008.

[25] M. Q. Wang, "GREET 1.5—transportation fuel-cycle model volume 1: methodology, development, use, and results," Tech. Rep., Center for Transportation Research, Energy Systems Division, Argonne National Laboratory, 1999.

[26] C. P. Liao, C. Z. Wu, Y. J. Yan, and H. T. Huang, "Chemical elemental characteristics of biomass fuels in China," *Biomass and Bioenergy*, vol. 27, no. 2, pp. 119–130, 2004.

[27] X. H. Song, *Analysis of development trend of petroleum refining industry [Master thesis of School of Economics and Management]*, Tsinghua University, 2004 (Chinese).

[28] H. Z. Tian, J. M. Hao, and Y. Q. Lu, "Nitrogen oxides emissions arising from commercial energy consumption in China," *Environmental Science*, vol. 22, no. 6, pp. 24–28, 2001 (Chinese).

[29] Y. J. Jia, *A methodology and application for sustainability assessment of bioenergy systems [Ph.D. thesis]*, Department of Thermal

Science and Energy Engineering, University of Science and Technology of China, 2004.

[30] D. A. Tillman, "Biomass cofiring: the technology, the experience, the combustion consequences," *Biomass and Bioenergy*, vol. 19, no. 6, pp. 365–384, 2000.

Hindawi Publishing Corporation
The Scientific World Journal
Volume 2014, Article ID 139653, 5 pages
http://dx.doi.org/10.1155/2014/139653

Research Article

Synergistic Microbial Consortium for Bioenergy Generation from Complex Natural Energy Sources

Victor Bochuan Wang,[1,2] Joey Kuok Hoong Yam,[1,3] Song-Lin Chua,[1,4] Qichun Zhang,[2] Bin Cao,[1,5] Joachim Loo Say Chye,[1,2] and Liang Yang[1,6]

[1] *Singapore Centre on Environmental Life Sciences Engineering (SCELSE), Nanyang Technological University, Singapore 637551*
[2] *School of Materials Science and Engineering, Nanyang Technological University, Singapore 639798*
[3] *Interdisciplinary Graduate School, Nanyang Technological University, Singapore 637551*
[4] *Graduate School of Integrative Sciences and Engineering, National University of Singapore, Singapore 117543*
[5] *School of Civil and Environmental Engineering, Nanyang Technological University, Singapore 639798*
[6] *School of Biological Sciences, Nanyang Technological University, Singapore 637551*

Correspondence should be addressed to Joachim Loo Say Chye; joachimloo@ntu.edu.sg and Liang Yang; yangliang@ntu.edu.sg

Received 7 May 2014; Accepted 16 June 2014; Published 6 July 2014

Academic Editor: Yang-Chun Yong

Microbial species have evolved diverse mechanisms for utilization of complex carbon sources. Proper combination of targeted species can affect bioenergy production from natural waste products. Here, we established a stable microbial consortium with *Escherichia coli* and *Shewanella oneidensis* in microbial fuel cells (MFCs) to produce bioenergy from an abundant natural energy source, in the form of the sarcocarp harvested from coconuts. This component is mostly discarded as waste. However, through its usage as a feedstock for MFCs to produce useful energy in this study, the sarcocarp can be utilized meaningfully. The monospecies *S. oneidensis* system was able to generate bioenergy in a short experimental time frame while the monospecies *E. coli* system generated significantly less bioenergy. A combination of *E. coli* and *S. oneidensis* in the ratio of 1 : 9 (v : v) significantly enhanced the experimental time frame and magnitude of bioenergy generation. The synergistic effect is suggested to arise from *E. coli* and *S. oneidensis* utilizing different nutrients as electron donors and effect of flavins secreted by *S. oneidensis*. Confocal images confirmed the presence of biofilms and point towards their importance in generating bioenergy in MFCs.

1. Introduction

Unprecedented industrialization and the continued spurt in population growth have vastly depleted global natural energy sources. This has led to an acute need for alternative, clean, and renewable energy sources. In particular, extensive efforts have been invested into increasing efficiencies of solar cells [1], which has been envisioned as the next frontier in renewable energy. Another potential source of alternate energy lies in producing bioenergy from agricultural waste products via microbial activity.

One potential approach to producing bioenergy from natural waste products is through microbial fuel cells (MFCs) which employ the extracellular electron transport (EET) functionalities of electrochemically active bacteria (EAB) to facilitate electron transport and thus produce electricity from diverse energy sources [2]. The free electrons and protons originate from microbial metabolism of organic components found in the media within an anaerobic anode chamber. Metabolism is achieved when electrons move along the cascading energy pathway of the electron transport chain, which releases energy for continued survival of the microorganism. These electrons are further transported by various EET mechanisms to the external terminal electron acceptors. A voltage is generated in the process of electrons moving across the external resistor towards the cathode. Protons diffuse simultaneously across the selective proton exchange membrane to the aerobic cathode chamber. In this compartment, oxygen is reduced by electrons and protons to produce water molecules in order to complete the charge

balance. Although this technology has matured over time and shows promise in concurrent bioremediation and power generation [3], it has seen little commercial success. This is due to high material cost and low power performance that is partly caused by limitations in inferior charge transport at the inherently insulating microbe-electrode interface. Much effort has been invested in circumventing these bottlenecks. Recently, enhanced power output in MFCs has been demonstrated through chemical modification of the insulating interface junction across *Escherichia coli* cellular membrane [4, 5] and genetic engineering of *Pseudomonas aeruginosa* to enhance endogenous secretion of pyocyanin mediators [6]. Further, small-scale stacked MFCs have been shown to power mobile devices using human urine as an energy source [7]. Better understanding of microbial species interactions employing EET processes has been proposed as a promising strategy to improve the performance of MFCs [8, 9].

In this contribution, a synergistic microbial consortium was established and modified for bioenergy generation from a complex energy source, in the form of the coconut sarcocarp, which is defined as the fleshy part of the fruit. According to statistics from the Food and Agriculture Organization of the United Nations, ~54 million tonnes of coconut were produced in 2010 from mainly tropical coastal countries, of which a large amount is wasted [10, 11]. However, coconuts are known to be rich sources of sugars, fats, oil, and carbohydrates with small beneficial concentrations of vitamins and salts [12]. Hence, coconuts which are considered as waste products can be potentially used as an alternative and natural energy source for tropical coastal countries.

By choosing the model non-EAB (*E. coli*) and the EAB (*Shewanella oneidensis*), we demonstrate that modification of the ratio of bacterial strains introduced into the microbial consortium can significantly improve MFC performance.

2. Materials and Methods

2.1. Media Preparation and Bacterial Strains. The sarcocarp from a fresh coconut was removed and homogenized using a Bio-Gen PRO200 Homogenizer (PRO Scientific Inc, USA) at maximum speed for 5 min. All parts of the equipment were dismantled and wiped down with 70% ethanol to adhere to sterility requirements. Further, the homogenization process took place inside a sterile biosafety cabinet to avoid contamination. The resulting slurry was further diluted 2x with sterile deionized water to form the medium for dispensing into the MFCs. Monocultures of *E. coli* (red fluorescent protein (RFP) tagged) and *S. oneidensis* (green fluorescent protein (GFP) tagged) [13] were grown aerobically overnight in lysogeny broth (LB) at 37°C and 30°C, respectively, while shaking at 200 rpm.

2.2. Setup of MFCs. All materials were used as received, unless otherwise stated. Dual-chamber MFCs were constructed as previously described [3, 4, 6]. 19 mL of diluted sarcocarp slurry was dispensed into the anode chamber, prior to inoculation of the bacterial strains. 1 mL of culture (OD_{600}~1.0) for each bacterial strain was then inoculated into the anode chamber only. Final volume of each chamber is maintained at 20 mL. The incubator housing of the MFCs was set to 33°C. Data recording started immediately after inoculation. Glass tubes (17 mm O.D. × 1.8 mm wall thickness) forming the anode and cathode chambers of the MFCs, carbon felt (3.18 mm thickness), and stainless steel pinch clamps (#28) were purchased from VWR Pte. Ltd. Titanium wire (0.25 mm diameter), Nafion N117 proton exchange membrane (PEM), and serrated silicone septa (18 mm O.D.) were purchased from Sigma-Aldrich. Nylon screws and nuts were purchased from Small Parts, Inc. 90° O-ring-groove-to-plain-end glass tubes were separated from each other by a piece of Nafion N117 proton exchange membrane. The joints of the glass tubes were greased and sealed against a circular piece of Nafion membrane (diameter of 2 cm). The whole assembly was held in place and tightened with a stainless steel pinch clamp. Carbon felt electrodes were cut to 2 cm × 5 cm dimensions (width × length) and connected to the titanium wire via the screws and nuts. The electrodes were then seated inside the glass tubes. Prior to MFC operation, the devices were filled with ultrapure water and autoclaved to sterilize the internal components in the devices. After sterilization, the water was dispensed and diluted sarcocarp slurry was introduced to both chambers. The anode chamber was sealed with a silicone septum through which the titanium wire was threaded, while the cathode chamber was loosely capped with an inverted glass scintillation vial to provide an aerobic environment. The cathode electrodes were only partly submerged in the catholyte to allow for an "air-wicking" aerobic configuration. The electrodes were then connected to a 1 kΩ resistor and voltage measurements across the resistors were recorded at a rate of 1 point per 5 minutes using an eDAQ e-corder data acquisition system (Bronjo Medi) equipped with Chart software. Voltage readings are collected as raw data and further converted to current density for presentation. Current is calculated according to the following equation:

$$I = \frac{V}{R}, \tag{1}$$

where I is the current in amperes (A), V is the potential difference in volts (V), and R is the resistance in ohms (Ω). Current density is obtained by dividing the equation above by the geometrical surface area of the electrode (by 20 cm^2).

2.3. Biofilm Imaging. Electrodes from the anode chamber were removed from the corresponding MFCs. All microscopy images of RFP-tagged *E. coli* and GFP-tagged *S. oneidensis* biofilms formed on the electrode surface were acquired by Carl Zeiss Confocal Laser Scanning Microscope (CLSM model LSM 780) (Carl Zeiss, Germany) with 40x objective lens after mounting the electrode fibers onto microscope slides. Image processing was performed with the software package, Zen 2011, provided by Carl Zeiss.

3. Results and Discussion

3.1. Electrical Performance. Dual-chamber MFCs were employed to investigate the bioenergy generated as the coconut sarcocarp is broken down through microbial oxidation by

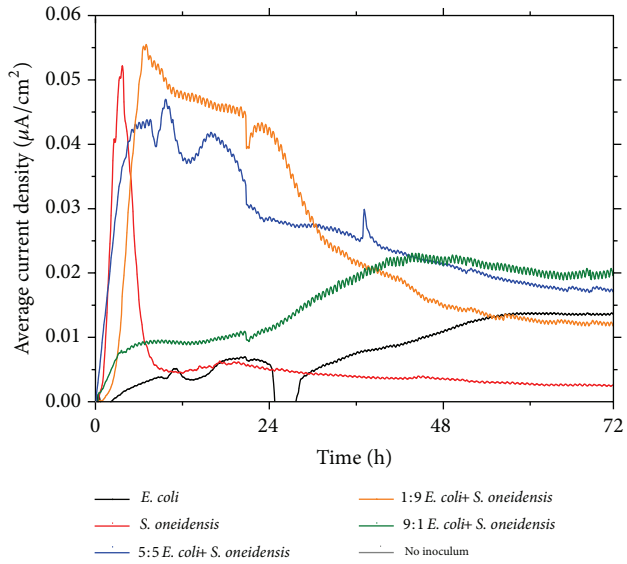

FIGURE 1: Average current density versus time of MFCs with various bacterial species and ratios.

the respective bacterial species. The average current densities generated over 72 h were recorded (Figure 1). The consistently low current densities from all operated MFCs were attributed to high internal resistances within the bioelectrochemical devices, which impede charge movement. Further, the media in the anode and cathode chambers contained the sarcocarp slurry, which has limited conductivity. This can be averted through various forms of optimization, such as adopting different device architectures [14], apparatus components, or electrode engineering [15]. However, the focus of this study was to demonstrate facile bioenergy generation through the use of a natural, abundant, and readily available energy source, coconut sarcocarp, by employing common bacterial species. MFCs inoculated with *E. coli* generated an average maximum current density of ~0.015 μA/cm^2 (Figure 1, black trace), whereas *S. oneidensis* MFCs generated ~0.05 μA/cm^2 (Figure 1, red trace). The rapid decrease in average current density generated by the *S. oneidensis* MFCs after ~6 h is caused by the depletion of suitable energy sources available for *S. oneidensis*. This is because the single fed batch MFC system was employed in this study, which is in contrast to a continuous fed system, where the energy source can be renewed through a steady exchange of spent and fresh medium. The average current density generated by the *S. oneidensis* MFCs stabilized at a significantly lower current density of ~0.005 μA/cm^2 up to 72 h. MFCs without any inoculum were also operated and negligible current density was generated (Figure 1, grey trace). This indicates that the observed current densities were driven by the microbial actions of *E. coli* and *S. oneidensis* mono- and cocultures on the sarcocarp.

It has been well established that electrochemically active *S. oneidensis* has various forms of EET mechanisms, such as conducting outer membrane cytochromes [16], nanoappendages [17], and secretion of flavins [18], which act as charge transport mediators. These mechanisms are electrical conduits to transfer microbially released electrons to terminal electron acceptors. The ~3-fold difference in average maximum current density from monoculture systems is attributed to poorly evolved *E. coli* EET mechanisms which lack the diversity and effectiveness of EET mechanisms in *S. oneidensis*. Notably, significant bioenergy generation by *S. oneidensis* started from an early stage, while output from *E. coli* only started to increase later. This suggests that *S. oneidensis* and *E. coli* might utilize different energy sources present in the sarcocarp for bioenergy generation. It is further hypothesized that, in coculture MFCs containing *E. coli* and *S. oneidensis*, a possible synergistic effect involving flavins has been created. To test this hypothesis, coculture systems utilizing various ratios of *E. coli* and *S. oneidensis* were operated to investigate possible synergistic interactions. Interestingly, a 5 : 5 (50% : 50%, v : v) coculture system produced a maximum current density of ~0.045 μA/cm^2 (Figure 1, blue trace). As compared to the monoculture systems (Figure 1, red trace for *S. oneidensis*, black trace for *E. coli*), the 5 : 5 coculture system could generate a relatively sustainable and significant current density over 72 h. It is thus noteworthy to further probe the effect of different bacterial ratios on the extent of bioenergy generation. A 1 : 9 (v : v) *E. coli* and *S. oneidensis* system generated a maximum current density of ~0.055 μA/cm^2 (Figure 1, orange trace), whereas a 9 : 1 (v : v) *E. coli* and *S. oneidensis* system generated a maximum current density of ~0.025 μA/cm^2 (Figure 1, green trace). The ratio modification study suggests that introducing a higher concentration of *S. oneidensis* in the coculture systems allows for maximum exploitation of suitable energy sources for *S. oneidensis*. This strategy may minimize consumption of such energy sources by *E. coli*,which generates significantly lesser bioenergy, and facilitate generation of excess secreted flavins to enhance *E. coli* bioenergy generation at a later stage when the species uses suitable energy sources for itself.

3.2. Biofilm Characterization. Further, the role of biofilms in the bioelectrochemical systems was elucidated by confocal microscopy characterization. Representative overlaid bright-field and confocal images were acquired from random strands of electrodes in respective MFCs. Biofilms were formed in all systems (Figures 2(a) and 2(b)). To differentiate between each species, *E. coli* was tagged with red fluorescent protein (RFP), whereas *S. oneidensis* was tagged with green fluorescent protein (GFP). The RFP-tagged *E. coli* biofilm and GFP-tagged *S. oneidensis* biofilm were evident on the electrode fiber surfaces (Figures 2(a) and 2(b)). The confocal images corroborate the importance of the biofilm in the electrical performances with specific bacterial strains.

3.3. Mechanistic Insights of the Functional Coculture System. The following possible mechanisms occurring in the coculture system were proposed (Figure 3). Various favourable nutrients (represented by blue and green dots) present in the sarcocarp can be broken down specifically by the independent microbial oxidative actions of non-EAB (*E. coli*) and

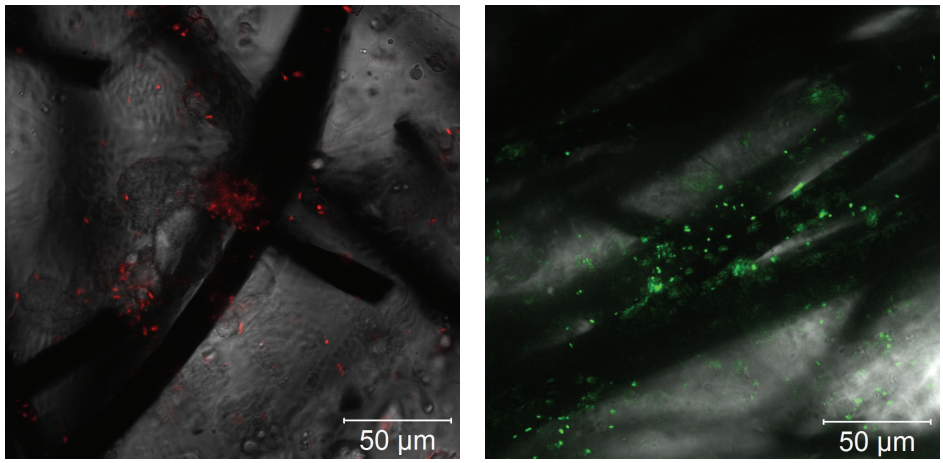

(a) (b)

Figure 2: Overlaid brightfield and confocal microscopy images of stained biofilms on respective electrodes. (a) *E. coli* biofilm. (b) *S. oneidensis* biofilm.

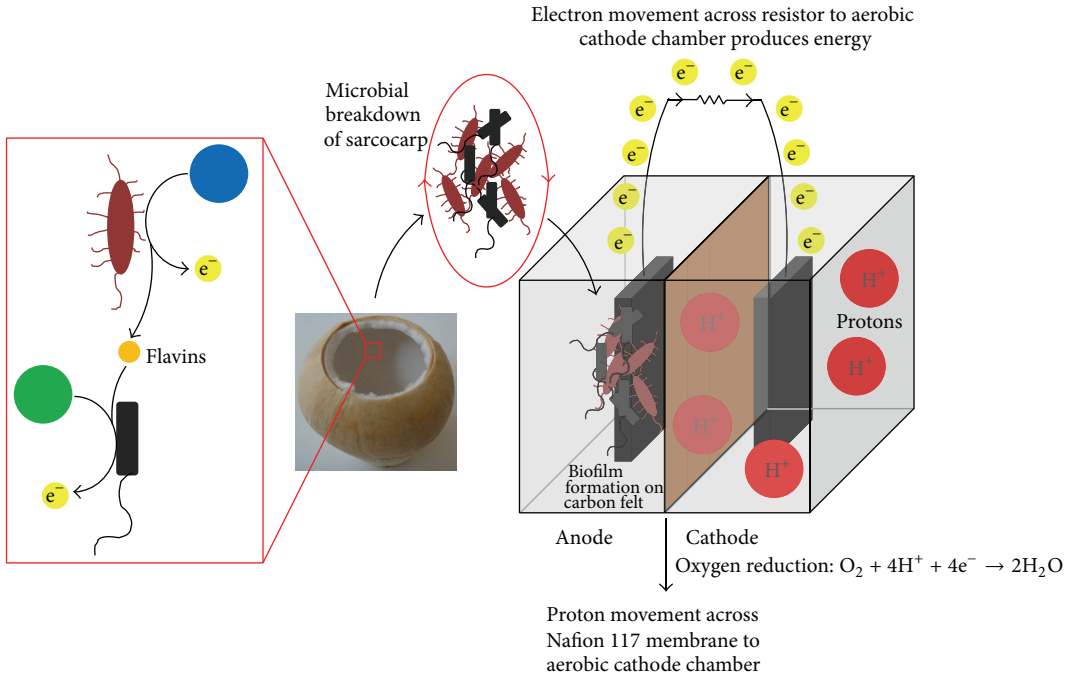

Figure 3: Diagram illustrating mechanistic reactions in coculture MFCs. Black schematic depicting nonelectrochemically active microorganisms, such as *E. coli*; red schematic depicting electrochemically active microorganisms, such as *S. oneidensis*; blue and green schematics depicting energy sources most favourable for breakdown by electrochemically active and nonelectrochemically active microorganisms, respectively.

EAB (*S. oneidensis*) in different stages of MFC operation to produce bioenergy. From the electrical data (Figure 2), it is suggested that, for significant and sustained bioenergy production, the EAB should be introduced at a higher concentration. This is to restrict nutrient consumption by non-EAB. The EAB also breaks down its suitable energy source and secretes flavins, which can be utilized by non-EAB at a later stage to facilitate EET. Gradual decline in current densities is due to lack of available nutrients in the closed system (Figure 1).

4. Conclusions

In summary, we have demonstrated bioenergy generation in MFCs by employing a natural and abundant feedstock, coconut sarcocarp. The common EAB, *S. oneidensis*, and the non-EAB, *E. coli*, were employed and a possible synergy was suggested, based on the ratio of microbial species introduced to the system. This demonstration paves the way forward for exploration of alternative and natural energy sources using mixed species consortia.

Conflict of Interests

The authors declare that there is no conflict of interests regarding the publication of this paper.

Acknowledgments

The authors acknowledge financial support from the Singapore Centre on Environmental Life Sciences Engineering (SCELSE) (M4330001.C70.703012), School of Materials Science and Engineering (M020070110), Nanyang Technological University, Singapore, and MOE Tier 2 Programme (MOE 2012-t2-2-024, ARC 2/13).

References

[1] G. Xing, N. Mathews, S. Sun et al., "Long-range balanced electron- and hole-transport lengths in organic-inorganic $CH_3NH_3PbI_3$," *Science*, vol. 342, pp. 344–347, 2013.

[2] D. R. Lovley, "The microbe electric: conversion of organic matter to electricity," *Current Opinion in Biotechnology*, vol. 19, no. 6, pp. 564–571, 2008.

[3] V. B. Wang, S.-L. Chua, Z. Cai et al., "A stable synergistic microbial consortium for simultaneous azo dye removal and bioelectricity generation," *Bioresource Technology*, vol. 155, pp. 71–76, 2014.

[4] V. B. Wang, J. Du, X. Chen et al., "Improving charge collection in *Escherichia coli*-carbon electrode devices with conjugated oligoelectrolytes," *Physical Chemistry Chemical Physics*, vol. 15, no. 16, pp. 5867–5872, 2013.

[5] H. Hou, X. Chen, A. W. Thomas et al., "Conjugated oligoelectrolytes increase power generation in *E. coli* microbial fuel cells," *Advanced Materials*, vol. 25, no. 11, pp. 1593–1597, 2013.

[6] V. B. Wang, S. Chua, B. Cao et al., "Engineering PQS biosynthesis pathway for enhancement of bioelectricity production in *Pseudomonas aeruginosa* microbial fuel cells," *PLoS ONE*, vol. 8, no. 5, Article ID e63129, 2013.

[7] I. A. Ieropoulos, P. Ledezma, A. Stinchcombe, G. Papaharalabos, C. Melhuish, and J. Greenman, "Waste to real energy: the first MFC powered mobile phone," *Physical Chemistry Chemical Physics*, vol. 15, no. 37, pp. 15312–15316, 2013.

[8] Z. Du, H. Li, and T. Gu, "A state of the art review on microbial fuel cells: A promising technology for wastewater treatment and bioenergy," *Biotechnology Advances*, vol. 25, no. 5, pp. 464–482, 2007.

[9] D. R. Lovley, "Microbial fuel cells: novel microbial physiologies and engineering approaches," *Current Opinion in Biotechnology*, vol. 17, no. 3, pp. 327–332, 2006.

[10] S. Sumathi, S. P. Chai, and A. R. Mohamed, "Utilization of oil palm as a source of renewable energy in Malaysia," *Renewable & Sustainable Energy Reviews*, vol. 12, no. 9, pp. 2404–2421, 2008.

[11] C. S. Goh, K. T. Tan, K. T. Lee, and S. Bhatia, "Bio-ethanol from lignocellulose: status, perspectives and challenges in Malaysia," *Bioresource Technology*, vol. 101, no. 13, pp. 4834–4841, 2010.

[12] D. M. Mourao, J. Bressan, W. W. Campbell, and R. D. Mattes, "Effects of food form on appetite and energy intake in lean and obese young adults," *International Journal of Obesity*, vol. 31, no. 11, pp. 1688–1695, 2007.

[13] Y. Zhang, C. K. Ng, Y. Cohen, and B. Cao, "Cell growth and protein expression of *Shewanella oneidensis* in biofilms and hydrogel-entrapped cultures," *Molecular BioSystems*, vol. 10, no. 5, pp. 1035–1042, 2014.

[14] B. R. Ringeisen, E. Henderson, P. K. Wu et al., "High power density from a miniature microbial fuel cell using *Shewanella oneidensis* DSP10," *Environmental Science & Technology*, vol. 40, no. 8, pp. 2629–2634, 2006.

[15] T. Zhang, Y. Zeng, S. Chen, X. Ai, and H. Yang, "Improved performances of *E. coli*-catalyzed microbial fuel cells with composite graphite/PTFE anodes," *Electrochemistry Communications*, vol. 9, no. 3, pp. 349–353, 2007.

[16] D. Coursolle, D. B. Baron, D. R. Bond, and J. A. Gralnick, "The Mtr respiratory pathway is essential for reducing flavins and electrodes in *Shewanella oneidensis*," *Journal of Bacteriology*, vol. 192, no. 2, pp. 467–474, 2010.

[17] M. Y. El-Naggar, G. Wanger, K. M. Leung et al., "Electrical transport along bacterial nanowires from *Shewanella oneidensis* MR-1," *Proceedings of the National Academy of Sciences of the United States of America*, vol. 107, no. 42, pp. 18127–18131, 2010.

[18] H. Von Canstein, J. Ogawa, S. Shimizu, and J. R. Lloyd, "Secretion of flavins by *Shewanella* species and their role in extracellular electron transfer," *Applied and Environmental Microbiology*, vol. 74, no. 3, pp. 615–623, 2008.

Hindawi Publishing Corporation
The Scientific World Journal
Volume 2014, Article ID 451919, 9 pages
http://dx.doi.org/10.1155/2014/451919

Research Article

Effect of Catalytic Cylinders on Autothermal Reforming of Methane for Hydrogen Production in a Microchamber Reactor

Yunfei Yan,[1,2] Hongliang Guo,[2] Li Zhang,[1,2] Junchen Zhu,[2] Zhongqing Yang,[1,2] Qiang Tang,[1,2] and Xin Ji[2]

[1] *Key Laboratory of Low-Grade Energy Utilization Technologies and Systems, Chongqing University, Ministry of Education, Chongqing 400030, China*
[2] *College of Power Engineering, Chongqing University, Chongqing 400030, China*

Correspondence should be addressed to Yunfei Yan; yunfeiyan@cqu.edu.cn

Received 23 April 2014; Accepted 14 June 2014; Published 3 July 2014

Academic Editor: Bin Cao

A new multicylinder microchamber reactor is designed on autothermal reforming of methane for hydrogen production, and its performance and thermal behavior, that is, based on the reaction mechanism, is numerically investigated by varying the cylinder radius, cylinder spacing, and cylinder layout. The results show that larger cylinder radius can promote reforming reaction; the mass fraction of methane decreased from 26% to 21% with cylinder radius from 0.25 mm to 0.75 mm; compact cylinder spacing corresponds to more catalytic surface and the time to steady state is decreased from 40 s to 20 s; alteration of staggered and aligned cylinder layout at constant inlet flow rates does not result in significant difference in reactor performance and it can be neglected. The results provide an indication and optimize performance of reactor; it achieves higher conversion compared with other reforming reactors.

1. Introduction

The development and application of micro-electro-mechanical system (MEMS) are collecting growing attentions. The reactor scale of order of millimeter offers a high degree of compactness and minimises heat as well as mass transport resistances [1], increasing effects of flame-wall interaction, and molecular diffusion are the major problems. Some scholars demonstrate the catalytic reforming of premixed hydrocarbon fuel and vapor to produce hydrogen. The addition of hydrogen maintains the stable and efficient hydrocarbon fuel combustion in microreactor.

Steam reforming of methane (SRM), an endothermic process, is well known as the main process for hydrogen production in industry [2]. While the partial oxidation of methane (POM) is an exothermic process, autothermal reforming of methane is the coupling for both. By combining two reactions, it is possible to operate under autothermal conditions, in which the enthalpy of SRM is balanced by that of POM. Extensive reviews about steam reforming of hydrocarbons discussed the conventional process; some scholars presented the multichannel reactors (MCR), typically dimensions which ranged from a few hundred micrometers to 3–5 mm, proved to be more efficiently to produce hydrogen [3–7]. A numerical method was also employed to simulate the catalytic partial oxidation of methane [8], exergy analysis was conducted to account for the heat recovery in waste steam. Ávila-Neto et al. [9] proposed a simulation code for the methane autothermal reforming where a methane conversion of about 50% can be reached by operating in the temperature range of 450–500°C. Murphy et al. [10] presented a ceramic microchannel reactor that combining heat-exchanger and catalytic-reactor functions to produce syngas; the research achieved high methane conversion. Yan et al. [11, 12] conducted numerical analysis of hydrogen-assisted catalytic combustion of methane; the effect of hydrogen addition on combustion of preheated mixtures of methane-hydrogen-air in a microcombustor was investigated including

an elementary-step surface reaction mechanism. In previous works [13, 14], the activity of Ni-Al_2O_3 and Ni-MgO catalyst was tested for methane steam reforming using two different reaction systems and the highest reaction rates were found with monolith configuration. Besides, researches on several kinds of catalyst had also been carried out and the catalysts based on Ni, Rh, and Pt on various supports had been widely tested [15–17].

The above researches are mostly concerned with the chemical mechanism and theory of the reforming reaction. It demonstrated that the multicylinder affects the performance of reaction; in our work we simulate the reforming reaction in a microchamber reactor and carry out parametric studies that can provide guidance for practical application and similar reactor design.

2. Numerical Simulation

2.1. Description of Reacting System. The reaction system considered in this work is the endothermic steam reforming of methane and methane catalytic combustion taking place in a microchamber with multicylinder inside. The main chemical reactions involved in the process are

methane steam reforming:

$$CH_4 + H_2O \longleftrightarrow CO + 3H_2, \qquad \Delta H = +206.1\ \text{kJ/mol}, \tag{1}$$

methane partial oxidation:

$$CH_4 + 0.5O_2 \longleftrightarrow CO + 2H_2, \qquad \Delta H = -35.2\ \text{kJ/mol}, \tag{2}$$

methane autothermal reforming:

$$CH_4 + 0.5O_2 \longleftrightarrow CO + 2H_2, \qquad \Delta H = -35.2\ \text{kJ/mol}, \tag{3}$$

$$CH_4 + H_2O \longleftrightarrow CO + 3H_2, \qquad \Delta H = +206.1\ \text{kJ/mol}. \tag{4}$$

In this study, steam reforming of methane and partial oxidation of methane are coupled and the overall process is endothermic. Figure 1 presents schematically the structure of the microchamber reactor: the mixed gas flow into the microchamber (length 15 mm, width 5 mm, and height about 3 mm) at inlet; two rows and five columns of cylinders (height 2.5 mm, radius and spacing various from 0.25 mm ~ 0.75 mm and 0.7 mm ~ 1.1 mm), covered with Ni-based catalyst, are placed to adjust the performance and thermal behavior of reactor.

The mechanism of reforming reaction with methane, steam, and oxygen over Ni catalyst dominates the reaction in microchamber reactor. The inner flow field is calculated according to following fundamental assumptions: steady state is considered for reactor operation; fully developed laminar flow is employed in microchamber reactor; the flow is incompressible and the gravitational influence is neglected; the walls within the chamber are catalytic surface and in constant temperature; the effect of volume force and dissipation function is neglected; no phase change occurred from gas to liquid phases; the basic operating parameters used in this paper are given in Table 1.

Table 1: The basic operating parameters.

Inlet flow rate of mixed gas/(m·s^{-1})	Inlet temperature of mixed gas/(K)	Temperature of catalytic surface/(K)	Mole ratio (H : C : O)
0.005	300	1190	2 : 1 : 0.4

Table 2: Grid division in microchamber and methane conversion.

Interval size/(mm)	0.3	0.4	0.5	0.6
Methane conversion	99.57%	99.29%	99.14%	98.74%

In the present work, analysis on methane autothermal reforming has been carried out to assess the performance of the microchamber reactor by varying the structural variables. In particular, results including methane conversion and mass fraction of methane/hydrogen have been studied.

2.2. Mesh Generation. A three-dimensional model of microchamber reactor with 1 : 1 proportions is built using the CFD preprocessing software GAMBIT, which is used for the three-dimensional flow passage and grid generation. FLUENT is based on the finite volume method and used to conduct the full passage numerical simulations.

The solution domain is divided into limited control volumes by grids. Thus grid generation has a great influence on the calculation accuracy and stability. A grid-independent study confirmed that grids provided sufficient grid independency. The grid independence is examined with 0.3, 0.4, 0.5, and 0.6 mm of interval size, respectively. As given in Table 2, the accuracy of the calculation is confirmed as the difference of methane conversion is 0.8% with interval size of 0.3 mm and 0.6 mm; thus, the interval size of 0.3 mm is adopted. To improve the computing accuracy, the mesh consisting of 48638 hybrid forms of triangular and hexahedral elements is adopted with special care for meshing around cylinders, as shown in Figure 2. In addition, grid point distributions near the catalytic surface (surface of cylinders and walls) are fined for accuracy.

The simulation carried out in the Fluent 6.3 environment and is integrated with Chemkin programs including mechanism of multiple reactions of methane, steam, and oxygen on Ni catalyst.

2.3. Governing Equations. To describe the reaction process of the methane, water vapor and the oxygen, the governing equations are given by

continuous equation:

$$\frac{\partial \rho}{\partial t} + \frac{\partial}{\partial x_i}\left(\rho u_i\right) = 0 \tag{5}$$

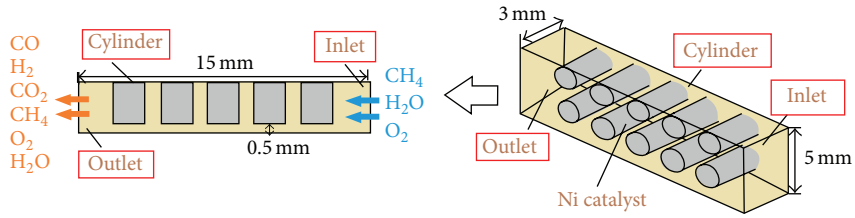

Figure 1: The schematic drawing of the microchamber reactor.

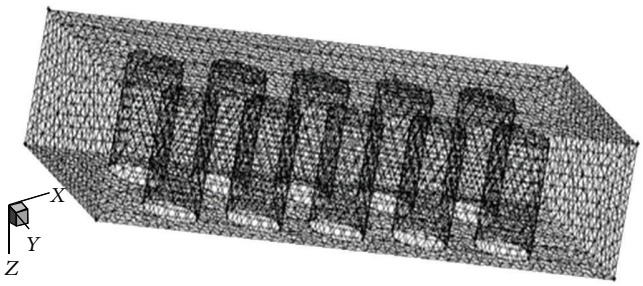

Figure 2: Three-dimensional mesh of the microchamber reactor.

component equation:

$$\frac{\partial}{\partial t}\left(\rho Y_i\right) + \nabla\left(\rho \vec{u} Y_i\right) = -\nabla \vec{J}_i + R_i \tag{6}$$

momentum equation:

$$\frac{d\left(\rho \vec{V}\right)}{dt} = -\text{grad}\, p + \nabla^2\left(\mu \vec{V}\right) \tag{7}$$

energy equation:

$$\rho\frac{Dh}{Dt} - \frac{\partial p}{\partial t} = \frac{\partial}{\partial x_i}\left(\lambda\frac{\partial T}{\partial x_j}\right) + \frac{\partial}{\partial x_j}\left(\sum_i D\rho\frac{\partial Y_i}{\partial x_j}h_i\right) + q \tag{8}$$

gas state equation:

$$p = \rho RT\sum\frac{Y_i}{M_i}. \tag{9}$$

In (7), (8), and (9), the variable p is pressure; T is temperature; ρ is the density; q in (8) is the heat; h is the enthalpy; λ is the thermal conductivity; u is the flow rate; μ in (7) is the dynamic viscosity; R in (6), (9) is the gas constant; Y_i is the mass fraction of the component i and $\sum Y_i = 1$; J_i in (6) is the diffusion flux of component i, which is caused by the concentration gradient and can be calculated by

$$J_i = -\rho D_i \nabla Y_i, \tag{10}$$

where the variable D_i is the diffusion coefficient of the component i in the mixture.

Arrhenius equation is used to calculate chemical source term for laminar finite rate model, R_i in (11) is the net production rate of reaction i, which can be calculated by a sum of Arrhenius reaction source term in N_r chemical reactions

$$R_i = M_i\sum_{i=1}^{N_r}\hat{R}_{i,r}, \tag{11}$$

where M_i is the molecular weight of the material i and $\hat{R}_{i,r}$ in (11) is the generation or decomposition rate of material i in the formula $r$and is given by

$$\hat{R}_{i,r} = \Gamma\left(v'_{i,r} - v''_{i,r}\right)\left\{k_{f,r}\prod_{j=1}^{N_r}\left[C_{j,r}\right]\eta'_{j,r} - k_{b,r}\prod_{j=1}^{N_r}\left[C_{j,r}\right]\eta''_{j,r}\right\}, \tag{12}$$

where Γ is the net effect of the third substance on the reaction rate; $v'_{i,r}$ is the stoichiometric coefficient of reactant i in reaction r; $v''_{i,r}$ is the stoichiometric coefficient of resultant i in reaction r; $k_{f,r}$ is the forward reaction rate in reaction r; $k_{b,r}$ is the backward reaction rate in reaction r; $\eta'_{j,r}$ is the forward reaction speed index of each reactant or product j in reaction r; $\eta''_{j,r}$ is the backward reaction speed index of each reactant or product j in reaction r; $C_{j,r}$ is the molar concentration of each reactant or product j in reaction r.

3. Results and Discussion

3.1. Effect of Cylinder Radius. It identified that the location of the catalytic cylinders placed in microchamber may offer a degree of flexibility to adjust the temperature profile and prevent the detrimental reverse reaction in the endothermic side, avoiding at the same time severe hot spots [18]. The reactor performance with cylinder radius of 0.25, 0.50, and 0.75 mm are explored and the operating parameters are shown in Table 3.

The numerical analysis has been carried out in order to verify the effect of cylinder radius (0.25 mm, 0.50 mm, and 0.75 mm) on reforming reaction. As shown in Figure 3, the mass fraction of methane decreases from 26% to 21% with cylinder radius of 0.75 mm at 3 s, while cylinder radius of 0.50 mm and 0.25 mm decreases to 23.5% and 25.3%, indicating that larger cylinder radius (from 0.25 mm to 0.75 mm) promotes the reactor performance. The methane conversion with different cylinder radius generally achieves

Table 3: Operating parameters with different cylinder radius.

Number	Radius/(mm)	Inlet flow rate/(m·s^{-1})	Mole ratio (H : C : O)	Wall temperature/(K)	Cylinder spacing/(mm)	Cylinder layout
1	0.25	0.005	2 : 1 : 0.4	1190	0.9	Aligned
2	0.50	0.005	2 : 1 : 0.4	1190	0.9	Aligned
3	0.75	0.005	2 : 1 : 0.4	1190	0.9	Aligned

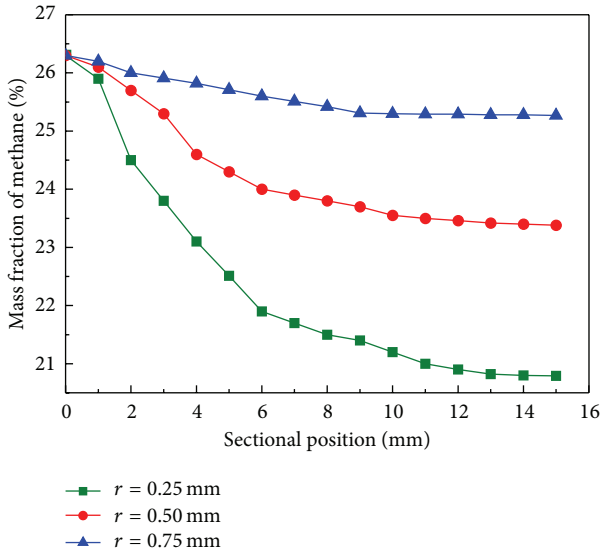

Figure 3: Mass fraction of methane along sectional position with cylinder radius of 0.25 mm (■), 0.50 mm (●), and 0.75 mm (▲) at reaction time of 3 s.

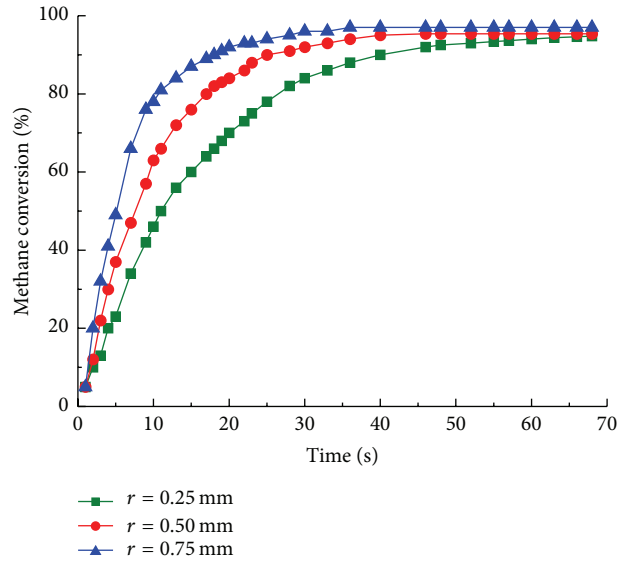

Figure 4: Methane conversion with cylinder radius of 0.25 mm (■), 0.50 mm (●), and 0.75 mm (▲) for different reaction time.

Table 4: Mass fraction of hydrogen and methane conversion with different cylinder radius.

Radius/(mm)	0.25	0.5	0.75
Methane conversion	99.37%	99.49%	99.74%
Mass fraction of hydrogen	9.26%	9.38%	9.33%

97% (see Figure 4) with operating temperature of 1190 K, higher than the conventional research [8, 19], partially due to the adjusted temperature profile and reaction heat flux caused by catalytic cylinders. Larger cylinder radius corresponds to more catalytic surface and the time to steady state reaction is decreased from 50 s to 30 s. Hence, expanding the cylinder radius is one option to improve reforming performance, subject to limited physical size of micro-chamber reactor.

As shown in Figures 5(a) and 5(b), it can be seen that larger cylinder radius typically increased hydrogen yield. Particularly at sectional position of 3 mm, the mass fraction of hydrogen with cylinder radius of 0.75 mm is 2% higher than that of 0.25 mm, the mass fraction of methane with cylinder radius of 0.25 mm is 7% higher than that of 0.75 mm, indicating that larger cylinder radius results in increase of conversion mainly due to more efficient heat transfer. Rather small differences in mass fraction of methane and hydrogen are observed after 8 mm in steady state. The methane conversion and mass fraction of hydrogen with different radius are reported in Table 4, the effect of cylinder radius can be neglected in steady state. Thus the alteration of the cylinder radius does not affect significantly the outlet conversion and outlet reactor performance, partially for that reactant molecules have enough time to reach the wall before they exit the reactor [18].

3.2. Effect of Cylinder Spacing. The study has been carried out in order to verify the effect of cylinder spacing. The cylinder spacing is concerned with catalyst loading and flow field distribution in microchamber, turbulent flow and hot spots occurs when not properly designed [18]. The spacing of catalytic cylinders are 0.7, 0.9, and 1.1 mm, respectively, all other parameters are kept in constant and presented in Table 5.

Figures 6(a) and 6(b) show results of a series of numerical simulations. Mass fraction of methane with cylinder spacing of 0.7, 0.9, and 1.1 mm are plotted on sectional position along reactor length at reaction time of 5 s and 25 s. Mass fraction of methane generally decreases from 26% to 16% (see Figure 6(a)) and coincides at 3 mm (reaction time of 5 s). After that methane mass fraction with cylinder spacing of 0.7 mm decreases from 16% to 7%, while the spacing of 0.9 mm and 1.1 mm moves downstream to 14% and 10%, this

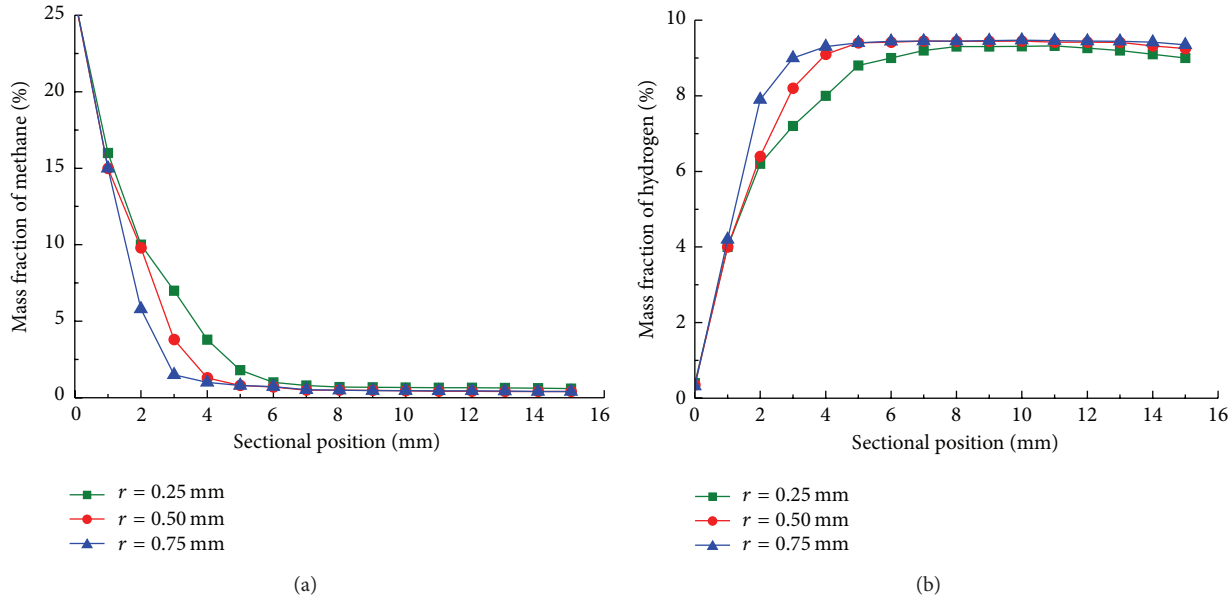

Figure 5: Mass fraction of (a) methane and (b) hydrogen along sectional position with cylinder radius of 0.25 mm (■), 0.50 mm (●), and 0.75 mm (▲) in steady state.

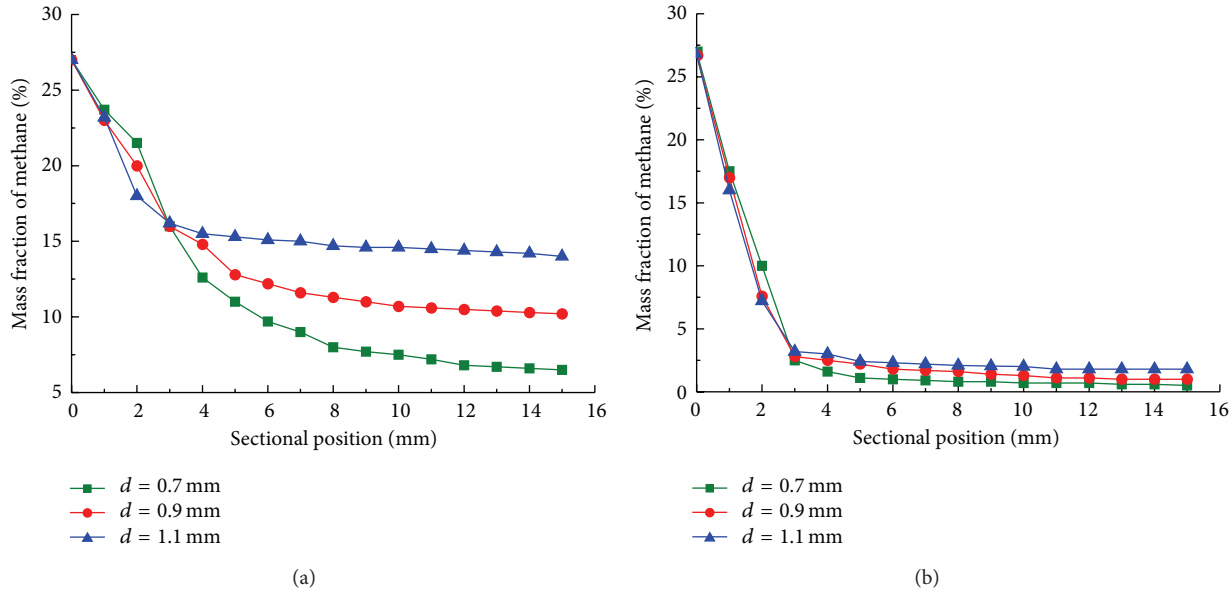

Figure 6: Mass fraction of methane along sectional position with cylinder spacing of 0.7 mm (■), 0.9 mm (●), and 1.1 mm (▲) at reaction time of 5 s (a) and 25 s (b).

Table 5: Operating parameters with different cylinder spacing.

Number	Cylinder spacing/(mm)	Inlet flow rate/(m·s^{-1})	Mole ratio (H : C : O)	Wall temperature/(K)	Radius/(mm)	Cylinder layout
1	0.7	0.005	2 : 1 : 0.4	1190	0.75	Aligned
2	0.9	0.005	2 : 1 : 0.4	1190	0.75	Aligned
3	1.1	0.005	2 : 1 : 0.4	1190	0.75	Aligned

Table 6: Operating parameters with different cylinder layout.

Number	Cylinder layout	Inlet flow rate/(m·s^{-1})	Mole ratio (H : C : O)	Wall temperature/(K)	Radius/(mm)	Cylinder spacing/(mm)
1	Aligned	0.005	2 : 1 : 0.4	1190	0.75	0.7
2	Staggered	0.005	2 : 1 : 0.4	1190	0.75	0.7

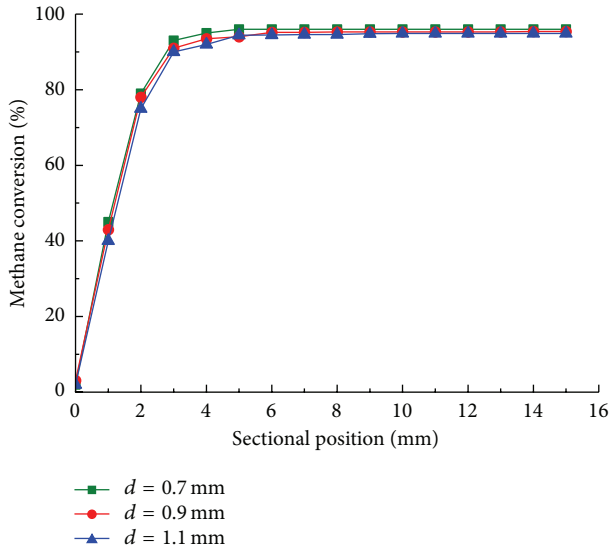

Figure 7: Methane conversion along sectional position with cylinder spacing of 0.7 mm (■), 0.9 mm (●), and 1.1 mm (▲) in steady state.

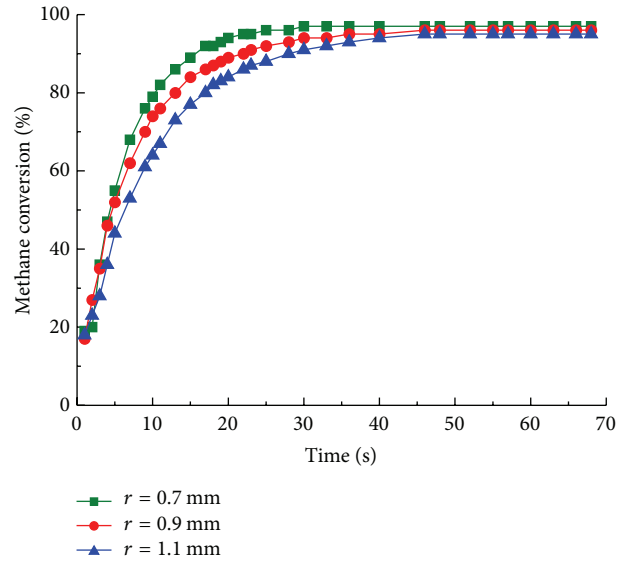

Figure 8: Methane conversion with cylinder spacing of 0.7 mm (■), 0.9 mm (●), and 1.1 mm (▲) for different reaction time.

Table 7: The finalized structure of microchamber.

Cylinder radius/(mm)	Cylinder spacing/(mm)	Cylinder layout
0.75	0.7	Aligned

indicates that a decrease in cylinder spacing (from 1.1 mm to 0.7 mm) promotes the reactor performance at outlet section. As a contrast, the same alteration of cylinder spacing is made and mass fraction of methane is approaching at reaction time of 25 s (see Figure 6(b)), partially due to fully developed and adjusted flow field and temperature profile, thus rather small differences are observed after 3 mm.

As shown in Figure 7, alteration of cylinder spacing leads to no significant difference in steady state. It illustrates that the spacing of cylinders has no significant effect on the final state of reaction. The present work achieves a methane conversion of 95% (see Figure 7); it generally higher than improved performance of 91% and 93% conversion in previous experimental research [20, 21] (inlet flow rate 0.75 and 2; temperature of feed 873 K and 943 K), partially due to higher operating temperature. As shown in Figure 8, larger cylinder spacing results in higher conversion and the time to steady state is decreased (from 40 s to 20 s). The cylinder spacing is concerned with catalyst loading and more reactants contact catalytic surface with compact cylinder spacing. The methane conversion of cylinder spacing varied in Figure 8 approaches in steady state, indicating that the parameter is unlikely to optimize performance for the steady state reaction. The result also shows that operating temperature is the major factor limiting reforming performance; thus, a cooler reactor leads to lower final conversions.

3.3. Effect of Cylinder Layout. The arrangement of cylinders is separated with aligned and staggered layout. The reactor behavior and performance are studied for different cylinder layout and all other parameters shown in Table 6 are kept at constant value.

Mass fraction of hydrogen and methane along sectional position with aligned and staggered layout at reaction time of 25 s is illustrated in Figures 9(a) and 9(b). It indicates a small benefit of staggered layout, since the mass fraction of hydrogen is generally higher in staggered arrangement before 6 mm. As a contrast, the mass fraction of methane is higher in aligned arrangement and after that no significant differences are observed. Methane partial oxidation reaction, an exothermic process, dominates the reaction initially and the staggered arrangement enhances heat transfer and the turbulence intensity.

Methane and hydrogen conversion with staggered and aligned cylinder layout are illustrated in Figures 10(a) and 10(b); rather small differences with staggered and aligned cylinder layout are observed, indicating that the influence of cylinder layout for the overall reaction is negligible, despite

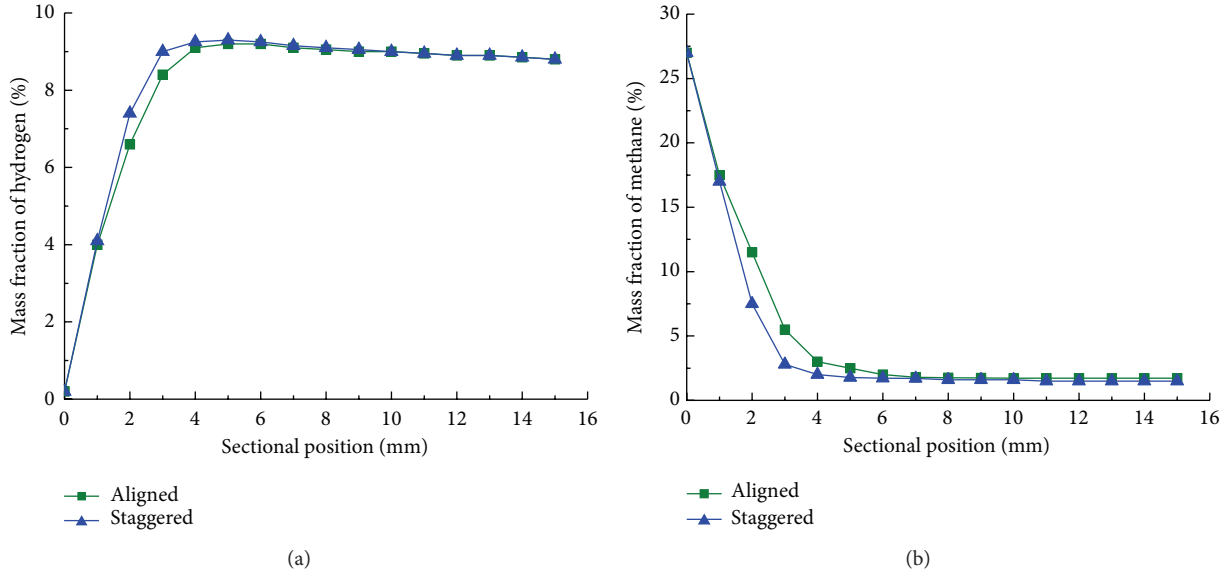

FIGURE 9: Mass fraction of (a) hydrogen and (b) methane along sectional position with aligned (■) and staggered (▲) layout of cylinder: reaction time t_r = 25 s.

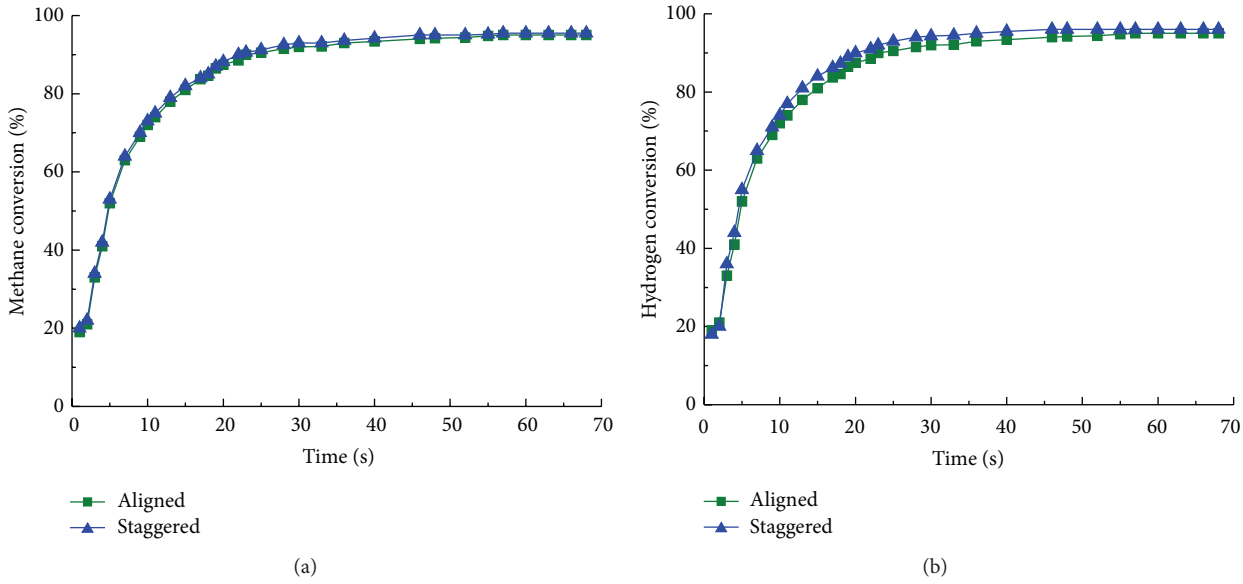

FIGURE 10: (a) Methane and (b) hydrogen conversion with aligned (■) and staggered (▲) layout of cylinder for different reaction time.

the fact that the choice of aligned arrangement can reduce wear and tear on cylinders.

As shown in Table 7, the finalized structural parameters of cylinders in microchamber derived with cylinder radius of 0.75 mm, cylinder spacing of 0.7 mm, and aligned layout. The optimized parameters of the microchamber reactor provide guidance for its application and similar reactor design.

4. Conclusions

The performance of the reforming reaction was investigated by varying the cylinders covered with Ni catalysts in microchamber. It was concluded that larger cylinder radius resulted in more catalytic surface area and therefore it reduced the mass fraction of methane from 26% to 21%, while such effect was neglected for steady state reaction. The methane conversion with different cylinder radius generally achieves 97%. Smaller cylinder spacing enhanced the turbulence intensity and promoted the efficiency of heat transfer. Thus the reaction was fully developed and the time required to reach the steady state was decreased from 40 s to 20 s. At constant inlet flow rates, alteration of cylinder layout for staggered and aligned did not introduce significant differences in reactor performance. Staggered layout could

partially enhance the methane conversion and hydrogen yield. While the promotion was insignificant after 6 mm and thus the effect of cylinder layout was negligible.

The results indicate that autothermal reforming of methane in microchamber was affected by catalytic cylinders inside and it should be properly designed; the optimized microchamber reactor with cylinder radius of 0.75 mm, cylinder spacing of 0.7 mm, and aligned layout was derived.

Nomenclature

Variables

$C_{j,r}$: The molar concentration of each reactant or product j in reaction r (–)
D_i: Diffusion coefficient of component I (m^2 s^{-1})
h: Enthalpy (kJ kg^{-1})
J: Diffusion flux (mol m^{-2} s^{-1})
$k_{f,r}$: Forward reaction rate in reaction r (–)
$k_{b,r}$: Backward reaction rate in reaction r (–)
M: Relative molecular mass (–)
P: Pressure (Pa)
q: Heat (kJ)
R: Universal gas constant = 8.314 (J mol^{-1} K^{-1})
R_i: Net production rate of reaction i (mol m^{-3} s^{-1})
t: Time (s)
T: Temperature (K)
u: Flowrate (m s^{-1})
$v'_{i,r}$: The stoichiometric coefficient of reactant i in reaction r (–)
$V''_{i,r}$: The stoichiometric coefficient of resultant i in reaction r (–)
Y: Mass fraction (%).

Greek Letters

η: Efficiency (%)
$\eta'_{i,r}$: The forward reaction speed index of each reactant or product j in reaction r (–)
$\eta''_{i,r}$: The backward reaction speed index of each reactant or product j in reaction r (–)
ρ: Density (kg m^{-3})
∇: Gradient operator (–)
λ: Thermal conductivity (W m^{-1} k^{-1})
μ: Dynamic viscosity (N s m^{-2})
Γ: Index of the third substance on the reaction rate (–).

Conflict of Interests

The authors declare that there is no conflict of interests regarding the publication of this paper.

Acknowledgments

The authors gratefully acknowledge financial support from the Fundamental Research Funds for the Central Universities (Project no. CDJZR14145501), National Natural Science Foundation of China (Project no. 50906103), and Chongqing Science and Technology talent training plan (cstc2013kjrc-qnrc90002).

References

[1] M. Zanfir and A. Gavriilidis, "Catalytic combustion assisted methane steam reforming in a catalytic plate reactor," *Chemical Engineering Research & Design*, vol. 58, no. 17, pp. 3947–3960, 2003.

[2] Q. S. Jing, L. X. Fang, and H. Lou, "Progress of catalytic conversion of methane to syngas in the presence of oxygen," *Chemical Industry and Engineering Progress*, vol. 27, no. 4, pp. 503–507, 2008.

[3] G. G. Park, S. D. Yim, Y. G. Yoon et al., "Hydrogen production with integrated microchannel fuel processor for portable fuel cell systems," *Journal of Power Sources*, vol. 145, no. 2, pp. 702–706, 2005.

[4] S. K. Ryi, J. S. Park, S. H. Cho, and S. H. Kim, "Fast start-up of microchannel fuel processor integrated with an igniter for hydrogen combustion," *Journal of Power Sources*, vol. 161, no. 2, pp. 1234–1240, 2006.

[5] A. L. Y. Tonkovich, B. Yang, S. T. Perry, S. P. Fitzgerald, and Y. Wang, "From seconds to milliseconds to microseconds through tailored microchannel reactor design of a steam methane reformer," *Catalysis Today*, vol. 120, no. 1, pp. 21–29, 2007.

[6] K. R. Hwang, S. K. Ryi, C. B. Lee, S. W. Lee, and J. S. Park, "Simplified, plate-type Pd membrane module for hydrogen purification," *International Journal of Hydrogen Energy*, vol. 36, no. 16, pp. 10136–10140, 2011.

[7] A. Vigneault, S. S. E. H. Elnashaie, and J. R. Grace, "Simulation of a compact multichannel membrane reactor for the production of pure hydrogen via steam methane reforming," *Chemical Engineering & Technology*, vol. 35, no. 8, pp. 1520–1533, 2012.

[8] W. H. Chen, Y. C. Cheng, and C. I. Hung, "Transient reaction and exergy analysis of catalytic partial oxidation of methane in a Swiss-roll reactor for hydrogen production," *International Journal of Hydrogen Energy*, vol. 37, no. 8, pp. 6608–6619, 2012.

[9] C. N. Ávila-Neto, S. C. Dantas, F. A. Silva et al., "Hydrogen production from methane reforming: thermodynamic assessment and autothermal reactor design," *Journal of Natural Gas Science and Engineering*, vol. 1, no. 6, pp. 205–215, 2009.

[10] D. M. Murphy, A. Manerbino, M. Parker, J. Blasi, R. J. Kee, and N. P. Sullivan, "Methane steam reforming in a novel ceramic microchannel reactor," *International Journal of Hydrogen Energy*, vol. 38, no. 21, pp. 8741–8750, 2013.

[11] Y. Yan, W. Pan, L. Zhang et al., "Numerical study on combustion characteristics of hydrogen addition into methane-air mixture," *International Journal of Hydrogen Energy*, vol. 38, no. 30, pp. 13463–13470, 2013.

[12] Y. Yan, W. Tang, L. Zhang et al., "Numerical simulation of the effect of hydrogen addition fraction on catalytic micro-combustion characteristics of methane-air," *International Journal of Hydrogen Energy*, vol. 39, no. 4, pp. 1864–1873, 2014.

[13] N. de Miguel, J. Manzanedo, and P. L. Arias, "Testing of a Ni-Al2O3 catalyst for methane steam reforming using different

reaction systems," *Chemical Engineering and Technology*, vol. 35, no. 4, pp. 720–728, 2012.

[14] N. de Miguel, J. Manzanedo, J. Thormann, P. P. feifer, and P. L. Arias, "Ni catalyst coating on Fecralloy microchanneled foils and testing for methane steam reforming," *Chemical Engineering & Technology*, vol. 33, no. 1, pp. 155–166, 2010.

[15] C. Lei, L. W. Pan, C. J. Ni, Z. S. Yuan, and S. D. Wang, "Autothermal reforming of methane over $Rh/Ce_{0.5}Zr_{0.5}O_2$ catalyst: effects of the crystal structure of the supports," *Fuel Processing Technology*, vol. 91, no. 3, pp. 306–312, 2010.

[16] J. A. C. Ruiz, F. B. Passos, J. M. C. Bueno, E. F. Souza-Aguiar, L. V. Mattos, and F. B. Noronha, "Syngas production by autothermal reforming of methane on supported platinum catalysts," *Applied Catalysis A: General*, vol. 334, no. 1-2, pp. 259–267, 2008.

[17] J. C. Escritori, S. C. Dantas, R. R. Soares, and C. E. Hori, "Methane autothermal reforming on nickel-ceria-zirconia based catalysts," *Catalysis Communications*, vol. 10, no. 7, pp. 1090–1094, 2009.

[18] M. Zanfir and A. Gavriilidis, "Influence of flow arrangement in catalytic plate reactors for methane steam reforming," *Chemical Engineering Research and Design*, vol. 82, no. 2, pp. 252–258, 2004.

[19] S. Ayabe, H. Omoto, T. Utaka et al., "Catalytic autothermal reforming of methane and propane over supported metal catalysts," *Applied Catalysis A: General*, vol. 241, no. 1-2, pp. 261–269, 2003.

[20] N. de Miguel, J. Manzanedo, and P. L. Arias, "Active and stable Ni-MgO catalyst coated on a metal monolith for methane steam reforming under low steam-to-carbon ratios," *Chemical Engineering & Technology*, vol. 35, no. 12, pp. 2195–2203, 2012.

[21] J. Ryu, K. Lee, H. La, H. Kim, J. Yang, and H. Jung, "Ni catalyst wash-coated on metal monolith with enhanced heat-transfer capability for steam reforming," *Journal of Power Sources*, vol. 171, no. 2, pp. 499–505, 2007.

Hindawi Publishing Corporation
The Scientific World Journal
Volume 2014, Article ID 723092, 11 pages
http://dx.doi.org/10.1155/2014/723092

Research Article

Syngas Production from Pyrolysis of Nine Composts Obtained from Nonhybrid and Hybrid Perennial Grasses

Adéla Hlavsová,[1] Agnieszka Corsaro,[1] Helena Raclavská,[1,2] Dagmar Juchelková,[1,3] Hana Škrobánková,[2] and Jan Frydrych[4]

[1] *ENET-Energy Units for Utilization of Non-Traditional Energy Sources, VŠB-Technical University of Ostrava, 17. listopadu 15/2172, 708 33 Ostrava-Poruba, Czech Republic*
[2] *Institute of Geological Engineering, Faculty of Mining and Geology, VŠB-Technical University of Ostrava, 17. listopadu 15/2172, 708 33 Ostrava-Poruba, Czech Republic*
[3] *Department of Energy, Faculty of Mechanical Engineering, VŠB-Technical University of Ostrava, 17. listopadu 15/2172, 708 33 Ostrava-Poruba, Czech Republic*
[4] *OSEVA PRO s.r.o., Grass Research Institute, Rožnov-Zubří, Hamerská 698, 756 54 Zubří, Czech Republic*

Correspondence should be addressed to Adéla Hlavsová; adela.hlavsova@vsb.cz

Received 6 March 2014; Revised 9 June 2014; Accepted 13 June 2014; Published 1 July 2014

Academic Editor: Bin Cao

A pyrolysis of compost for the production of syngas with an explicit $H_2/CO = 2$ or $H_2/CO = 3$ was investigated in this study. The composts were obtained from nonhybrid (perennial) grasses (NHG) and hybrid (perennial) grasses (HG). Discrepancies in H_2 evolution profiles were found between NHG and HG composts. In addition, positive correlations for NHG composts were obtained between (i) H_2 yield and lignin content, (ii) H_2 yield and potassium content, and (iii) CO yield and cellulose content. All composts resulted in $H_2/CO = 2$ and five of the nine composts resulted in $H_2/CO = 3$. Exceptionally large higher heating values (HHVs) of pyrolysis gas, very close to HHVs of feedstock, were obtained for composts made from mountain brome (MB, 16.23 MJ/kg), hybrid Becva (FB, 16.45 MJ/kg), and tall fescue (TF, 17.43 MJ/kg). The MB and FB composts resulted in the highest syngas formation with $H_2/CO = 2$, whereas TF compost resulted in the highest syngas formation with $H_2/CO = 3$.

1. Introduction

The pressing demands for greater generation of energy at a lower cost, associated with a diminution of greenhouse gases (GHG) emission, have compelled researchers to expand their search for an energy source outside conventional and primary energy sources, such as fossil fuels. This pursuit is facilitated by the utilization of renewable energy sources and based on Directive 2001/77/EC of the European Parliament that must consist of 13% of the total energy consumption by 2020 in the Czech Republic [1]. Biomass, specifically energy crops, is of particular interest among these renewable energy resources. It has been predicted that by 2050 energy crops will have the potential to supply around 200–400 EJ/year at a competitive cost [2], and up to 161 EJ/year of the 200–400 EJ/year range will come from projected surplus cropland and grassing areas [3]. The competitive costs are based upon the incentives made available through the scheme for energy crops according to the Article 88 of Regulation (EC) No. 1782/2003 [4]. The preference of energy crops over other types of biomass for energy generation is due to their (i) higher productivity, (ii) lower investment cost, (iii) low environmental maintenance, (iv) short time between plantation and harvesting, and (v) high energy values [5–7]. Another reason for which energy crops, in particular grasses, are being considered as a source of energy is the overproduction of grass and/or hay from permanent grasslands. This overproduction is a result of a diminution of livestock. According to the Czech Statistical Office, the land used for agriculture reached 959,131 ha with harvest of 3.22 t/ha in 2012 [8]. Comparatively, livestock numbers decreased since 1990 by 60.78% for cattle and 66.74% for pigs reaching 1375 cattle and 1593 pigs in 2012 [9]. Therefore, it is necessary to find an appropriate technology to manage and utilize the excess of grass.

The number of technologies available to convert biomass to energy has developed greatly in recent years and they are focused in general on production of synthesis gas (syngas) [10, 11]. Syngas which is a mixture of hydrogen (H_2) and carbon monoxide (CO) can then be directly converted to energy through combustion or to a variety of fuels: (i) liquid hydrocarbons from methanol, (ii) liquid hydrocarbons through Fischer-Tropsch synthesis, and (iii) synthetic natural gas (SNG) [11, 12]. The selective conversion of syngas to liquid hydrocarbons or SNG requires, however, specific ratios of H_2 to CO in the amount of 2 or 3, respectively [12]. Obtaining those explicit values is not a straightforward task as the yields of produced noncondensable gases depend on several factors such as raw material composition and operating conditions of the converting process [13–15].

Two methods in particular have been reported in the literature that convert biomass to syngas, namely, gasification and pyrolysis. Gasification is a thermochemical method which converts a variety of biomass in an oxygen environment. Typical reactions involved in any gasification process are the reactions using oxygen (O_2) (combustion) represented by (1) and (2), the reverse Boudouard reaction represented by (3), the water-gas reaction represented by (4), and the water-gas shift (WGS) reaction represented by (5) [16, 17]:

Partial oxidation:

$$2C + O_2 \longrightarrow 2CO \quad \Delta H_r^0 = -222\,\text{kJ/mol} \tag{1}$$

Oxidation of carbon:

$$C + O_2 \longrightarrow CO_2 \quad \Delta H_r^0 = -394\,\text{kJ/mol} \tag{2}$$

Revers Boudouard reaction:

$$C + CO_2 \longrightarrow 2CO \quad \Delta H_r^0 = 173\,\text{kJ/mol} \tag{3}$$

Water-gas reaction:

$$C + H_2O \longrightarrow CO + H_2 \quad \Delta H_r^0 = 131\,\text{kJ/mol} \tag{4}$$

Water-gas shift reaction:

$$CO + H_2O \longrightarrow CO_2 + H_2 \quad \Delta H_r^0 = -41\,\text{kJ/mol} \tag{5}$$

As a consequence of these reactions, a wide range of H_2/CO ratios (0.45–2) are obtained [18]. Pyrolysis on the other hand is a process in which biomass undergoes thermal degradation in an oxygen-free atmosphere. The final products are pyrolysis solid, liquid, and gas containing mainly CO, carbon dioxide (CO_2), H_2, and lower hydrocarbons (C_1 –C_3). The remaining reactions involved in the process apart from previously mentioned reactions (3), (4), and (5) are the following [19]:

Steam reforming of methane:

$$CH_4 + H_2O \longrightarrow CO + 3H_2 \quad \Delta H_r^0 = 206\,\text{kJ/mol} \tag{6}$$

Steam reforming of tar:

$$C_nH_mO_p + (2n - p)\,H_2O \longrightarrow nCO_2 + (1/2m + 2n - p)\,H_2 \quad \Delta H_r^0 \geq 0\,\text{kJ/mol} \tag{7}$$

Thermal cracking:

$$C_nH_m \longrightarrow C_{n-x}O_{m-y} + H_2 + CH_4 + C \quad \Delta H_r^0 \geq 0\,\text{kJ/mol} \tag{8}$$

Methanation:

$$C + 2H_2 \longrightarrow CH_4 \quad \Delta H_r^0 = -75\,\text{kJ/mol} \tag{9}$$

The obtained H_2/CO ratios are dependent on pyrolysis temperature and increase as the latter increases [15, 20–22]. Their values are, however, somewhat lower (i.e., 0.1–1.42 in the 500–1000°C range) when compared to the values obtained from biomass gasification [15, 20, 22]. In addition, in order to make syngas suitable for commercial application (i.e., reduce economic investment and improve its quality (obtain an appropriate H_2/CO ratio, *ipso facto* increase H_2 formation)), the obtained gas mixture needs to be cleaned and processed [18, 23]. These requirements can be avoided or minimized by pretreatments of biomass raw material such as composting [10, 24].

Composting is a naturally occurring, biological decomposition process in which bacteria, fungi, and other microorganisms break down the organic matter into a more stable form called compost [10, 24, 25]. The process occurs in two stages. The first stage (i.e., organic matter degradation) results in the formation of CO_2, NH_3, H_2O, saccharides, and humic substances (fulvic and humic acids) with emission of heat [23, 26]. The second stage involves the maturation and stabilization of formed material [26]. As a result of both stages, the newly formed organic matter has a different chemical composition, *ipso facto* thermal behavior [10, 23, 24, 27]. Composting reduces the content of two of the major biomass components, namely, cellulose and hemicellulose, while increasing the content of lignin [10, 23, 24]. These changes are of particular importance, since lignin is the component responsible for the highest H_2 and CH_4 formation, hemicellulose is responsible for the highest CO_2 emission, and cellulose is responsible for the highest CO release [28–31]. Yang et al. [29] examined pyrolysis characteristics of lignin, cellulose, and hemicellulose and concluded that the main source of H_2 release was lignin. Lignin resulted in four times more emission of H_2 than cellulose and three times more than hemicellulose [29]. Similar results were obtained by Barneto et al. [31] who extended the investigation of H_2 origin and reported that although most of H_2 is emitted from thermal degradation of lignin, three times more H_2 is released from charring than from volatilization of lignin. In addition, hemicellulose is the least stable from the three biochemical components and, therefore, reacts at the lowest temperatures, followed by cellulose and lignin [32]. Consequently, the changes in the chemical composition due to composting result in the changes in pyrolysis gaseous products. That is, a mixture of H_2 and CO becomes the primary product, not a mixture of CO_2 and CO which are the major products of biomass pyrolysis [21, 28]. For this reason also, the composts obtained from perennial grasses rather than grasses alone are considered as a feedstock for pyrolysis experiments in this research.

Table 1: Names and abbreviations of composts.

Grass type	Grass name	Compost abbreviation
Nonhybrid	Redtop-Rožnovský (*Agrostis gigantea* Roth)	R
	Reed canary grass-Chrastava (*Phalaris arundinacea* L.)	RC
	Tall fescue-Kora (*Festuca arundinacea* Schreb.)	TF
	Tall oat grass-Rožnovský (*Arrhenatherum elatius* L.)	TO
	Mountain brome-Tacit (*Bromus marginatus* Nees ex Steud.)	MB
	Mixture of clover (*Trifolium pratense*)	MC
Hybrid	Festulolium Perun	FP
	Festulolium Becva	FB
	Festulolium Lofa	FL

Table 2: Proximate and ultimate analyses of composts.

Compost	Ultimate analysis (wt%)[a,b]				Proximate analysis (wt%)				HHV (MJ/kg)
	C	N	H	O[c]	Moisture[d]	Volatile matter[a]	Ash[a]	Fixed carbon[a,c]	
R	47.24	0.91	6.6	45.25	4.54	74.88	09.83	15.29	17.45
RC	46.43	0.49	6.88	46.2	6.29	76.02	07.6	16.38	17.61
TF	46.39	0.56	7.09	45.97	4.38	74.17	10.3	15.53	17.3
TO	48.84	1.11	6.7	43.34	5.66	72.3	12.72	14.98	17.53
MB	47.9	0.59	7.14	44.37	5.87	73.1	11.42	15.48	17.21
MC	44.43	0.96	5.93	48.68	5.23	71.98	13.3	14.72	16.69
FP	46.5	0.83	6.6	46.07	6.12	73.29	10.52	16.19	18.29
FB	44.64	0.64	6.42	48.3	5.5	75.73	07.95	16.32	18.11
FL	48.11	0.77	6.52	44.6	5.68	74.26	08.94	16.8	18.21

[a]Dry basis.
[b]Ash free.
[c]Calculated by difference.
[d]As received.

The purpose of this study was to compare the composition, yields, and evolution of gaseous products from pyrolysis of nine composts. The examined composts were obtained from two types of perennial grasses: nonhybrid and hybrid. The main objective was selective formation of syngas with an explicit H_2/CO ratio in the amount of 2 : 1 or 3 : 1.

2. Materials and Methods

2.1. Materials. Nine composts made from perennial grasses (six nonhybrid grasses (NHG) and three hybrid grasses (HG)) were investigated in this study. The grass crops were obtained from OSEVA PRO s.r.o., Grass Research Institute, Rožnov-Zubří, CZ. The names and abbreviation of the composts examined are displayed in Table 1.

2.2. Composting. The composting experiments were carried out at the Institute of Geological Engineering, VŠB-Technical University of Ostrava (VŠB-TU Ostrava), CZ. The nine perennial grasses were finely chopped (<2 cm) and mechanically mixed with sawdust and soil in the ratio of 4 : 2 : 1 in order to obtain the appropriate C/N ratio. The composting of each blend (perennial grass, sawdust, and soil) was conducted in a microcomposter (NM125, NatureMill) for 10 days, whereas the maturation of composts was carried out for 14 days.

2.3. Chemical Characterization of Composts. All nine composts were subjected to proximate and ultimate analyses. The following standard test methods were applied: CSN EN 15402 (volatile matter), CSN EN 15403 (ash), CSN EN 15104 (carbon (C), nitrogen (N), and hydrogen (H)), and CSN EN 15400 (higher heating value (HHV)). The summarized results are presented in Table 2. The biochemical components were determined according to the CSN EN ISO 13906 standard test method (lignin) and the method described by Kačík and Solár [33] (cellulose and hemicellulose). Humic acids (HA) and fulvic acids (FA) were extracted from composts according to the method described by Swift [34]. In addition, analysis of water-soluble alkali was conducted according to the EN 15105 standard test method. The summarized results are shown in Table 3.

2.4. Pyrolysis Experiments. The pyrolysis experiments were conducted in a stainless steel fixed bed reactor equipped with an electric heater (Parr). The temperature of the heater was controlled by a temperature controller (Parr, 4836 controller), while the reaction temperature was monitored by a K-type thermocouple. The experiments were carried out in

Table 3: Biochemical components, humic to fulvic acids ratio, and water-soluble alkali contents of composts.

Compost	Lignin (wt%)	Cellulose (wt%)	Hemicellulose (wt%)	HA/FA	Na (mg/g)	K (g/kg)
R	37.47	43.07	19.07	2.63	1.4	7.76
RC	34.04	51.71	02.51	2.57	4.92	3.44
TF	36.27	51.49	06.99	2.58	1.16	4.71
TO	38.2	46.2	17.92	3.13	1.51	7.7
MB	30.48	55.41	05.98	2.58	2.09	3.93
MC	38.24	43.62	09.07	3.12	3.01	7.76
FP	34.66	54.75	07.18	2.87	4.42	7.86
FB	36.54	53.47	07.78	2.58	1.35	2.87
FL	34.75	50.28	05.77	2.57	1.12	6.7

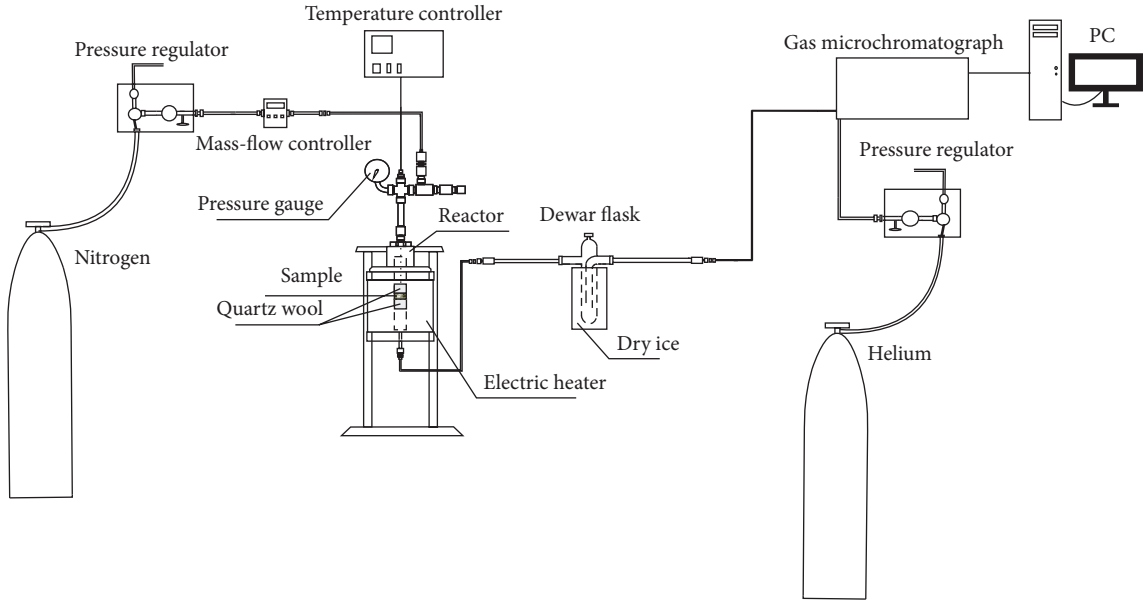

Figure 1: Experimental setup.

N_2 atmosphere and the flow of gas was controlled by a mass- flow controller (SIERRA C100 Serie, Smart-Trak). The experimental setup is presented in Figure 1. For all pyrolysis experiments, 0.5 g of compost was loaded into the reactor and heated to a final temperature of 700°C. The flow of N_2 was maintained at 20 smL/min for all experiments. The experiments were considered completed when N_2 was the only gas detected by online gas chromatography (GC).

2.5. Analysis of Gas Product. The noncondensable pyrolysis product was analyzed by online 2-channel GC (Agilent 3000) equipped with thermal conductivity detectors. The channels were equipped with the following columns: Molsieve for separation of H_2, N_2, CO, and CH_4 and PLOT U for separation of CO_2, C_2, and C_3.

2.6. Statistical Analysis. The relationships between components of chemical analyses and pyrolysis gaseous products yields were tested by bivariate correlation analysis, specifically Pearson's correlations. SPSS 17 statistical software was applied.

3. Results and Discussion

3.1. Gas Yield and Evolution. The yield of gaseous products obtained from pyrolysis of NHG and HG composts referred to as a gram of compost used is presented in Figure 2. The highest yield of pyrolysis gaseous products among NHG composts (328.81 mL/g, also the highest yield among all composts pyrolyzed) was obtained for RC compost, whereas the lowest yield of pyrolysis gaseous products (281.74 mL/g) among NHG composts was obtained for MC compost. The highest pyrolysis gas yield among HG composts was obtained for FL compost (286.41 mL/g), whereas the lowest pyrolysis gas yield was obtained for FP compost (251.77 mL/g) which also exhibited the lowest gas yield among all composts examined. The yield of pyrolysis gas decreased in the following order: RC > R > TF > TO > MB > MC for composts made from nonhybrid grasses and FL > FB > FP for composts made from hybrid grasses.

Figure 3 shows the evolution profiles of released pyrolysis gas as a function of temperature. Figure 3(a) presents the evolution profiles of gas released during pyrolysis of NHG composts, while Figure 3(b) shows the evolution profiles of

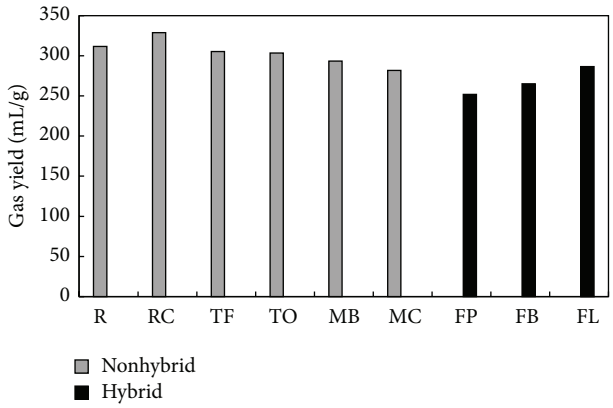

Figure 2: Total gas yield of composts.

gas released during pyrolysis of HG composts. The emission of noncondensable pyrolysis gases at temperature below 500°C is related in majority to degradation of the biochemical structures of compost as well as humic substances formed during the composting process [21, 23, 35, 36], whereas the release of gases at temperature >500°C is likely associated with secondary reactions of char formed from biochemical components or humic substances [21, 23, 28, 35, 36]. In general, pyrolysis gases began to release at 170°C for all compost samples examined which is equivalent to the beginning of thermal degradation of hemicellulosic fraction [23]. The distinction was only observed for the pyrolysis experiment conducted on compost made from hybrid grass (FB) for which a beginning of gas evolution at 247°C was observed. Apart from TO compost which exhibited a three-stage evolution profile (three peaks were observed), all composts investigated resulted in two-stage evolution profiles (two peaks were observed). The composts made from nonhybrid grasses exhibited the maximum of the first peak at temperature range of 315–430°C which is a typical temperature range of thermal degradation of cellulose fraction [29, 30, 37]. The maximum of the second peak was observed at 472°C for TF compost, 508°C for R, RC, and MC composts, and 539°C for TO and MB composts and can be mainly attributed to thermal degradation of lignin and secondary reactions of chars and liquids [23, 29, 30, 37]. The third peak observed for TO compost was detected at 588°C and is also likely due to thermal degradation of lignin and secondary reactions of chars and liquids [23, 29, 30, 37]. As previously mentioned, composts made from hybrid grasses resulted in two-stage gas evolution profiles as well, although more noticeable shifts in the peaks maximum were observed. Specifically, a shift from maximum at 315°C to maximum at 377°C was observed for FP, FB, and FL composts, respectively, and a shift from maximum at 430°C to maximum at 472°C and to maximum at 539°C for the second peak was observed for FP, FL, and FB composts, correspondingly. The change of peaks maximum noted for the FB composts is likely due to the delay of starting point of pyrolysis gas release.

3.2. Pyrolysis Gas Composition. The yields of major pyrolysis gaseous products (H_2, CO_2, CO, and CH_4) from grass composts are presented in Figure 4. Other products such as short-chain hydrocarbons (i.e., C_2 and C_3) were also detected but in sizably lower amounts (less than 1 vol%) and will not be discussed. Figure 4(a) shows yields of NHG composts gaseous products, whereas Figure 4(b) shows yields of HG composts gaseous products. The yields were calculated at 700°C (after 112 min) and at N_2 free-vol%. Among NHG composts, MC compost resulted in the highest production of H_2 (62.17 vol%), the lowest formation of CO (12.74 vol%) and CH_4 (5.10 vol%), and the second lowest formation of CO_2 (18.93 vol%). The lowest yield of H_2 (48.32 vol%) was observed for MB compost and as expected it also resulted in the highest CO (21.34 vol%) and CH_4 (8.01 vol%) formation and a moderately high formation of CO_2 (20.30 vol%). The majority of these observations are directly related to the biochemical composition of examined composts and the contents of water-soluble alkali. Specifically, lignin, cellulose, and potassium (K) contents were found to be associated with H_2 as well as CO and CH_4 formation. A positive correlation was observed between H_2 yield and lignin ($R = 0.916$, $P < 0.05$), and stronger negative correlations were observed between CO yield and lignin ($R = -0.974$, $P < 0.01$) and between CH_4 yield and lignin ($R = -0.929$, $P < 0.01$). The relationship between H_2 and lignin is consistent with the results obtained by Barneto et al. [10] who examined the effect of *Leucaena* and tagasaste composts on the production of volatiles from pyrolysis and reported 75 wt% production of H_2 from lignin. A positive correlation was also observed between H_2 yield and K content ($R = 0.750$, $P < 0.1$) and negative correlations were obtained between CO and CH_4 yields and K content ($R = -0.901$, $P < 0.05$ and $R = -0.742$, $P < 0.1$, correspondingly). Negative relationships between K content and CO and CH_4 were likewise observed by Couhert et al. [38] who reported that mineral matter can influence pyrolysis reactions occurring inside the component's particle and decrease the formation of aforementioned gases. As previously mentioned, these correlations can also be explained by the occurrence of char gasification reactions ((4) and (5)) which are likely to be a result of combination of lignin and K contents. A higher lignin content is associated with a higher K content (i.e., Pearson's correlation coefficient between lignin and K content was 0.832, $P < 0.05$) [28, 39]. Potassium, on the other hand, is known to be an effective catalyst for char gasification [20, 24, 39]. Both MC and MB composts have shown the highest and the lowest lignin and K contents which would explain their H_2 and CO yields, the highest and lowest for MC compost, and the opposite for MB compost, respectively. As previously noted, the formation of H_2 in majority from charring reactions was also confirmed by Barneto et al. [10]. Opposite correlations to those observed between lignin content and CO, CH_4, and H_2 yields were found for cellulose. That is, a negative correlation was calculated between H_2 yield and cellulose content ($R = -0.860$, $P < 0.05$), and positive correlations were found between CO yield and cellulose content ($R = 0.952$, $P < 0.01$) and between CH_4 yield and cellulose content ($R = 0.876$, $P < 0.05$). The strong positive relationship between CO yield and cellulose content is directly related to higher content of carbonyl groups in cellulose, which is consistent with results obtained by Qu et al.

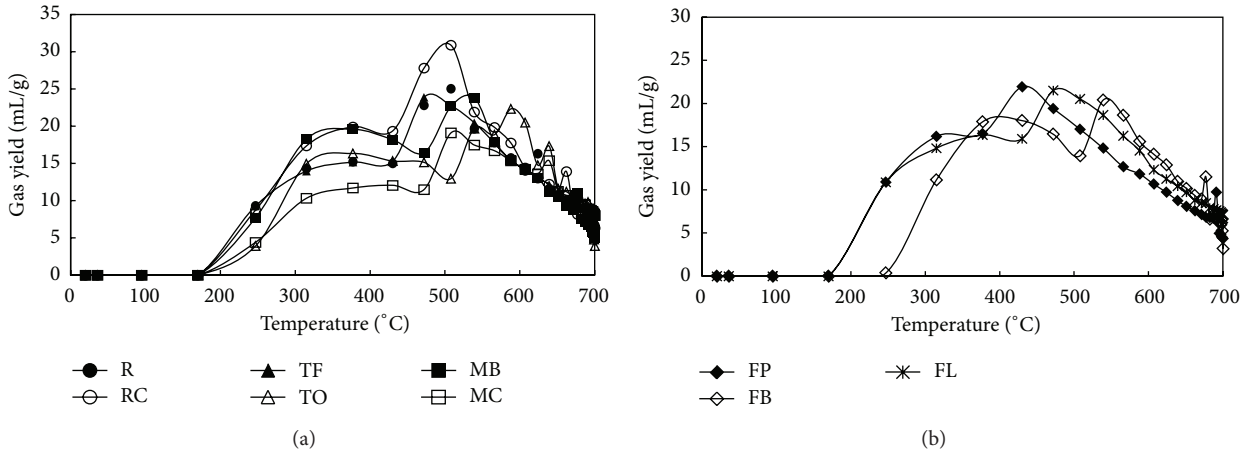

Figure 3: Evolution of gas released during pyrolysis of composts: (a) NHG and (b) HG as a function of temperature.

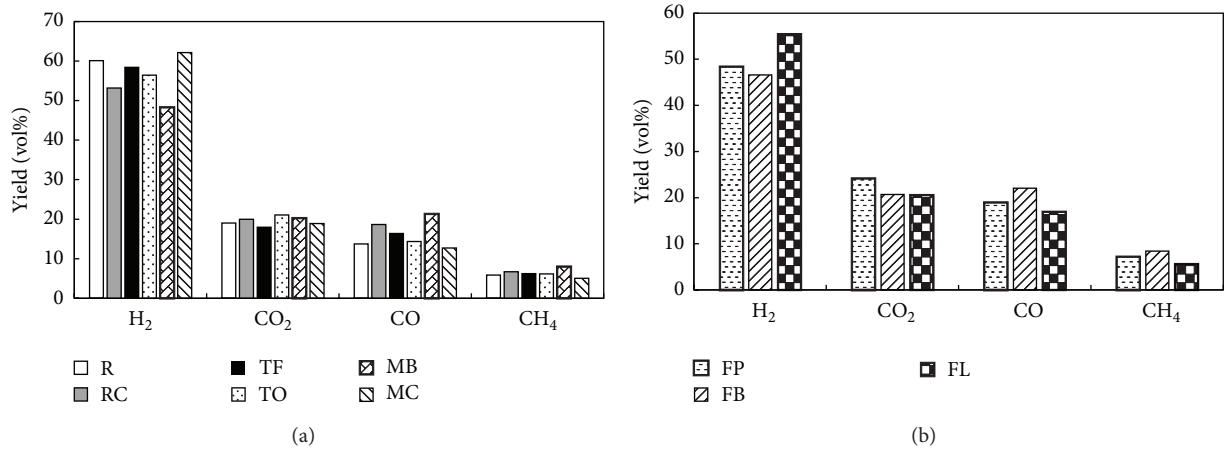

Figure 4: Yields of individual gaseous products from pyrolysis of (a) NHG composts and (b) HG composts at 700°C and N_2 free-vol%.

[28] and Yang et al. [29]. The exception to the observed correlations was observed for CO_2 yield which was found to be unrelated to either biochemical composition or water-soluble alkali. Instead, a weaker and marginally significant correlation to one of the components of proximate analysis, moisture, was observed ($R = 0.780$, $P < 0.1$), which is a further confirmation of presence of water-gas shift reaction.

The individual products yields trends observed for NHG composts were also observed for two out of three HG composts, namely, FP and FB (Figure 4(b)). The remaining compost, FL, resulted in the highest yield of H_2 (55.43 vol%) and the lowest yields of CO_2 (20.58 vol%), CO (16.95 vol%), and CH_4 (5.60 vol%). The analogy of NHG composts cannot be, however, applied to these samples as the correlation between lignin and K contents was in the opposite direction ($R = -0.983$) with a value which fell just shy of the statistical significance threshold ($P = 0.127$). A negative correlation between lignin and K was also reported by Fahmi et al. [40] who investigated the effect of alkali metals on pyrolysis of *Lolium* and *Festuca* independently. For this reason, the NHG and HG composts samples were also separated in this study when examining the possible relationships between gaseous product yields and composts composition. In addition, the correlations between individual products' (H_2, CO, and CH_4) yields and lignin content were no longer applicable and insignificant due to the small number of observations. The observed changes may, however, suggest that as much as both lignin and K contents affect the H_2 formation during pyrolysis of NHG composts, in the case of HG composts, it may be K content that has the greatest influence on H_2 production.

Figure 5 presents the evolution profiles of pyrolysis gaseous products of NHG composts (Figure 5(a)) and HG composts (Figure 5(b)) as a function of temperature. The products released at temperature below 450°C consisted mainly of CO_2, CO, and CH_4 which is consistent with the prior literature [21]. A further increase of pyrolysis temperature changed the emission of pyrolysis gases as the yield of CO and CO_2 began to decrease in expense of greater H_2 and CH_4 formation. The greatest discrepancies in the emission profiles of primary noncondensable gases were observed for H_2 profiles. The differences occurred not only in the gas release temperature but in the shape of evolution profiles as

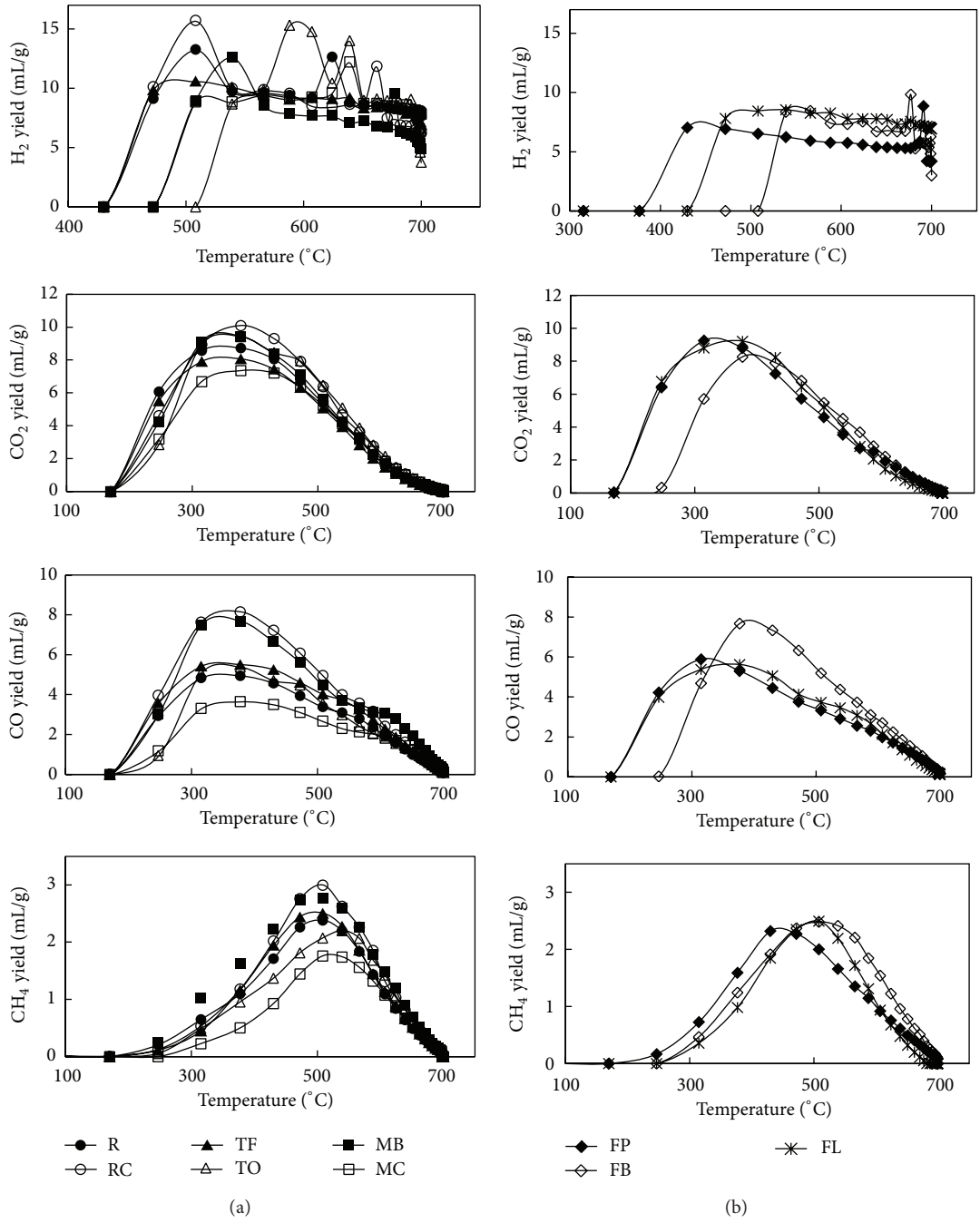

Figure 5: Evolution profiles of individual gaseous products from pyrolysis of (a) NHG composts and (b) HG composts.

well. The emission of H_2 during pyrolysis of NHG composts began at 430°C (R, RC, and TF composts), 472°C (MC and MB composts), and 508°C (TO compost), whereas the release of H_2 during pyrolysis of HG composts began at 377°C (FP compost), 430°C (FL compost), and 508°C (FB compost). The majority of NHG composts (R, RC, TO, and MB) exhibited double-peak profiles with some shift of both the first peak maximum (observed in the 508–588°C range) and the second peak maximum (observed in the 624–677°C range). The maximum of the first peak is the highest and is attributed to cracking of C–H bonds of lignin and cellulose and its shift is a consequence of a change of released temperature [29], whereas the second peak is smaller and is associated with pyrolytic reactions of lignin due to its higher content of aromatic ring (i.e., cracking and deformation of C=C and C-H bonds) and charring reactions [29, 31]. The observed changes are also a further confirmation of the fact that the formation of H_2 at temperature >400°C is mostly contributed by pyrolysis of biochemical components, whereas the release of H_2 at temperature >500°C is mainly attributed to thermal degradation of lignin and the occurrence of charring reactions [21, 35, 36]. As aforementioned, these reactions are

more pronounced in the energy grasses than in other biomass type materials (i.e., wood) due to a greater amount of alkali metals responsible for catalyzing these types of reactions [35, 36]. The remaining NHG composts, MC and TF, resulted in single-peak or no-peak evolution profiles, respectively. Similar H_2 profiles were exhibited by HG compost; specifically, a single-peak profile was obtained for FP and FB composts, whereas a no-peak profile was obtained for FL compost. The resemblance between HG composts corresponds well with the profile obtained for TF compost since HG composts are a cross between *Festuca* (FT) and *Lolium*. The overall yield of formed H_2 in these samples is also related to a combination of both pyrolytic reactions of biochemical compounds and charring reactions.

No significant discrepancies between NHG and HG composts were observed in the emission profiles of the remaining gaseous products. All samples displayed wide single-peak profiles and, in general, a starting point of emission at 170°C. The shift of a starting point of emission to 247°C was only observed for FB compost for CO and CO_2 evolution profiles. The majority of CO_2 release took place in the temperature ranges of 250–450°C for FP and FL (hybrid grasses) composts, and 300–500°C for NHG and FB (hybrid grass) composts. This corresponds well with CO_2 release from all biochemical components through cracking and reforming of carboxyl groups [28, 29, 41] and is in agreement with calculated Pearson's correlations (i.e., no single statistically significant relationship towards one particular biochemical component was observed). A reduction of CO_2 emission at temperature >500°C is likely due to secondary reactions of volatiles as temperature at this point has a limited influence [21, 42]. A minor difference between both types of composts was observed in the emission of CO. That is, a single evolution profile with a release of majority of the product in 300–500°C range was obtained for RC, MB (nonhybrid grasses), and FB (hybrid grass) composts. The remaining samples exhibited a wider but shorter CO peak at temperature ranges of 300–500°C and 250–500°C with a break of possible second peak at 500–640°C range for R, TF, TO, and MC (nonhybrid grasses) and FP and FL (hybrid grasses) composts, correspondingly. The CO emission is mainly attributed to cracking of carbonyl and carboxyl groups from cellulose [28, 29, 41]. The most constant evolution profile was obtained for CH_4 as its emission focused mainly at a temperature range of 450–550°C and was attributed to cracking of methoxyl groups [28, 29, 41].

3.3. Syngas Production. The high variability of CO and H_2 yields led to gas mixtures with equally high variability of H_2/CO ratios. Figure 6 presents total yield of formed syngas with respect to the particular H_2/CO ratio, specifically, the total yield of syngas produced with H_2/CO = 2 used in Fischer-Tropsch and methanol syntheses and with H_2/CO = 3 used for synthetic natural gas production. All compost samples investigated resulted in syngas formation with H_2/CO = 2. However, only five composts resulted in the production of syngas with H_2/CO = 3 (i.e., R, TF, TO, and MC composts obtained from nonhybrid grasses and FL compost from hybrid grass). The highest amount of syngas with H_2/CO = 2 was obtained for MB (nonhybrid grass) and FB (hybrid grass) composts, 67.23 vol% and 67.38 vol%, respectively. These two composts also resulted in the lowest H_2 and the highest CO yields, correspondingly, whereas the highest amount of syngas with H_2/CO = 3 (72.10 vol%) was obtained from pyrolysis of TF (nonhybrid grass) compost.

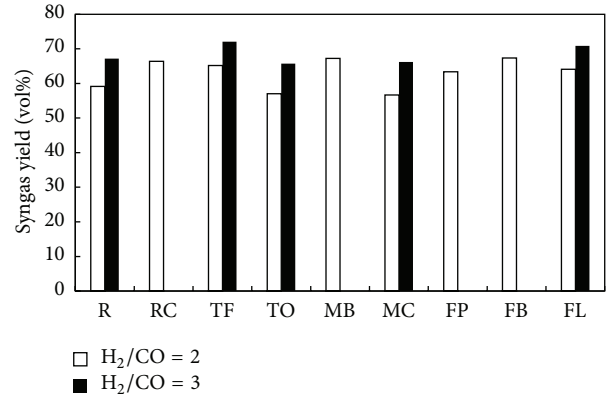

Figure 6: Total yield of syngas at H_2/CO = 2 and H_2/CO = 3.

The change of H_2/CO ratio with pyrolysis temperature is shown in Figure 7. In general, apart from two samples, TO and MC composts, all composts displayed a gradual increase of H_2/CO ratio with a pyrolysis temperature increase up to 650°C. A further increase of pyrolysis temperature resulted in a steep H_2/CO ratio increase which corresponds well with obtained CO evolution profiles and indicates mostly H_2 generation. The TO and MC composts exhibited a more abrupt increase of H_2/CO ratio with a pyrolysis temperature increase, which can indicate a higher rate of charring and cracking reactions for these particular samples. It was not a surprise that in regard to the specific value of H_2/CO ratio, these two composts reached this value at the lowest temperature. That is, a H_2/CO ratio = 2 was obtained at 624 and 639°C, whereas a H_2/CO ratio = 3 was obtained at 673 and 684°C, for MC and TO composts, respectively. Among samples for which H_2/CO ratios increased gradually, only one sample in particular reached the required H_2/CO ratio at a similar temperature range. Specifically, R composts resulted in H_2/CO ratio = 2 at 624°C and in H_2/CO ratio = 3 at 682°C. The remaining samples reached the essential H_2/CO ratio in higher temperature ranges of 660–700°C and 695–700°C for H_2/CO ratio = 2 and H_2/CO ratio = 3, correspondingly. The temperature necessary to obtain the specific H_2/CO ratios increased, therefore, in the following composts type order: (i) H_2/CO = 2: R, MC < TO < TF < FL < RC < FP < MB < FB and (ii) H_2/CO = 3: MC < R < TO < TF < FL.

3.4. Pyrolysis Gas HHV. The HHVs of pyrolysis gas with respect to its total yield and syngas yield are displayed in Figure 8. The size of the bubble represents the HHV expressed in MJ/kg_{gas} obtained at a specific pyrolysis temperature at which an explicit H_2/CO ratio was reached. Figure 8(a) shows the HHVs of pyrolysis gas obtained at H_2/CO = 2, and

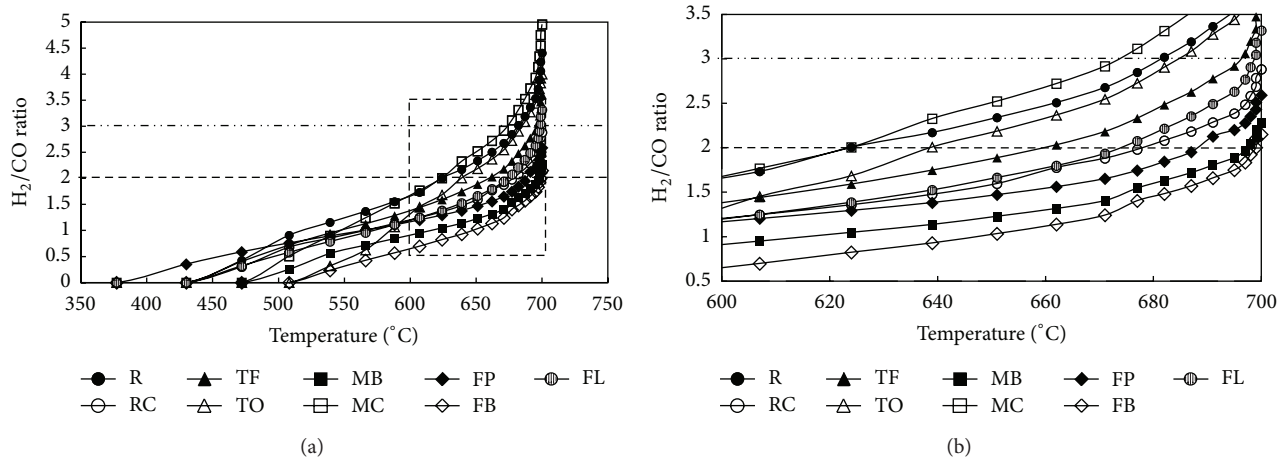

Figure 7: H_2/CO ratio as a function of temperature.

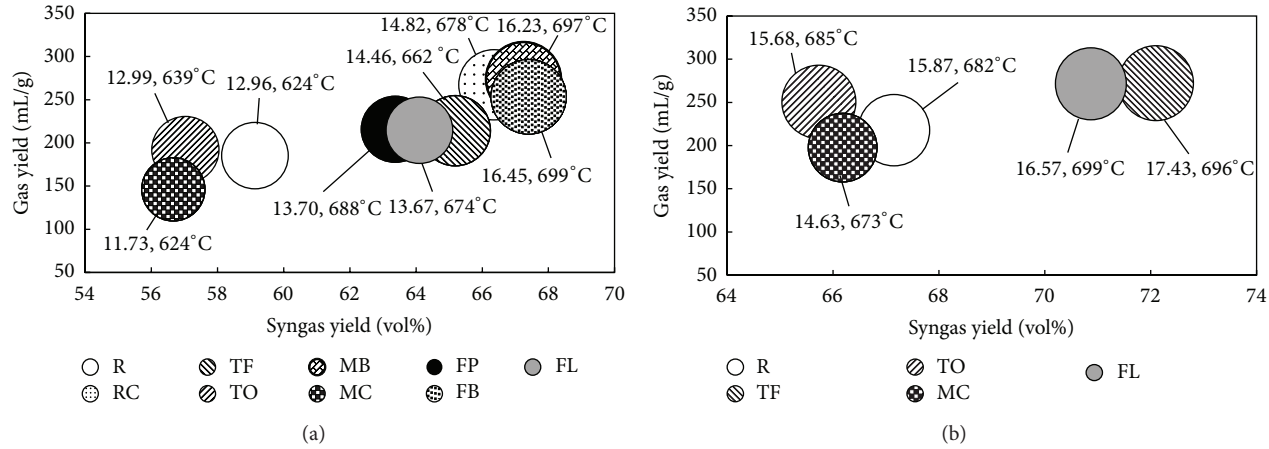

Figure 8: HHVs of pyrolysis gas with respect to its yield and syngas yield: (a) H_2/CO = 2 and (b) H_2/CO = 3.

Figure 8(b) shows the HHVs of pyrolysis gas obtained at H_2/CO = 3. The HHV was directly associated with pyrolysis temperature; that is, as pyrolysis temperature increased, the HHV increased as well. As a consequence, the optimal HHV was reached at the highest syngas yield, which is consistent with the prior literature [21, 43, 44], but not at the highest gas yield. For example, the highest HHV at H_2/CO = 2 in the amount of 16.23 and 16.45 MJ/kg_{gas} was obtained for MB (nonhybrid grass) and FB (hybrid grass) composts, respectively, which also resulted in the highest syngas formation; however, they exhibited one of the lowest total gas yields, whereas the highest HHV at H_2/CO = 3 was obtained for TF (nonhybrid grass) and FL (hybrid grass) composts, 16.57 and 17.43 MJ/kg_{gas}, correspondingly, which corresponded to the highest syngas yield and third highest total gas yield for TF compost and the highest total gas yield and second highest syngas yield for FL compost. It is important to note that these values are only marginally lower than the HHVs obtained for raw materials (i.e., by 5.69%, 9.17%, 4.22%, and 4.28% for MB, FB, TF, and FL composts, resp.) and are comparable to those obtained from pyrolysis of wood or coir pith [39, 45]. The HHVs of pyrolysis gas reported in the literature are significantly lower (4–12 MJ/kg_{gas}) and are given mainly for products obtained from pyrolysis of grasses rather than grass composts [12, 42, 43, 46]. The significant increase of observed pyrolysis gases HHV is likely due to (i) composting process which results in lignin enriched material, *ipso facto* greater H_2 formation, and (ii) sawdust addition to the composting process [47].

4. Conclusions

The syngas generation from pyrolysis of nine composts was investigated in this study. Composts were divided into two groups: composts obtained from nonhybrid perennial grasses and composts obtained from hybrid perennial grasses. The pyrolysis experiments were conducted in a fixed bed reactor to a final temperature of 700°C. Apart from compost obtained from tall oatgrass which exhibited the evolution gas profile with three peaks, all the remaining materials displayed two-peak evolution profiles indicating formation of gases based on two main processes: (i) thermal decomposition of biochemical components and (ii) secondary reactions of

char. A distinction between NHG and HG composts was observed for the evolution profiles of individual gaseous products, in particular H_2. HG composts resulted in no-peak evolution profiles, whereas NHG composts displayed two-peak and one-peak distributions. A no-peak distribution was only observed for one of the NHG composts made from tall fescue which belongs to the same genus as hybrid grasses. The remaining gaseous products (CO, CO_2, and CH_4) did not result in significant changes in emission profiles. It was found that all examined composts resulted in H_2/CO necessary for future utilization in the amount of 2 and only five of the studied composts resulted in H_2/CO = 3. A close relationship was established between H_2, CO, and syngas yields, HHV of pyrolysis gas, and temperature required to obtain the essential H_2/CO ratio. Specifically, composts obtaining the highest H_2 yield resulted in the lowest CO yield, following the lowest syngas yield, HHV, and temperature required to obtain the specific H_2/CO ratio, whereas composts obtaining the lowest H_2 yield resulted in the highest CO yield, following the highest syngas yield, HHV, and temperature required to obtain the essential H_2/CO ratio. It was also found that the formation of H_2 was significantly correlated with lignin and K contents for nonhybrid grass. That is, strong positive correlations were obtained between (i) lignin and K contents, (ii) lignin content and H_2 yield, and (iii) K content and H_2 yield. Comparatively, a negative correlation (that just barely fell outside statistical significance) was observed for HG composts between lignin and K contents. The remaining correlations (i.e. between lignin content and H_2 yield and between K content and H_2 yield) were not statistically significant. Remarkable results were also obtained for HHV of pyrolysis gas. Specifically, values close to the HHVs of raw materials, 16.23, 17.43, and 16.45 MJ/kg, were calculated for composts obtained from mountain brome, tall fescue, and festulolium Becva composts, respectively. The increase was attributed to the composting process (i.e., an increase of lignin content) and sawdust addition. Finally, the composts made from mountain brome grass and hybrid Becva were recognized as the optimal materials for fuel/energy generation due to their (i) highest syngas formation and (ii) highest HHV.

Conflict of Interests

The authors declare that there is no conflict of interests regarding the publication of this paper.

Acknowledgments

This research was supported by the Czech Republic Ministry of Education, Youth and Sport, and the Centre ENET research project, Reg. no. CZ.1.05/2.1.00/03.0069, and the Czech Republic Ministry of Agriculture research project, Reg. no. MZ QI101C246, elaborated in the framework of the project New Creative Teams in Priorities of Scientific Research, Reg. no. CZ.1.07/2.3.00/30.0055, supported by Operational Programme Education for Competitiveness, and cofinanced by the European Social Fund and the state budget of the Czech Republic.

References

[1] European Commission, *Report from the Commission to the European Parliament, the Council, the European Economic and Social Committee and the Committee of the Regions*, 2013.

[2] R. E. H. Sims, A. Hastings, B. Schlamadinger, G. Taylor, and P. Smith, "Energy crops: current status and future prospects," *Global Change Biology*, vol. 12, no. 11, pp. 2054–2076, 2006.

[3] H. Haberl, K. Erb, F. Krausmann et al., "Global bioenergy potentials from agricultural land in 2050: sensitivity to climate change, diets and yields," *Biomass and Bioenergy*, vol. 35, no. 12, pp. 4753–4769, 2011.

[4] Commission of the European Communities, "Report from the Commission to the Council on the review of the energy crops scheme," 2006, http://iet.jrc.ec.europa.eu/remea/sites/remea/files/files/documents/com_2006_500_energy_crops_scheme.pdf.

[5] L. Potter, M. J. Bingham, M. G. Baker, and S. P. Long, "The potential of two perennial C_4 grasses and a perennial C_4 sedge as ligno-cellulosic fuel crops in N. W. Europe. Crop establishment and yields in E. England," *Annals of Botany*, vol. 76, no. 5, pp. 513–520, 1995.

[6] M. Rahman, S. B. Mostafiz, J. V. Paatero, and R. Lahdelama, "Extension of energy crops on surplus agricultural lands: a potentially viable option in developing countries while fossil fuel reserves are diminishing," *Renewable and Sustainable Energy Reviews*, vol. 29, pp. 108–119, 2014.

[7] C. Wrobel, B. E. Coulman, and D. L. Smith, "The potential use of reed canarygrass (*Phalaris arundinacea* L.) as a biofuel crop," *Acta Agriculturae Scandinavica B: Soil and Plant Science*, vol. 59, no. 1, pp. 1–18, 2009.

[8] Czech Statistical Office, "Harvest of permanent grassland in hay in 2012 by regions," 2013, http://www.czso.cz/csu/2013edicniplan.nsf/engt/1000218C20/$File/21021326.pdf.

[9] Czech Statistical Office, "Agriculture—3rd quarter of 2013. Meat production at the last year level, agricultural producer prices increased," 2013, http://www.czso.cz/csu/csu.nsf/informace/czem103113.doc.

[10] A. G. Barneto, J. A. Carmona, and M. Jesús Díaz Blanco, "Effect of the previous composting on volatiles production during biomass pyrolysis," *Journal of Physical Chemistry A*, vol. 114, no. 11, pp. 3756–3763, 2010.

[11] R. C. Baliban, J. A. Elia, V. Weekman, and C. A. Floudas, "Process synthesis of hybrid coal, biomass, and natural gas to liquids via Fischer-Tropsch synthesis, ZSM-5 catalytic conversion, methanol synthesis, methanol-to-gasoline, and methanol-to-olefins/distillate technologies," *Computers & Chemical Engineering*, vol. 47, pp. 29–56, 2012.

[12] A. A. Boateng, K. B. Hicks, and K. P. Vogel, "Pyrolysis of switchgrass (Panicum virgatum) harvested at several stages of maturity," *Journal of Analytical and Applied Pyrolysis*, vol. 75, no. 2, pp. 55–64, 2006.

[13] A. Moutsoglou, "A comparison of prairie cordgrass and switchgrass as a biomass for syngas production," *Fuel*, vol. 95, pp. 573–577, 2012.

[14] A. Gomez-Barea, S. Nilsson, F. V. Barrero, and M. Campoy, "Devolatilization of wood and wastes in fluidized bed," *Fuel Processing Technology*, vol. 91, no. 11, pp. 1624–1633, 2010.

[15] S. Li, S. Xu, S. Liu, C. Yang, and Q. Lu, "Fast pyrolysis of biomass in free-fall reactor for hydrogen-rich gas," *Fuel Processing Technology*, vol. 85, no. 8–10, pp. 1201–1211, 2004.

[16] P. Chaiwatanodom, S. Vivanpatarakij, and S. Assabumrungrat, "Thermodynamic analysis of biomass gasification with CO_2

recycle for synthesis gas production," *Applied Energy*, vol. 114, pp. 10–17, 2014.

[17] Y. Bai, Y. Wang, S. Zhu, L. Yan, F. Li, and K. Xie, "Synergistic effect between CO_2 and H_2O on reactivity during coal chars gasification," *Fuel*, vol. 126, pp. 1–7, 2014.

[18] M. J. A. Tijmensen, A. P. C. Faaij, C. N. Hamelinck, and M. R. M. Van Hardeveld, "Exploration of the possibilities for production of Fischer Tropsch liquids and power via biomass gasification," *Biomass and Bioenergy*, vol. 23, no. 2, pp. 129–152, 2002.

[19] M. Widyawati, T. L. Church, N. H. Florin, and A. T. Harris, "Hydrogen synthesis from biomass pyrolysis with in situ carbon dioxide capture using calcium oxide," *International Journal of Hydrogen Energy*, vol. 36, no. 8, pp. 4800–4813, 2011.

[20] A. Domínguez, J. A. Menéndez, Y. Fernández et al., "Conventional and microwave induced pyrolysis of coffee hulls for the production of a hydrogen rich fuel gas," *Journal of Analytical and Applied Pyrolysis*, vol. 79, no. 1-2, pp. 128–135, 2007.

[21] D. Neves, H. Thunman, A. Matos, L. Tarelho, and A. Gómez-Barea, "Characterization and prediction of biomass pyrolysis products," *Progress in Energy and Combustion Science*, vol. 37, no. 5, pp. 611–630, 2011.

[22] A. Dufour, P. Girods, E. Masson, Y. Rogaume, and A. Zoulalian, "Synthesis gas production by biomass pyrolysis: effect of reactor temperature on product distribution," *International Journal of Hydrogen Energy*, vol. 34, no. 4, pp. 1726–1734, 2009.

[23] A. G. Barneto, J. A. Carmona, J. A. Conesa Ferrer, and M. J. Díaz Blanco, "Kinetic study on the thermal degradation of a biomass and its compost: composting effect on hydrogen production," *Fuel*, vol. 89, no. 2, pp. 462–473, 2010.

[24] A. G. Barneto, J. A. Carmona, A. Gálvez, and J. A. Conesa, "Effects of the composting and the heating rate on biomass gasification," *Energy & Fuels*, vol. 23, no. 2, pp. 951–957, 2009.

[25] M. P. Bernal, J. A. Alburquerque, and R. Moral, "Composting of animal manures and chemical criteria for compost maturity assessment: a review," *Bioresource Technology*, vol. 100, no. 22, pp. 5444–5453, 2009.

[26] D. Plachá, H. Raclavská, M. Kučerova, and J. Kuchařova, "Volatile fatty acid evolution in biomass mixture composts prepared in open and closed bioreactors," *Waste Management*, vol. 33, no. 5, pp. 1104–1112, 2013.

[27] M. Blanco and G. Almendros, "Maturity assessment of wheat straw composts by thermogravimetric analysis," *Journal of Agricultural and Food Chemistry*, vol. 42, no. 11, pp. 2454–2459, 1994.

[28] T. Qu, W. Guo, L. Shen, J. Xiao, and K. Zhao, "Experimental study of biomass pyrolysis based on three major components: hemicellulose, cellulose, and lignin," *Industrial and Engineering Chemistry Research*, vol. 50, no. 18, pp. 10424–10433, 2011.

[29] H. Yang, R. Yan, H. Chen, D. H. Lee, and C. Zheng, "Characteristics of hemicellulose, cellulose and lignin pyrolysis," *Fuel*, vol. 86, no. 12-13, pp. 1781–1788, 2007.

[30] H. Yang, R. Yan, H. Chen, C. Zheng, D. H. Lee, and D. T. Liang, "In-depth investigation of biomass pyrolysis based on three major components: hemicellulose, cellulose and lignin," *Energy & Fuels*, vol. 20, no. 1, pp. 388–393, 2006.

[31] A. G. Barneto, J. A. Carmona, J. E. M. Alfonso, and J. A. C. Ferrer, "Use of thermogravimetry/mass spectrometry analysis to explain the origin of volatiles produced during biomass pyrolysis," *Industrial and Engineering Chemistry Research*, vol. 48, no. 15, pp. 7430–7436, 2009.

[32] F. Collard, J. Blin, A. Bensakhria, and J. Valette, "Influence of impregnated metal on the pyrolysis conversion of biomass constituents," *Journal of Analytical and Applied Pyrolysis*, vol. 95, pp. 213–226, 2012.

[33] F. Kačík and R. Solár, *Analytická chémia dreva*, Technical University in Zvolen, Zvolen, Slovakia, 2000.

[34] R. S. Swift, "Organic matter characterization," in *Methods of Soil Analysis, Part 3 Chemical Methods*, D. L. Sparks, A. L. Page, P. A. Helmke et al., Eds., pp. 1011–1069, Soil Science Society of America and American Society of Agronomy, Madison, Wis, USA, 1996.

[35] C. J. Gómez, E. Mészáros, E. Jakab, E. Velo, and L. Puigjaner, "Thermogravimetry/mass spectrometry study of woody residues and an herbaceous biomass crop using PCA techniques," *Journal of Analytical and Applied Pyrolysis*, vol. 80, no. 2, pp. 416–426, 2007.

[36] R. A. Khalil, E. Mészáros, M. G. Grønli et al., "Thermal analysis of energy crops: part I: the applicability of a macro-thermobalance for biomass studies," *Journal of Analytical and Applied Pyrolysis*, vol. 81, no. 1, pp. 52–59, 2008.

[37] K. Raveendran, A. Ganesh, and K. C. Khilar, "Pyrolysis characteristics of biomass and biomass components," *Fuel*, vol. 75, no. 8, pp. 987–998, 1996.

[38] C. Couhert, J. Commandre, and S. Salvador, "Is it possible to predict gas yields of any biomass after rapid pyrolysis at high temperature from its composition in cellulose, hemicellulose and lignin?" *Fuel*, vol. 88, no. 3, pp. 408–417, 2009.

[39] K. Raveendran, A. Ganesh, and K. C. Khilar, "Influence of mineral matter on biomass pyrolysis characteristics," *Fuel*, vol. 74, no. 12, pp. 1812–1822, 1995.

[40] R. Fahmi, A. V. Bridgwater, L. I. Darvell et al., "The effect of alkali metals on combustion and pyrolysis of *Lolium* and *Festuca* grasses, switchgrass and willow," *Fuel*, vol. 86, no. 10-11, pp. 1560–1569, 2007.

[41] L. Jiang, S. Hu, L. Sun et al., "Influence of different demineralization treatments on physicochemical structure and thermal degradation of biomass," *Bioresource Technology*, vol. 146, pp. 254–260, 2013.

[42] A. A. Boateng, W. F. Anderson, and J. G. Phillips, "Bermudagrass for biofuels: effect of two genotypes on pyrolysis product yield," *Energy and Fuels*, vol. 21, no. 2, pp. 1183–1187, 2007.

[43] A. A. Boateng, H. G. Jung, and P. R. Adler, "Pyrolysis of energy crops including alfalfa stems, reed canarygrass, and eastern gamagrass," *Fuel*, vol. 85, no. 17-18, pp. 2450–2457, 2006.

[44] D. Beneroso, J. M. Bermúdez, A. Arenillas, and J. A. Menéndez, "Microwave pyrolysis of microalgae for high syngas production," *Bioresource Technology*, vol. 144, pp. 240–246, 2013.

[45] K. Raveendran and A. Ganesh, "Heating value of biomass and biomass pyrolysis products," *Fuel*, vol. 75, no. 15, pp. 1715–1720, 1996.

[46] J. A. Conesa and A. Domene, "Synthesis gas production from various biomass feedstocks," *AIMS Energy*, vol. 1, pp. 17–27, 2013.

[47] S. M. Troy, T. Nolan, J. J. Leahy, P. G. Lawlor, M. G. Healy, and W. Kwapinski, "Effect of sawdust addition and composting of feedstock on renewable energy and biochar production from pyrolysis of anaerobically digested pig manure," *Biomass & Bioenergy*, vol. 49, pp. 1–9, 2013.

Hindawi Publishing Corporation
The Scientific World Journal
Volume 2014, Article ID 537826, 10 pages
http://dx.doi.org/10.1155/2014/537826

Review Article

Assessment of the GHG Reduction Potential from Energy Crops Using a Combined LCA and Biogeochemical Process Models: A Review

Dong Jiang,[1] Mengmeng Hao,[1,2] Jingying Fu,[1,2] Qiao Wang,[3] Yaohuan Huang,[1] and Xinyu Fu[1,2]

[1] *Institute of Geographical Sciences and Natural Resources Research, Chinese Academy of Sciences, 11A Datun Road, Chaoyang District, Beijing 100101, China*
[2] *University of Chinese Academy of Sciences, Beijing 100049, China*
[3] *Satellite Environmental Application Center, Ministry of Environmental Protection, Beijing 100094, China*

Correspondence should be addressed to Jingying Fu; fujy@lreis.ac.cn

Received 17 April 2014; Accepted 26 May 2014; Published 17 June 2014

Academic Editor: Yang-Chun Yong

The main purpose for developing biofuel is to reduce GHG (greenhouse gas) emissions, but the comprehensive environmental impact of such fuels is not clear. Life cycle analysis (LCA), as a complete comprehensive analysis method, has been widely used in bioenergy assessment studies. Great efforts have been directed toward establishing an efficient method for comprehensively estimating the greenhouse gas (GHG) emission reduction potential from the large-scale cultivation of energy plants by combining LCA with ecosystem/biogeochemical process models. LCA presents a general framework for evaluating the energy consumption and GHG emission from energy crop planting, yield acquisition, production, product use, and postprocessing. Meanwhile, ecosystem/biogeochemical process models are adopted to simulate the fluxes and storage of energy, water, carbon, and nitrogen in the soil-plant (energy crops) soil continuum. Although clear progress has been made in recent years, some problems still exist in current studies and should be addressed. This paper reviews the state-of-the-art method for estimating GHG emission reduction through developing energy crops and introduces in detail a new approach for assessing GHG emission reduction by combining LCA with biogeochemical process models. The main achievements of this study along with the problems in current studies are described and discussed.

1. Introduction

The increasing consumption of fossil fuel and current ecological environmental problems are global challenges. Plant-based bioenergy liquid fuel (including biofuel ethanol and biodiesel) is an effective way to relieve the energy crisis and also protect the environment due to its advantages of cleanness, safety, and reproducibility [1, 2]. After nearly 10 years, the worldwide production of liquid fuel is developing very rapidly, increasing from 0.96 billion in 2001 to 21.4 billion in 2011. The European Union, the USA, and Brazil are the main forces in the development of the biomass energy industry [3]. Although the development of the global biofuel industry has shown a great trend driven by the energy requirement and related policies, there are still many challenges in large-scale production. The main raw material of liquid biofuel production is currently cultivated crops. Soybean and corn are widely used in the USA and rapeseed and soybean are used in the European Union for biodiesel development. In Brazil, sugarcane is used for ethanol development [4]. Relatively accurate conclusions regarding productivity and environmental benefits may be drawn based on years of cultivated experience. The production of bioethanol and biodiesel by different energy plants and process techniques can reduce greenhouse gas (GHG) emissions by 12–125% compared with traditional fossil fuels [5–7]. Adler et al. used the DAYCENT biogeochemistry model to assess the soil GHG fluxes and biomass yields for corn, soybean, alfalfa,

hybrid poplar, reed canarygrass, and switchgrass as bioenergy crops in Pennsylvania, USA. The results showed that all cropping systems considered provided net GHG sinks. The net GHG emissions of switchgrass, reed canarygrass, corn-soybean rotation, corn-soybean-alfalfa rotation, and hybrid poplar were reduced by −114%, −84%, −38%, −41%, and −117%, respectively [6]. Large-scale production of biodiesel in the UK was found to save 26% of GWP [8]. However, Jatropha and other noncrop energy plants have not been used long enough to generate sufficient data. The key problem of noncrop energy plants scale development is how to scientifically estimate the potential of GHG emission reduction [9]. If this problem can be solved, the development of biological liquid fuels can be more accurately evaluated and more reasonably planned.

The main purpose for the development of biological liquid fuel is to reduce GHG emissions, but great uncertainty remains regarding its comprehensive environmental impact. Some researchers believe that the patterns of land use change will affect the GHG emissions. These researchers believe that biological liquid fuel development would have a negative impact on the environment if the GHG emissions caused by the land use pattern changes were under consideration [10, 11]. However, according to the latest survey of the American Department of Energy, certain assumptions in the studies above have obvious problems. They assumed that 30 billion gallons of ethanol would be produced from corn annually until 2015, but only 1.5 billion gallons were planned to be produced according to the Energy Independence and Security Act [12]. They also assumed that massive deforestation would occur during the development of biomass energy, but most of the forests were excluded in the planning. Therefore, the assumption of a large amount of cultivated land being occupied is not correct because the biomass energy is developed based on the sparse forest land, sparse shrub land, sparse grassland, shoal/bottomland, and bare land rather than the cultivated land [13].

Regarding the net energy balance problems during production, ethanol from corn yields 25% more energy than the energy invested in its production, whereas biodiesel from soybeans yields 93% more [5]. Switchgrass produces 540% more bioethanol than nonrenewable energy consumed [12], which shows a great advantage of the second generation of biological liquid fuel. Some controversy also exists as to whether the development of bioliquid fuel will reduce GHG emissions. Some studies have indicated that GHG emissions can be reduced by 12–125% with bioliquid fuel production compared to traditional fossil fuels [12]. Bioethanol production from corn can reduce GHG emissions by 13%. The second generation biofuel can reduce more GHG emissions along with the development of process techniques [14]. Bioethanol production from switchgrass instead of fossil fuels can reduce GHG emissions by 94% [15]. Sasaki et al. [16] developed biomass change and harvest models to estimate the woody biomass availability in forests under the current management regime. The total annual production of woody biomass is 563.4 million tons (11.3 EJ) over the same period between 1990 and 2020. The total energy consumption in Southeast Asia was estimated at 6.4 EJ in 1990 and 15.7 EJ in 2006, increasing approximately by 9.0% yr^{-1}. Energy from wood fuels in Southeast Asia (excluding Singapore and Brunei) was estimated at 2.4 EJ in 1993 or approximately 33.1% of the total energy consumption in that year. Energy from wood fuels in this region increased by approximately 2.5% yr^{-1} on average between 1992 and 1995 [17, 18]. Therefore, without effective policies to reduce deforestation and forest degradation, an energy shortage is likely to occur in Southeast Asia. The carbon emission reductions associated with using woody biomass instead of fossil fuels to generate energy are estimated at 281.7 TgC yr^{-1} for replacing coal, 225.3 TgC yr^{-1} for replacing petroleum products, and 169.0 TgC yr^{-1} for replacing natural gas throughout the modeling period using carbon coefficients of 25 kgC GJ^{-1} for coal, 20 kgC GJ^{-1} for petroleum products, and 15 kgC GJ GJ^{-1} for natural gas [16].

Some controversy remains about the effects of biological liquid fuel development on the economy, society, and environment. Therefore, many countries have begun to reevaluate their future biofuel development strategies, exploring strategies that have smaller negative effects on the economy, society, and environment. For example, the European Union decided to postpone the implementation of their goal of replacing 10% of their transportation energy with biological liquid fuel by 2020, and the United States government claimed to assess and monitor the sustainability of biological liquid fuel development [19]. China's biofuel industry is also witnessing rapid development. However, the development of the biodiesel industry is still faced with many uncertainties, among which the accurate estimation of the potentiality of raw material supply, net energy production, and GHG emission reduction is the most crucial issue.

The main objectives of this study are the following: (1) to review the state-of-the-art method for assessing the GHG emission reduction by developing energy crops and (2) to introduce a new approach for assessing the GHG emission reduction by combining life cycle analysis (LCA) with biogeochemical process models. This paper focuses on estimating the GHG reduction of noncrop energy plants, especially in the stages of growing, managing, and harvesting. In addition, the GHG caused by direct land-use changes were considered, while the GHG caused by indirect land-use change were beyond the scope of this paper.

2. Life Cycle Analysis

To become a substitute for fossil fuels, bioliquid fuel should be able to provide net energy, bring environmental and economic benefits, and not reduce the food supply during mass production [6]. LCA is used to evaluate the energy consumption of a product or system throughout its life cycle, including raw material acquisition, production, product use, and postprocessing [3]. In recent years, LCA has been widely used as a complete comprehensive analysis method in bioenergy assessment studies. By comparison with fossil fuels, the consumption across the whole life cycle of biofuels, GHG emission, and primary energy usage can be reduced. Xing et al. [20] calculated and evaluated the land use and water and

energy consumption of three feedstocks, namely, rape seed oil, *Jatropha curcas* L. oil, and waste oil, using LCA that considered planting, harvesting, transportation, pretreatment, biodiesel production, distribution, and consumption. Hu et al. established a life cycle energy consumption and emission assessment model for soybean, rape seed, Cornus wilsoniana wanaer (CWW), and *Jatropha curcas* L. as bases for biodiesel [21]. Wang and Lu analyzed the life cycle energy consumption and pollutant emissions during biodiesel production from *Jatropha curcas* [22]. The costs, energy consumption, and environmental impact of a bioethanol life cycle that used wheat, corn, and sweet potato as raw materials were analyzed by Zhang [23]. Dai et al. [24] evaluated the energy efficiency of the cassava fuel ethanol life cycle in the Guangxi province, China. Nguyen et al. [25] assessed the energy balance and GHG emissions of the cassava fuel ethanol life cycle in Thailand. Sobrino et al. [1] compared energy consumption of bioliquid fuels with fossil fuels throughout the life cycle and found a lower consumption of primary energy and a CO_2 emission reduction after bioliquid fuel replaced certain fossil fuels. Razon and Tan [26] analyzed the net energy gain of bioliquid fuel and biogas using algae. Finally, Lu et al. [27] and Li et al. [28] established the energy and GHG reduction potential of *Pistacia chinensis*.

Most of the current literature is devoted to experimental or theoretical evaluations in estimating the GHG reduction effects of a certain energy plant for unit volume or mass using LCA. The mean value is used when applied on a district level [29]. The result is that the spatial differences in the GHG reduction potential resulting from the spatial heterogeneity of climate, soil, and terrain features cannot be determined. Hence, the GHG reduction potential is difficult to evaluate on a regional scale.

Addressing this problem, some studies proposed introducing spatial data and spatial analysis methods that couple LCA with GIS to evaluate the GHG reduction potential. A multifactor analysis method based on geographic information system (GIS) techniques was adopted to identify marginal lands for bioenergy development. Marginal lands with potential for planting energy plants were identified for each 1 km × 1 km grid across China. The net energy and emission reduction efficiency of biological liquid fuel were identified at each grid and the total GHG emission reduction was then obtained by accumulating the grids [30]. GIS techniques and multifactor comprehensive analysis methods are applied to calculate the potential for planting large-scale cassava in Southwest China. Then, the life cycle net energy and GHG emission reduction capacities of cassava on marginal land with different suitability degrees were calculated based on the expanded life cycle model for cassava ethanol fuel. The results indicate that adopting spatial data (such as the climate, soil, and terrain conditions) as well as a spatial analysis model provides a preliminary solution to solve the GHG reduction evaluation problem on a regional scale. The more reasonable results for GHG reduction potential were estimated at relatively fine geographical scale [31]. Dresen and Jandewerth integrated spatial analyses into LCA-calculated GHG emissions with GIS systems. Using the example of the energetic utilization of biomass via conditioned biogas, the authors presented a GIS-based calculation tool that combines geodata on biomass potentials, infrastructure, land use, cost, and technology with analysis tools for the planning of biogas plants to identify the most efficient plant locations and to calculate the emission balances, biomass streams, and costs in the lower Rhine region and the Altmark region in Germany. The results of the GHG balances were presented. The balances of the individual sites, the regional balances, and their temporal development can be calculated in GIS using LCA methods. GIS tools not only allow the assessment of individual plants but also allow the determination of the GHG reduction potential, the biogas potential, and the necessary investment costs for entire regions. Thus, exploiting regional biogas potentials in a way that is sustainable and climate-friendly becomes simple [32]. Environmental integration, such as GIS and LCA, provides a methodology capable of providing enough information and results to determine an energy crop implementation strategy for reducing the energy consumption and CO_2 eq. emissions. The methodology was applied and verified in a study area in Catalonia (southern Europe). The results showed that a high impact reduction in GHG could be achieved annually (annual reduction of 1,954,904 Mg of CO_2 eq.) [33]. However, some obvious problems remain in the current research. The same parameters were used in the "GHG reduction efficiency" model without considering natural or social conditions. Meanwhile, the total GHG emission reduction potential is not exactly equal to the sum of the grid values, as mutual influences and interactions exist between each grid [29].

3. Model

In recent years, many methods, including LCA, have been widely used in bioenergy assessment studies. However, previous studies typically only calculated the unit mass or unit area of a biofuel life cycle based on a laboratory dataset, that is, the "GHG emission reduction efficiency." Regional total GHG emission reduction potentials were simply considered as "efficiency times total yield." The spatiotemporal variation of environmental factors, such as solar radiation, temperature, soil, and water, was not well described in previous studies. To solve this problem, various models have been adopted for estimating the GHG emission of energy plants. IPCC Tier 1 provided a very practical method for calculating GHG emissions. Ecosystem process models and land surface models have also been used. According to the latest progress in this field, the process-based biogeochemical models were introduced into the framework of LCA to quantitatively calculate the C, N, and GHG emissions during the growth of energy plants and obtain their spatial distribution as well.

3.1. Three-Tier Approaches of IPCC. De Klein et al. (New Zealand) used a three-tier approach to estimate the nitrous oxide (N_2O) emissions from managed soils, including indirect N_2O emissions from the additions of N to land due to deposition and leaching and emissions of carbon dioxide (CO_2) following the additions of liming materials and urea-containing fertilizer. In the most basic form, direct N_2O

emissions from managed soils are estimated using Tier 1 methods ((A.1); see the appendix). If more detailed emission factors and corresponding activity data are available to a country than are presented in Tier 1, then Tier 2 can be undertaken. Tier 3 methods are modeling or measurement approaches that can relate the soil and environmental variables responsible for N_2O emissions to the sizes of those emissions [34]. Tier 1 methods were most widely used because of the data acquisition convenience. Ruesch and Gibbs created a new global map using the IPCC Tier 1 method of biomass carbon stored in above- and below-ground living vegetation. However, the methods they employed are not directly linked to ground-based measures of carbon stocks and have not been validated with field data [35]. At the national level, the intergovernmental panel on climate change (IPCC) has produced a set of guidelines for estimating the GHG inventories at different tiers of quality, ranging from Tier 1 up to Tier 3. The biome averages used in the Tier 1 approach to estimate forest carbon stocks are freely and immediately available and currently provide the only source of globally consistent forest carbon information; however, there are uncertainties caused by natural disturbance, topography, microclimate, and soil type. Additionally, the estimates may be too high or too low for some locations. A study suggested that the default values used in this approach underestimate the carbon stocks for ecosystems, such as temperate moist forests [36–39]. In addition to the weaknesses above, the IPCC guidelines provide the default values of regular crops without the default values of most specific energy plants, such as sugarcane, Miscanthus and Cassava.

3.2. Ecosystem Process Model and Land Surface Model. Wu et al. used a modified version of the soil and water assessment tool (SWAT) as a basic tool to simulate a series of biofuel production scenarios involving crop rotation and land cover changes in the James River Basin of the Midwestern United States. The grasslands could be classified based on the simulations in terms of biomass productivity and nitrogen loads. The group further derived the relationship of biomass production targets and the resulting nitrogen loads, and they projected the annual average water yield NO_3-N load and soil NO_3-N concentration during the 18-year simulation period (1991–2008) [40]. PnET (photosynthetic/evapotranspiration model) is a nested series of models of carbon, water, and nitrogen dynamics for forest ecosystems. The models were developed and validated in the Northeastern USA at both the site and the grid level (to 1 km resolution) by Aber et al. [41]. To contribute toward more reliable estimates of the N_2O source strength of tropical rainforest ecosystems on a regional scale, Kiese et al. modified a process-oriented biogeochemical model, PnET-N-DNDC, and parameterized it to simulate C and N turnover and the production of associated N_2O emissions in and from tropical rainforest ecosystems. The daily simulated N_2O emissions based on site data were in good agreement (model efficiencies up to 0.83) with field observations in the wet tropics of Australia and Costa Rica [42]. A simulation model, Wetland-DNDC, for C dynamics and methane (CH_4) emissions in wetland ecosystems was reported; the model's main structure was adopted from PnET-N-DNDC. The model has been validated against various observations from three wetland sites in Northern America. The validation results agree with the field measurement data [43]. Predictions using PnET-II at the stand or community level indicated that the lumped parameter approach worked well at both large (i.e., multiple community types) and small (within community types) spatial scales [44, 45]. However, this type of approach will provide inaccurate parameter estimates without the right "mix" of species to offset over- and underestimates because the mixture of species resulted in a compensating error [46].

3.3. Biogeochemical Process Models. DAYCENT is a daily time series biogeochemical model used in agroecosystems to simulate the fluxes of carbon and nitrogen in the atmosphere, vegetation, and soil [47, 48]. The model is a version of the CENTURY biogeochemical model using a daily scale. The DAYCENT land surface submodel simulated the soil water and soil temperature dynamics well for a variety of sites ranging from dry grassland, wet managed grassland, and wet crop land systems. The simulated results were compared with observed snow cover data, weekly 0–10 cm soil water data, daily AET data, and soil temperature data. The r^2 values from the observed versus simulated results were between 0.58 and 0.96 [49]. The ability of DAYCENT to simulate NPP, soil organic carbon, N_2O emissions, and NO_3 leaching has been tested with data from various native and managed systems [50–52]. The DAYCENT biogeochemical model was used to represent GHG emissions more realistically for nonrice major crop types (corn, wheat, and soybean). The results indicate a significant potential to the reduce GHG emissions from cropped soils and to increase yields. Using nitrification inhibitors and split fertilizer applications both led to increased (~6%) crop yields, but the inhibitor led to a larger reduction in N losses (~10%). No-till cultivation, which led to C storage, combined with nitrification inhibitors resulted in reduced GHG emissions of ~50% and increased crop yields of ~7% [53]. DAYCENT, used in this study, is likely to be an improvement over the IPCC method that estimates N_2O emissions based solely on N inputs and does not account for weather and soil class. However, the dataset used during the simulation was mapped to an extremely coarse resolution at 1.9olutio, and the nonspatial data (e.g., rates and dates of fertilizer applications) were assumed to be identical within crop types across regions. Lee et al. calibrated and validated DAYCENT and predicted the biomass yield potential of switchgrass across the Central Valley of California. Six common cultivars were calibrated using published data across the USA and validated with data generated from four field trials in California (2007–2009). After calibration and validation, the model explained 66–90% of observed yield variation in 2007–2009. The model (2.0–9.9 $Mg\,ha^{-1}\,yr^{-1}$) agreed well with the observed yield variance (1.3–12.2 $Mg\,ha^{-1}\,yr^{-1}$) in the establishment year. The Alamo and Kanlow cultivars were estimated to have biomass production potential within the Central Valley of California under the selected management practices. The

biomass management options of switchgrass were suggested to differ depending on the temperature and on the yields of the different ecotypes [54].

RothC-26.3 was originally developed and parameterized to model the organic C turnover in arable topsoils from the Rothamsted long term field experiments, hence the name. The model uses a monthly time step to calculate the total organic carbon ($t\,ha^{-1}$), microbial biomass carbon ($t\,ha^{-1}$), and D14C (from which the equivalent radiocarbon age of the soil can be calculated) on timescales from years to centuries [55–58]. The model has been evaluated for a range of climates and vegetation types (e.g., cropland, grassland, and forests) and has been previously used for prediction on both regional and global scales [59–64]. Hillier et al. have conducted a study for England and Wales, using the yield maps of four bioenergy crops, Miscanthus (*Miscanthus giganteus*), short rotation coppice (SRC) poplar (*Populus trichocarpa* Torr. & Gray *P. trichocarpa*, var. Trichobel), winter wheat, and oilseed rape, with RothC to simulate the soil C turnover over a 20-year period. The GHG emissions from soil are placed in context with the life cycle emissions and then quantify the potential fossil fuel C that could be displaced. The GHG balance is estimated for each of the 12 land use change transitions associated with replacing arable, grassland, or forest/seminatural land with each of the four bioenergy crops. Miscanthus and SRC are likely to have a mostly beneficial impact in reducing GHG emissions, while oilseed rape and winter wheat have either a net GHG cost or only a marginal benefit [65].

Biome-BGC version 4.1.2 was provided by Peter Thornton at the National Center for Atmospheric Research (NCAR, sponsored by the National Science Foundation) and by the Numerical Terradynamic Simulation group (NTSG) at the University of Montana. The model is a computer model that simulates the storage and fluxes of water, carbon, and nitrogen within the vegetation, litter, and soil components of a terrestrial ecosystem. Biome-BGC is primarily a research tool and many versions have been developed for particular purposes [66]. Biome-BGC was applied to simulate the behavior of three Mediterranean species (*Quercus ilex* L., *Quercus cerris* L., and *Pinus pinaster* Ait.) [67]. The model was also adapted to managed stands with long term observations of biomass production. The exercise includes a model analysis for 33 stands exemplifying typical forest management of beech, oak, pine, and spruce, that is, the four major tree species important to Central-European forestry [68]. In this area, Schmid et al. analyzed the carbon dynamics along an altitudinal gradient across the alpine treeline; the analysis provided insights into the sensitivity of simulated average carbon pools to the changes in environmental factors [69]. The Biome-BGC model was also applied in a forested area of Sweden. The current carbon balance of the forested area and its sensitivity to global change was simulated [70]. Eastaugh et al. applied the species-specific adaptation of the biogeochemical model Biome-BGC to Norway spruce across a range of Austrian climatic change zones using the Austrian National Forest Inventory. The relative influence of current climate change on forest growth was quantified. At the national scale, climate change was found to have negligible effect on Norway spruce productivity, due in part to opposing effects at the regional level [71]. Based on the Biome-BGC model, a modified net primary productivity (NPP) calculation is used to estimate the *Jatropha curcas* Linnaeus (JCL) yields. A zoning scheme that considers land cover status and potential yield levels was formulated and used to evaluate the potential area and production of future plantations at the global, regional, and national levels. The estimated potential area of JCL plantations is 59–1486 million hectares worldwide and the potential production is 56–3613 million ton dry seed y^{-1} [72]. The Biome-BGC outputs are useful for the following: (1) establishing the amount and distribution of C storage by plants; (2) predicting the behavior of different ecosystems in cases of CO_2 concentration changes in the air; (3) exploring the controls of water stress and drought on plant carbon balances; (4) exploring the interannual variability of climate on growing season; and (5) furnishing important parameters useful to managing ecosystems, particularly forests [67].

The models most used for energy plant GHG simulations are listed in Table 1. It is worth noting that hundreds of different types of models have been used in the literature. Table 1 presents only select models that are relatively operable and widely applied.

4. Discussion and Conclusion

During the last decade, great effort has been directed at establishing an efficient method for comprehensively estimating the GHG emission reduction potential from large-scale cultivation of energy plants by combining LCA with ecosystem/biogeochemical process models. LCA presents a general framework for evaluating the energy consumption and GHG emission from energy crop plantation, yield acquisition, production, product use, and postprocessing. Meanwhile, ecosystem/biogeochemical process models are adopted to simulate the fluxes and storage of energy, water, carbon, and nitrogen in the soil-plant (energy crops) soil continuum. Although clear progress has been made in recent years, some problems remain in current studies and should be addressed.

(1) Localization of key parameters: in some of the "GHG reduction efficiency" models, such as [27, 31] the key parameters are derived from the reference values of the American Oregon National Laboratory. The same parameters were used without considering local geographical and social conditions. Good examples of models that incorporate geographical and social conditions were presented by Qin et al. [73] and Gelfand et al. [74]. The terrestrial ecosystem model (TEM), a process-based global-scale ecosystem model, was used to estimate the C fluxes and pool sizes of switchgrass and Miscanthus in China. For each crop, TEM was calibrated against driving data and the rate limiting parameters for several biogeochemical processes were obtained from the parameterization [73]. Many more details regarding the parameterization of the process model were also presented in

Table 1: Models mostly used for GHG simulation of energy plant.

Model	Study object	Study area	Author(s)
Tier 1	Vegetation	Global	Ruesch and Gibbs 2008 [35]
	Eucalyptus regnans forests	Australian	Keith et al. 2009 [36]
SWAT	Biofuel	James River Basin of the Midwestern United States	Wu et al. 2012 [40]
PnET	Forest ecosystems	Northeastern USA	Aber et al. 2005 [41]
	Tropical rainforest ecosystems	Wet tropics of Australia and Costa Rica	Kiese et al. 2005 [42]
	Wetland	Northern America	Zhang et al. 2002 [43]
DAYCENT	Dry grassland, wet managed grassland, and wet crop land systems	Minneapolis, Minnesota, USA	Parton et al. 1994 [49]
	Crops	USA	del Grosso et al. 2005 [50]
	Corn, wheat, and soybean	Worldwide	del Grosso et al. 2009 [53]
	Switchgrass	The Central Valley of California	Lee et al. 2012 [54]
RothC	Cropland	European Russia and the Ukraine	Smith et al. 2007 [59]
	Nonwaterlogged soils	Germany, England, the USA, the Czech Republic, and Australia	Coleman et al. 1997 [60]
	Miscanthus, poplar, winter wheat, and oilseed rape	England and Wales	Hillier et al. 2009 [65]
Biome-BGC	*Quercus ilex* L., *Quercus cerris* L., and *Pinus pinaster* Ait.	The Mediterranean area	Chiesi et al. 2007 [67]
	Beech, oak, pine, and spruce	Central-European forestry	Cienciala and Tatarinov 2006 [68]
	Forest	Central-European forestry	Schmid et al. 2006 [69]
	Forest	Sweden	Lagergren et al. 2006 [70]
Biome	Norway spruce	Austrian	Eastaugh et al. 2011 [71]
	Jatropha curcas Linnaeus	Global	Li et al. 2010 [72]

[74]. To achieve qualified and reliable results, the localization of key parameters and sensitivity analysis are very important and worth greater attention in further studies.

(2) Acquisition of spatially explicit estimations: the total GHG emission reduction potential is not simply equal to the sum of the grid values, as in the Biome-BGC model. Mutual influences and interactions exist between each grid [29]. For example, the Biome-BGC team recently presented a new model, the regional hydrological and ecological simulation system (RHESSys), that combines the terrestrial ecosystem process model Biome-BGC with spatially explicit meteorological information and the TOPMODEL hydrologic routing model to make spatial and temporal predictions of carbon, water, and nitrogen dynamics over landscapes [75]. Xu et al. suggested developing a spatially explicit agent-based LCA analysis framework for improving the environmental sustainability of bioenergy systems [76]. Hence, spatially explicit process-based biogeochemical models are much important for deriving both the amount and the spatial distribution of the C, N, and GHG emissions during the growth of energy plants. Using these models, the GHG reduction efficiency of scale development of energy plants can be accurately evaluated.

(3) Assessment of the effect of management system. The effect of management system has been neglected in many existing models. However, the environmental policy integrated climate (EPIC), provided by Blackland Research & Extension Center and USDA Grassland, Soil, and Water Laboratory, could predict the effects of management decisions on soil, water, nutrient, and pesticide movements [77]. Gelfand et al. implemented an EPIC-based spatially explicit integrative modeling framework to simulate the yields of perennial species grown on marginal lands across the ten-state study area in the US north-central region [74]. The international institute for applied systems analysis (IIASA) suggests that EPIC has accurately simulated the agricultural conditions and practices for hundreds of years into the past, providing an excellent basis for projecting future trends in global change [78]. Therefore, more attention should be paid to the management system or the practice of energy crop plantation in future studies.

Appendix

Consider

$$N_2O_{Direct}\text{-}N = N_2O\text{-}N_{N\,inputs} + N_2O\text{-}N_{OS} + N_2O\text{-}N_{PRP}$$

$$
\begin{aligned}
N_2O\text{-}N_{N\,inputs} &= \left[\left[\left(F_{SN} + F_{ON} + F_{CR} + F_{SOM}\right) \bullet EF_1\right]\right. \\
&\quad \left. + \left[\left(F_{SN} + F_{ON} + F_{CR} + F_{SOM}\right)_{FR} + EF_{1FR}\right]\right] \\
N_2O\text{-}N_{OS} &= \left[\left(F_{OS,CG,Temp} \bullet EF_{2CG,Temp}\right)\right. \\
&\quad + \left(F_{OS,CG,Trop} \bullet EF_{2F,Temp,NP}\right) \\
&\quad + \left(F_{OS.F.Temp,NR} \bullet EF_{2F,Temp,NR}\right) \\
&\quad + \left(F_{OS,F,Temp,NP} \bullet EF_{2F,Temp,np}\right) \\
&\quad \left. + \left(F_{OS,F,Trop} \bullet EF_{2F,Trop}\right)\right] \\
N_2O\text{-}N_{PRP} &= \left[\left(F_{PRP,CPP} \bullet EF_{3PRP,CPP}\right)\right. \\
&\quad \left. + \left(F_{PRP,SO} \bullet EF_{3PRP,SO}\right)\right], \qquad \text{(A.1)}
\end{aligned}
$$

where

N_2O_{Direct}-N = annual direct N_2O-N emissions produced from managed soils, kg N_2O-N yr^{-1},

$N_2O\text{-}N_{Ninputs}$ = annual direct N_2O-N emissions from N inputs to managed soils, kg N_2O-N yr^{-1},

$N_2O\text{-}N_{OS}$ = annual direct N_2O-N emissions from managed organic soils, kg N_2O-N yr^{-1},

$N_2O\text{-}N_{PRP}$ = annual direct N_2O-N emissions from urine and dung inputs to grazed soils, kg N_2O-N yr^{-1},

F_{SN} = annual amount of synthetic fertilizer N applied to soils, kg N yr^{-1},

F_{ON} = annual amount of animal manure, compost, sewage sludge, and other organic N additions applied to soils (note: if including sewage sludge, cross-check with waste sector to ensure that the N_2O emissions are not double-counted from the N in sewage sludge), kg N yr^{-1},

F_{CR} = annual amount of N in crop residues (above-ground and below-ground), including N-fixing crops, and from forage/pasture renewal, returned to soils, kg N yr^{-1},

F_{SOM} = annual amount of N in mineral soils that is mineralized, in association with loss of soil C from soil organic matter as a result of changes to land use or management, kg N yr^{-1},

F_{OS} = annual area of managed/drained organic soils, ha (note: the subscripts CG, F, Temp, Trop, NR, and NP refer to cropland and grassland, forest land, temperate, tropical, nutrient rich, and nutrient poor, resp.),

F_{PRP} = annual amount of urine and dung N deposited by grazing animals on pasture, range, and paddock, kg N yr^{-1} (note: the subscripts CPP and SO refer to cattle, poultry, and pigs and sheep and other animals, resp.),

EF_1 = emission factor for N_2O emissions from N inputs, kg N_2O-N (kg N input)$^{-1}$,

EF_{1FR} is the emission factor for N_2O emissions from N inputs to flooded rice, kg N_2O-N (kg N input)$^{-1}$,

EF_2 = emission factor for N_2O emissions from drained/managed organic soils, kg N_2O-N ha^{-1} yr^{-1}; (note: the subscripts CG, F, Temp, Trop, NR, and NP refer to cropland and grassland, forest land, temperate, tropical, nutrient fich, and nutrient poor, resp.),

EF_{3PRP} = emission factor for N_2O emissions from urine and dung N deposited on pasture, range, and paddock by grazing animals, kg N_2O-N (kg N input)$^{-1}$ (note: the subscripts CPP and SO refer to cattle, poultry, and pigs, and sheep and other animals, resp.).

Conflict of Interests

The authors declare that there is no conflict of interest regarding the publication of this paper.

Acknowledgments

The work presented here was supported by the Chinese Academy of Sciences (Grant no. KZZD-EW-08) and the Chinese Earthquake Administration (Grant no. 201208018-3).

References

[1] F. Hernandez Sobrino, C. Rodriguez Monroy, and J. Luis Hernandez Perez, "Biofuels and fossil fuels: Life Cycle Analysis (LCA) optimisation through productive resources maximisation," *Renewable & Sustainable Energy Reviews*, vol. 15, no. 6, pp. 2621–2628, 2011.

[2] I. Gelfand, R. Sahajpal, X. Zhang, R. C. Izaurralde, K. L. Gross, and G. P. Robertson, "Sustainable bioenergy production from marginal lands in the US Midwest," *Nature*, vol. 493, no. 7433, pp. 514–517, 2013.

[3] B. Dudley, *BP Statistical Review of World Energy*, 2012.

[4] E. Martinot, "Renewables 2005," Global Status Report, Worldwatch Institute, Washington, DC, USA, 2005.

[5] J. Hill, E. Nelson, D. Tilman, S. Polasky, and D. Tiffany, "Environmental, economic, and energetic costs and benefits of biodiesel and ethanol biofuels," *Proceedings of the National Academy of Sciences of the United States of America*, vol. 103, no. 30, pp. 11206–11210, 2006.

[6] P. R. Adler, S. J. D. Grosso, and W. J. Parton, "Life-cycle assessment of net greenhouse-gas flux for bioenergy cropping systems," *Ecological Applications*, vol. 17, no. 3, pp. 675–691, 2007.

[7] W. Thompson, S. Meyer, and T. Green, "The U.S. biodiesel use mandate and biodiesel feedstock markets," *Biomass & Bioenergy*, vol. 34, no. 6, pp. 883–889, 2010.

[8] A. L. Stephenson, J. S. Dennis, and S. A. Scott, "Improving the sustainability of the production of biodiesel from oilseed rape in the UK," *Process Safety and Environmental Protection*, vol. 86, no. 6, pp. 427–440, 2008.

[9] S. Gmünder, R. Singh, S. Pfister, A. Adheloya, and R. Zah, "Environmental impacts of Jatropha curcas biodiesel in India," *Journal of Biomedicine & Biotechnology*, vol. 2012, Article ID 623070, 10 pages, 2012.

[10] J. Fargione, J. Hill, D. Tilman, S. Polasky, and P. Hawthorne, "Land clearing and the biofuel carbon debt," *Science*, vol. 319, no. 5867, pp. 1235–1238, 2008.

[11] T. Searchinger, R. Heimlich, R. A. Houghton et al., "Use of U.S. croplands for biofuels increases greenhouse gases through emissions from land-use change," *Science*, vol. 319, no. 5867, pp. 1238–1240, 2008.

[12] U. Congress, "Energy independence and security act of 2007," Public Law, no. 110–140: p. 2, 2007.

[13] Energy, U.S.D.o. DOE Actively Engaged in Investigating the Role of Biofuels in Greenhouse Gas Emissions from Indirect Land Use Change, 2008.

[14] A. E. Farrell, R. J. Plevin, B. T. Turner, A. D. Jones, M. O'Hare, and D. M. Kammen, "Ethanol can contribute to energy and environmental goals," *Science*, vol. 311, no. 5760, pp. 506–508, 2006.

[15] M. R. Schmer, K. P. Vogel, R. B. Mitchell, and R. K. Perrin, "Net energy of cellulosic ethanol from switchgrass," *Proceedings of the National Academy of Sciences of the United States of America*, vol. 105, no. 2, pp. 464–469, 2008.

[16] N. Sasaki, W. Knorr, D. R. Foster et al., "Woody Biomass & Bioenergy potentials in Southeast Asia between 1990 and 2020," *Applied Energy*, vol. 86, no. 1, pp. S140–S150, 2009.

[17] F. Richter, "Financial and economic assessment of timber harvesting operations in Sarawak, Malaysia," Forest Harvesting Case-Study, 2001.

[18] E. I. Administration, *International Energy Outlook 2006*, EIA, Office of Integrated Analysis and Forecasting, US Department of Energy, Washington, DC, USA, 2006.

[19] W. Wu and H. Jikun, *Potential Land for Plantation of Jatropha Curcas as Feedstocks for Biodiesel in Southwest China*, China Agriculture Press, Beijing, China, 2010.

[20] A.-H. Xing, J. Ma, Y.-H. Zhang, Y. Wang, and Y. Jin, "Life cycle assessment of resource and energy consumption for production of biodiesel," *The Chinese Journal of Process Engineering*, vol. 10, no. 2, pp. 314–320, 2010.

[21] Z. Hu, P. Tan, D. Lou, and Y. Dong, "Assessment of life cycle energy consumption and emissions for several kinds of feedstock based biodiesel," *Transactions of the Chinese Society of Agricultural Engineering*, vol. 22, no. 11, pp. 141–146, 2006.

[22] Z. X. Wang and Y. Lu, "Jatropha curcas seed oil life cycle of the economy, environment and energy efficiency," *Resources and Environment in the Yangtze Basin*, vol. 20, no. 001, pp. 61–67, 2011.

[23] C. X. Zhang, *Potential and Impact Assessment of Bio-Ethanol in China*, Graduate University of Chinese Academy of Sciences, Beijing, China, 2010.

[24] D. Dai, Z. Hu, G. Pu, H. Li, and C. Wang, "Energy efficiency and potentials of cassava fuel ethanol in Guangxi region of China," *Energy Conversion and Management*, vol. 47, no. 13-14, pp. 1686–1699, 2006.

[25] T. L. T. Nguyen, S. H. Gheewala, and S. Garivait, "Energy balance and GHG-abatement cost of cassava utilization for fuel ethanol in Thailand," *Energy Policy*, vol. 35, no. 9, pp. 4585–4596, 2007.

[26] L. F. Razon and R. R. Tan, "Net energy analysis of the production of biodiesel and biogas from the microalgae: haematococcus pluvialis and Nannochloropsis," *Applied Energy*, vol. 88, no. 10, pp. 3507–3514, 2011.

[27] L. Lu, D. Jiang, D. Zhuang, and Y. Huang, "Evaluating the marginal land resources suitable for developing Pistacia chinensis-based biodiesel in China," *Energies*, vol. 5, no. 7, pp. 2165–2177, 2012.

[28] Y. Li, X. Xie, X. Bin et al., "Study on pilot scale biodiesel production from Pistacia chinensis oil," *Renewable Energy Resources*, vol. 28, no. 4, pp. 54–57, 2010.

[29] G. Fiorese and G. Guariso, "A GIS-based approach to evaluate biomass potential from energy crops at regional scale," *Environmental Modelling & Software*, vol. 25, no. 6, pp. 702–711, 2010.

[30] D. Zhuang, D. Jiang, L. Liu, and Y. Huang, "Assessment of bioenergy potential on marginal land in China," *Renewable & Sustainable Energy Reviews*, vol. 15, no. 2, pp. 1050–1056, 2011.

[31] L. Lei, D. Zhuang, D. Jiang et al., "Assessing the potential of the cultivation area and greenhouse gas (GHG) emission reduction of cassava-based fuel ethanol on marginal land in Southwest China," *African Journal of Agricultural Research*, vol. 7, no. 41, pp. 5594–5603, 2012.

[32] B. Dresen and M. Jandewerth, "Integration of spatial analyses into LCA-calculating GHG emissions with geoinformation systems," *International Journal of Life Cycle Assessment*, vol. 17, no. 9, pp. 1094–1103, 2012.

[33] C. M. Gasol, X. Gabarrell, M. Rigola, S. González-García, and J. Rieradevall, "Environmental assessment: (LCA) and spatial modelling (GIS) of energy crop implementation on local scale," *Biomass & Bioenergy*, vol. 35, no. 7, pp. 2975–2985, 2011.

[34] C. De Klein, R. S. A. Novoa, S. Ogle et al., "N_2O emissions from managed soils, and CO_2 emissions from lime and urea application," in *IPCC Guidelines for National Greenhouse Gas Inventories*, vol. 4, National Greenhouse Gas Inventories Programme, 2006.

[35] A. Ruesch and H. K. Gibbs, *New IPCC Tier-1 Global Biomass Carbon Map for the Year 2000*, 2008.

[36] H. Keith, B. G. Mackey, and D. B. Lindenmayer, "Re-evaluation of forest biomass carbon stocks and lessons from the world's most carbon-dense forests," *Proceedings of the National Academy of Sciences of the United States of America*, vol. 106, no. 28, pp. 11635–11640, 2009.

[37] H. K. Gibbs, S. Brown, J. O. Niles, and J. A. Foley, "Monitoring and estimating tropical forest carbon stocks: making REDD a reality," *Environmental Research Letters*, vol. 2, no. 4, Article ID 045023, 2007.

[38] P. C. West, H. K. Gibbs, C. Monfreda et al., "Trading carbon for food: global comparison of carbon stocks vs. crop yields on agricultural land," *Proceedings of the National Academy of Sciences of the United States of America*, vol. 107, no. 46, pp. 19645–19648, 2010.

[39] S. N. Djomo and R. Ceulemans, "A comparative analysis of the carbon intensity of biofuels caused by land use changes," *GCB Bioenergy*, vol. 4, no. 4, pp. 392–407, 2012.

[40] Y. Wu, S. Liu, and Z. Li, "Identifying potential areas for biofuel production and evaluating the environmental effects: a case study of the James River Basin in the Midwestern United States," *GCB Bioenergy*, vol. 4, no. 6, pp. 875–888, 2012.

[41] J. D. Aber, C. T. Federer, C. A. Ollinger et al., *PnET Models: Carbon, Nitrogen, Water Dynamics in Forest Ecosystems (Vers. 4 and 5)* , vol. 10, Oak Ridge National Laboratory Distributed Active Archive Center, Oak Ridge, Tenn, USA, 2005, http://daac.ornl.gov/.

[42] R. Kiese, C. Li, D. W. Hilbert, H. Papen, and K. Butterbach-Bahl, "Regional application of PnET-N-DNDC for estimating the N2O source strength of tropical rainforests in the wet tropics of Australia," *Global Change Biology*, vol. 11, no. 1, pp. 128–144, 2005.

[43] Y. Zhang, C. Li, C. C. Trettin, H. Li, and G. Sun, "An integrated model of soil, hydrology, and vegetation for carbon dynamics in wetland ecosystems," *Global Biogeochemical Cycles*, vol. 16, no. 4, pp. 1–9, 2002.

[44] J. D. Aber and C. A. Federer, "A generalized, lumped-parameter model of photosynthesis, evapotranspiration and net primary production in temperate and boreal forest ecosystems," *Oecologia*, vol. 92, no. 4, pp. 463–474, 1992.

[45] J. D. Aber, P. B. Reich, and M. L. Goulden, "Extrapolating leaf CO_2 exchange to the canopy: a generalized model of forest photosynthesis compared with measurements by eddy correlation," *Oecologia*, vol. 106, no. 2, pp. 257–265, 1996.

[46] J. M. Vose and P. V. Bolstad, "Challenges to modelling NPP in diverse eastern deciduous forests: Species-level comparisons of foliar respiration responses to temperature and nitrogen," *Ecological Modelling*, vol. 122, no. 3, pp. 165–174, 1999.

[47] W. J. Parton, M. Hartman, D. Ojima, and D. Schimel, "DAYCENT and its land surface submodel: Description and testing," *Global and Planetary Change*, vol. 19, no. 1, pp. 35–48, 1998.

[48] S. J. del Grosso, W. J. Parton, P. R. Adler, S. C. Davis, C. Keough, and E. Marx, "Simulated interaction of carbon dynamics and nitrogen trace gas fluxes using the DAYCENT model," *Modeling Carbon and Nitrogen Dynamics for Soil Management*, pp. 303–332, 2012.

[49] W. J. Parton, D. S. Ojima, and C. V. Cole, "A general model for soil organic matter dynamics: sensitivity to litter chemistry, texture and management," in *Quantitative Modeling of Soil Forming Processes: Proceedings of a Symposium Sponsored by Divisions S-5 and S-9 of the Soil Science Society of America in Minneapolis, MinnesotA, USA, 2 November 1992*, R. B. Bryant and R. W. Arnold, Eds., Soil Science Society of America, 1994.

[50] S. J. del Grosso, A. R. Mosier, W. J. Parton, and D. S. Ojima, "DAYCENT model analysis of past and contemporary soil N_2O and net greenhouse gas flux for major crops in the USA," *Soil and Tillage Research*, vol. 83, no. 1, pp. 9–24, 2005.

[51] S. J. Del Grosso, W. J. Parton, A. R. Mosier et al., "Simulated effects of land use, soil texture, and precipitation on N gas emissions using DAYCENT.," *Nitrogen in the Environment: Sources, Problems and Management*, pp. 413–431, 2001.

[52] S. del Grosso, D. Ojima, W. Parton, A. Mosier, G. Peterson, and D. Schimel, "Simulated effects of dryland cropping intensification on soil organic matter and greenhouse gas exchanges using the DAYCENT ecosystem model," *Environmental Pollution*, vol. 116, no. 1, pp. S75–S83, 2002.

[53] S. J. del Grosso, D. S. Ojima, W. J. Parton et al., "Global scale DAYCENT model analysis of greenhouse gas emissions and mitigation strategies for cropped soils," *Global and Planetary Change*, vol. 67, no. 1-2, pp. 44–50, 2009.

[54] J. Lee, G. Pedroso, B. A. Linquist, D. Putnam, C. van Kessel, and J. Six, "Simulating switchgrass biomass production across ecoregions using the DAYCENT model," *GCB Bioenergy*, vol. 4, no. 5, pp. 521–533, 2012.

[55] D. Jenkinson, P. Hart, J. Rayner, and L. Parry, "Modelling the turnover of organic matter in long-term experiments at Rothamsted," 1987.

[56] D. S. Jenkinson and K. Coleman, "Calculating the annual input of organic matter to soil from measurements of total organic carbon and radiocarbon," *European Journal of Soil Science*, vol. 45, no. 2, pp. 167–174, 1994.

[57] D. S. Jenkinson, D. E. Adams, and A. Wild, "Model estimates of CO_2 emissions from soil in response to global warming," *Nature*, vol. 351, no. 6324, pp. 304–306, 1991.

[58] D. S. Jenkinson, S. P. S. Andrew, J. M. Lynch, M. J. Goss, and P. B. Tinker, "The turnover of organic carbon and nitrogen in soil," *Philosophical Transactions of the Royal Society of London B*, vol. 329, no. 1255, pp. 361–368, 1990.

[59] J. Smith, P. Smith, M. Wattenbach et al., "Projected changes in the organic carbon stocks of cropland mineral soils of European Russia and the Ukraine, 1990–2070," *Global Change Biology*, vol. 13, no. 2, pp. 342–356, 2007.

[60] K. Coleman, D. S. Jenkinson, G. J. Crocker et al., "Simulating trends in soil organic carbon in long-term experiments using RothC-26.3," *Geoderma*, vol. 81, no. 1-2, pp. 29–44, 1997.

[61] P. Falloon, P. Smith, R. I. Bradley et al., "RothCUK—a dynamic modelling system for estimating changes in soil C from mineral soils at 1-km resolution in the UK," *Soil Use and Management*, vol. 22, no. 3, pp. 274–288, 2006.

[62] Y. P. Wang and P. J. Polglase, "Carbon balance in the tundra, boreal forest and humid tropical forest during climate change: scaling up from leaf physiology and soil carbon dynamics," *Plant, Cell & Environment*, vol. 18, no. 10, pp. 1226–1244, 1995.

[63] J. O. Skjemstad, L. R. Spouncer, B. Cowie, and R. S. Swift, "Calibration of the Rothamsted organic carbon turnover model (RothC ver. 26.3), using measurable soil organic carbon pools," *Australian Journal of Soil Research*, vol. 42, no. 1, pp. 79–88, 2004.

[64] P. Smith, J. U. Smith, D. S. Powlson et al., "A comparison of the performance of nine soil organic matter models using datasets from seven long-term experiments," *Geoderma*, vol. 81, no. 1-2, pp. 153–225, 1997.

[65] J. Hillier, W. Carly, G. Dailey et al., "Greenhouse gas emissions from four bioenergy crops in England and Wales: integrating spatial estimates of yield and soil carbon balance in life cycle analyses," *GCB Bioenergy*, vol. 1, no. 4, pp. 267–281, 2009.

[66] P. E. Thornton, B. E. Law, H. L. Gholz et al., "Modeling and measuring the effects of disturbance history and climate on carbon and water budgets in evergreen needleleaf forests," *Agricultural and Forest Meteorology*, vol. 113, no. 1, pp. 185–222, 2002.

[67] M. Chiesi, F. Maselli, M. Moriondo, L. Fibbi, M. Bindi, and S. W. Running, "Application of BIOME-BGC to simulate Mediterranean forest processes," *Ecological Modelling*, vol. 206, no. 1-2, pp. 179–190, 2007.

[68] E. Cienciala and F. A. Tatarinov, "Application of BIOME-BGC model to managed forests. 2. Comparison with long-term observations of stand production for major tree species," *Forest Ecology and Management*, vol. 237, no. 1–3, pp. 252–266, 2006.

[69] S. Schmid, B. Zierl, and H. Bugmann, "Analyzing the carbon dynamics of central European forests: comparison of Biome-BGC simulations with measurements," *Regional Environmental Change*, vol. 6, no. 4, pp. 167–180, 2006.

[70] F. Lagergren, A. Grelle, H. Lankreijer, M. Mölder, and A. Lindroth, "Current carbon balance of the forested area in Sweden and its sensitivity to global change as simulated by Biome-BGC," *Ecosystems*, vol. 9, no. 6, pp. 894–908, 2006.

[71] C. S. Eastaugh, E. Pötzelsberger, and H. Hasenauer, "Assessing the impacts of climate change and nitrogen deposition on Norway spruce (Picea abies L. Karst) growth in Austria with BIOME-BGC," *Tree Physiology*, vol. 31, no. 3, pp. 262–274, 2011.

[72] Z. Li, B.-L. Lin, X. F. Zhao, M. Sagisaka, and R. Shibazaki, "System approach for evaluating the potential yield and plantation of jatropha curcas l on a global scale," *Environmental Science & Technology*, vol. 44, no. 6, pp. 2204–2209, 2010.

[73] Z. Qin, Q. Zhuang, X. Zhu, X. Cai, and X. Zhang, "Carbon consequences and agricultural implications of growing biofuel crops on marginal agricultural lands in China," *Environmental Science & Technology*, vol. 45, no. 24, pp. 10765–10772, 2011.

[74] I. Gelfand, R. Sahajpal, X. Zhang, R. C. Izaurralde, K. L. Gross, and G. P. Robertson, "Sustainable bioenergy production from marginal lands in the US Midwest," *Nature*, vol. 493, no. 7433, pp. 514–517, 2013.

[75] S. Running, J. Golinkoff, and R. Anderson, "Ecosystem modeling," 2013, http://www.ntsg.umt.edu/taxonomy/term/59.

[76] M. Xu, S. A. Miller, S. Choudhary, and A. Heairet, "Developing a spatially-explicit agentbased life cycle analysis framework for improving the environmental sustainability of bioenergy systems," 2011, http://css.snre.umich.edu/project/developing-spatially-explicit-agent-based-life-cycle-analysis-framework-improving.

[77] Research, T.A.M.A. EPIC & APEX Models, http://epicapex.tamu.edu/epic/.

[78] (IIASA), I.I.f.A.S.A. The Environmental Policy Integrated Model (EPIC)—a model assessing how land management affects the environment, 2012, http://www.iiasa.ac.at/web/home/research/modelsData/EPIC.en.html.

Hindawi Publishing Corporation
The Scientific World Journal
Volume 2014, Article ID 210504, 10 pages
http://dx.doi.org/10.1155/2014/210504

Review Article

Coupling of Algal Biofuel Production with Wastewater

Neha Chamoli Bhatt, Amit Panwar, Tara Singh Bisht, and Sushma Tamta

Algae Laboratory, Department of Biotechnology, Kumaun University, Bhimtal Campus, Bhimtal, Nainital, Uttarakhand-263136, India

Correspondence should be addressed to Neha Chamoli Bhatt; nehachamoli2508@gmail.com

Received 19 February 2014; Accepted 13 March 2014; Published 26 May 2014

Academic Editors: Y.-C. Yong, S.-G. Zhou, and L. Zhuang

Microalgae have gained enormous consideration from scientific community worldwide emerging as a viable feedstock for a renewable energy source virtually being carbon neutral, high lipid content, and comparatively more advantageous to other sources of biofuels. Although microalgae are seen as a valuable source in majority part of the world for production of biofuels and bioproducts, still they are unable to accomplish sustainable large-scale algal biofuel production. Wastewater has organic and inorganic supplements required for algal growth. The coupling of microalgae with wastewater is an effective way of waste remediation and a cost-effective microalgal biofuel production. In this review article, we will primarily discuss the possibilities and current scenario regarding coupling of microalgal cultivation with biofuel production emphasizing recent progress in this area.

1. Introduction

World biofuel production has increased sevenfold since 2000 but still meets only 2.3% of final liquid fuel demands [1]. Worldwide energy consumption is projected to increase by 49% from 522 exajoules (EJ) in 2007 to 780 EJ in 2035 [2]. It is expected that two main energy resources, crude oil and natural gas, will be diminished by 45.7 and 62.8 years and estimated energy requirement will be tripled in 2025 [3]. Transportation is one of the fastest growing sectors using 27% of primary energy in current scenario and in India annual oil consumption is about 5.5% which is going to increase in the next decade [4]. Currently in India, diesel alone meets an estimated 73% of transportation fuel demand followed by gasoline at 20%; moreover, it is estimated that, by the end of this decade, the average demand for transport fuels will rise from an estimated 117 billion litres in 2013 to 167 billion litres and would grow further to reach 195 million liters by 2023 [5]. Fossil fuels make up 88% and 86.2% of the energy consumed by the world and USA [6]. The transportation and energy sectors are the major sources in European Union (EU) responsible for more than 20% and 60% of greenhouse gas (GHG) emissions, respectively [7]. It is fully accepted that global warming increases in response to (GHG) emissions [8] which reveals that there is vital need for cleaner alternative to fossil fuels. Due to continuous depletion of natural resources emerging energy crisis and increasing fuel prices demands for an alternative, scalable and sustainable energy source. Moreover, the entire globe is facing two major challenges of freshwater shortage and energy crisis [9]. Recently, renewable energies including water, wind, solar, geothermal and especially biofuels have gained much attention as a substitute to conventional energy resources as they are sustainable, ecofriendly, and carbon neutral and have potential to fulfil the energy needs of the transportation sector.

Microalgae have potential to become an alternative source of petrodiesel due to their sustainable photosynthetic efficiency, ecofriendly approach, increasing depletion of nonrenewable energy resources, and use of nonarable land. Coupling wastewater with microalgae cultivation can be a promising approach for biofuel production. This integration can offer an economically viable and environmentally friendly means for sustainable algal biofuel production since enormous amounts of water and nutrient (e.g., nitrogen and phosphorus) can be recycled for algal growth in wastewater-based algal cultivation system [10, 11]. Microalgae have dual application of biomass production for sustainable biofuels production and phycoremediation [12]. They have higher photosynthetic efficiency and lipid content which can be

harnessed for biofuels including biodiesel, bioethanol, biohydrogen, and combustible gases. Microalgal biofuel systems are capable of producing clean and sustainably produced fuels for the future while eradicating the food versus fuel and forest versus fuel concerns associated with first generation biofuels and lignocellulosic processes based on wood feedstocks [13]. Although there had been enough debate on algal biofuels, still they are not commercialized as their economic viability is questionable. Despite being so advantageous, the technoeconomics of present microalgal biofuel production systems is not effective to compete with petroleum-based conventional fuels as it is accompanied with high cost production. The major expenditure of a current algae biofuel technology depends on algae cultivation system, harvesting, and lipid extraction methods. But certainly their outlook is promising, and both the developed nations and the emerging economies are interested in algal fuels [14].

2. Microalgae: Advantages as a Source of Biofuel

Microalgae are prokaryotic or eukaryotic photosynthetic microorganisms, some of which can also form a chain or colony ranging from a few micrometers to a few hundred micrometers and are generally ubiquitous in nature. Algae are a broad category that has no proper taxonomic classification [15]. They are primitive plants (thallophytes), that is, lacking roots, stems, and leaves, have no sterile covering of cells around the cells, and have chlorophyll as their primary photosynthetic pigment [16]. Algae can be divided into two main categories, that is, macroalgae which are multicellular and size up to several meters and microalgae are small size organisms ranging from sizes 0.2 μm to 100 μm or even higher [17]. Microalgae have high rate of areal biomass productivity compared to traditional agricultural crops like corn and soya bean and oil content in microalgae can exceed 80% dry weight of biomass [18]. Generally algae are divided into five main groups:

(i) blue-green algae (Cyanophyceae),

(ii) green algae (Chlorophyceae),

(iii) diatoms (Bacillariophyceae),

(iv) red algae (Rhodophyceae),

(v) brown algae (Phaeophyceae).

Although Cyanobacteria (blue-green algae) are classified to the domain of bacteria, being photosynthetic prokaryotes, they are often considered as "algae" [19]. There are many promising attributes of microalgae which make them desirable for biofuel production. The main source of carbon for the growth of microalgae is atmospheric carbon dioxide [20]. Several microalgae species can grow well on nonpotable water (brackish, wastewater, and seawater); their is a possibility that biofuel production can be coupled with one of these systems in future. This coupling does not compete for arable land which can be used for agricultural purpose and also for eliminating the use of freshwater resources. The production of biofuels from algae can be coupled with flue gas CO_2 mitigation, wastewater treatment, and production of high-value chemicals [21, 22]. Many species of microalgae produce significant quantities of lipids which can be converted to biodiesel through process of transesterification. Microalgal biodiesel has characteristics related to petroleum-based diesel including density, viscosity, flash point, cold flow, and calorific value. Microalgae can be harvested batch-wise nearly all year round providing a reliable and constant supply of oil [20]. Microalgae does not require the use of chemical unlike terrestrial plants requiring herbicides or pesticides which affect the environment adversely and increase the cost of production. Lignin is generally absent in microalgae and other large biopolymers (found in woody biomass) that may hinder with biomass processing and conversion [23]. Apart from this, the residual algal biomass mainly composed of proteins and carbohydrates can be processed to various biofuels, including methane and alcohol fuels, and it can also produce other nonfuel coproducts which can be recovered and formulated into products with high market value such as nutriceuticals, therapeutics, and animal feeds [24].

3. Microalgal Farming Using Wastewater for Biofuel Production

Due to global expansion of human population and advanced living standards of people, a high level of water pollution is generated worldwide. Wastewater is basically end product generated by domestic, municipal, agricultural, and industrial sources [25]. The composition of wastewater is a reflection of the life styles and technologies practiced in the producing society [26]. Wastewater generally contains organic mass like proteins, carbohydrates, lipids, volatile acids, and inorganic content containing sodium, calcium, potassium, magnesium, chlorine, sulphur, phosphate, bicarbonate, ammonium salts, and heavy metals [27]. Excess of these nutrient loads in surrounding water bodies causes eutrophication or algal blooms often due to anthropogenic waste production.

More than 300 million tonnes of biodegradable household and household-like wastes, industrial wastes, and other wastes are generated every year in the European Union and stay mostly unexploited [45]. Human beings generate approximately ~3 billion tonnes of domestic wastewater every year [46]. In India, annually, due to migration of people into cities, the figures are expected to reach about 600 million by 2030 making and simultaneously increasing pressure on urban return flow (wastewater) which is usually about 70–80% of the water supply [47]. The recent reports of Central Pollution Control Board [48], New Delhi, India, revealed that the wastewater generation in the nation is around 40 billion litres per day largely from urban areas and ironically only 20–30% of the generated wastewater is subjected to treatment. In majority of the developing nations, the main sources of wastewater generation are domestic, municipal, agricultural, and industrial activities which are foremost released into environment without having sufficient treatment steps. Many species of microalgae are able to efficiently grow in wastewater environment through their capability to use abundant

organic carbon and inorganic N and P in the wastewater [11]. Algae take up these nutrients along with CO_2 and produce biomass through the process of photosynthesis. Microalgae are the main microorganisms used in treatment of domestic wastewater in units such as oxidation ponds or oxidation ditches. Algae have also been deployed for low cost and environmentally friendly wastewater treatment [49–51]. The idea of coupling of wastewater as a medium for biofuel production from algae is not innovative, as it was previously suggested in report of the Aquatic Species Program (ASP) conducted from 1978 to 1996, U.S.A [10]. The main constraint for wastewater-based algae biofuel production system is to find ideal microalgae strains which could be able to grow in wastewater environment with significant nutrient removal efficiency showing high biomass and lipid productivity.

Extensive work has been conducted by researchers [35, 37, 40, 52–54] from numerous parts of the world to explore the feasibility of using microalgae for biofuel potential from wastewater with nutrient removal property particularly nitrogen and phosphorus from effluents. Researchers had more focus on microalgal culture for N and P removal from domestic sewage in comparison to industrial wastewater. The reason behind this is that industrial wastewater, such as tannery wastewater and chemical industry wastewater, has more metal ions in addition to various organic N and P compounds [39] and it is more toxic having heavy metal contamination which does not facilitate the algal growth. The total biofuel potential of algae, when grown in domestic wastewater generated by 1000 urban centres in India, is ~0.16 Mt/annum considering the lipid fraction as 20% [55].

3.1. Biomass Production from Wastewater Grown Microalgae. Species selection, optimization of growth, lipid content, and harvesting at large scale are the important factors which govern the commercialization potential of algal biofuels. The algal biomass produced and harvested from these wastewater treatment systems could be transformed through a variety of pathways to biofuels, for example, anaerobic digestion to biogas, transesterification of lipids to biodiesel, fermentation of carbohydrate to bioethanol, and high temperature alteration to biocrude oil [56]. Economic feasibility of algal biofuel production from wastewater treatment can be achieved by high rate algal ponds (HRAPs) with low environmental impact compared to commercial algal production by HRAPs which consume freshwater and fertilisers [57]. The major challenge in the microalgae research for the existing high rate ponds is designing an efficient and economical carbonation system to fulfill the needs of high CO_2 requirement that might improve the biomass productivity [58]. Viswanath and Bux [59] isolated *Chlorella* sp. from wastewater pond and screened it for its efficiency in lipid production by cultivating both photoautotrophic and heterotrophic conditions in bioreactor. Maximum amount of biomass was recovered from the *Chlorella* sp. grown under heterotrophic growth conditions with $8.90\,gL^{-1}$ compared to photoautotrophic growth conditions which were about 3.6-fold lesser than the former, resulting in the accumulation of high lipid content in cells compared to autotrophic growth by enhancing lipid production by 4.4-fold. This study suggested that heterotrophic growth of microalgae is an efficient method for the production of biomass and high lipid content in the cells, which can reduce the cost of microalgal biomass production.

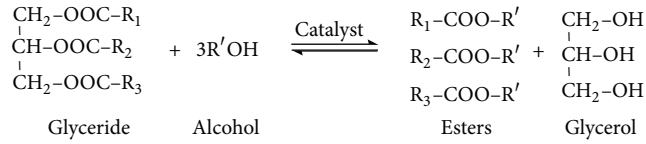

Figure 1: The chemical reaction of transesterification process.

4. Harvesting Methods of Microalgae

Dewatering and harvesting of algal biomass are a necessary step for concentrating algal biomass and for further releasing triacylglycerols (TAGs) which can then be transesterified to produce biodiesel (as shown in Figure 1). Harvesting and dewatering are one of the challenging areas of current biofuel technology as microalgae have small size and low density increasing the capital cost. The difficulty is in releasing the lipids from their intracellular location in the most energy-efficient and economical way possible, avoiding the use of large amounts of solvent, such as hexane, and utilising as much of the carbon in the biomass as liquid biofuel as possible, potentially with the recovery of minor high-value products [60]. The major techniques presently applied in microalgae harvesting and recovery include centrifugation, flocculation, filtration, and flotation.

4.1. Flocculation. Flocculation is a process of forming aggregates known as algae flocs that are often performed as a pretreatment to destabilize algae cells from water and to increase the cell density by natural, chemical, or physical means. Chemicals called flocculants are usually added to induce flocculation, and commonly used flocculants are inorganic flocculants such as alum [61, 62] or organic flocculants such as chitosan [63] or starch [64]. The surface charge of microalgal cells is generally negatively charged due to the ionization of functional groups on the microalgal cell walls and also by the adsorption of ions from the culture medium which can be neutralized by applying positively charged electrodes and cationic polymers, also commonly used to flocculate the microalgal biomass. This harvesting method is pretty expensive because of the cost of flocculants; hence flocculants need to be inexpensive, easily produced, and nontoxic.

4.2. Centrifugation. Centrifugation is a widely used method of separation on the basis of particle size and density separation. Separation efficiency is dependent upon the size of desired algal species. Numerous centrifugal techniques have been employed in various types and sizes depending on the uses such as tubular centrifuge, multichamber centrifuges, imperforate basket centrifuge, decanter, solid retaining disc centrifuge, nozzle type centrifuge, solid ejecting type disc

centrifuge, and hydrocyclone [65]. Despite being energy intensive method, it is rapid and a preferred method for microalgal cell recovery, whereas cell viability was found to be significantly dependent on the microalgal species and the method of centrifugation [66]. Even though it is very effective, centrifugation is considered unfeasible in large-scale algal culture system due to the high capital and operational costs.

4.3. Filtration. Filtration harvests microalgal biomass through filters on which the algae accumulate forming thick algae paste and allow the liquid medium to pass through. Filtration systems can be classified as macrofiltration (pore size of >10 μm), microfiltration (pore size of 0.1–10 μm), ultrafiltration (pore size of 0.02–2 μm), and reverse osmosis (pore size of <0.001 μm) [67]. There are many different forms of filtration, such as dead end filtration, microfiltration, ultrafiltration, pressure filtration, vacuum filtration, and tangential flow filtration (TFF) [68]. Nevertheless, it is accompanied with extensive running costs and time consuming.

4.4. Flotation. Microalgae cells are trapped on microair bubbles and float at the surface of water [69]. Generally, the flotation efficiency is dependent on the size of the created bubble: nanobubbles (<1 μm), microbubbles (1–999 μm), and fine bubbles (1–2 mm) [70]. Dissolved air flotation is a widely used technique in which microalgal cells are usually flocculated first and then air is bubbled through the liquid causing the flocs to float to the surface for easier harvesting. Hydrophobic interaction and surface charge of microalgae play crucial role for attachment of microalgae to the bubbles.

5. Lipid Extraction Methods

Lipid is polymer of fatty acids which is generally hydrophobic in nature and is classified as a polar (membrane lipids) and nonpolar lipid (neutral lipids). Polar lipids interact with polar solvents like ethanol and methanol and similarly nonpolar lipids interact with nonpolar solvents like chloroform and benzene which is the basis of designing solvent system for lipid extraction methods [71]. This solvent system mainly disrupts noncovalent interactions, hydrophobic interactions, and hydrogen bonding between lipid and associated macromolecule like protein. Lipids are mainly composed of 90–98% (weight) of TAGs, small amounts of mono- and diglycerides, free fatty acids (1–5%), and residual amounts of phospholipids, phosphatides, carotenes, tocopherols, sulphur compounds, and traces of water [72]. The majority of the lipid fraction is comprised of TAG content, an important parameter for biodiesel production. The saturated (16 : 0) and monounsaturated (18 : 1) fatty acids also play essential role in determining the fuel properties of biodiesel such as cetane number, oxidative stability, and cold flow [73]. Usually, extraction of lipid from microalgae consists of dual steps: cell disruption and solvent extraction. The lipid extraction methods might work differently on a variety of algal species as algae have an enormous variation in cell shape, size, cell wall composition, and types of algal lipids.

Microalgae cell disruption can be achieved by sonication, homogenisation, grinding, bead beating, or freezing [74]. The Folch et al. [75] method was originally optimized for isolation and purification of total lipids from animal tissues is also used for the extraction of total lipids from microalgae using chloroform-methanol 2 : 1. The most commonly used method for total lipid extraction from microalgae is the Bligh and Dyer method [76] which uses chloroform and methanol in 1 : 2. Another method for extraction of biooil or other molecule is to carry out extraction using safe and nonflammable solvent supercritical carbon dioxide (SC-CO_2) which solubilizes non polar compounds; when the molecule of interest is not soluble, the solvent power can be increased using a safe and polar modifier, such as ethanol [77]. But it has few disadvantages; it is uneconomical for large-scale, energy-consuming step of drying pretreatment which limits its application for biofuel production. Ryckebosch et al. [78] optimized procedure for extraction of total and nonpolar lipids from microalgae showing chloroform-methanol 1 : 1 to be the best solvent mixture for extraction of total lipids from microalgae. Sathish and Sims [79] developed wet lipid extraction procedure capable of extracting 79% of transesterifiable lipids from wet algal biomass (84% moisture) via acid and base hydrolysis (90°C and ambient pressures), and 76% of extracted lipids were further converted to FAMEs. Ultimately, it is necessary to develop extraction method having less organic solvent use, reduce contamination, and avoid drying of algae to obtain significant cost reduction for scaling up mass algal culture system for biodiesel production.

5.1. Lipid Analysis Methods. After lipid extraction, it is important to identify and quantify lipid contents to screen the desirable algal strains for their biofuel efficiency. Further quantification of lipids requires separation of the crude extract and quantification of the lipid fraction by thin-layer chromatography (TLC), HPLC, or gas chromatography (GC) [80]. The Nile red fluorescence method is also employed for the determination of both neutral and polar lipids in algae but has been unsuccessful in many others, particularly in those with thick rigid cell walls that prevent the penetration of this lipid soluble fluorescence dye [81]. Mostly, microalgal lipid profiling is done by gas chromatography with flame ionization detector (GC-FID) and is carried out using the methylated ester form of the lipid [82].

5.2. Transesterification. Transesterification or alcoholysis is the reaction of a lipid with an alcohol to form esters and a by-product, glycerol [71]. This reaction actually converts highly viscous raw lipid/oil into low molecular weight molecules in the form of fatty acid alkyl esters which can be used as an alternative fuel for diesel engines. Biodiesel is a term used to describe "fuel comprised of monoalkyl esters of long-chain fatty acids that are derived from vegetable oils or animal fats" [83]. In a typical biodiesel reaction, TAGs enter into a reaction with methanol which yields fatty acid methyl esters (biodiesel) and glycerol as a waste product (as shown in Figure 1). Mainly three approaches are used to produce biodiesel; they are base catalyzed transesterification, acid

catalyzed transesterification (with simultaneous esterification of free fatty acids), and noncatalytic conversion [84, 85].

6. Lipid Productivity from Wastewater Grown Algae

Lipid productivity takes into account both the lipid concentration within cells and the biomass produced by these cells and is therefore a more useful indicator of the potential costs of liquid biofuel production [86]. High lipid productivity is a key characteristic of a microalgal species for biodiesel production [87]. Generally, algae produce lipids between C_{14} and C_{20} in length. During stressful conditions like nutrient limitation, algae change their biosynthetic pathways and produce TAGs, which accumulate in the cytoplasm for the purpose of energy and carbon storage [88, 89]. Nevertheless, deliberately, cultivation of algae in stressful conditions can inhibit cell division, leading to decrease in overall lipid productivity [33, 90]. This is one of the reasons that it is difficult to maximize both high biomass and lipid productivity simultaneously. But still to achieve substantial cost reduction for the commercialization of biofuel production; it is suggested that the near-term research should be focused on maximizing lipid content with the help of altering the phycological metabolism of the microalgal cell and manipulation of cultivation system with the application of advanced engineering and design system.

Although, in many cases, most of the microalgal species reported with high lipid content does not adapt well to grow in wastewater, many researchers had screened microalgal isolates able to grow in wastewater effluents showing high lipid content. Xin et al. [54] isolated a freshwater microalga *Scenedesmus* sp. LX1 with high lipid content (around 25–35%) from low nutrient environment, and they compared *Scenedesmus* sp. LX1 with other reported 11 oily microalgal species based on the growth and lipid accumulation properties while growing in the secondary effluent of domestic wastewater. *Scenedesmus* sp. LX1 showed best growth and accumulated the maximum lipid content in microalgal cells in comparison to other microalgal species which could not grow in the secondary effluent of domestic wastewater. Zhou et al. [35] screened 17 top-performing strains isolated from water bodies including wastewater from Minnesota which grew well in centrate (highly concentrated municipal) wastewater. Five strains were promising, that is, *Chlorella* sp., *Heynigia* sp., *Hindakia* sp., *Micractinium* sp., and *Scenedesmus* sp., regarding their ability to adapt to centrate municipal wastewater showing high growth rates (0.455–0.498 d^{-1}) and higher lipid productivities (74.5–77.8 mg L^{-1} d^{-1}). Bhatnagar et al. [52] isolated three robust mixotrophic microalgae isolated from industrial wastewater and evaluated their growth potential in media supplemented with different organic carbon substrates and wastewaters, which showed 3–10 times more biomass production relative to phototrophy. Devi et al. [53] evaluated the effect of sequential growth phase (GP) and starvation phase (SP) on the lipid productivity of heterotrophically grown mixed microalgae using domestic wastewater as a substrate. The mixotrophic microalgae used in this study were *Chlorella, Scenedesmus* sp., *Cosmarium* sp., and facultative heterotrophs (centric and pinnate diatoms) along with few photoautotrophs (*Cyclotella* and *Oedogonium*) and obligate photoautotrophs (*P. boryanum*). Effect of nutrient supplementation and the results showed that in growth phase (GP) operation with maximum N + P condition higher biomass (1.69 mg/mL) was observed, while higher lipid productivity was observed in starvation phase with maximum in C condition (28.2%) showing good wastewater treatment efficiency in terms of substrate degradation and nutrient removal during the growth phase operation. Moreover, when supplemented with CO_2 sparging period and interval, it influences growth and lipid accumulation of microalgae cultivated in domestic wastewater under mixotrophic microenvironment. Sparging period of 120 s documented maximum biomass growth (GP, 3.4 mg/mL) and lipid productivity (SP, 27.3%), while, in intervals, 4 h (120 s) condition showed maximum biomass (3.2 mg/mL) and lipid productivity (27.8%). Fatty acid composition revealed high degree of saturated fatty acids (SFAs) varied with the experimental variations signifying their utility as biodiesel [91]. They also documented microalgal efficiency to utilize acid-rich effluents from biohydrogen production process as carbon source for lipid accumulation under heterotrophic nutritional mode. Two types of substrates, namely, synthetic volatile fatty acids (SVFAs) and fermentative fatty acids (FFAs) collected from acidogenic H_2 producing bioreactor were used for evaluating the lipid accumulation potential in microalgae. Comparatively, FFAs documented higher biomass and lipid productivity (1.42 mg/mL (wet weight); 26.4%) than SVFAs 0.60 mg/mL; 23.1%) [92].

In another study, fatty acid methyl ester (FAME) analysis of *A. protothecoides* UMN280 showed that the microalgal lipids were mainly composed of C_{16}/C_{18} fatty acids (accounting for over 94% of total fatty acid) making it suitable for high-quality biodiesel production [36]. He et al. [93] checked the feasibility of cultivating *Chlorella vulgaris* with wastewater containing high ammonia nitrogen concentrations. This study found that increasing NH_4^+-N from 17 to 207 mg L^{-1} yielded additional short-chain and saturated fatty acids. Lipid productivity peaked in its value of 23.3 mg L^{-1} d^{-1} at 39 mgL^{-1} NH_4^+-N. Hence, microalgae components could be manipulated by NH_4^+-N concentration of the initial feeds. The biomass and lipid productvities of some of the microalgal species grown in different wastewater resources reported till date is given in Table 1.

7. Nutrient Removal Efficiency

Growing algae depends on the availability of principal nutrients like nitrogen, phosphorus, carbon, sulphur and micronutrients including silica, calcium, magnesium, potassium, iron, manganese, sulphur, zinc, copper, and cobalt. Algal cells have the capability to uptake nitrogen and phosphorus from water [94, 95]. Microalgae can be efficiently used to remove significant amount of nutrients because they need high amounts of nitrogen and phosphorus for protein (45–60% of microalgae dry weight), nucleic acid, and phospholipid synthesis [12]. The nitrogen in sewage effluent arises

Table 1: Biomass and lipid productivities of microalgae grown in different wastewater resources.

Microalgae species	Wastewater type	Biomass productivity ($mg\,L^{-1}\,d^{-1}$)	Lipid content (% DW)	Lipid productivity ($mg\,L^{-1}\,d^{-1}$)	Reference
Chlorella pyrenoidosa	Activated sludge extract	11.55	NA	NA	[28]
Chlorella pyrenoidosa	Digested sludge Extract	51.82	NA	NA	[28]
Chlorella pyrenoidosa	Settled sewage	275	NA	NA	[29, 30]
Chlorella pyrenoidosa and *Scenedesmus* sp.	Activated sewage	92.31	NA	NA	[29, 30]
Botryococcus braunii	Secondarily treated sewage	35.00	NA	NA	[31]
Scenedesmus sp.	Artificial Wastewater	126.54	12.80	16.2	[32]
Polyculture of *Chlorella* sp., *Micractinium* sp., *Actinastrum* sp.	Dairy Wastewater	NA	29.00	17	[33]
Polyculture of *Chlorella* sp., *Micractinium* sp. *Actinastrum* sp.	Primary clarifier Effluent	NA	9.00	24.4	[33]
Chlorella asccharophila	Carpet mill	23	18.10	4.2	[34]
Scenedesmus sp.	Carpet mill	126.54	12.80	16.2	[34]
Chlorella sp.	Centrate Muinicipal Wastewater	231.4	33.53	77.5	[35]
Hindakia sp.	Centrate Muinicipal Wastewater	275.0	28.30	77.8	[35]
Chlorella sp.	Centrate Muinicipal Wastewater	241.7	30.91	74.7	[35]
Scenedesmus sp.	Centrate Muinicipal Wastewater	247.5	30.09	74.5	[35]
Auxenochlorella protothecoides	Concentrated Muinicipal Wastewater	268.8	28.9	77.7	[36]
Chlamydomonas Mexicana	Piggery Wastewater	NA	33 ± 3.4[a]	0.31 ± 0.03[a]	[37]
Scenedesmus obliquus	Piggery Wastewater	NA	31 ± 0.8[a]	0.24 ± 0.03[a]	[37]

*NA: Not Available.
[a]Expressed in dwt/L.

primarily from metabolic interconversions of extra derived compounds, whereas 50% or more of phosphorus arises from synthetic detergents [27]. Nitrogen and phosphorus are the two important nutrient compounds to analyze a water source for potential algae growth. The principal forms in which they arise in wastewater are NH_4 (ammonia), NO^{-2} (nitrite), NO^{-3} (nitrate), and $PO_4{}^{3-}$ (orthophosphate). The nutrient removal efficiency of some of the microalgal species reported till date is given in Table 2.

Algal growth and nutrient removal characteristics of microalgae *Chlorella vulgaris* using artificial wastewater in batch experiments showed that *C. vulgaris* can completely remove up to $21.2\,mg\,L^{-1}$ ammonia-nitrogen concentration but showed low phosphorus removal with $7.7\,mg\,L^{-1}$ initial PO_4-P concentration with 78% efficiency [94]. A promising strain *A. protothecoides* UMN280 isolated from a local municipal wastewater plant shows high nutrient removal efficiency as well as its high growth rate and lipid productivity. The results of the six-day batch cultivation showed that the maximal removal efficiencies for total nitrogen, total phosphorus, chemical oxygen demand (COD), and total organic carbon (TOC) were over 59%, 81%, 88%, and 96%, respectively, with high growth rate ($0.490\,d^{-1}$), high biomass productivity ($269\,mg\,L^{-1}\,d^{-1}$), and high lipid productivity ($78\,mg\,L^{-1}\,d^{-1}$) [36]. Studies have demonstrated ability of *Euglena sp*. originally isolated from the sewage treatment plants and showing good lipid content of 24.6% (w/w), efficient nutrient uptake within a short span of eight days, and profuse biomass productivity ($132\,mg\,L^{-1}\,d^{-1}$) [44].

Sturm and Lamer [96] do an assessment on energy balance of microalgal production in open ponds coupled with nutrient removal from wastewater energy for algal biodiesel production. They studied microalgal yields and nutrient removal rate from four pilot scale reactors (2500 gallons each) fed with wastewater effluent from a municipal wastewater treatment plant for six months, using a total of 12 million gallons per day processed by the wastewater treatment plant. Hence, it shows that the direct combustion of algal biomass may be a more viable energy source than biofuel production, especially when the lipid content of dry biomass (10% in this field experiment) is lower than the high values reported in lab scale reactors (50 60%). Yang et al. [97] examined nutrients usages to generate 1 kg of microalgae biodiesel using nonrecycled freshwater. It will require 3726 kg

Table 2: Nutrient removal efficiency of microalgal species.

Microalgal species	Wastewater type	Nitrogen	Phosphate	COD	Reference
Chlorella vulgaris	Textile wastewater	(44.4–45.1%)	(33.1–33.3%)	(38.3–62.3%)	[38]
Scenedesmus sp. LX1	Modified effluent of a wastewater treatment plant of an electric factory by photo-membrane bioreactor	46%	100%	NA	[39]
Chlorella sorokiniana and aerobic bacteria	Potato processing industry	>95	80.7	84.8	[40]
Chlorella sorokiniana and aerobic bacteria	Pig manure	82.7	58.0	62.3	[40]
Chlamydomonas sp. TAI-2	Industrial wastewater	100%	33%	NA	[41]
Auxenochlorella protothecoides UMN280	Concentrated municipal wastewater	59%	81%	88%	[36]
Chlorella Mexicana	Piggery wastewater	62%	28%	NA	[37]
Scenedesmus obliquus	Piggery effluent	23–58%	48–69%	NA	[42]
Chlamydomonas Polypyrenoideum	Dairy industry wastewater	74%–90%	70%	NA	[43]
Euglena sp.	Sewage treatment plant	93%	66%	NA	[44]

*NA: Not Available.

of water, 0.33 kg of nitrogen, and 0.71 kg of phosphate and also shows decrease of water and nutrients usage by 84% and 55% using recycling harvest water and reduction in 90% of water requirement, eliminating the need for all the nutrients except phosphate by using sea/wastewater as culture medium. In another study, 1L biodiesel was produced consuming nutrient between 0.23 and 1.55 kg nitrogen and 29–145 g of phosphorus depending on the cultivation conditions for microalgae [98].

8. Conclusion

Presently, key bottleneck of biofuel production from microalgae is that the current technologies do not allow an economic and sustainable biofuel production at today's energy prices, although high biomass, lipid productivity, and nutrient removal efficiency of wastewater grown microalgae make them promising as a feedstock for renewable energy. Furthermore, there is need to analyse nutrient consumption rates of wastewater derived algal biofuels, bioprospecting of different wastewater habitats to explore indigenous oil producing microalgal strains. Moreover, efforts should be made by focusing research on development of large-scale cost-effective cultivation systems. The coupling of microalgae cultivation with wastewater might provide possibility of phycoremediation, CO_2 sequestration, and low cost nutrient supply for the algal biomass utilization which will enhance the economic outlook of microalgae-based biofuel production systems.

Conflict of Interests

The authors declare that there is no conflict of interests regarding the publication of this paper.

Acknowledgments

The authors would like to thank Department of Biotechnology, Kumaun University, Nainital, for providing necessary facilities to carry out this work and also thank Dr. Alok Shukla, Department of Plant Physiology, and G. B. Pant University of Agriculture and Technology, Pantnagar, for their suggestions and comments that greatly improved the paper.

References

[1] International Energy Agency, *Tracking Clean Energy Progress*, OCED/IEA, Paris, France, 2013, http://www.iea.org.

[2] US DOE, *International Energy Outlook. Energy Information Administration*, U. S. Department of Energy, Washington, DC, USA, 2010.

[3] BP Statistical Review of World Energy, 2011, http://www.bp.com/statistical review.

[4] S. A. Khan, R. Rashmi, M. Z. Hussain, S. Prasad, and U. C. Banerjee, "Prospects of biodiesel production from microalgae in India," *Renewable and Sustainable Energy Reviews*, vol. 13, no. 9, pp. 2361–2372, 2009.

[5] IndiaBiofuelAnnals, 2013, http://gain.fas.usda.gov/Recent%20GAIN%20Publications/Biofuels%20Annual_New%20Delhi_India_8-13-2013.pdf.

[6] International Energy Agency, *Energy Balances of OECD Countries 2004-2005*, IEA, Paris, France, 2007, http://www.iea.org.

[7] Energy Information Agency, "Annual energy review," Tech. Rep. DOE/EIA-384, EIA, 2005, http://www.eia.doe.gov.

[8] Intergovernmental Panel on Climate Change, "IPCC summary for policymakers," in *Climate Change 2007: The Physical Science Basis. Contribution of Working Group I to the Fourth Assessment Report of the Intergovernmental Panel on Climate Change*, pp. 7–22, Cambridge University Press, 2007.

[9] H. Y. Hu, X. Li, Y. Yu, Y. H. Wu, M. Sagehashi, and A. Sakoda, "Domestic wastewater reclamation coupled with biofuel/biomass production based on microalgae: a novel

wastewater treatment process in the future," *Journal of Water and Environment Technology*, vol. 9, pp. 199–207, 2011.

[10] J. Sheehan, T. Dunahay, J. Benemann, and P. Roessler, "A look back at the US Department of Energy's Aquatic Species Program—Biodiesel from algae," Tech. Rep. NREL/TP-580-24190, Prepared for the U. S. Department of Energy by the National Renewable Energy Laboratory, Golden, Colo, USA, 1998.

[11] J. K. Pittman, A. P. Dean, and O. Osundeko, "The potential of sustainable algal biofuel production using wastewater resources," *Bioresource Technology*, vol. 102, no. 1, pp. 17–25, 2011.

[12] I. Rawat, R. Ranjith Kumar, T. Mutanda, and F. Bux, "Dual role of microalgae: phycoremediation of domestic wastewater and biomass production for sustainable biofuels production," *Applied Energy*, vol. 88, no. 10, pp. 3411–3424, 2011.

[13] E. Stephens, I. L. Ross, J. H. Mussgnug et al., "Future prospects of microalgal biofuel production systems," *Trends in Plant Science*, vol. 15, no. 10, pp. 554–564, 2010.

[14] Y. Chisti and J. Yan, "Energy from algae: current status and future trends. Algal biofuels—a status report," *Applied Energy*, vol. 88, no. 10, pp. 3277–3279, 2011.

[15] L. Barsanti and P. Gualtiery, *Algae: Anatomy, Biochemistry and Biotechnology*, CRC Taylor & Francis, New York, NY, USA, 2006.

[16] R. E. Lee, *Phycology*, Cambridge University Press, New York, NY, USA, 1980.

[17] G. Markou, I. Angelidaki, and D. Georgakakis, "Microalgal carbohydrates: an overview of the factors influencing carbohydrates production, and of main bioconversion technologies for production of biofuels," *Applied Microbiology and Biotechnology*, vol. 96, pp. 631–645, 2012.

[18] Y. Chisti, "Biodiesel from microalgae," *Biotechnology Advances*, vol. 25, no. 3, pp. 294–306, 2007.

[19] J. Brodie and J. Lewis, *Unravelling the Algae: The Past, Present, and Future of Algal Systematics*, vol. 75 of *Systematics Association Special Volumes*, CRC Press, London, UK, 2007.

[20] P. M. Schenk, S. R. Thomas-Hall, E. Stephens, U. C. Marx, J. H. Mussgnug, and C. Posten, "Second generation biofuels: high efficiency microalgae for biodiesel production," *Bioenergy Research*, vol. 1, pp. 20–43, 2008.

[21] J. R. Benemann, J. C. van Olst, M. J. Massingill et al., "The controlled eutrophication process: using microalgae for CO_2 utilization and agricultural fertilizer recycling," in *Greenhouse Gas Control Technologies—6th International Conference*, pp. 1433–1438, Pergamon, Oxford, UK, 2003.

[22] A. Demirbas, "Use of algae as biofuel sources," *Energy Conversion and Management*, vol. 51, no. 12, pp. 2738–2749, 2010.

[23] P. Alvira, E. Tomás-Pejó, M. Ballesteros, and M. J. Negro, "Pretreatment technologies for an efficient bioethanol production process based on enzymatic hydrolysis: a review," *Bioresource Technology*, vol. 101, no. 13, pp. 4851–4861, 2010.

[24] P. J. McGinn, K. E. Dickinson, S. Bhatti, J. Frigon, S. R. Guiot, and S. J. O'Leary, "Integration of microalgae cultivation with industrial waste remediation for biofuel and bioenergy production: opportunities and limitations," *Photosynth Research*, vol. 109, pp. 231–247, 2011.

[25] T. G. Ellis, "Chemistry of wastewater," in *Environmental and Ecological Chemistry, Volume II*, p. 452, Department of Civil, Construction and Environmental Engineering, Ames, Iowa, USA, 2011.

[26] N. F. Gray, *Biology of Wastewater Treatment*, Oxford University Press, Oxford, UK, 1989.

[27] N. Abdel-Raouf, A. A. Al-Homaidan, and I. B. M. Ibraheem, "Microalgae and wastewater treatment," *Saudi Journal of Biological Sciences*, vol. 19, pp. 257–275, 2012.

[28] Y. H. Cheung and M. H. Wong, "Properties of animal manures and sewage sludges and their utilization for algal growth," *Agricultural Wastes*, vol. 3, no. 2, pp. 109–122, 1981.

[29] N. F. Y. Tam and Y. S. Wong, "Wastewater nutrient removal by *Chlorella pyrenoidosa* and *Scenedesmus* sp," *Environmental Pollution*, vol. 58, no. 1, pp. 19–34, 1989.

[30] N. F. Y. Tam and Y. S. Wong, "The comparison of growth and nutrient removal efficiency of *Chlorella pyrenoidosa* in settled and activated sewages," *Environmental Pollution*, vol. 65, no. 2, pp. 93–108, 1990.

[31] S. Sawayama, T. Minowa, Y. Dote, and S. Yokoyama, "Growth of the hydrocarbon-rich microalga *Botryococcus braunii* in secondarily treated sewage," *Applied Microbiology and Biotechnology*, vol. 38, no. 1, pp. 135–138, 1992.

[32] D. Voltolina, B. Cordero, M. Nieves, and L. P. Soto, "Growth of *Scenedesmus* sp. in artificial wastewater," *Bioresource Technology*, vol. 68, no. 3, pp. 265–268, 1999.

[33] I. Woertz, A. Feffer, T. Lundquist, and Y. Nelson, "Algae grown on dairy and municipal wastewater for simultaneous nutrient removal and lipid production for biofuel feedstock," *Journal of Environmental Engineering*, vol. 135, no. 11, pp. 1115–1122, 2009.

[34] S. Chinnasamy, A. Bhatnagar, R. W. Hunt, and K. C. Das, "Microalgae cultivation in a wastewater dominated by carpet mill effluents for biofuel applications," *Bioresource Technology*, vol. 101, no. 9, pp. 3097–3105, 2010.

[35] W. Zhou, Y. Li, M. Min, B. Hu, P. Chen, and R. Ruan, "Local bioprospecting for high-lipid producing microalgal strains to be grown on concentrated municipal wastewater for biofuel production," *Bioresource Technology*, vol. 102, no. 13, pp. 6909–6919, 2011.

[36] W. Zhou, Y. Li, M. Min et al., "Growing wastewater-born microalga *Auxenochlorella protothecoides* UMN280 on concentrated municipal wastewater for simultaneous nutrient removal and energy feedstock production," *Applied Energy*, vol. 98, pp. 433–440, 2012.

[37] R. A. Abou-Shanab, M. K. Ji, H. C. Kim, K. J. Paeng, and B. H. Jeon, "Microalgal species growing on piggery wastewater as a valuable candidate for nutrient removal and biodiesel production," *Journal of Environmental Management*, vol. 115, pp. 257–264, 2013.

[38] S. L. Lim, W. L. Chu, and S. M. Phang, "Use of *Chlorella vulgaris* for bioremediation of textilewastewater," *Bioresource Technology*, vol. 101, pp. 7314–7322, 2010.

[39] S. Zhen-Feng, L. Xin, H. Hong-Ying, W. Yin-Hu, and N. Tsutomu, "Culture of *Scenedesmus* sp. LX1 in the modified effluent of a wastewater treatment plant of an electric factory by photo-membrane bioreactor," *Bioresource Technology*, vol. 102, no. 17, pp. 7627–7632, 2011.

[40] D. Hernández, B. Riaño, M. Coca, and M. C. García-González, "Treatment of agro-industrial wastewater using microalgae-bacteria consortium combined with anaerobic digestion of the produced biomass," *Bioresource Technology*, vol. 135, pp. 598–603, 2012.

[41] L. F. Wu, P. C. Chen, A. P. Huang, and C. M. Lee, "The feasibility of biodiesel production by microalgae using industrial wastewater," *Bioresource Technology*, vol. 113, pp. 14–18, 2012.

[42] M. Ji, R. Abou-Shanab, J. Hwang et al., "Removal of nitrogen and phosphorus from piggery wastewater effluent using the green microalga *Scenedesmus obliquus*," *Journal of Environmental Engineering*, vol. 139, pp. 1198–1205, 2013.

[43] R. Kothari, R. Prasad, V. Kumar, and D. P. Singh, "Production of biodiesel from microalgae *Chlamydomonas polypyrenoideum* grown on dairy industry wastewater," *Bioresource Technology*, vol. 144, pp. 499–503, 2013.

[44] D. M. Mahapatra, H. N. Chanakya, and T. V. Ramachandra, "*Euglena* sp. as a suitable source of lipids for potential use as biofuel and sustainable wastewater treatment," *Journal of Applied Phycology*, vol. 25, pp. 855–865, 2013.

[45] European Nations, *Innovating for Sustainable Growth: A Bioeconomy for Europe*, European Nations, Brussels, Belgium, 2012, http://www.ec.europa.eu/bioeconomy/pdf/2012_commision_staff_working.pdf.

[46] L. Fahm, *The Waste of Nations: The Economic Utilisation of Human Waste in Agriculture*, Allenhand, Osmun & Co. Pu, Montclair, NJ, USA, 1980.

[47] P. Amerasinghe, R. M. Bhardwaj, C. Scott, K. Jella, and F. Marshall, "Urban wastewater and agricultural reuse challenges in India," IWMI Research Report 147, International Water Management Institute (IWMI), Colombo, Sri Lanka, 2013, http://ageconsearch.umn.edu/bitstream/1158342/2/H045769.pdf.

[48] CPCB (Central Pollution Control Board), pp. 1–9, 2011, http://unstats.un.org/unsd/environment/envpdf/pap_wasess3-b6india.pdf.

[49] J. de la Noue, G. Laliberte, and D. Proulx, "Algae and waste water," *Journal of Applied Phycology*, vol. 4, pp. 247–254, 1992.

[50] F. B. Green, T. J. Lundquist, and W. J. Oswald, "Energetics of advanced integrated wastewater pond systems," *Water Science and Technology*, vol. 31, no. 12, pp. 9–20, 1995.

[51] W. J. Oswald, H. B. Gotaas, C. G. Golueke, and W. R. Kellen, "Algae in waste treatment," *Sewage and Industrial Wastes*, vol. 29, pp. 437–455, 1957.

[52] A. Bhatnagar, S. Chinnasamy, M. Singh, and K. C. Das, "Renewable biomass production by mixotrophic algae in the presence of various carbon sources and wastewaters," *Applied Energy*, vol. 88, no. 10, pp. 3425–3431, 2011.

[53] M. Prathima Devi, G. Venkata Subhash, and S. Venkata Mohan, "Heterotrophic cultivation of mixed microalgae for lipid accumulation and wastewater treatment during sequential growth and starvation phases: effect of nutrient supplementation," *Renewable Energy*, vol. 43, pp. 276–283, 2012.

[54] L. Xin, H. Hong-Ying, and Y. Jia, "Lipid accumulation and nutrient removal properties of a newly isolated freshwater microalga, *Scenedesmus* sp. LX1, growing in secondary effluent," *New biotechnology*, vol. 27, no. 1, pp. 59–63, 2010.

[55] H. N. Chanakya, D. M. Mahapatra, S. Ravi, V. S. Chauhan, and R. Abitha, "Sustainability of large-scale algal biofuel production in India," *Journal of the Indian Institute of Science*, vol. 92, no. 1, pp. 63–98, 2012.

[56] R. J. Craggs, S. Heubeck, T. J. Lundquist, and J. R. Benemann, "Algal biofuels from wastewater treatment high rate algal ponds," *Water Science and Technology*, vol. 63, no. 4, pp. 660–665, 2011.

[57] J. B. K. Park, R. J. Craggs, and A. N. Shilton, "Wastewater treatment high rate algal ponds for biofuel production," *Bioresource Technology*, vol. 102, no. 1, pp. 35–42, 2011.

[58] R. Putt, M. Singh, S. Chinnasamy, and K. C. Das, "An efficient system for carbonation of high-rate algae pond water to enhance CO_2 mass transfer," *Bioresource Technology*, vol. 102, no. 3, pp. 3240–3245, 2011.

[59] B. Viswanath and F. Bux, "Biodiesel production potential of wastewater microalgae *Chlorella* sp. Under photoautotrophic and Heterotrophic growth conditions," *British Journal of Engineering and Technology*, vol. 1, pp. 251–264, 2012.

[60] S. A. Scott, M. P. Davey, J. S. Dennis et al., "Biodiesel from algae: challenges and prospects," *Current Opinion in Biotechnology*, vol. 21, no. 3, pp. 277–286, 2010.

[61] R. M. Knuckey, M. R. Brown, R. Robert, and D. M. F. Frampton, "Production of microalgal concentrates by flocculation and their assessment as aquaculture feeds," *Aquacultural Engineering*, vol. 35, no. 3, pp. 300–313, 2006.

[62] A. Papazi, P. Makridis, and P. Divanach, "Harvesting *Chlorella minutissima* using cell coagulants," *Journal of Applied Phycology*, vol. 22, no. 3, pp. 349–355, 2010.

[63] J. Morales, J. de la Noüe, and G. Picard, "Harvesting marine microalgae species by chitosan flocculation," *Aquacultural Engineering*, vol. 4, no. 4, pp. 257–270, 1985.

[64] D. Vandamme, I. Foubert, B. Meesschaert, and K. Muylaert, "Flocculation of microalgae using cationic starch," *Journal of Applied Phycology*, vol. 22, no. 4, pp. 525–530, 2010.

[65] G. Shelef, A. Sukenik, and M. Green, *Microalgae Harvesting and Processing: A Literature Review*, Technion Research and Development Foundation, Haifa, Israel, 1984.

[66] N. Uduman, Y. Qi, M. K. Danquah, G. M. Forde, and A. Hoadley, "Dewatering of microalgal cultures: a major bottleneck to algae-based fuels," *Journal of Renewable and Sustainable Energy*, vol. 2, no. 1, Article ID 012701, 15 pages, 2010.

[67] S. O. Gultom and B. Hu, "Review of microalgae harvesting via co-pelletization with filamentous fungus," *Energies*, vol. 6, pp. 5921–5939, 2013.

[68] R. Harun, M. Singh, G. M. Forde, and M. K. Danquah, "Bioprocess engineering of microalgae to produce a variety of consumer products," *Renewable and Sustainable Energy Reviews*, vol. 14, no. 3, pp. 1037–1047, 2010.

[69] K. K. Sharma, S. Garg, Y. Li, A. Malekizadeh, and P. M. Schenk, "Critical analysis of current microalgae dewatering techniques," *Biofuels*, vol. 4, pp. 397–407, 2013.

[70] J. Kim, G. Yoo, H. Lee et al., "Methods of downstream processing for the production of biodiesel from microalgae," *Biotechnology Advances*, vol. 31, no. 6, pp. 862–876, 2013.

[71] S. F. Sing, A. Isdepsky, M. A. Borowitzka, and N. R. Moheimani, "Production of biofuels from microalgae," *Mitigation and Adaptation Strategies for Global Change*, vol. 18, pp. 47–72, 2011.

[72] K. Bozbas, "Biodiesel as an alternative motor fuel: production and policies in the European Union," *Renewable and Sustainable Energy Reviews*, vol. 12, no. 2, pp. 542–552, 2008.

[73] S. Kaur, M. Sarkar, R. B. Srivastava, H. K. Gogoi, and M. C. Kalita, "Fatty acid profiling and molecular characterization of some freshwater microalgae from India with potential for biodiesel production," *New Biotechnology*, vol. 29, no. 3, pp. 332–344, 2012.

[74] A. R. Medina, E. M. Grima, A. G. Gimenez, and M. J. I. Gonzalez, "Downstream processing of algal polyunsaturated fatty acids," *Biotechnology Advances*, vol. 3, pp. 517–580, 1998.

[75] J. Folch, M. Lees, and G. H. S. Stanley, "A simple method for the isolation and purification of total lipids from animal tissues," *The Journal of Biological Chemistry*, vol. 226, pp. 497–509, 1957.

[76] E. G. Bligh and W. J. Dyer, "A rapid method of total lipid extraction and purification," *Canadian Journal of Biochemistry and Physiology*, vol. 37, no. 8, pp. 911–917, 1959.

[77] C. Crampon, O. Boutin, and E. Badens, "Supercritical carbon dioxide extraction of molecules of interest from microalgae and seaweeds," *Industrial and Engineering Chemistry Research*, vol. 50, no. 15, pp. 8941–8953, 2011.

[78] E. Ryckebosch, K. Muylaert, and I. Foubert, "Optimization of an analytical procedure for extraction of lipids from microalgae," *Journal of the American Oil Chemists' Society*, vol. 89, pp. 189–198, 2011.

[79] A. Sathish and R. C. Sims, "Biodiesel from mixed culture algae via a wet lipid extraction procedure," *Bioresource Technology*, vol. 118, pp. 643–647, 2012.

[80] M. L. Eltgroth, R. L. Watwood, and G. V. Wolfe, "Production and cellular localization of neutral long-chain lipids in the haptophyte algae *Isochrysis galbana* and *Emiliania huxleyi*," *Journal of Phycology*, vol. 41, no. 5, pp. 1000–1009, 2005.

[81] W. Chen, C. Zhang, L. Song, M. Sommerfeld, and Q. Hu, "A high throughput Nile red method for quantitative measurement of neutral lipids in microalgae," *Journal of Microbiological Methods*, vol. 77, no. 1, pp. 41–47, 2009.

[82] T. Mutanda, D. Ramesh, S. Karthikeyan, S. Kumari, A. Anandraj, and F. Bux, "Bioprospecting for hyper-lipid producing microalgal strains for sustainable biofuel production," *Bioresource Technology*, vol. 102, no. 1, pp. 57–70, 2011.

[83] Z. Zhao, "Comment on heterogeneous catalytic deoxygenation of stearic acid for production of biodiesel," *Industrial and Engineering Chemistry Research*, vol. 45, no. 20, p. 6874, 2006.

[84] A. Demirbaş, "Biodiesel fuels from vegetable oils via catalytic and non-catalytic supercritical alcohol transesterifications and other methods: a survey," *Energy Conversion and Management*, vol. 44, no. 13, pp. 2093–2109, 2003.

[85] C. V. McNeff, L. C. McNeff, B. Yan et al., "A continuous catalytic system for biodiesel production," *Applied Catalysis A: General*, vol. 343, no. 1-2, pp. 39–48, 2008.

[86] L. Brennan and P. Owende, "Biofuels from microalgae—a review of technologies for production, processing, and extractions of biofuels and co-products," *Renewable and Sustainable Energy Reviews*, vol. 14, no. 2, pp. 557–577, 2010.

[87] M. J. Griffiths and S. T. L. Harrison, "Lipid productivity as a key characteristic for choosing algal species for biodiesel production," *Journal of Applied Phycology*, vol. 21, no. 5, pp. 493–507, 2009.

[88] Q. Hu, M. Sommerfeld, E. Jarvis et al., "Microalgal triacylglycerols as feedstocks for biofuel production: perspectives and advances," *Plant Journal*, vol. 54, no. 4, pp. 621–639, 2008.

[89] L. L. Beer, E. S. Boyd, J. W. Peters, and M. C. Posewitz, "Engineering algae for biohydrogen and biofuel production," *Current Opinion in Biotechnology*, vol. 20, no. 3, pp. 264–271, 2009.

[90] L. Lardon, A. Hélias, B. Sialve, J. Steyer, and O. Bernard, "Life-cycle assessment of biodiesel production from microalgae," *Environmental Science and Technology*, vol. 43, no. 17, pp. 6475–6481, 2009.

[91] M. P. Devi and S. Venkata Mohan, "CO_2 supplementation to domestic wastewater enhances microalgae lipid accumulation under mixotrophic microenvironment: effect of sparging period and interval," *Bioresource Technology*, vol. 112, pp. 116–123, 2012.

[92] S. Venkata Mohan and M. P. Devi, "Fatty acid rich effluent from acidogenic biohydrogen reactor as substrate for lipid accumulation in heterotrophic microalgae with simultaneous treatment," *Bioresource Technology*, vol. 123, pp. 627–635, 2012.

[93] P. J. He, B. Mao, C. M. Shen, L. M. Shao, D. J. Lee, and J. S. Chang, "Cultivation of *Chlorella vulgaris* on wastewater containing high levels of ammonia for biodiesel production," *Bioresource Technology*, vol. 129, pp. 177–181, 2013.

[94] S. Aslan and I. K. Kapdan, "Batch kinetics of nitrogen and phosphorus removal from synthetic wastewater by algae," *Ecological Engineering*, vol. 28, no. 1, pp. 64–70, 2006.

[95] J. García, B. F. Green, T. Lundquist, R. Mujeriego, M. Hernández-Mariné, and W. J. Oswald, "Long term diurnal variations in contaminant removal in high rate ponds treating urban wastewater," *Bioresource Technology*, vol. 97, no. 14, pp. 1709–1715, 2006.

[96] B. S. M. Sturm and S. L. Lamer, "An energy evaluation of coupling nutrient removal from wastewater with algal biomass production," *Applied Energy*, vol. 88, no. 10, pp. 3499–3506, 2011.

[97] J. Yang, M. Xu, Q. Hu, M. Sommerfeld, and Y. Chen, "Life-cycle analysis on biodiesel production from microalgae: water footprint and nutrients balance," *Bioresource Technology*, vol. 102, pp. 159–165, 2011.

[98] C. Rösch, J. Skarka, and N. Wegerer, "Materials flow modeling of nutrient recycling in biodiesel production from microalgae," *Bioresource Technology*, vol. 107, pp. 191–199, 2012.

Hindawi Publishing Corporation
The Scientific World Journal
Volume 2014, Article ID 130185, 5 pages
http://dx.doi.org/10.1155/2014/130185

Research Article

Carbon Nanofibers Modified Graphite Felt for High Performance Anode in High Substrate Concentration Microbial Fuel Cells

Youliang Shen,[1,2] Yan Zhou,[3] Shuiliang Chen,[3] Fangfang Yang,[3] Suqi Zheng,[3] and Haoqing Hou[1,3]

[1] *School of Materials Science and Engineering, Nanchang University, Nanchang 330031, China*
[2] *Jiangxi Key Laboratory of Surface Engineering, Jiangxi Science & Technology Normal University, Nanchang 330013, China*
[3] *Department of Chemistry and Chemical Engineering, Jiangxi Normal University, Nanchang 330022, China*

Correspondence should be addressed to Shuiliang Chen; slchenjxnu@jxnu.edu.cn and Haoqing Hou; haoqing@jxnu.edu.cn

Received 25 December 2013; Accepted 19 February 2014; Published 22 April 2014

Academic Editors: B. Cao, H.-C. Tao, and Y.-C. Yong

Carbon nanofibers modified graphite fibers (CNFs/GF) composite electrode was prepared for anode in high substrate concentration microbial fuel cells. Electrochemical tests showed that the CNFs/GF anode generated a peak current density of 2.42 mA cm^{-2} at a low acetate concentration of 20 mM, which was 54% higher than that from bare GF. Increase of the acetate concentration to 80 mM, in which the peak current density of the CNFs/GF anode greatly increased and was up to 3.57 mA cm^{-2}, was seven times as that of GF anode. Morphology characterization revealed that the biofilms in the CNFs/GF anode were much denser than those in the bare GF. This result revealed that the nanostructure in the anode not only enhanced current generation but also could tolerate high substrate concentration.

1. Introduction

Microbial fuel cells (MFCs) are electrochemical devices that use electroactive microorganisms to oxidize organic chemicals and generate electric power [1]. Based on the "green" power source characteristic, the MFCs show great potential in many applications including wastewater treatment, biosensors, water desalination, remote power sources, biohydrogen production, and heavy metal removal and recovery [2–4]. Currently, the limited performance is one of main obstacles for the MFC on the way to practical application.

Anode related to the biofilm growth plays a crucial role on the performance of MFCs. Recently, some measures have been taken to improve the performance of anode, which mainly included architecture design and surface modification. Various macroporous carbons were developed for anodes in MFCs, such as carbon papers [5], carbon cloth [6], graphite rod [7], graphite fiber brush [8], reticulated vitrified carbon (RVC) [7], graphite felt [9], electrospun carbon fiber mats [10], natural plant derived carbon materials [11], and layered corrugated carbon [12]. Simultaneously, some composite materials prepared by surface modification were also studied as high performance anodes in MFCs, such as redox or conducting polymer [13–15] and nanocarbons [16], modified carbon materials [17, 18], and carbon nanotube-coated macroporous polymers [19, 20].

Though the highest anodic current density of 400 A m^{-2} was obtained in one of our previous studies by using layered corrugated carbon [12], the performance of these anodes was measured under relatively low-concentration substrate, for example, below 20 mM acetate. Though a diversity of substrates were employed as substrates in MFCs, including saccharides, alcohols, and different kinds of wastewater, which had been summarized in some review such as [21], the study on the performance of anode in MFCs under high concentration substrate was rare. The tolerance of high

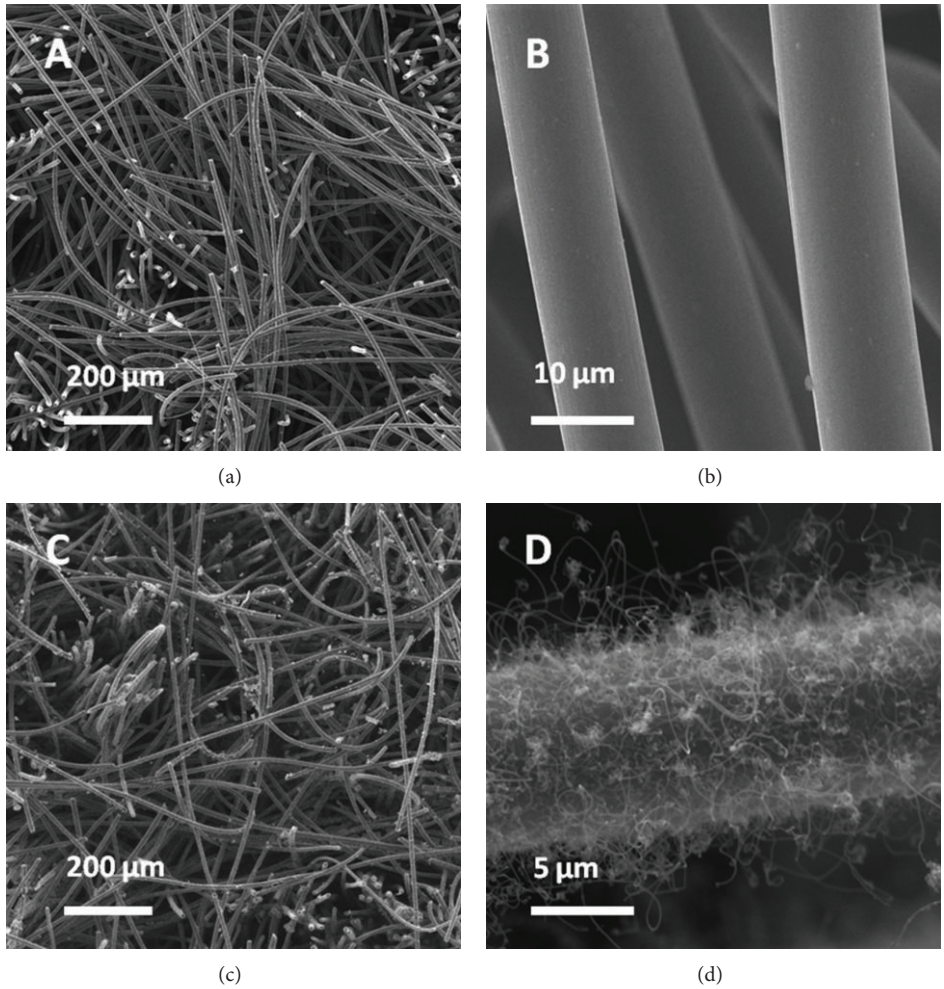

(a) (b)

(c) (d)

Figure 1: SEM images of ((a) and (b)) GF and ((c) and (d)) CNFs/GF.

concentration substrate would expand the application of MFCs to treat high strength wastewater, thus showing great help for practical application.

In this study, we report carbon nanofiber modified graphite felt (CNFs/GF) for anode in high substrate concentration microbial fuel cells. CNFs/GF anode is prepared by growth of CNFs on GF via chemical vapor deposition. The anodic performance of the CNFs/GF anode in different concentration of acetate is investigated, as well as the behavior of biofilms in the CNFs/GF, and compared with the bare graphite felt.

2. Method

2.1. Materials Preparation and Characterization. Graphite felt (GF) (Hunan Jiuhua Carbon High-Tech Co., Xiangtan, Hunan, China) was firstly soaked in 10 wt% $FeCl_3$ for 1 h and then dried in a vacuum oven at 100°C for 1 h. The growth of carbon nanofibers onto GF was conducted in a furnace equipped with a quartz tube. The GF was heated to 850°C at a rate of 5°C/min in N_2 atmosphere, then inlet the mixture of H_2 and N_2 ($H_2/N_2 = 1:4$) at a total flow of 100 mL min^{-1} for 1 h to reduce the Fe (III) to Fe (0). Subsequently, let the furnace cool down to about 750°C and then inlet acetylene with rate of 10 mL min^{-1} for 5 min. After cooling down to room temperature naturally, the CNFs/GF was taken out. The residue Fe in the CNFs/GF was removed by socking it in 0.5 M hydrochloric acid solution and rinsed with distilled water. At last, the samples were dried in the drying oven at 100°C for 1 h. The morphology characterization of samples was observed by a Tescan Vega-3 scanning electron microscope (SEM).

2.2. Electrode Preparation. Graphite plate (GP) cut into pieces with size of $1 \times 1\,cm^2$ was connected with stainless wire and encapsulated by epoxy resin. One side of GP was polished by 2000 mesh sandpaper and used as support for anode electrode. The CNFs/GF and GF were cut into pieces with the same size as the GP and glued onto the polished GP by conductive glue.

2.3. Electrochemical Measurement. Primary domestic wastewater was collected from the wastewater treatment plant (Qingshan, Nanchang, China) and used as the inoculum to

select secondary biofilms through procedures following previous report [11]. All current density data in this paper refer to secondary biofilms and the electrochemical performance tests were conducted when the biofilms activity reached stationary level.

The electrochemical measurements were carried out in three-electrode half-cell, in which a 500 mL bottle was assembled with six working electrodes, one Ag/AgCl reference electrode (saturated KCl, 0.198 V versus standard hydrogen electrode (SHE)) and one carbon felt counter electrode (8 cm^2). The experiments were carried out with computer controlled potentiostat (CHI1040B) which was equipped with eight channels in parallel. For the chronoamperometric (CA) measurement, a potential of +0.2 V was applied onto the working electrodes and the current was recorded. All experimental operations were conducted anaerobically at 35°C which was the optimal growth temperature of bacteriain 50 mM phosphate buffer solution (pH = 7.0) with different concentrations of acetate substrate. All of the electrode potentials were given as versus Ag/AgCl and all of the current density values were normalized to the projected surface area.

2.4. Biofilm SEM Imaging. The morphology of the biofilm was characterized by scanning electron microscopy (SEM). The biofilm samples for SEM characterization were prepared as follows [11], biofilm samples were firstly fixed by 5 wt% glutaric aldehydes in 50 mM phosphate buffer solution (pH = 7.0), then dehydrated in a graded series of ethanol aqueous solution (10%, 25%, 40%, 55%, 70%, 80%, 90%, and 100%), and finally dried naturally at room temperature. After coating a layer of gold, the biofilm samples were observed under SEM.

3. Results and Discussion

3.1. Morphologies of GF and CNFs/GF. Figure 1 shows the SEM images of GF and CNFs. The diameter of graphite fiber in the GF is about 10 μm. The GF has a macroporous structure with pore size in the tens of micrometers. Detailed SEM image in Figure 1(b) shows that the surface of GF is smooth. After a CVD process, a layer of long length carbon nanofibers with diameter of about 100 nm was successfully grown onto the graphite fibers surface to form CNFs/GF composite (Figure 1(d)), which is in accordance with the micro/nano structures of carbon composite in [22]. The CNFs/GF displays a hierarchical micro-/nanostructures which would be beneficial for the attachment of bacteria to the anode and enhancement of electron transfer from inside bacteria to the anode simultaneously.

3.2. Biocatalytic Current Generation of GF and CNFs/GF Anode. The biocatalytic current generation curves of GF and CNFs/GF anodes under different concentration of acetate are shown in Figure 2. It can be observed that the CNFs/GF anode achieves the maximum current density at the second cycle, while the GF requires three cycles. This result demonstrates the CNFs modification enhances the attachment of the bacteria to the anode. After running for six cycles under low acetate concentration of 20 mM, the GF and CNFs/GF anodes

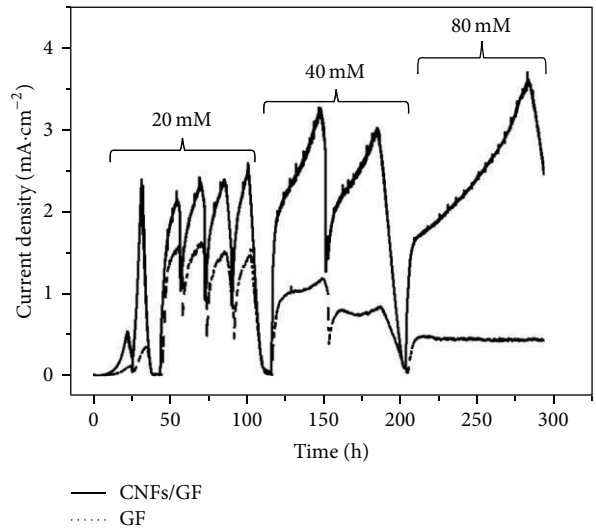

Figure 2: Biocatalytic current generation curves of GF (curves of dotted line) and CNFs/GF (curves of solid line) under different concentration of acetate measured in a half cell at 35°C. The arrows indicate the replenishment of the substrate with different concentration of acetate.

all delivered a stable maximum current density. The CNFs/GF anode generates a maximum geometric current density of about 2.42 mA cm^{-2}, which is 54% higher than that from GF of about 1.57 mA cm^{-2}. By increasing the concentration of acetate to 40 mM, the current density of GF anode shows a slight decrease to 1.17 mA cm^{-2}, while the CNFs/GF anode produces a much higher current density of 3.23 mA cm^{-2}, about 33% higher than that under 20 mM acetate. By further increasing the concentration of acetate to 80 mM, the maximum current density of the CNFs/GF anode keeps increasing to about 3.57 mA cm^{-2}, in contrast, that of the bare GF anode greatly decreases to only about 0.50 mA cm^{-2}. It could be concluded that the CNFs/GF anode shows excellent performance of tolerating high strength substrate and that excellent performance is brought by the CNFs modification. It was reported that nanocarbons modification could enhance the attachment of the biofilm and the electron transfer from inside bacteria to the surface of anode and thus increased and stabled the anodic current generation [16–18, 22]. In this paper, the CNFs modification not only increases the current generation, but also shows high performance of tolerating high strength substrate. That could also be attributed to the enhancement of electron transfer (respiration) by the CNFs modification and acceleration of the metabolism of the biofilms in the anode.

3.3. Morphology of Biofilms on GF and CNFs/GF. In order to verify the anodic performance, after current generation in media with 80 mM acetate, the GF and CNFs/GF anodes with biofilms are taken out. After fixation and drying, the biofilms in the GF and CNFs/GF are observed under the SEM. Figure 3 shows the images of biofilms grown in the GF and CNFs/GF. It can be seen from the overview images

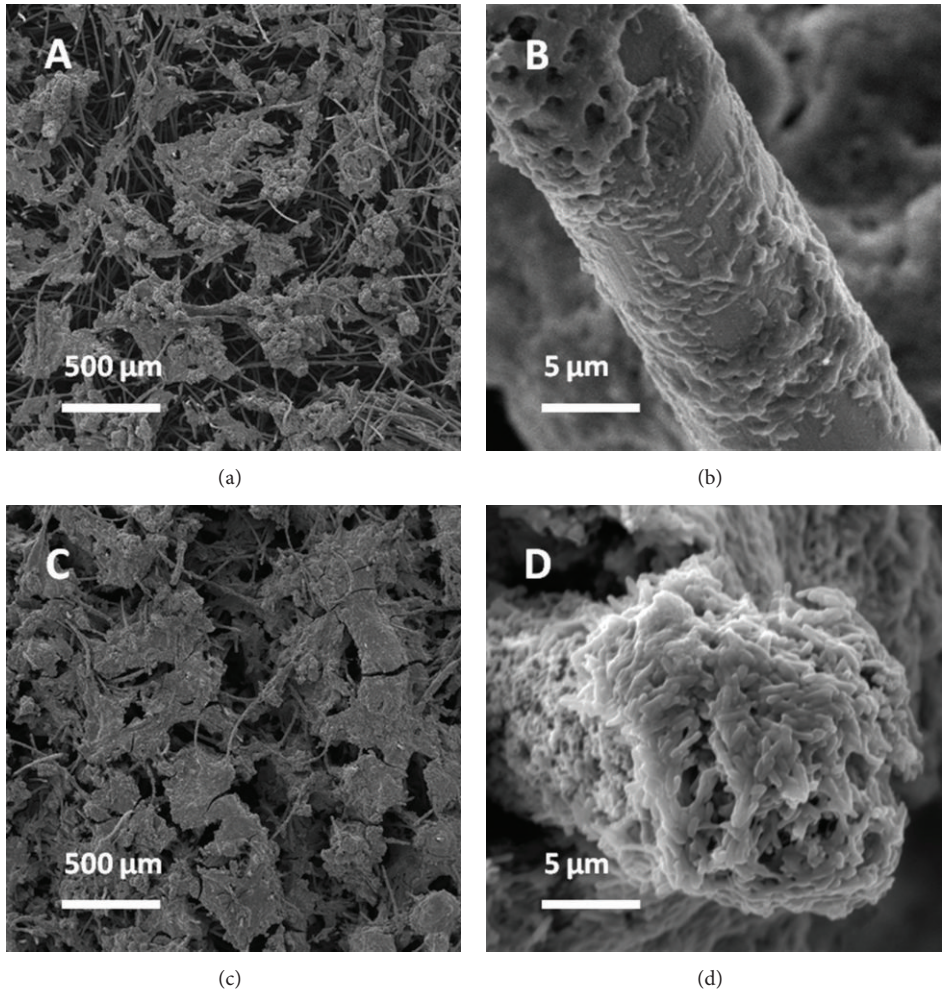

(a) (b)

(c) (d)

Figure 3: Overview and detailed SEM images of ((a) and (b)) biofilms in GF and ((c) and (d)) CNFs/GF.

(Figures 3(a) and 3(c)) that the biofilms grown in the CNFs/GF anode are denser than those in the GF anode. Detailed observation of biofilms on individual fiber (Figures 3(b) and 3(d)) reveals that the biofilms on bare graphite fibers are sparse, while those on the CNFs modified fibers are very thick and have a thickness of about 5 μm on individual graphite fiber according to the SEM image in Figure 3(d). That confirms that the current generation for the CNFs/GF is higher than that of the bare GF.

4. Conclusion

The performance of tolerating high strength substrate for the CNFs modified GF was demonstrated. The CNFs/GF not only generate enhanced current density in low strength acetate media of 20 mM comparing to the bare GF but also could generate a much higher current density of 3.57 mA cm^{-2} in high strength acetate media of 80 mM, which was 7 times higher than that generated from bare GF. The performance of tolerating high strength substrate was attributed to the nanostructured CNFs which enhanced the electron transfer from inside bacteria to anode (respiration) and accelerated the metabolism of bacteria. Anode materials tolerating high strength substrate would expand the applications of MFCs in high concentration of substrate environment, for example, high strength wastewater treatment from oil and food industry.

Conflict of Interests

The authors declare that there is no conflict of interests regarding the publication of this paper.

Acknowledgments

This research was supported by the National Natural Science Foundation of China (Grant no. 51202096) and the Science and Technology Project of Jiangxi Province (no. 20121BBE50024).

References

[1] K. Rabaey and W. Verstraete, "Microbial fuel cells: novel biotechnology for energy generation," *Trends in Biotechnology*, vol. 23, no. 6, pp. 291–298, 2005.

[2] F. Harnisch and U. Schröder, "From MFC to MXC: chemical and biological cathodes and their potential for microbial bioelectrochemical systems," *Chemical Society Reviews*, vol. 39, no. 11, pp. 4433–4448, 2010.

[3] Y. Qiao, S. J. Bao, and C. M. Li, "Electrocatalysis in microbial fuel cells-from electrode material to direct electrochemistry," *Energy & Environmental Science*, vol. 3, no. 5, pp. 544–553, 2010.

[4] K. R. Fradler, I. Michie, R. M. Dinsdale, A. J. Guwy, and G. C. Premier, "Augmenting microbial fuel cell power by coupling with supported liquid membrane permeation for zinc recovery," *Water Research*, vol. 55, pp. 115–125, 2014.

[5] B. Min and B. E. Logan, "Continuous electricity generation from domestic wastewater and organic substrates in a flat plate microbial fuel cell," *Environmental Science & Technology*, vol. 38, no. 21, pp. 5809–5814, 2004.

[6] S. Cheng, H. Liu, and B. E. Logan, "Increased power generation in a continuous flow MFC with advective flow through the porous anode and reduced electrode spacing," *Environmental Science & Technology*, vol. 40, no. 7, pp. 2426–2432, 2006.

[7] Z. He, S. D. Minteer, and L. T. Angenent, "Electricity generation from artificial wastewater using an upflow microbial fuel cell," *Environmental Science & Technology*, vol. 39, no. 14, pp. 5262–5267, 2005.

[8] B. Logan, S. Cheng, V. Watson, and G. Estadt, "Graphite fiber brush anodes for increased power production in air-cathode microbial fuel cells," *Environmental Science & Technology*, vol. 41, no. 9, pp. 3341–3346, 2007.

[9] Y. Liu, F. Harnisch, K. Fricke, U. Schröder, V. Climent, and J. M. Feliu, "The study of electrochemically active microbial biofilms on different carbon-based anode materials in microbial fuel cells," *Biosensors and Bioelectronics*, vol. 25, no. 9, pp. 2167–2171, 2010.

[10] S. L. Chen, H. Q. Hou, F. Harnisch et al., "Electrospun and solution blown three-dimensional carbon fiber nonwovens for application as electrodes in microbial fuel cells," *Energy & Environmental Science*, vol. 4, no. 4, pp. 1417–1421, 2011.

[11] S. Chen, G. He, X. Hu et al., "A three-dimensionally ordered macroporous carbon derived from a natural resource as anode for microbial bioelectrochemical systems," *ChemSusChem*, vol. 5, no. 6, pp. 1059–1063, 2012.

[12] S. Chen, G. He, Q. Liu et al., "Layered corrugated electrode macrostructures boost microbial bioelectrocatalysis," *Energy & Environmental Science*, vol. 5, no. 12, pp. 9769–9772, 2012.

[13] K. Scott, G. A. Rimbu, K. P. Katuri, K. K. Prasad, and I. M. Head, "Application of modified carbon anodes in microbial fuel cells," *Process Safety and Environmental Protection*, vol. 85, no. 5, pp. 481–488, 2007.

[14] D. Q. Jiang and B. K. Li, "Novel electrode materials to enhance the bacterial adhesion and increase the power generation in microbial fuel cells (MFCs)," *Water Science & Technology*, vol. 59, no. 3, pp. 557–563, 2009.

[15] Y. Zhao, K. Watanabe, R. Nakamura et al., "Three-dimensional conductive Nanowire networks for maximizing anode performance in microbial fuel cells," *Chemistry-A European Journal*, vol. 16, no. 17, pp. 4982–4985, 2010.

[16] H. Y. Tsai, C. C. Wu, C. Y. Lee, and E. P. Shih, "Microbial fuel cell performance of multiwall carbon nanotubes on carbon cloth as electrodes," *Journal of Power Sources*, vol. 194, no. 1, pp. 199–205, 2009.

[17] Y. Zhang, G. Mo, X. Li et al., "A graphene modified anode to improve the performance of microbial fuel cells," *Journal of Power Sources*, vol. 196, no. 13, pp. 5402–5407, 2011.

[18] N. Thepsuparungsikul, N. Phonthamachai, and H. Ng, "Multi-walled carbon nanotubes as electrode material for microbial fuel cells," *Water Science & Technology*, vol. 65, no. 7, pp. 1208–1214, 2012.

[19] X. Xie, M. Ye, L. Hu et al., "Carbon nanotube-coated macroporous sponge for microbial fuel cell electrodes," *Energy & Environmental Science*, vol. 5, no. 1, pp. 5265–5270, 2012.

[20] X. Xie, L. Hu, M. Pasta et al., "Three-dimensional carbon nanotube-textile anode for high-performance microbial fuel cells," *Nano Letters*, vol. 11, no. 1, p. 291, 2011.

[21] D. Pant, G. Van Bogaert, L. Diels, and K. Vanbroekhoven, "A review of the substrates used in microbial fuel cells (MFCs) for sustainable energy production," *Bioresource Technology*, vol. 101, no. 6, pp. 1533–1543, 2010.

[22] Y. Zhao, K. Watanabe, and K. Hashimoto, "Hierarchical micro/nano structures of carbon composites as anodes for microbial fuel cells," *Physical Chemistry Chemical Physics*, vol. 13, no. 33, pp. 15016–15021, 2011.

Hindawi Publishing Corporation
The Scientific World Journal
Volume 2014, Article ID 186016, 7 pages
http://dx.doi.org/10.1155/2014/186016

Research Article

Effective Control of Bioelectricity Generation from a Microbial Fuel Cell by Logical Combinations of pH and Temperature

Jiahuan Tang,[1,2] Ting Liu,[3] Yong Yuan,[2] and Li Zhuang[2]

[1] *Guangzhou Institute of Geochemistry, Chinese Academy of Sciences, Guangzhou 510640, China*
[2] *Guangdong Institute of Eco-Environmental and Soil Sciences, Guangzhou 510650, China*
[3] *College of Bioscience and Biotechnology, Hunan Agricultural University, Changsha 410128, China*

Correspondence should be addressed to Yong Yuan; yuanyong@soil.gd.cn

Received 27 December 2013; Accepted 27 January 2014; Published 11 March 2014

Academic Editors: B. Cao, Y.-C. Yong, and S.-G. Zhou

In this study, a microbial fuel cell (MFC) with switchable power release is designed, which can be logically controlled by combinations of the most physiologically important parameters such as "temperature" and "pH." Changes in voltage output in response to temperature and pH changes were significant in which voltage output decreased sharply when temperature was lowered from 30°C to 10°C or pH was decreased from 7.0 to 5.0. The switchability of the MFC comes from the microbial anode whose activity is affected by the combined medium temperature and pH. Changes in temperature and pH cause reversible activation-inactivation of the bioanode, thus affecting the activity of the entire MFC. With temperature and pH as input signals, an AND logic operation is constructed for the MFC whose power density is controlled. The developed system has the potential to meet the requirement of power supplies producing electrical power on-demand for self-powered biosensors or biomedical devices.

1. Introduction

Microbial fuel cells (MFCs) are energy-producing devices that can directly generate electric energy from the oxidation of various organic matters with the aid of microbes. Since MFCs are capable of generating electricity in an environmentally friendly manner, they have attracted a great deal of research attention over the past decades [1–3]. One of the potentially important applications of MFCs is powering sensors or biomedical devices. Tender et al. [4] and Zhang et al. [5] succeeded in powering temperature sensors using MFCs in natural environments. Siu et al. proposed that MFCs were capable of powering biological microelectromechanical systems (bioMEMS) [6]. Recently, major research concerns have been raised about increasing energy output of MFCs as power supplies. In the case of powering sensors or biomedical devices, switchable or tunable electrical power release would be a great advantage for their application, given their adaptive behavior and power production on demand.

Enzyme-based biofuel cells with self-regulating power release have been intensively studied using switchable biocatalytic electrodes controlled by physical or biochemical signals [7]. In such devices, the biocatalytic electrodes were usually modified with signal-responsive materials that were sensitive to triggering actions to make the electrodes electrochemically active or inactive. For instance, Katz and Willner reported that the power production of a biofuel cell was switched ON and OFF by integrating a biocatalyst with a copper polyacrylic acid matrix of controllable conductivity properties [8]. Amir et al. regulated the power release of a biofuel cell using a pH-sensitive redox polymer [9]. The polymer allowed switching between redox active and inactive states by pH-induced swelling and shrinking processes, respectively. Other biofuel cell systems with controllable power release were also realized by being integrated with enzyme- or immune-based systems, enabling the switchable and tunable functions of the biofuel cells [10, 11]. Although promising progress has

been achieved for enzyme-based biofuel cells, their long-term stability and scalability need to be improved, and the complicated manufacturing process of enzyme electrodes severely limit their practical application. MFCs are promising alternatives to enzyme-biofuel cells due to the use of whole bacterial cells which are stable for a long time, scalable, self-attachable on the electrodes as catalysts. Microbial electrodes or assembled MFCs are capable of switching the electron transfer process or self-regulating power release as well. Yuan et al. developed a switchable microbial electrode with electrical signal output by controlling the presence of acetate and oxygen [12]. For the first time, Li et al. integrated an MFC with an AND logic gate to self-regulate power release [13]. However, a *Pseudomonas aeruginosa* lasI/rhlI double mutant was employed as the biocatalyst and two quorum-sensing signaling molecules were used as input signals in their study, involving rather complex genetic operations and slow switching speed.

In this study, we demonstrated a simple method to regulate the electricity generation from an MFC by controlling the most important physiological parameters (pH and temperature), where a sharp thermal and pH response of the microbial anode of the MFC has been logically designed. The bioanode could switch between electrochemically active and inactive states in response to the operation environment, resulting in the "smart" bioelectricity generation from the assembled MFC. The present paper extends the fundamental research activity in bioelectricity generation of MFCs with switchable or tunable functions.

2. Materials and Methods

2.1. MFC Construction and Startup. MFCs with an inner volume of 12 mL were constructed as previously reported with minor modification on the anodes [14]. A cylindrical MFC chamber with a length of 1.7 cm and a diameter of 3.0 cm in the cathode side and 1.8 cm in the anode side was made of plexiglass, resulting in a surface area of 7.0 cm^2 for the cathode and 2.5 cm^2 for the anode. The cathode was prepared with a 30% wet-proof carbon cloth (type B, E-TEK, USA) with four layers of polytetrafluoroethylene (PTFE) (PTFE30, DuPont, USA) coating. Pt/C (20% Pt, E-TEK, USA) was used as the cathode catalyst with a Pt loading of 0.5 mg cm^{-2}. Carbon cloth (type A, E-TEK, USA) was used as the anode electrode. Reactors were inoculated with 2 mL activated sludge (Liede Wastewater Treatment Plant, Guangzhou, China) in 10 mL sodium acetate (1000 mg L^{-1}) culture medium. Besides sodium acetate, the culture medium contained KH_2PO_4 (13.6 g L^{-1}), NaOH (2.32 g L^{-1}), NH_4Cl (0.31 g L^{-1}), NaCl (1.0 g L^{-1}), a vitamin stock solution (12.5 mL L^{-1}), and a mineral stock solution (12.5 mL L^{-1}). Power density curves were obtained by changing the circuit resistor from 50 Ω to 5000 Ω. All tests were conducted in duplicate, and mean values were presented.

2.2. UV-Vis Spectroscopy. Prior to spectroscopy measurements, pure *Geobacter* strain was cultured and harvested. *Geobacter sulfurreducens* strain PCA (ATCC 51573) was cultured as previously reported at 30°C using a vitamin-free anaerobic medium [15]. Acetate was provided as an electron donor at 30 mM and 40 mM fumarate as electron acceptor. UV-Vis spectra of intact cells of PCA were recorded in diffused transmission mode with bacterial cells suspended in a bicarbonate buffer [16]. The cell suspension was injected into a cuvette, and it was mounted in front of an integrating sphere to measure the diffuse transmission light. Full reduction of the cells was achieved by adding sodium dithionite (25 mM) to the cell suspension and oxidation of the whole cell was obtained by purging oxygen into the cell suspension for 10 min before measuring.

2.3. Electrochemical Measurements. Electrochemical characterization of the mixed-culture anode was carried out with cyclic voltammetry (CV) using a CHI660D workstation (Shanghai CH Instrument Company, China) with a three-electrode system, where the biofilm-attached anode served as the working electrode, saturated calomel electrode (SCE) as the reference electrode, and the cathode as the counter electrode. A phosphate buffer (0.05 M; no culture medium) was used as the electrolyte under no-turnover conditions. CV under turnover conditions was measured when the voltage output of the MFC at 1000 Ω was maximized and stabilized.

2.4. Scanning Electron Microscopy. Prior to scanning electron microscopy (SEM) measurements, the mixed-culture biofilm-attached electrode was first fixed in a 2.5% glutaraldehyde solution for 1 h, then in a series of ethanol dehydration solution (i.e., 25%, 50%, 75%, and 100% v/v EtOH; 0.5 h each treatment), and after that, dried at the CO_2-critical point for 3 h. The resultant specimen was coated with gold using a coating device (Emitech K550X; UK) and observed under a SEM (JEOL, JSM-6330F; Japan) at 20 kV.

3. Results and Discussion

3.1. Responses of Voltage Output to pH and Temperature Variations. An MFC can be a very robust device when it is subjected to short-term changes of operating parameters such as temperature and pH. To probe the response of MFC performance to these parameters, an MFC inoculated with a mixed consortium was constructed. The structure and morphology of the self-assembled mixed-culture bioanode were characterized with SEM (Figure 1(a)). Nearly the entire surface of the solid carbon cloth electrode was covered with rod-shaped bacterial cells. Changes in voltage output in response to temperature and pH changes were shown in Figure 1(b). Voltage output decreased sharply when temperature was lowered from 30°C to 10°C or pH was decreased from 7.0 to 5.0. Previous studies reported similar changes of the voltage output in response to temperature and pH changes [14, 17, 18]. Gonzalez del Campo et al. pointed out that temperature could affect MFC voltage output by influencing microbial metabolism, membrane permeability, and ohmic resistance of the electrolyte [17]. In the case of effects of medium pH on the power generation of an MFC, it was found that acidification of the anode affected

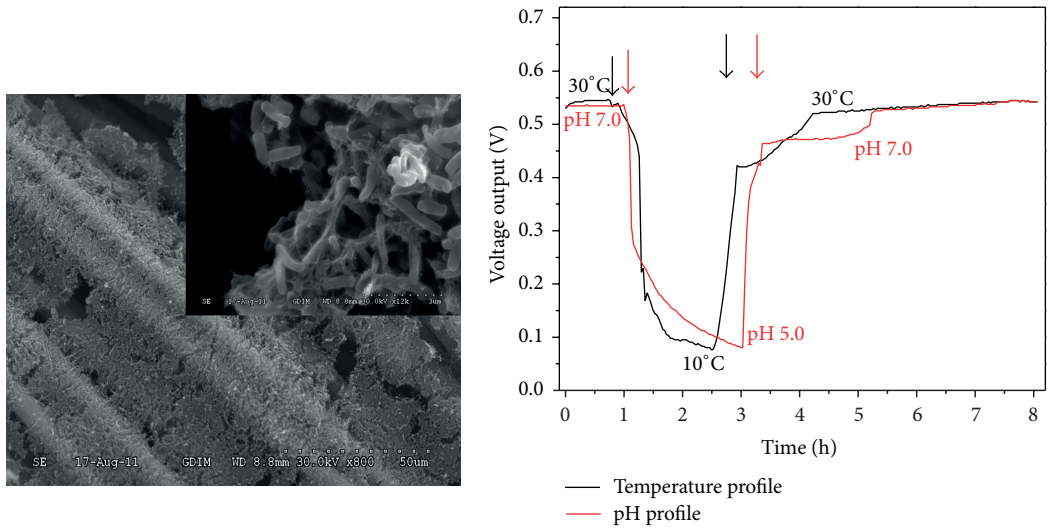

(a) (b)

Figure 1: (a) SEM images of the anode biofilm (inset: high resolution image); (b) voltage output versus time curves with the variation of temperature and pH.

electricity generation by inhibiting the microbial activity [18]. In addition, alkaline medium increased biosynthesis of riboflavin from *Shewanella*, which could also enhance bioanode performance [19]. It was important to note here that a rather fast switching speed of voltage output (~0.5 h) was achieved by controlling the pH and temperature, benefiting the next generation of bacteria-based computing circuits or sensors [20].

3.2. CVs of Mixed Biofilm as Affected by pH and Temperature. In addition to the above mentioned reasons, the electrochemical activity of the redox species in the microbial electron transfer chains is also greatly influenced by temperature and pH, further affecting the whole extracellular electron transfer process. Numerous studies claimed that c-type cytochromes (c Cyts) located on the outer membrane of the microbes were the key redox species participating in the extracellular electron transfer [21, 22]. Figure 2 showed the electrochemical properties of the living c Cyts in the mixed-culture biofilm under different temperature and pH conditions, which have been rarely reported in previous studies. As shown in Figure 2(a), similar to the CV features of a pure *Geobacter* strain, there were two pairs of distinct redox peaks on the CV curve for the biofilm in the nonturnover state, with formal potential at −0.46 V and −0.39 V (versus SCE), respectively, at 30°C and pH 7.0. These two couples of redox peaks might belong to two different outer membrane c-type cytochromes of OmcB and OmcZ, respectively [21]. However, the redox peaks positively shifted when the temperature went down. The formal potentials were −0.44 V and −0.37 V (versus SCE) at 20°C and −0.42 V and −0.35 V, respectively (versus SCE), at 10°C. Moreover, the peak separations increased and the peak currents decreased as the temperature decreased, implying decreases in the electrochemical activities of c Cyts. As a result, the electrochemical catalytical activity of the anode biofilm dropped accordingly (Figure 2(b)). It is worth mentioning that temperature caused more significant change in the oxidation peak potential than in the reduction peak potential, demonstrating greater influence of temperature on the oxidation process of the c Cyts. Similar changes in the redox potential of c Cyts were also observed when medium pH was changed. As shown in Figure 2(c), when pH decreased, the redox potentials positively shifted by ca. 40 mV, suggesting that the redox processes of these redox active species were pH-dependent. The peak separations increased and the peak currents decreased as pH decreased, indicating decrease of the electrochemical activity of the c Cyts and the electrochemical catalytical activity of the anode biofilm (Figure 2(d)).

3.3. UV-Vis Spectroscopy Measurements of In Vivo c Cyts as Affected by pH and Temperature. The effects of temperature and pH on *in vivo* c Cyts were further evidenced by investigating the whole cell using a UV-Vis spectroscopy. Bacteria with outer membrane bonded c-type cytochromes showed distinguished UV-Vis spectra with different redox states [23]. The oxidized c Cyts have a Soret band at 409 nm and a broad band at 528 nm (Figure 3). After c Cyts were reduced by sodium dithionite, reduced c Cyts show the Soret, β, and α bands at 419, 520, and 550 nm, respectively. A similar shift in the Soret absorption band was reported for purified c Cyts [24]. These spectral features are typical of hexacoordinated low-spin hemes and are obviously affected by environmental stimuli. An apparent red shifting of the Soret band and the absence of the peaks at 522 and 552 nm was observed for the oxidized living c Cyts while the temperature went down (Figure 3(a)). However, no shifting but a decrease in intensity of the absorbance peaks for the reduced c Cyts was observed when temperature decreased (Figure 3(b)). The spectral features also changed when the medium pH was

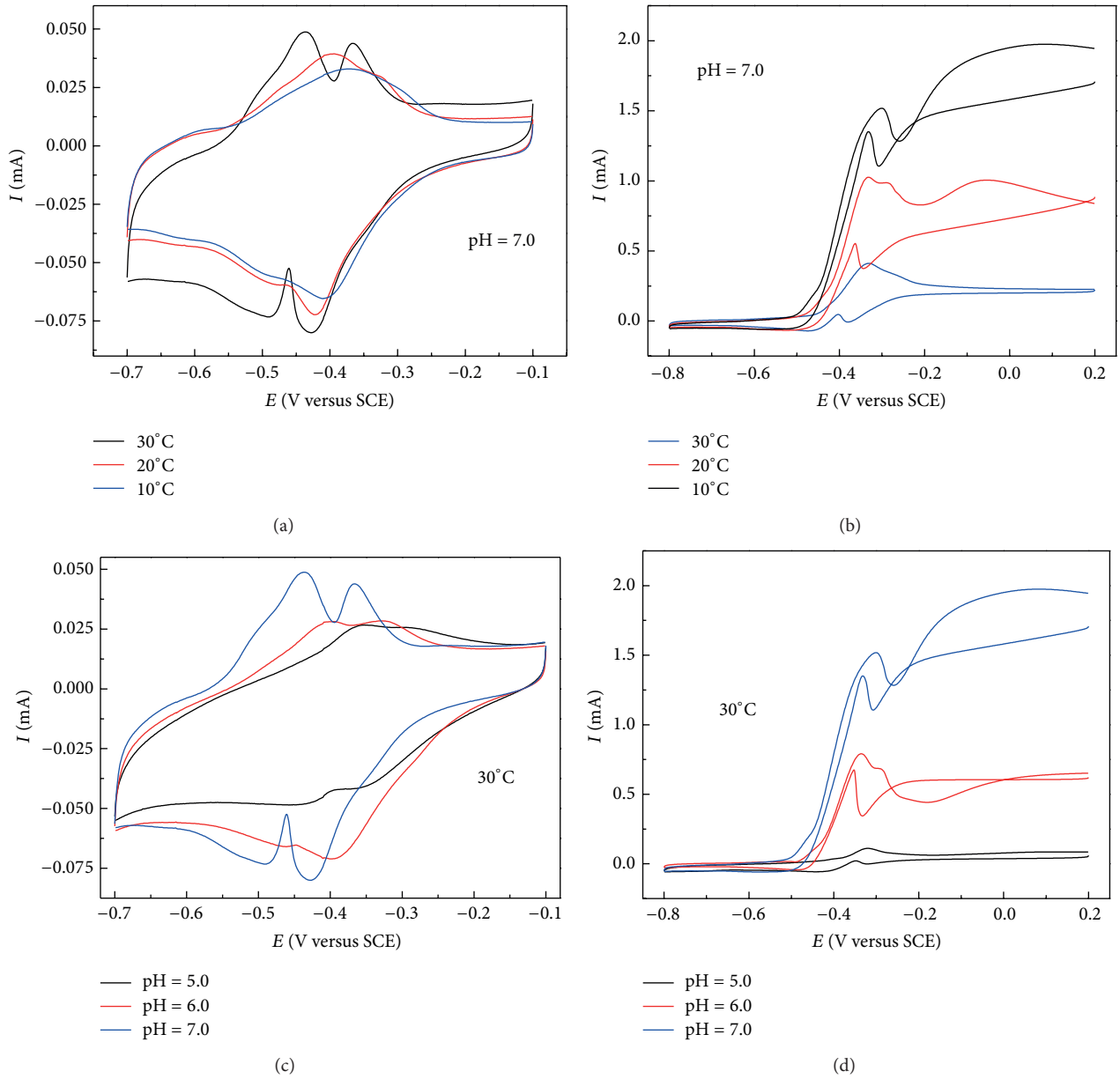

Figure 2: CVs of the anode biofilm under various temperatures by fixing pH condition under no-turnover state (a) and turnover state (b); CVs of the anode biofilm under various pH levels by fixing temperature condition under no-turnover state (c) and turnover state (d).

adjusted. The Soret band of the oxidized c Cyts shifted to 393 nm with a lower intensity (Figure 3(c)). The position and the intensity of the Soret absorption band were related to the conformational state of the heme group in c Cyts and the weakening of the heme crevice [25]. The appearance of the Soret band at 393 nm demonstrated the formation of a fully high-spin heme complex. No obvious shifts of the Soret band but a weakening in absorption intensity for all the bands were observed when the medium became acid. On the other hand, the blue shifts of the Soret absorption band of both the oxidized and reduced cytochromes were also observed under an alkaline condition. The results suggested that environmental stimuli apparently had an effect on the conformational state of the heme groups in c Cyts and in turn the electrochemical properties of the c Cyts, which provided an opportunity for tuning the extracellular electron transfer of the whole cell.

3.4. The Combined Effect of pH and Temperature on the Bioelectricity Generation from the MFC. To take advantage of the switchable electrochemical activity of the whole cell by the combined effect of pH and temperature, we constructed a "smart" MFC. In such a device, bioelectricity generation from the MFC could be controlled by temperature and pH. As shown in Figure 4(a), the highest power output was achieved

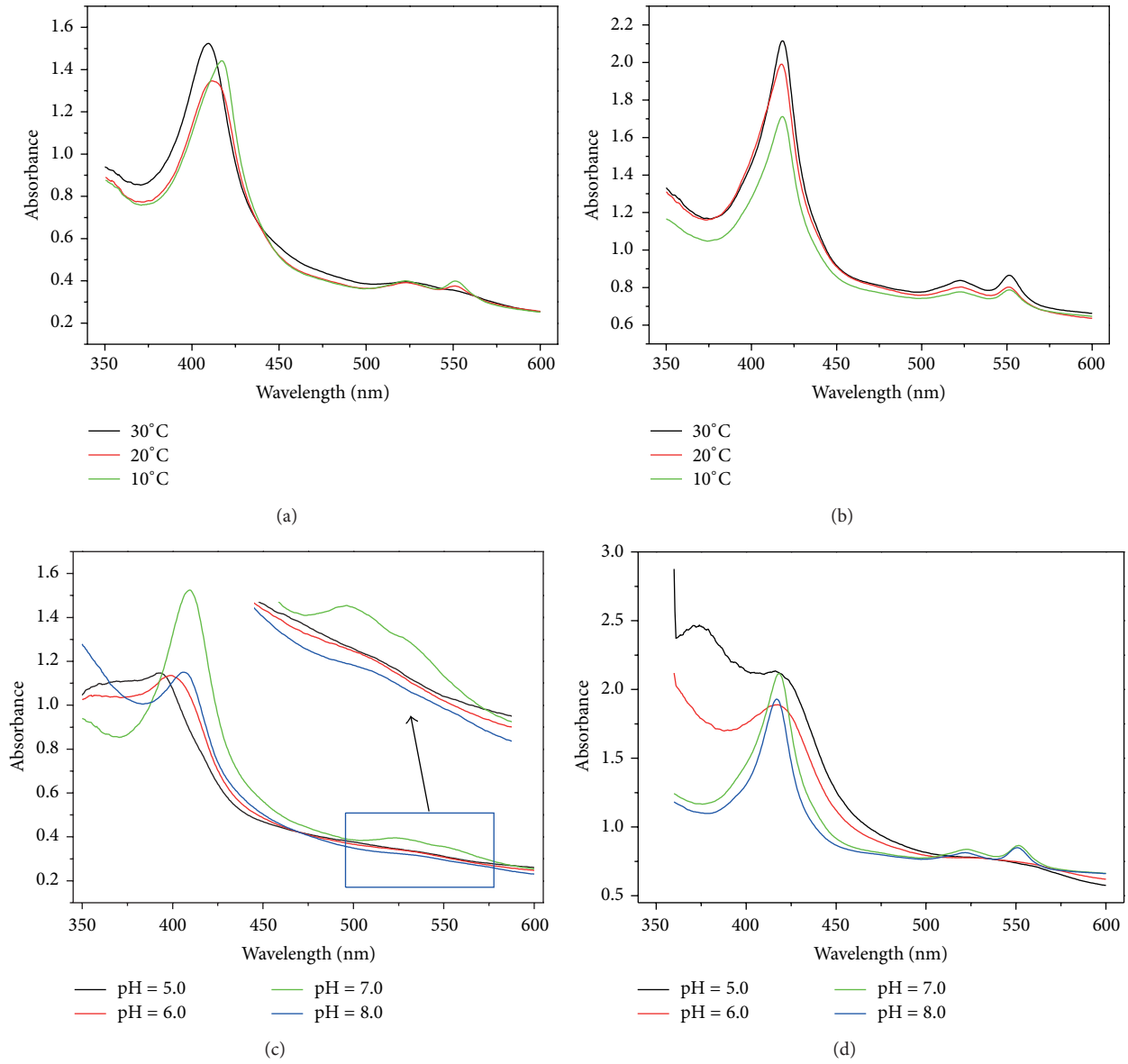

Figure 3: Electronic absorption spectra of *G. sulfurreducens* under various temperatures at pH 7.0 in oxidized state (a) and reduced state (b); electronic absorption spectra under various pH values at 30°C in oxidized state (c) and reduced state (d).

under the conditions of 30°C and pH 7.0, while a very low power output was generated under conditions of lower temperature or pH. Based on this, a Boolean AND logic operation was developed for power generation. In this logic operation, pH and temperature were designed as input signals (A and B signals, resp.), and the maximum power output was taken as output signal (Figure 4(b)). Conditions of pH 7.0 and 30°C were considered as logic input 1, and conditions of pH 5.0 and 10°C were considered as logic input 0. The input signals were applied in all four combinations (0,0; 0,1; 1,0; and 1,1) as shown in Figures 4(c) and 4(d). The highest power density for all MFC tests was obtained for input 1,1 (1600 mW m^{-2}). In contrast, the power output was at a low level when input was 0,0, 0,1, or 1,0. The threshold of the Boolean logic AND gate for the MFC was 180 mW m^{-2}.

4. Conclusion

In this study, the "smart" MFC presented above demonstrated for the first time the possibility to control the power output of an MFC by adjusting environmental conditions according to Boolean logic operations. This provides opportunities for future sensor and bioelectronic devices logically controlled by physiological parameters. "Smart" MFCs can be a promising alternative to enzyme-based biofuel cell systems due to their long-term stability, scalability, and easy handling properties.

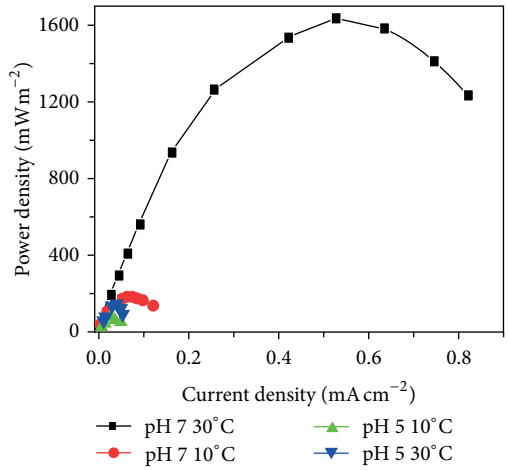

(a)

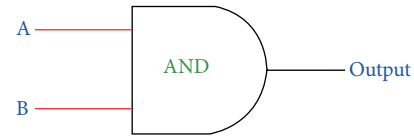

(b)

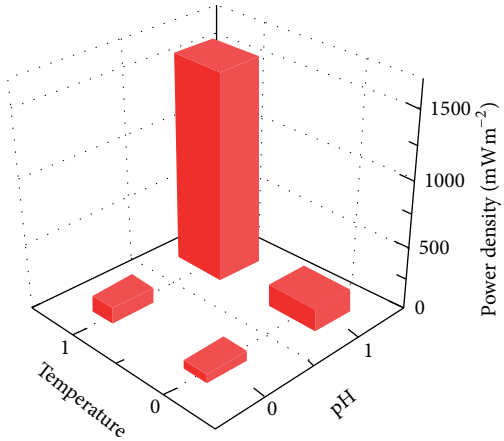

(c)

Input A (pH)	Input B (temperature)	Output (power density)
0 (5)	0 (10°C)	0
0 (5)	1 (30°C)	0
1 (7)	0 (10°C)	0
1 (7)	1 (30°C)	1

(d)

Figure 4: Polarization curves of the MFC under various conditions (a); equivalent circuit of an AND logic gate based on the MFC (b); the maximum power output of the MFC for four different input combinations (c); and truth table for the logically controlled power output (d).

An MFC with switchable and tunable power release might broaden its application in sensor, medical, and environmental fields.

Conflict of Interests

The authors declared that they have no conflict of interests regarding this work.

Acknowledgments

This study was supported jointly by the National Natural Science Foundation of China (no. 21277035), the Foundation for Excellent Young Scientist in Guangdong Academy of Sciences (no. rcjj201101), the Agricultural Science and Technology Achievements Transformation Fund Programs of Guangdong Province, China (2012NL040), and Guangzhou Science and Technology Development Foundation, China (2011J2200039).

References

[1] B. E. Logan, B. Hamelers, R. Rozendal et al., "Microbial fuel cells: methodology and technology," *Environmental Science and Technology*, vol. 40, no. 17, pp. 5181–5192, 2006.

[2] K. Rabaey and W. Verstraete, "Microbial fuel cells: novel biotechnology for energy generation," *Trends in Biotechnology*, vol. 23, no. 6, pp. 291–298, 2005.

[3] V. B. Wang, S. L. Chua, B. Cao et al., "Engineering PQS biosynthesis pathway for enhancement of bioelectricity production in *Pseudomonas aeruginosa* microbial fuel cells," *PLoS ONE*, vol. 8, no. 5, Article ID e63129, 2013.

[4] L. M. Tender, S. A. Gray, E. Groveman et al., "The first demonstration of a microbial fuel cell as a viable power supply: powering a meteorological buoy," *Journal of Power Sources*, vol. 179, no. 2, pp. 571–575, 2008.

[5] F. Zhang, L. Tian, and Z. He, "Powering a wireless temperature sensor using sediment microbial fuel cells with vertical arrangement of electrodes," *Journal of Power Sources*, vol. 196, no. 22, pp. 9568–9573, 2011.

[6] C.-P. Siu and M. Chiao, "A microfabricated PDMS microbial fuel cell," *Journal of Microelectromechanical Systems*, vol. 17, no. 6, pp. 1329–1341, 2008.

[7] E. Katz and M. Pita, "Biofuel cells controlled by logically processed biochemical signals: towards physiologically regulated bioelectronic devices," *Chemistry*, vol. 15, no. 46, pp. 12554–12564, 2009.

[8] E. Katz and I. Willner, "A biofuel cell with electrochemically switchable and tunable power output," *Journal of the American Chemical Society*, vol. 125, no. 22, pp. 6803–6813, 2003.

[9] L. Amir, T. K. Tam, M. Pita, M. M. Meijler, L. Alfonta, and E. Katz, "Biofuel cell controlled by enzyme logic systems," *Journal of the American Chemical Society*, vol. 131, no. 2, pp. 826–832, 2009.

[10] K. T. Tsz, G. Strack, M. Pita, and E. Katz, "Biofuel cell logically controlled by antigen-antibody recognition: towards immune-regulated bioelectronic devices," *Journal of the American Chemical Society*, vol. 131, no. 33, pp. 11670–11671, 2009.

[11] M. Zhou, Y. Du, C. Chen et al., "Aptamer-controlled biofuel cells in logic systems and used as self-powered and intelligent logic aptasensors," *Journal of the American Chemical Society*, vol. 132, no. 7, pp. 2172–2174, 2010.

[12] Y. Yuan, S. Zhou, J. Zhang, L. Zhuang, G. Yang, and S. Kim, "Multiple logic gates based on reversible electron transfer of self-organized bacterial biofilm," *Electrochemistry Communications*, vol. 18, no. 1, pp. 62–65, 2012.

[13] Z. Li, M. A. Rosenbaum, A. Venkataraman, T. K. Tam, E. Katz, and L. T. Angenent, "Bacteria-based and logic gate: a decision-making and self-powered biosensor," *Chemical Communications*, vol. 47, no. 11, pp. 3060–3062, 2011.

[14] Y. Yuan, S. Zhou, N. Xu, and L. Zhuang, "Electrochemical characterization of anodic biofilms enriched with glucose and acetate in single-chamber microbial fuel cells," *Colloids and Surfaces B*, vol. 82, no. 2, pp. 641–646, 2011.

[15] Y. Liu, H. Kim, R. Franklin, and D. R. Bond, "Gold line array electrodes increase substrate affinity and current density ofelectricity-producing G. sulfurreducens biofilms," *Energy and Environmental Science*, vol. 3, no. 11, pp. 1782–1788, 2010.

[16] A. Esteve-Núñez, J. Sosnik, P. Visconti, and D. R. Lovley, "Fluorescent properties of c-type cytochromes reveal their potential role as an extracytoplasmic electron sink in Geobacter sulfurreducens," *Environmental Microbiology*, vol. 10, no. 2, pp. 497–505, 2008.

[17] A. Gonzalez del Campo, J. Lobato, P. Cañizares, M. A. Rodrigo, and F. J. Fernandez Morales, "Short-term effects of temperature and COD in a microbial fuel cell," *Applied Energy*, vol. 101, pp. 213–217, 2013.

[18] S. Jung, M. M. Mench, and J. M. Regan, "Impedance characteristics and polarization behavior of a microbial fuel cell in response to short-term changes in medium pH," *Environmental Science and Technology*, vol. 45, no. 20, pp. 9069–9074, 2011.

[19] Y. Yong, Z. Cai, Y. Yu et al., "Increase of riboflavin biosynthesis underlies enhancement of extracellular electron transfer of Shewanella in alkaline microbial fuel cells," *Bioresource Technology*, vol. 130, pp. 763–768, 2013.

[20] M. A. Teravest, Z. Li, and L. T. Angenent, "Bacteria-based biocomputing with cellular computing circuits to sense, decide, signal, and act," *Energy and Environmental Science*, vol. 4, no. 12, pp. 4907–4916, 2011.

[21] K. Fricke, F. Harnisch, and U. Schröder, "On the use of cyclic voltammetry for the study of anodic electron transfer in microbial fuel cells," *Energy and Environmental Science*, vol. 1, no. 1, pp. 144–147, 2008.

[22] Y. Liu, F. Harnisch, K. Fricke, R. Sietmann, and U. Schröder, "Improvement of the anodic bioelectrocatalytic activity of mixed culture biofilms by a simple consecutive electrochemical selection procedure," *Biosensors and Bioelectronics*, vol. 24, no. 4, pp. 1006–1011, 2008.

[23] B. Cao, B. Ahmed, D. W. Kennedy et al., "Contribution of extracellular polymeric substances from Shewanella sp. HRCR-1 biofilms to U(VI) immobilization," *Environmental Science and Technology*, vol. 45, no. 13, pp. 5483–5490, 2011.

[24] R. Nakamura, K. Ishii, and K. Hashimoto, "Electronic absorption spectra and redox properties of C type cytochromes in living microbes," *Angewandte Chemie*, vol. 48, no. 9, pp. 1606–1608, 2009.

[25] M. Collinson and E. F. Bowden, "UV-visible spectroscopy of adsorbed cytochrome c on tin oxide electrodes," *Analytical Chemistry*, vol. 64, no. 13, pp. 1470–1476, 1992.

Hindawi Publishing Corporation
The Scientific World Journal
Volume 2014, Article ID 791672, 6 pages
http://dx.doi.org/10.1155/2014/791672

Research Article

Hydrothermal Synthesis of Nanostructured Manganese Oxide as Cathodic Catalyst in a Microbial Fuel Cell Fed with Leachate

Yuan Haoran,[1,2] Deng Lifang,[1,2] Lu Tao,[1,2] and Chen Yong[3]

[1] *Guangzhou Institute of Energy Conversion, Chinese Academy of Sciences, Guangzhou 510640, China*
[2] *Key Laboratory of Renewable Energy and Gas Hydrate, Chinese Academy of Sciences, Guangzhou 510640, China*
[3] *Guangzhou Division Academy, Chinese Academy of Sciences, Guangzhou 510070, China*

Correspondence should be addressed to Deng Lifang; denglf@ms.giec.ac.cn

Received 14 November 2013; Accepted 27 January 2014; Published 27 February 2014

Academic Editors: B. Cao, Y.-C. Yong, S.-G. Zhou, and L. Zhuang

Much effort has been devoted to the synthesis of novel nanostructured MnO_2 materials because of their unique properties and potential applications as cathode catalyst in Microbial fuel cell. Hybrid MnO_2 nanostructures were fabricated by a simple hydrothermal method in this study. Their crystal structures, morphology, and electrochemical characters were carried out by FESEM, N_2-adsorption-desorption, and CV, indicating that the hydrothermally synthesized MnO_2 (HSM) was structured by nanorods of high aspect ratio and multivalve nanoflowers and more positive than the naturally synthesized MnO_2(NSM), accompanied by a noticeable increase in oxygen reduction peak current. When the HSM was employed as the cathode catalyst in air-cathode MFC which fed with leachate, a maximum power density of 119.07 mW/m^2 was delivered, 64.68% higher than that with the NSM as cathode catalyst. Furthermore, the HSM via a 4-e pathway, but the NSM via a 2-e pathway in alkaline solution, and as 4-e pathway is a more efficient oxygen reduction reaction, the HSM was more positive than NSM. Our study provides useful information on facile preparation of cost-effective cathodic catalyst in air-cathode MFC for wastewater treatment.

1. Introduction

Microbial fuel cell (MFC) is a promising biotechnology that utilizes microorganisms as catalysts to decompose organic or inorganic matter and simultaneously harvest electricity, which present a new approach for generating electricity from waste and biomass [1–4]. Air breathing microbial fuel cells, typically characterized by using natural convection air-flow to their cathodes, are attractive for wastewater treatment applications due to their simple single-chamber construction and their unique ability to remove organic matter and generate bioelectricity. In such oxygen cathode system, the function of MFC would be significantly affected by the cathode performance due to the poor kinetics of oxygen reduction reaction (ORR).

To improve ORR and simultaneously maximize the power density, various kinds of electrocatalysts such as Pt [5], lead dioxide [6], iron (III) phthalocyanine(FePc) and cobalt tetramethoxyphenyl porphyrin(COTMPP) [7–10], Prussian blue/polyaniline [11], iron related ethylenediaminetetraacetic acid [12], Co/Fe/N/CNT [13], and Co-naphthalocyanine [14] have been evaluated for their ORR activity in MFC cathodes and the MFCs all exhibited good performances. However, the high cost of platinum, the toxicity of lead dioxide, long-term instability of the transition metal macrocycles, and phthalocyanines make these alternatives impractical.

In the past decade, manganese dioxide has been studied as one of the most promising cathode catalyst for alkaline fuel cell and metal-air batteries application [15], and several research groups have previously shown that nonprecious manganese dioxide electrocatalysts were highly efficient for catalyzing ORR and lowering overall cost at the same time [16–18]. Recent studies had paid their attention towards carbon nanotubes (CNTs) coated with manganese dioxide and MnO_2 nanoparticles [19–21]. However, very limited efforts have been made to evaluate the activities of nanostructured manganese oxides. Roche et al. [22] found that the power density of the MFC with carbon-supported MnO_2 nanoparticles can reach 161 mW/m^2 compared to 19 mW/m^2 for a benchmark Pt/C at room temperature, and when

using nanostructured MnO_x as cathode catalyst the MFC can achieved a peak power density of 772.8 mW/m^3 [23]. Thus, it is of significant to develop manganese oxides with controllable morphology and nanostructures by using facile methods for enhancing oxygen reduction and lowering the cost of single-chamber MFC for wastewater treatment. In this study, nanostructure manganese oxide prepared by hydrothermal synthesis method is applied on MFC cathode, which shows comparable catalytic capability to naturally synthesized manganese oxide, and it could further facilitate the scaling up of MFC.

2. Materials and Methods

2.1. Catalysts Preparation. The hydrothermally synthesized nanostructure MnO_2 (HSM) was synthesized as described elsewhere [24]. Briefly, 0.2 g $MnSO_4{\cdot}H_2O$ and 0.5 g $KMnO_4$ were dissolved in 100 mL distilled water; then well-mixed aqueous solution of $KMnO_4$ and hydrated $MnSO_4$ were transferred to a Teflon-lined pressure vessel (QiangQiang Instrument, Shanghai.) and loaded into an oven preheated to 140°C; the dwell time for the reaction chose 8 h when the nanostructure MnO_2 was prepared. After the reaction was finished, the pressure vessel cooled to room temperature naturally. The precipitation formed was filtered and washed with distilled water until the pH of the wash water was 7 and finally dried at 100°C in air. The same amounts of starting materials were left in a beaker overnight for the formation of MnO_2 precipitate in order to see the structural evolution of nanostructured MnO_2 from room temperature to the hydrothermal treatment. After the reaction was finished, all operations were the same as the synthesis of nanostructure MnO_2.

2.2. Characterization of MnO_2

2.2.1. FESEM. The morphology of MnO_2 was characterized with field emission scanning electronic microscopy (FESEM) (HITACHI, S-4800). The specific surface areas of MnO_2 were measured by the Brunauer-Emmett-Teller (BET) method, in which N_2 adsorption at 77 K was applied and Carlo Erba Sorptometer was used.

2.2.2. CV. Cyclic voltammetric (CV) measurements were performed with an Autolab potentiostat (model PGSTAT 30) with a three-electrode system (Ecochemie, Netherlands). The glass carbon electrode (GCE, with a diameter of 3.0 mm) coated by catalyst severs as the working electrode a Pt wire and Ag/AgCl (sat. KCl, 222 mV versus SHE) were used as the counter and reference electrodes, respectively. CV measurements were performed from –0.6 V to 0.2 V at a scan rate of 100 mV·S^{-1} in a 0.l M KOH electrolyte. The electrolyte solution is bubbled with O_2 or N_2 to establish aerobic or anaerobic environment, respectively, for 30 min prior to each scan series, and 3 min between every two scans.

2.3. MFC Configuration and Operation. All MFCs were operated at 30 ± 1°C in a temperature-controlled incubator (HPG-280H, China). The air-cathode MFC consisted of a plastic (Plexiglas) cuboid chamber ($2 \times 5 \times 5$ cm^3) [25] and with a membrane electrode assembly on one side. Carbon felt (8×8 cm^2, Panex 33160K, Zoltex) was used as the anode. Carbon cloth and cation-exchange membrane was hot-pressed together to be cathode. Titanium wire was inserted inside the carbon felt and carbon cloth to connect the circuit. Active area of the cathode was 25 cm^2. For all tests, a 1000 Ω external resistance was fixed except as noted. And the anode chamber of the MFC was filled with 40 mL of leachate (collected during the biodrying pretreatment of MSW from Boluo waste treatment).

2.4. Data Acquisition. The cell voltage outputs were measured by a precision multimeter (Victory 9807A, China) and a 16-channel voltage collection instrument (AD8223, China) which continuously monitored the voltages and transferred data to the computer at an interval of 2 min. To obtain a polarization curve, the external resistor varied from 50 Ω to 10000 Ω when the voltage output approached steady state. The corresponding voltages at different external resistances were recorded and the power output (W), power density (W·m^{-2}), and current output density (A·m^{-2}) were calculated according to $P = U^2/R$, $P = IU/A$, $I = U/RA$, where U(V) is the measured voltage, I(A) is the current, R(Ω) is the external resistance, and A(cm^2) is the active surface area of the cathode, and individual electrode potentials were measured versus saturated calomel electrode (SCE). The external resistance was fixed at 1000 Ω throughout all the experiments except as noted.

3. Results and Discussion

3.1. Synthesis and Characterization of the Catalysts. The nanostructured MnO_2 is synthesized by hydrothermal method and MnO_2 (NSM) is precipitated at room temperature naturally. SEM images of the obtained MnO_2 are displayed in Figure 1. As can be seen from the pictures, the flowerlike whiskers of MnO_2 were formed as the material prepared at room temperature by natural synthesis, and when hydrothermally treated for 8 h, there has been an increase in the size of the individual whiskers which replicates the formation of nanostructured surface with a distinct platelike morphology, and the nanoarchitecture with few rods evolving in addition to nanostructured platelike morphology was observed, the same as Subramanian found [24]. Moreover, the BET surface areas of hydrothermal and NSM were determined to be 24.91 and 111.89 m^2/g, respectively (Table 1). For the HSM, the nanostructure increases the BET surface area and is easier for the organic substrates to be adsorbed on the cathodes, and the high BET surface areas of MnO_2 catalysts could enhance the oxygen absorption and electron acceptance on catalysts surface. Oxygen vacancies created to fulfill an overall charger balance can migrate onto the surface of MnO_2 nanorod and play important roles in catalysis [18]. With the nanorod surface properties and the existence of oxygen vacancies, the MnO_2 should substantially increase the oxygen reaction rate and electron acceptance capability. On the other hand, the specific nanorod and platelike structure of the MnO_2 catalysts facilitated oxygen adhesion.

Table 1: Performance of MFCs based on different cathodic catalysts.

Catalyst	OCV (V)	Internal resistance (Ω)	Maximum power density (mW/m^2)	Maximum current density (A/m^2)	BET (m^2/g)
Without catalyst	0.33	250	32.11	0.22	—
Naturally synthesized MnO_2	0.47	200	42.05	0.29	24.91
Hydrothermally synthesized MnO_2	0.50	150	119.07	0.49	111.89

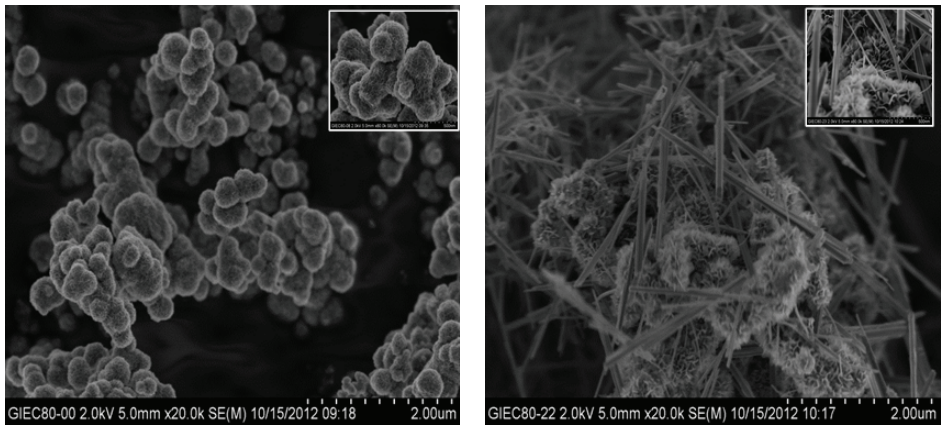

(a) (b)

Figure 1: SEM images of MnO_2 prepared by different methods: (a) natural process; (b) hydrothermal process. The inset images are the higher magnifications.

3.2. Electrochemical Characterization of the Catalysts. Cyclic voltammograms recorded at scan rate of 100 mV/s for naturally and hydrothermally synthesized MnO_2 in a 0.1 M KOH electrolyte under aerobic (bubbled with O_2) and anaerobic (bubbled with N_2) environment are shown in Figure 2. It can be seen from the figures that the MnO_2 possesses a reduction peak (−0.5 to −0.3 V) in aerobic environment but no peak in anaerobic environment (Figure 2), indicating the peak attribution to the catalyzed ORR process.

Comparing with the naturally synthesized MnO_2, the peak potential of HSM was −0.385 V versus Ag/AgCl, more positive than that for naturally synthesized MnO_2 (−0.443 V) and the HSM with a noticeable increase in oxygen reduction peak current (Figure 2). This may suggest an effective disproportionation of the electrogenerated hydrogen peroxide by the HSM nanorods and nanostructured platelike [23]. More importantly, the improved dispersion of nanostructured MnO_2 favors oxygen adsorption due to its larger BET, facilitating electron transfer through the film and decreasing the ORR over potential. In addition, the presence of oxygenated groups on the surface of cathode catalyst, partially due to oxidation by permanganate, may facilitate oxygen reduction, as reported by Kinoshita [26]. Thus, as the NSM is relatively low adsorption of oxygen and weaker ORR performance, it was expected that between the naturally and hydrothermally synthesized MnO_2, the HSM would constitute a more effective cathode catalyst material for MFCs.

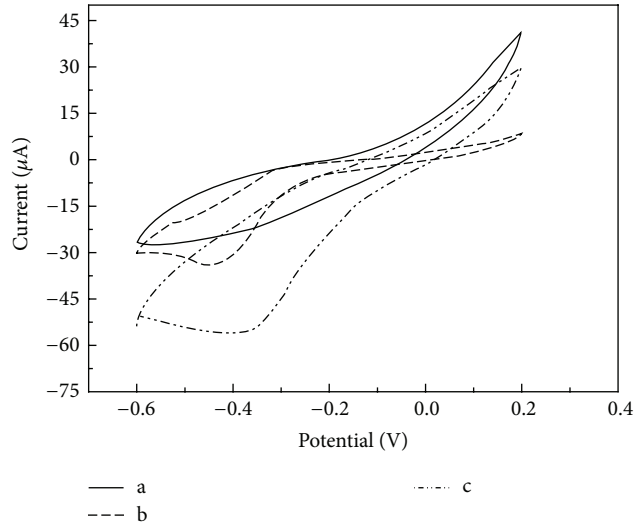

Figure 2: Cyclic voltammograms of MnO_2 for ORR at scan rate of 100 mV/s in 0.1 M KOH. (a) Electrolyte bubbled with N_2; (b) NSM; (c) HSM. (b)-(c) Electrolyte bubbled with O_2.

3.3. MFC Performances with Various Catalysts. The performance of MFCs with the NSM and HSM was evaluated alongside that of the cathode without loading catalyst by monitoring cell voltage output, anode and cathode polarization, and power density. As shown in Figure 3, a maximum stable voltage of 0.42 V was delivered by the MFC loading with HSM, which was larger than loading with NSM (0.34 V) and without loading catalyst (0.21 V) MFCs achieved. The main reason for the higher power generation of HSM MFC was that HSM possessed high oxygen reduction rates (ORRs), and the low voltage generation of MFC without loading

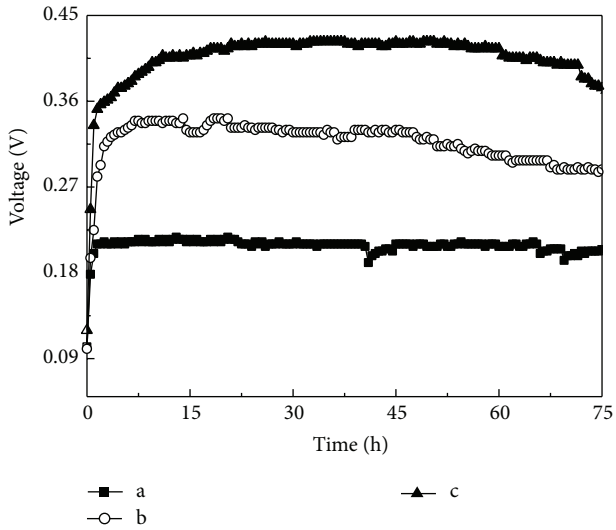

Figure 3: The voltage of MFCs with different cathode catalysts. (a) Cathode without loading catalyst; (b) cathode loading with NSM; (c) cathode loading with HSM.

catalyst could be explained by its higher R_{in} (250 Ω, as shown in Table 1). The difference of R_{in} among these MFCs may have been due to the electrical characteristics of the various catalysts, particularly conductivity [18]. Therefore, the sufficient dispersion of nanostructured MnO_2 over the cathode surface resulted in high conductivity and decreased the cathodic resistance, thus achieving a better performance in the MFC loading with HSM.

Power densities of different catalysts were compared using a polarization curve measurement. The HSM-based MFC had the highest maximum power density than NSM-based MFC and without loading catalyst MFC. The Maximum power density (based on 25 cm^2 projected anode surface area) of 119.07 mW/m^2 (about 5.95 W/m^3 based on 50 cm^3 anode volume, which was about 6.7 times higher than electrochemically deposition nanostructured MnO_x (772.8 mW/m^3) [23]), was obtained with HSM as cathode catalyst (with a current density of 0.49 A/m^2), while a maximum power density of 32.11 mW/m^2 and 42.05 mW/m^2 was achieved at current densities of 0.22 A/m^2 and 0.29 A/m^2 without any catalyst or with NSM as cathode catalyst (Figure 4(a)), about 73.03% and 64.68% lower than that with HSM, respectively. The results of this investigation on the dependency of power generation in MFCs are consistent with the results of the BET studies. To understand this observation better, the individual electrode potentials were also measured (Figure 4(b)). The anodic potentials were almost identical in all case due to the matured anodic biofilms, whereas the cathodic potentials were varied, so it was evident that the cathode was the limiting factor in these MFC reactors. For instance, in hydrothermally synthesized MnO_2 MFC, with the increased current densities of 0–0.8 A/m^2, the anode potential increased insignificantly from −0.52 to −0.46 V, whereas the cathode potential dropped from −0.17 to −0.36 V; the larger driving force with an over potential of 0.19 V required for the cathode compared to the value of 0.06 V required for the anode indicates that power generation from the MFC was dominated by cathode polarization. This is also consistent with the higher OCV (Table 1) and the lower internal resistance of HSM-based MFC than NSM-based MFC, since the lower internal resistance would result in a less ohmic loss and less polarization [27]. Therefore, the results indicated that MnO_2 prepared with a hydrothermal synthesis method could be effectively used as a catalyst in single-chamber air-cathode MFCs to generate current.

3.4. Oxygen Reduction Mechanisms. The ORR mechanism in alkaline media on MnO_x is usually described by the partial 2-electron reduction of O_2 as follows:

$$O_2 + H_2O + 2e^- \longrightarrow HO_2^- + OH^- \quad (1)$$

$$HO_2^- + H_2O + 2e^- \longrightarrow 3OH^- \quad (2)$$

$$2HO_2^- \longrightarrow O_2 + 2OH^- \quad (3)$$

Manganese oxides were found to facilitate the decomposition of hydrogen peroxides, according to the HO_2^- disproportionation reaction (3) [28]. Oxygen can then be reduced according to the reaction (1); the overall reaction is then the apparent 4-electron reduction of O_2:

$$O_2 + 2H_2O + 4e^- \longrightarrow 4OH^- \quad (4)$$

The 4-electron process to combine oxygen with electrons and protons directly to produce water as the end product; however, 2-electron processes involving the information of hydrogen peroxide ions as the intermediate. And the hydrogen peroxide ions are corrosive and can degrade the membrane and/or corrode the fuel cell cathode [29, 30]. Furthermore, Cao et al. [31] have studied the mechanism of the ORR in several MnO_2-catalysed air electrodes. It was found that the ORR is accompanied by the reduction of MnO_2 and that the catalytic activity is dependent on the electrochemical redox activity of these species. In addition, the oxygen reduction at MnO_2-catalyzed air cathode proceeds through chemical oxidation of the surface Mn^{3+} ions generated by the discharge of MnO_2 rather than through a direct two-electron reduction as previously suggested.

According to Bard and Faulkner [32], the number of electron transfer (n) involved in the oxygen reduction at 25°C could be estimated with Randles-sevcik equation (5):

$$i_p = 0.4463(Fn)^{(2/3)} A D_o C_o^* V^{(1/2)} (RT)^{(-1/2)}, \quad (5)$$

where i_p is peak current (A), F is Faraday's constant (96485 C/mol), n is the number of electrons appearing in half-reaction for the redox couple, A is the electrode area (cm^2), D_o is the electrolyte's diffusion coefficient (cm^2/s), C_o^* is the concentration of electrolyte at the electrode surface (mol/cm^3), V is the potential scanning rate (v/s), R is the universal gas constant (8.314 J/mol·K), and T is the absolute temperature (t+273.15 K). At 25°C, for A in cm^2, D_o in cm^2/s, C_o^* in mol/cm^3, and V in v/s, i_p in amperes is as follows:

$$i_p = \left(2.69 \times 10^5\right) n^{(2/3)} A D_o C_o^* V^{(1/2)}. \quad (6)$$

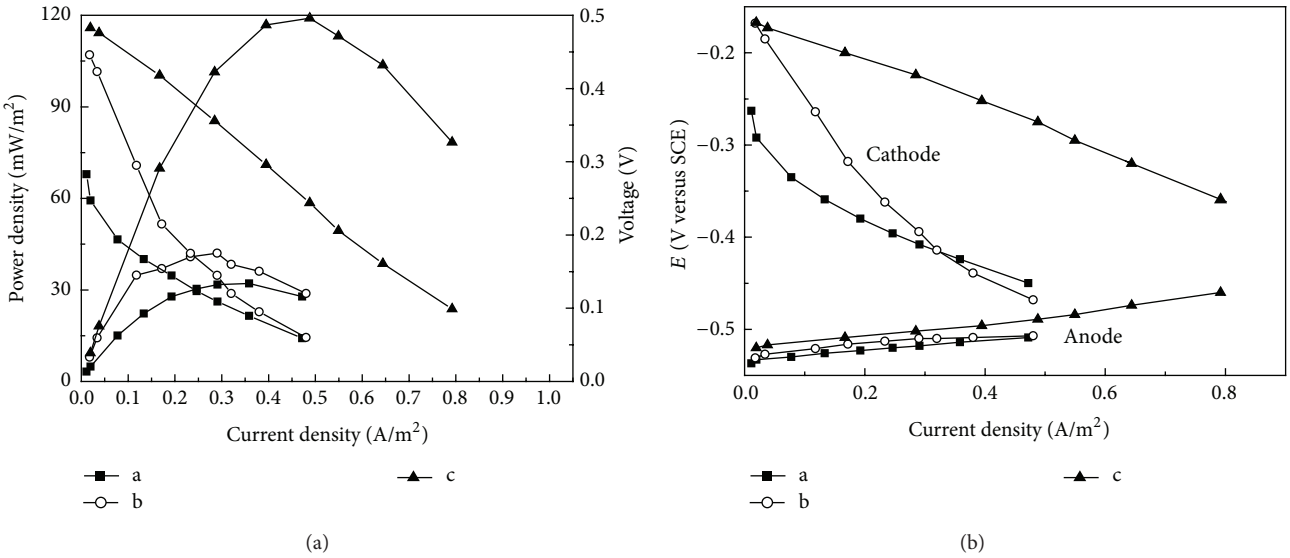

Figure 4: Performance of MFC equipped with different catalysts. (a) Cathode without loading catalyst; (b) cathode loading with NSM; (c) cathode loading with HSM.

A in this study was approximately 0.07 cm^2. Then according to the data shown in Figure 2, n in NSM is calculated to be 2.2, but in HSM it is calculated to be 4.3, suggesting that an apparent 2-e reduction of oxygen was achieved on the NSM in alkaline pH solution, but an apparent 4-e reduction of oxygen was achieved on the HSM. This result is the same as the one on MnO_x/C using ring-disc electrode in alkaline solution [22] and the one on electrochemically deposition MnO_x nanorods in neutral solution [23]. Moreover, the previous studies indicated that 4-e pathway is more efficient than 2-e pathway [30, 33]. This result further confirmed the previous outcome in this study.

4. Conclusions

In this study, by hydrothermal synthesis method a nanorods evolving in addition to nanostructure platelike morphology MnO_2 is synthesized, characterized, investigated by SEM and CV methods in alkaline solution and finally incorporated into air-cathode MFCs as cathode ORR catalysts. It is shown that the nanostructure MnO_2 has quite good capability for ORR catalysis and has an electrochemical activity towards ORR via a 4-e pathway in alkaline solution which is more efficient than 2-e pathway as the NSM undergo. When the MnO_2 are applied onto air-cathode MFC, the performance of the nanostructured MnO_2-based MFC is more efficient and stable than the natural synthesis MnO_2. Our findings provide useful information to develop appropriate nanostructured MnO_2 catalysts towards oxygen reduction in MFC using this facile method. Due to its low cost, easy preparation, and good MFC performance, this catalyst could be a very promising electrocatalyst for air-cathode MFC. It is believed that this efficient and economic catalyst could facilitate the scaling up and commercialization of MFC reactors for practical applications.

Conflict of Interests

The authors declare that there is no conflict of interests regarding the publication of this paper.

Acknowledgments

This work was financially supported by National 973 project of China (2011CB201501), supported by Projects of International Cooperation and Exchanges NSFC (51161140330), Knowledge Innovation Program of the Chinese Academy of Sciences (NKSCX2-EW-G-1-5), and The Program of Guangdong Province—Chinese Academy of sciences strategic cooperation (2010A090100035).

References

[1] B. Logan, "Generating electricity from wastewater treatment plants," *Water Environment Research*, vol. 77, no. 3, pp. 209–211, 2005.

[2] B. E. Logan, "Simultaneous wastewater treatment and biological electricity generation," *Water Science and Technology*, vol. 52, no. 1-2, pp. 31–37, 2005.

[3] K. Rabaey, P. Clauwaert, P. Aelterman, and W. Verstraete, "Tubular microbial fuel cells for efficient electricity generation," *Environmental Science and Technology*, vol. 39, no. 20, pp. 8077–8082, 2005.

[4] D. R. Lovley, "Bug juice: harvesting electricity with microorganisms," *Nature Reviews Microbiology*, vol. 4, no. 7, pp. 497–508, 2006.

[5] H. Liu and B. E. Logan, "Electricity generation using an air-cathode single chamber microbial fuel cell in the presence and absence of a proton exchange membrane," *Environmental Science and Technology*, vol. 38, no. 14, pp. 4040–4046, 2004.

[6] J. M. Morris, S. Jin, J. Wang, C. Zhu, and M. A. Urynowicz, "Lead dioxide as an alternative catalyst to platinum in microbial fuel

cells," *Electrochemistry Communications*, vol. 9, no. 7, pp. 1730–1734, 2007.

[7] F. Zhao, F. Harnisch, U. Schröder, F. Scholz, P. Bogdanoff, and I. Herrmann, "Application of pyrolysed iron(II) phthalocyanine and CoTMPP based oxygen reduction catalysts as cathode materials in microbial fuel cells," *Electrochemistry Communications*, vol. 7, no. 12, pp. 1405–1410, 2005.

[8] S. You, Q. Zhao, J. Zhang, J. Jiang, and S. Zhao, "A microbial fuel cell using permanganate as the cathodic electron acceptor," *Journal of Power Sources*, vol. 162, no. 2, pp. 1409–1415, 2006.

[9] S. Cheng, H. Liu, and B. E. Logan, "Power densities using different cathode catalysts (Pt and CoTMPP) and polymer binders (Nafion and PTFE) in single chamber microbial fuel cells," *Environmental Science and Technology*, vol. 40, no. 1, pp. 364–369, 2006.

[10] N. Duteanu, B. Erable, S. M. Senthil Kumar, M. M. Ghangrekar, and K. Scott, "Effect of chemically modified Vulcan XC-72R on the performance of air-breathing cathode in a single-chamber microbial fuel cell," *Bioresource Technology*, vol. 101, no. 14, pp. 5250–5255, 2010.

[11] L. Fu, S.-J. You, G.-Q. Zhang, F.-L. Yang, X.-H. Fang, and Z. Gong, "PB/PANI-modified electrode used as a novel oxygen reduction cathode in microbial fuel cell," *Biosensors and Bioelectronics*, vol. 26, no. 5, pp. 1975–1979, 2011.

[12] L. Wang, P. Liang, J. Zhang, and X. Huang, "Activity and stability of pyrolyzed iron ethylenediaminetetraacetic acid as cathode catalyst in microbial fuel cells," *Bioresource Technology*, vol. 102, no. 8, pp. 5093–5097, 2011.

[13] L. Deng, M. Zhou, C. Liu, L. Liu, C. Liu, and S. Dong, "Development of high performance of Co/Fe/N/CNT nanocatalyst for oxygen reduction in microbial fuel cells," *Talanta*, vol. 81, no. 1-2, pp. 444–448, 2010.

[14] J. R. Kim, J.-Y. Kim, S. B. Han, K.-W. Park, G. D. Saratale, and S.-E. Oh, "Application of Co-naphthalocyanine (CoNPc) as alternative cathode catalyst and support structure for microbial fuel cells," *Bioresource Technology*, vol. 102, pp. 342–347, 2011.

[15] Z. Wei, W. Huang, S. Zhang, and J. Tan, "Carbon-based air electrodes carrying MnO_2 in zinc-air batteries," *Journal of Power Sources*, vol. 91, no. 2, pp. 83–85, 2000.

[16] L. Zhang, C. Liu, L. Zhuang, W. Li, S. Zhou, and J. Zhang, "Manganese dioxide as an alternative cathodic catalyst to platinum in microbial fuel cells," *Biosensors and Bioelectronics*, vol. 24, no. 9, pp. 2825–2829, 2009.

[17] X. Li, B. Hu, S. Suib, Y. Lei, and B. Li, "Electricity generation in continuous flow microbial fuel cells (MFCs) with manganese dioxide (MnO_2) cathodes," *Biochemical Engineering Journal*, vol. 54, no. 1, pp. 10–15, 2011.

[18] X. Li, B. Hu, S. Suib, Y. Lei, and B. Li, "Manganese dioxide as a new cathode catalyst in microbial fuel cells," *Journal of Power Sources*, vol. 195, no. 9, pp. 2586–2591, 2010.

[19] Y. Zhang, Y. Hu, S. Li, J. Sun, and B. Hou, "Manganese dioxide-coated carbon nanotubes as an improved cathodic catalyst for oxygen reduction in a microbial fuel cell," *Journal of Power Sources*, vol. 196, no. 22, pp. 9284–9289, 2011.

[20] Y. Chen, Z. Lv, J. Xu et al., "Stainless steel mesh coated with MnO_2/carbon nanotube and polymethylphenyl siloxane as low-cost and high-performance microbial fuel cell cathode materials," *Journal of Power Sources*, vol. 201, pp. 136–141, 2012.

[21] M. Lu, L. Guo, S. Kharkwal, H. N. Wu, H. Y. Ng, and S. F. Y. Li, "Manganese-polypyrrole-carbon nanotube, a new oxygen reduction catalyst for air-cathode microbial fuel cells," *Journal of Power Source*, vol. 221, pp. 381–386, 2013.

[22] I. Roche, K. Katuri, and K. Scott, "A microbial fuel cell using manganese oxide oxygen reduction catalysts," *Journal of Applied Electrochemistry*, vol. 40, no. 1, pp. 13–21, 2010.

[23] X.-W. Liu, X.-F. Sun, Y.-X. Huang et al., "Nano-structured manganese oxide as a cathodic catalyst for enhanced oxygen reduction in a microbial fuel cell fed with a synthetic wastewater," *Water Research*, vol. 44, no. 18, pp. 5298–5305, 2010.

[24] V. Subramanian, H. Zhu, R. Vajtai, P. M. Ajayan, and B. Wei, "Hydrothermal synthesis and pseudocapacitance properties of MnO_2 nanostructures," *Journal of Physical Chemistry B*, vol. 109, no. 43, pp. 20207–20214, 2005.

[25] H. R. Yuan, L. F. Deng, Y. Chen, and S. G. Zhou, "Electricity generation from municipal solid waste leachate using microbial fuel cell technology," *Journal of Basic Science and Engineering*, vol. 20, no. 5, pp. 800–810, 2012.

[26] K. Kinoshita, *Electrochemical Oxygen Technology*, Wiley-Interscience, New York, NY, USA, 1992.

[27] L. Zhuang, S. Zhou, Y. Wang, C. Liu, and S. Geng, "Membraneless cloth cathode assembly (CCA) for scalable microbial fuel cells," *Biosensors and Bioelectronics*, vol. 24, no. 12, pp. 3652–3656, 2009.

[28] L. Mao, D. Zhang, T. Sotomura, K. Nakatsu, N. Koshiba, and T. Ohsaka, "Mechanistic study of the reduction of oxygen in air electrode with manganese oxides as electrocatalysts," *Electrochimica Acta*, vol. 48, no. 8, pp. 1015–1021, 2003.

[29] M. Chatenet, L. Genies-Bultel, M. Aurousseau, R. Durand, and F. Andolfatto, "Oxygen reduction on silver catalysts in solutions containing various concentrations of sodium hydroxide—comparison with platinum," *Journal of Applied Electrochemistry*, vol. 32, no. 10, pp. 1131–1140, 2002.

[30] M. Chatenet, M. Aurousseau, R. Durand, and F. Andolfatto, "Silver-platinum bimetallic catalysts for oxygen cathodes in chlor-alkali electrolysis. Comparison with pure platinum," *Journal of the Electrochemical Society*, vol. 150, no. 3, pp. D47–D55, 2003.

[31] Y. L. Cao, H. X. Yang, X. P. Ai, and L. F. Xiao, "The mechanism of oxygen reduction on MnO_2-catalyzed air cathode in alkaline solution," *Journal of Electroanalytical Chemistry*, vol. 557, pp. 127–134, 2003.

[32] A. J. Bard and L. R. Faulkner, *Electrochemical Methods: Fundamentals and Applications*, John Wiley & Sons, New York, NY, USA, 2001.

[33] K. Gong, F. Du, Z. Xia, M. Durstock, and L. Dai, "Nitrogen-doped carbon nanotube arrays with high electrocatalytic activity for oxygen reduction," *Science*, vol. 323, no. 5915, pp. 760–764, 2009.